AN ABSTRACT OF THE THESIS OF

Abdulrahim Al-Zahrani for the degree of Doctor of Philosophy in Chemical Engineering presented on November 23, 1988.

Title: Modeling and Control Studies of a Magnetically Staged Fluidized Bed

Abstract approved: Redacted for Privacy

Keith L. Levien

A column which contains a series of three fluidized beds for counter-current contacting of solid particles with a gas stream has been studied. Successful, independent control of solids holdup on each stage has been achieved by manipulating the field of a magnetic distributor-downcomer on each stage. Two methods to manipulate the field were investigated: an "on/off" method versus a continuous adjustment of the DC current used to create the field (the "leaking valve"). A model of the column ,which includes pressure fluctuations in each fluidized bed, was used to design a control law based on proportional feedback control with some logic statements to compensate for interactions. Both simulated and actual performances in setpoint and disturbance rejection experiments were obtained with solids

consisting of 100 percent iron, 50/50, and 25/75 percent mixtures of iron and sand. In all cases the gas stream was air.

The leaking valve approach was found to be more efficient in terms of average power consumption and in some experiments was found to yield better performances.

This is the first study of the magnetic distributor-downcomer under conditions where there is a net flow of solids through the fluidized bed. This is also the first study of a process where multiple fluidized bed stages are used and interactions are analyzed. The study of the staged fluidized beds when not all the solids are magnetic yielded new results on particle segregation within a bed as well as modifications needed in the control law.

Modeling and Control Studies of a Magnetically-Staged Fluidized Bed

by

Abdulrahim Al-Zahrani

A THESIS

submitted to

Oregon State University

in partial fulfillment of
the requirements for the
degree of

Doctor of Philosophy

Completed November 23, 1988

Commencement June, 1989

APPROVED:

Redacted for Privacy

Professor of Chemical Engineering in Charge of Major

Redacted for Privacy

Head of Department of Chemical Engineering

Redacted for Privacy

Dean of Graduate School

Date Thesis is Presented: November 23, 1988

Typed by: Donna Reyes

© 1990

ABDULRAHIM AL-ZAHRANI

All Rights Reserved

ACKNOWLEDGEMENTS

First and foremost, I would like to thank my advisor, Dr. Keith Levien. His guidance and assistance, which were available all the time, were the main reasons for the completion of this work. I thank him also for all the other things he taught me besides the research.

I would like to thank all the Chemical Engineering faculty members, especially Professors Levenspiel, Wicks, Knudsen and Mrazek, for their assistance and help. Special thanks goes to Dr. Levenspiel whose help I have often sought and have never been denied.

I would like to thank all the graduate students of the Chemical Engineering Department. In particular, I would like to thank Lounes Oufer for his friendship, which I enjoyed greatly.

My thanks goes to my friend, Nick Wannenmacher, whose help was available all the time and without it I would have been lost. I would like to thank him for his patience when he spent many hours repairing the electronics used in this work. I also thank him for teaching me many things besides those of the research.

I would like to thank my best friend, Mosaed Al-Ohally, without whose friendship and support I would not have made it this far.

I would like to thank Ahmad Al-Shadawi and Abdulrahman AL-Zahrani for their friendship and support.

My thanks goes to my brothers and sisters. In particular, I would like to recognize my brother Mohammed, whose support has a great deal to do with my achieving this goal.

Special thanks goes to my sons Ahmad and Mohammed. I deeply apologize to my son Ahmad for not giving him enough time and attention during this research.

Ultimately, I would like to thank my parents Ahmad and Fatimah for their love and support and also for setting me on the road to higher education.

My special thanks goes to Tharaya, my wife and best friend, for her love and support under difficult circumstances which allowed me to reach my goals. I would like to apologize to her for not spending enough time with her during this work.

To my father and mother,

to my wife, and to my sons,

Ahmad and Mohammed.

TABLE OF CONTENTS

I. INTRODUCTION AND PREVIOUS WORK 1

I.1 Introduction 1

I.1.1 Single Stage Fluidized Bed 3

I.1.2 Multistage Fluidized Bed 4

I.1.2.1 Advantages 4

I.1.2.2 Applications 5

I.1.2.3 Operational Problems 7

I.2 Previous Work 10

I.2.1 Use of Magnetic Field for Stabilization 10

I.2.1.1 Stabilization Diagram 11

I.2.1.2 Applications 11

I.2.1.3 Associated Problems 14

I.2.1.4 Operation with Mixtures 15

I.2.2 Use of Magnetic Field for Regulating the Flow Rate of Solids and the Design of Distributor and Downcomer 15

I.2.2.1 Applications 20

I.2.2.2 Advantages 22

I.2.3 Organization of the Thesis 23

II. EXPERIMENTAL EQUIPMENT 24

II.1 The Multistage Fluidized System 24

II.1.1 The Three Stage Fluidized Bed 24

II.1.2 Feed System 29

II.1.3 The Recycle Solids System 31

II.2 The Interface 35

II.2.1 IBM Data Acquisition and Control Adapter: 35

II.2.2 The Timer: 35

II.2.3 The Current Control Circuit Card: 38

II.2.4 The Differential Pressure Cell: 39

III. DYNAMIC BEHAVIOR OF THE PROCESS 40

III.1 Definitions of Input/Output Disturbances 40

III.2 Operation at Different Values of Fraction Open With Constant Period 42

III.3 Step Change in the Flow Rate of Solids into the Bed 47

III.4 Step Change in the Flow Rate Out of the Bed 49

III.5 Conclusions 50

IV. MODELING SOLIDS FLOW THROUGH A STAGE 53

IV.1 Simple Fundamental Model 53

IV.2 Regions Inside the Stage Valve 56

IV.2.1 Fluidized Region 56

IV.2.2 The Non-Fluidized Region Close to the Magnetic Valve 57

IV.2.2.1 Gravity Forces (F_g) 58

IV.2.2.2 The Drag Forces 58

IV.2.2.3 Magnetic Forces 60

IV.2.2.3.1 Derivation of the Magnetic Force Equation 64

IV.2.2.4 Ferromagnetic Material Hysteresis 67

IV.2.2.5 Mechanism of Valve Operation 72

IV.2.2.6 Model Equations for Solids Flow Rate 73

IV.3 On/Off Valve Operation v.s. "Leaking" Valve Operation 76

IV.3.1 On/off Operation 76

IV.3.1.1 Characterization of the Operation 77

IV.3.1.2 Glob Flow Region 81

IV.3.1.3 Continuous Flow Region 82

IV.3.1.4 Pulsed Flow Region 82

IV.3.1.5 Calculation of Average Current from a Fraction Open Specification 84

IV.3.2 "Leaking" Valve Operation 90

IV.4 Effect of Solids Holdup on the Flow Rate of Solids Out of the Stage Valve 93

V. PROCESS MEASUREMENT 96

V.I Relation Between Bed Height and Pressure Drop 96

V.2 Pressure Fluctuations 100

V.2.1 Motivation for Characterization of Pressure Fluctuations 100

V.2.1.1 Fluidization Quality 100

V.2.1.2 Influence on the Choice of Sampling Frequency for the Controller 101

V.2.1.3 Determining the Filter Time Constant 102

V.2.2 Previous Work in Gas Flow Systems 104

V.2.3 Sampling 105

V.2.4 Spectral Analysis Fluctuation Data Sets 106

V.2.5 Determination of Dominant Amplitude and Frequency of Fluctuation Data Sets 116

V.2.6 Correlating Dominant Amplitude and Frequency Measurements With the Average Pressure Drop Across the Stage 119

VI. SIMULATION PRELIMINARIES AND CLOSED-LOOP STUDIES FOR 100% IRON 125

VI.1 Introduction: 125

VI.1.1 Preliminary Studies for the Closed-Loop Simulation 126

VI.1.2 The Equations Used in the Simulation 127

VI.1.3 Interactions Between the Stages 129

VI.1.4 Decoupling 133

VI.1.5 Design of Control System Parameters via Simulation 140

VI.2 Closed-Loop Studies for 100% Iron 147

VI.2.1 Design of the Control System Parameters via Simulation 150

VI.2.1.1 Controller Gain 150

VI.2.1.2 Filter Time Constant 152

VI.2.1.2 Input Constraints 154

VI.2.2 Simulated Closed-Loop Performance 158

VI.2.2.1 Negative Setpoint Change in the Pressure Drop Across a Stage 158
VI.2.2.2 Positive Step Change in the Feed Flow Rate of Solids 161
VI.2.3 Closed-Loop Experiments 164
VI.2.3.1 Negative Step Change in the Pressure Drop Across a Stage 164
VI.2.3.2 Positive Step Change in the Feed Flow rate 166
VI.2.4 Comparison Between Experimental and Simulated Performances 170
VI.3 "Leaking" Valve Operation 172
VI.3.1 Design of the Control System Parameter via Simulations 172
VI.3.1.1 Controller Gain 174
VI.3.1.2 Filter Time Constant 176
VI.3.1.3 Input Constraints 176
VI.3.2 Simulated Closed-loop Performances 179
VI.3.2.1 Negative Setpoint Change in the Pressure Drop Across a Stage 179
VI.3.2.2 Positive Step Change in the Feed Flow Rate of Solids 185
VI.3.3 Closed-Loop Experiments 187
VI.3.3.1 Negative Setpoint Change in the Pressure Drop Across a Stage 187
VI.3.3.2 Positive Step Change in the Feed Flow Rate of Solids 191

VI.3.4 Comparison Between the Simulated and Experimental Performances 193

VI.4 Comparison Between On/Off and Leaking Valve Operations 195

VII. CLOSED-LOOP STUDIES FOR SOLIDS CONTAINING 50% IRON 198

VII.1 On/Off Operation 198

VII.1.1 Design of the Control System Parameters via Simulation 200

VII.1.1.1 Controller Gain 201

VII.1.1.2 Filter Time Constant 201

VII.1.1.3 Input Constraints 201

VII.1.2 Simulated Closed-Loop Performance 213

VII.1.2.1 Negative Step Change in the Pressure Drop Across a Stage 207

VII.1.2.2 Positive Step Change in the Feed Flow of Solids 210

VII.1.3 Closed-Loop Experiments 213

VII.1.3.1 Negative Setpoint Change in the Pressure Drop Across a Stage 213

VII.1.3.2 Positive Step Change in Feed Flow Rate of Solids 217

VII.1.4 Comparison Between the Simulated and Experimental Performances 217

VII.2 "Leaking" Valve Operation 221

VII.2.1 Evaluation of the Control System Parameters via Simulation 221

VII.2.1.1 Controller Gain 223

VII.2.1.2 Filter Time Constraint 223

VII.2.1.3 Input Constraints 226

VII.2.2 Simulated Closed-Loop Performance 229

VII.2.2.1 Negative Setpoint Change in the Pressure Drop across a Stage 229

VII.2.2.2 Positive Step Change in the Feed flow Rate of Solids 231

VII.2.3 Closed-Loop Experiment 235

VII.2.3.1 Negative Setpoint Change in the Pressure Drop Across a Stage 235

VII.2.3.2 Positive Step Change in the Feed Flow Rate of Solids 237

VII.2.4 Comparison Between Simulated and Experimental Results 241

VII.3 Comparison Between On/Off and "Leaking" Valve Operations 243

VIII. SEGREGATION AND CLOSED-LOOP STUDIES FOR SOLIDS CONTAINING 25% IRON 246

VIII.1 Iron's Weight Fraction Behavior Inside a Stage With Time 247

VIII.1.1 Experimental Procedures 247

VIII.1.2 Using Recycled Solids as a Feed to the Top Stage 249

VIII.1.3 Fresh Feed of Solids 255

VIII.1.4 Effect of Stage Position on Weight Fraction 257
VIII.1.5 Effect of Current on Weight Fraction 260
VIII.1.6 Determination of the Fixed Layer Thickness and Height 260
VIII.2 Control Difficulties 266
VIII.2.1 Steady-State Operation 266
VIII.2.2 Dynamic Operation 271
VIII.3 On/Off Operation 272
VIII.3.1 Design of the Controller Parameters via Simulation 274
VIII.3.1.1 Controller Gain 274
VIII.3.1.2 Filter Time Constant 274
VIII.3.1.3 Input Constraints 277
VIII.3.2 Simulated Closed-Loop Performance 280
VIII.3.2.1 Negative Setpoint Change in the Pressure Drop Across a Stage 280
VIII.3.2.2 Positive Step Change in the Flow Rate of Solids 282
VIII.3.3 Closed-Loop Experiments 286
VIII.3.3.1 Negative Setpoint Change in the Pressure Drop Across a Stage 286
VIII.3.3.2 Positive Step Change in the Feed Flow Rate of Solids 290
VIII.3.4 Comparison Between the Simulated and Experimental Performances 293
VIII.4 "Leaking" Valve Operation 294

VIII.4.1 Design of Controller Parameters via Simulations 296

VIII.4.1.1 Controller Gain 296

VIII.4.1.2 Filter Time Constant 296

VIII.4.1.3 Input Constraints 299

VIII.4.2 Simulated Closed-loop Performance 302

VIII.4.2.1 Negative Setpoint Change in the Pressure Drop Across a Stage 302

VIII.4.2.2 Positive Step Change in the Feed Flow Rate of Solids 307

VIII.4.3 Closed-Loop Experiments 307

VIII.4.3.1 Negative Setpoint Change in the Pressure Drop Across a Stage 307

VIII.4.3.2 Positive Change in the Feed Flow Rate of Solids 312

VIII.4.4 Comparison Between the Simulated and Experimental Performances 315

VIII.5 Comparison Between On/Off and "Leaking" Valve Operations 316

IX. CONCLUSIONS AND RECOMMENDATIONS FOR FUTURE WORK 319

IX.1 Conclusions 319

IX.2 Recommendations for Future Work 324

REFERENCES 326

APPENDIX A: DETAILS ABOUT THE INTERFACE 335

A-1 The Three Channel 8-bit Programmable Timer 335

A-1.1 Introduction 335

A-1.2 Description of the Three Channel Programmable Timer 335

A-1.3 The Timer Operation 339

A-2 The One Channel Programmable 8-bit Programmable Timer 340

A-2.1 The Current Controlling Circuit Card 341

A-3 The Pressure Transducer 345

A-3.1 Specifications: 345

A-3.2 Calibration of the Differential Pressure Cell 346

APPENDIX B: CALIBRATION OF THE FEED FLOW RATE FROM THE HOPPER 348

B-1 Calibration of Solids Flow Rate into the Bed 348

B-1.1 Calibration for Solids Containing 100% Iron 348

B-1.2 Calibration for Solids Containing 50% by Weight Iron 355

B-1.3 Calibration of Solids Containing 25% by Weight Magnetic 355

B-2 Effect of Screen Location On the Flow Rate of Solids Out of the Hopper 358

B-3 Effect of Solids Inventory in the Hopper On the Flow Rate of Solids 362

APPENDIX C: CHARACTERIZATION OF SOLIDS 364

C-1 Size Distribution of Solids 364

C-2 Typical Properties of the Solids Used in the Operation 372

C-2.1 The Magnetic Material 372

C-2.2 Bulk and Void Fraction 372

APPENDIX D: PRESSURE FLUCTUATIONS STUDIES 375

D-1 Some Information About Sampling 375

D-1.1 Very Fast Sampling Frequency 375

D-1.2 Controller Sampling Rate 377

D-2 Approximate Model for Pressure Fluctuations 380

D-2.1 Frequency 382

D-2.2 Amplitude 383

D-3 Pressure Fluctuations Without Solids Flow Through the Stage 387

D-4 Pressure Fluctuations with Solids Flow and 0.256 Second as a Controller iN Sampling Time 390

D-5 Effect of Level of Current on the Minimum Fluidization Velocity 393

LIST OF FIGURES

Figure		Page
(1)	Typical Pressure Drop Versus Gas Velocity Curve.	2
(2)	Exit Age Distribution for Single Stage and Multistage Fluidized Beds.	2
(3)	Conventional Multistage Fluidized Bed.	8
(4)	Magnetic Stabilization Diagram.	12
(5)	Magnetic Stabilized Beds.	12
(6)	Shapes of the Current Signal Flowing through the Grates.	17
(7)	The Complete Layout of the Experimental Equipment.	25
(8)	Details of Bed Chamber.	27
(9)	The Stage Valve with the Grates.	28
(10)	The Hopper.	30
(11)	The Recycle System.	32
(12)	Air Supply System.	34
(13)	The Main Components of the Interface.	36
(14)	Histories of Pressure Drop Across the Bed at Different Values of Fraction Open and h_i = 5".	43
(15)	Histories of Pressure Drop Across the Bed at Different Values of Fractions Open and h_i = 7".	44
(16)	Histories of Pressure Drop Across the Bed at Flow Rate = 80 gm/sec.	46
(17)	Histories of Pressure Drop Across the Bed for Positive Step in the Flow Rate of Solids into the Bed.	48

(18) Histories of Pressure Drop Across the Bed for Positive and Negative Step Change in the Flow Rate of Solids Out of the Stage. 51

(19) Sketch of the Behavior of Pressure Drop for Different Values of m_i and m_o. 55

(20) Regions Inside the Stage Valve. 55

(21) Orientation of the Particles in the Magnetic Field and the Various Forces Involved. 63

(22) The Magnetic Field Flux Lines with and without the Presence of the Magnetic Material. 63

(23) Typical Magnetization Curve for Ferromagnetic Material with Hysteresis. 69

(24) Magnetization Curve of Magnetic Materials when Using a D.C. Current. 69

(25) Experimental Magnetization Curve for Iron. 71

(26) Graphical Presentation of the Forces Acting on Solids Close to the Grates. 71

(27) Flow Regions of Solids Flow Through the Stage Valve. 78

(28) Actual Signal of the Current Flowing Through the Valve at Different Values of Fractions Open. 85

(29) Actual Signal of the Current Flowing Through the Valve at Different Values of Periods. 86

(30) Average Current Versus Fractions Open for Different Values of Working Currents. 88

(31) Hysteresis Associated with "Leaking" Valve Operation. 92

(32) Release and Holding Currents for Different Weight Fractions of Magnetic Particles. 92

(33) Effect of Pressure Drop Across the Stage on the Fraction Open Required for a Steady State. 94

(34) Effect of Pressure Drop Across the Stage on the Current Required for steady state. 94

(35) Illustration of the Pressure Measurement Locations. 97

(36) Average Pressure Drop vs. Settled Height for Different Solid's Composition. 99

(37) Pressure Drop Signal for Uniform Batch Fluidization. 108

(38) Pressure Drop Signal for Batch Fluidization. 110

(39) Autocorrelation Coefficient Plots of Pressure Drop for Batch Fluidization. 111

(40) Power Spectrum Plots for Batch Fluidization. 112

(41) Pressure Signal Plots for Continuous Solids Throughputs. 113

(42) Autocorrelation Coefficient of Pressure for Continuous Solids Throughputs. 114

(43) Power Spectrum Plots of Pressure Drop for Continuous Solids Throughputs. 115

(44) Frequency vs. Average Pressure for Various Magnetic Compositions. 120

(45) Amplitude vs. Average Pressure for Various Magnetic Compositions. 121

(46) The Closed-Loop Block Diagram of the Multistage Fluidized Bed. 131

(47) Pure Integrator Process and the Corresponding Closed-Loop Block Diagram. 139

(48) Average Pressure Drop Across a Stage vs. Time for Different Value of Filter Time Constant. 139

(49) Block Diagram for the Simulation. 143

(50) Plots of ISQERR and ISQMAN vs. time. 144

(51) Plots of Experimental Data, the Model Fit and Curve Fitted Model. 148

(52) ISQERR and ISQMAN for the Three Stages vs. the Controller Gain. 151

(53) ISQERR and ISQMAN for the Three Stages vs. the Filter Time Constant. 153

(54) ISQERR and ISQMAN for the Three Stages vs. the Upper Limit on Input Constraint. 155

(55) ISQERR and ISQMAN for the Three Stages v.s the Lower Limit on Input Constraint. 157

(56) Simulated Closed-Loop Performances for -0.2 psi Setpoint Change in the Top Stage without Decoupling. 159

(57) Simulated Closed-Loop Performances for -0.2 psi Setpoint in the Top Stage with Decoupling. 160

(58) Simulated Closed-Loop Performances for -0.2 psi Setpoint Change in the Middle Stage with Decoupling. 162

(59) Simulated Closed-Loop Performances for 35 gm/second Step Change in the Feed Flow of Solids into the Top Stage. 163

(60) Experimental Closed-Loop Performances for -0.2 psi Setpoint Change in the Top Stage without Decoupling. 165

(61) Experimental Closed-Loop Performances for -0.20 psi Setpoint Change in the Top Stage with Decoupling. 167

(62) Experimental Closed-Loop Performances for a -0.20 psi Setpoint Change in the Middle Stage With Decoupling. 168

(63) Experimental Closed-Loop Performances for a 35 gm/second Step Change in the Feed Flow of Solid into the Top Stage. 169

(64) Plots of Solids Flow Rate out of the Stage vs. the Average Current. 173

(65) ISQERR and ISQMAN for Three Stages vs. the Controller Gain ("Leaking" Valve Operation). 175

(66) ISQERR and ISQMAN for Three Stages vs. the Filter Time Constant for the "Leaking" Valve Operation. 177

(67) ISQERR and ISQMAN for Three Stages vs. the Upper Limit on Input Constraint. 178

(68) ISQERR and ISQMAN for Three Stages vs. the Lower Limit on Input Constraint. 180

(69) Simulated Closed-Loop Performances for a -0.20 psi Setpoint Change in the Top Stage without Decoupling in "Leaking" Valve Operation. 181

(70) Simulated Closed-Loop Performances for a -0.20 psi Setpoint Change in the Top Stage with Decoupling. 183

(71) Simulated Closed-Loop Performances for a -0.20 psi Setpoint Change in the Middle Stage with Decoupling. 184

(72) Simulated Closed-Loop Performances for a 35 gm/seconds Step Change in the Feed Flow. 186

(73) Experimental Closed-Loop Performances for a -0.20 psi Change in Setpoint in the Top Stage without Decoupling. 188

(74) Experimental Closed-Loop Performances for a -0.20 psi Change in the Setpoint of the Top Stage with Decoupling. 189

(75) Experimental Closed-Loop Performances for a -0.20 psi Change in the Setpoint of the Middle Stage with Decoupling. 190

(76) Experimental Closed-Loop Performances for a 35 gm/seconds Step Change in Solids Flow Rate. 192

(77) Comparison Between the On/Off and the "Leaking" Valve Operation. 196

(78) Solids Flow Rate Through the Stage vs. Fraction Open (On/Off Operation; 50%). 299

(79) ISQERR and ISQMAN for the Three Stages vs. the Controller Gain for On/Off Operation (50% Iron). 202

(80) ISQERR and ISQMAN for the Three Stages vs. Filter Time Constant for On/Off Operation (50% Iron). 203

(81) ISQERR and ISQMAN for the Three Stages vs. the Lower Limit on Input Constraint for On/Off Operation (50% Iron). 204

(82) ISQERR and ISQMAN for the Three Stages v.s the Upper Limit on Input Constraint for On/Off Operation (50% Iron). 206

(83) Simulated Closed-Loop Performances for a -0.2 psi Setpoint Change in the Top Stage without Decoupling (On/Off Operation and 50% Iron). 208

(84) Simulated Closed-Loop Performances for a -0.2 psi Setpoint Change in the Top Stage with Decoupling (On/Off Operation and 50% Iron). 209

(85) Simulated Closed-Loop Performances for a -0.20 psi Setpoint Change in the Middle Stage with Decoupling (On/Off Operation and 50% Iron). 211

(86) Simulated Closed-Loop Performances for a 35 gm/seconds Step Change in the Feed Flow of Solids into the Top Stage (On/Off Operation and 50% Iron). 212

(87) Experimental Closed-Loop Performances for a -0.20 psi Setpoint Change in the Top Stage without Decoupling (On/Off Operation and 50% Iron). 214

(88) Experimental Closed-Loop Performances for a -0.20 psi Setpoint Change in the Top Stage with Decoupling (On/Off Operation and 50% Iron). 215

(89) Experimental Closed-Loop Performances for a -0.20 psi Setpoint Change in the Middle Stage with Decoupling (On/Off Operation and 50% Iron). 216

(90) Experimental Closed-Loop Performances for a 35 gm/seconds Step Change in the Feed Flow of Solids into the Top Stage (On/Off Operation and 50% Iron). 218

(91) Plots of Solids Flow Rate out of the Stage vs. the Average Current ("Leaking" Valve Operation and 50% Solids). 222

(92) ISQERR and ISQMAN for the Three Stages vs. the Controller Gain. 224

(93) ISQERR and ISQMAN for the Thee Stages vs. Filter Time Constant ("Leaking" Valve Operation and 50% Iron). 225

(94) ISQERR and ISQMAN for the Three Stages vs. the Lower Limit on Input Constraint ("Leaking" Valve Operation and 50% Iron). 227

(95) ISQERR and ISQMAN for the Three Stages vs. the Upper Limit on Input Constraint ("Leaking" Valve Operation and 50% Iron). 228

(96) Simulated Closed-Loop Performances for a -0.20 psi Setpoint Change in the Top Stage without Decoupling ("Leaking" Valve Operation and 50% Iron). 230

(97) Simulated Closed-Loop Performances for a -0.20 psi Setpoint Change in the Top Stage with Decoupling ("Leaking" Valve Operation and 50% Iron). 232

(98) Simulated Closed-Loop Performances for a -0.20 psi Setpoint Change in the Middle Stage with Decoupling ("Leaking" Valve Operation and 50% Iron). 233

(99) Simulated Closed-Loop Performances for a 35 gm/seconds Step Change in Solids Flow Rate. 234

(100) Experimental Closed-Loop Performances for a -0.20 psi Setpoint Change in the Top Stage without Decoupling ("Leaking" Valve Operation and 50% Iron). 236

(101) Experimental Closed-Loop Performances for a -0.20 psi Setpoint Change in the Top Stage with Decoupling ("Leaking" Valve Operation and 50% Iron). 238

(102) Experimental Closed-Loop Performances for a -0.20 psi Setpoint Change in the Middle Stage with Decoupling ("Leaking" Valve Operation and 50% Iron). 239

(103) Experimental Closed-Loop Performances for a 35 gm/seconds Step Change in Solids Flow Rate. 240

(104) Comparison Between the ON/OFF and the "Leaking" Valve Operation. 244

(105) Actual vs. Measured Weight Fractions. 250

(106) Weight Fraction in the Fluidizing Region as a Function of Time for Recycled Solids at Different Feed Rates. 251

(107) Weight Fraction in the Fluidizing Region as a Function of Time for Fresh Solids at Different Feed Rates. 256

(108) Effect of the Stage Position on the Segregation of Solids Between the Two Regions. 258

(109) Effect of Working Current on the Segregation of Solids Between the Two Regions. 258

(110) Pressure Drop Histories Across Each Stage for Steady-State Operation and On/Off Operation. 268

(111) Pressure Drop Histories Across Each Stage for Steady-State Operation and "Leaking" Valve Operation. 269

(112) Solids Flow Rate Through the Stage vs. Fraction Open (ON/OFF Operation; 25%). 273

(113) ISQERR and ISQMAN for the Three Stages vs. the Controller Gain for On/Off Operation (25% Iron). 275

(114) ISQERR and ISQMAN for the Thee Stages vs. the Filter Time Constant for On/Off Operation (25% Iron). 276

(115) ISQERR and ISQMAN for the Three Stages vs. the Lower Limit on the Input Constraint for On/Off Operation (25% Iron). 278

(116) ISQERR and ISQMAN for the Three Stages vs. the Upper Limit on the Input Constraint for On/Off Operation (25% Iron). 279

(117) Simulated Closed-Loop Performances for a -0.20 psi Setpoint Change in the Top Stage without Decoupling. 281

(118) Simulated Closed-Loop Performances for a -0.20 psi Setpoint Change in the Top Stage with Decoupling. 283

(119) Simulated Closed-Loop Performances for a -0.20 psi Setpoint Change in the Top Stage with Decoupling. 284

(120) Simulated Closed-Loop Performances for a 30 gm/second Step Change in the Feed Flow of Solids. 285

(121) Experimental Closed-Loop Performances for a -0.20 psi Setpoint Change in the Top Stage without Decoupling. 287

(122) Experimental Closed-Loop Performances for a -0.20 psi Setpoint Change in the Top Stage with Decoupling. 289

(123) Experimental Closed-Loop Performances for a -0.20 psi Setpoint Change in the Middle Stage with Decoupling. 291

(124) Experimental Closed-Loop Performances for a 30 gm/second Step Change in Feed Flow of Solids. 292

(125) Solids Flow Rate Through the Stage Valve vs. Average Current ("Leaking" Valve Operation; 25% Iron). 295

(126) ISQERR and ISQMAN for the Three Stages vs. the Controller Gain. 297

(127) ISQERR and ISQMAN for the Three Stages vs. the Filter Time Constant. 298

(128) ISQERR and ISQMAN for the Three Stages vs. the Upper Limit on the Input Constraint. 300

(129) ISQERR and ISQMAN for the Three Stages vs. the Lower Limit on the Input constraint. 301

(130) Simulated Closed-Loop Performances for a -0.20 psi Setpoint Change in the Top Stage without Decoupling (On/Off Operation; 25% Iron). 303

(131) Simulated Closed-Loop Performances for a -0.20 psi Setpoint Change in the Top Stage with Decoupling ("Leaking" Valve Operation; 25% Iron). 304

(132) Simulated Closed-Loop Performances for a -0.20 psi Setpoint Change in the Middle Stage with Decoupling (25% Iron). 306

(133) Simulated Closed-Loop Performances for a 30 gm/second Step Change in Feed Flow of Solids (On/off Operation; 25% Iron). 308

(134) Experimental Closed-Loop Performances for a Step Change in the Setpoint in the Top Stage without Decoupling ("Leaking" Valve Operation). 309

(135) Experimental Closed-Loop Performances for a Step Change in the Setpoint in the Top Stage with Decoupling ("Leaking" Valve Operation; 25% Iron). 311

(136) Experimental Closed-Loop Performances for a -0.20 psi Setpoint Change in the Middle Stage ("Leaking" Valve Operation; 25% Iron). 313

(137) Experimental Closed-Loop Performances for a 30 gm/second Step Change Feed Flow of Solids("Leaking" Valve Operation; 25% Iron). 314

(138) Plots Flow Rate out of the Stage vs. the Average Current for the ON/OFF and "Leaking" Valve Operations. 318

LIST OF APPENDICES FIGURES

Figure		Page
(A-1)	Three Channel 8-Bit Computer Interfaced Programmable Timer Block Diagram.	336
(A-2)	Timing Diagram of the Programmable Timer.	337
(A-2.1)	Schematic Diagram of the Current Controller Circuit Card.	342
(A-2.2)	Block Diagram of the Current Controller Circuit Card.	343
(A-2.3)	Front and Back Panels Layouts of the Current Controller Circuit Card.	344
(B-1.1.1)	Flow Regimes Associated with the Collar Valve of the Hopper.	351
(B-1.1.2)	Flow Rate vs. Fraction Open at Different Periods.	353
(B-1.2)	Calibration Curves for the Feed Flow Rates of Solids Containing 50% and 25% by Weight Iron.	356
(B-2.1)	Effect of the Position of the Screen on the Flow Rate of Solids Through the Collar Valve Without Another Screen at the End of the Tube.	359
(B-2.2)	Effect of the Position of the Screen on the Flow Rate of Solids Through the Collar Valve With Another Screen at the End of the Tube.	360
(B-3)	Effect of Solids Inventory in the Hopper on the Flow Rate of Solids Through the Collar Valve.	363
(C-1)	Size Distribution of Solids Containing 100% at Various Times.	365

(C-2) Size Distributions of the Solids Consisting of 50% by Weight Iron at Various Times. 366

(C-3) Size Distribution of the Solids Consisting of 25% by weight Iron at Various Times. 368

(D-1.1) Fast Sampling Frequency of the Pressure Drop Across the Stage. 376

(D-1.2) Comparison Between the Controller Signal and the Actual Signal. 378

(D-1.3) Pressure Drop Across the Stage at Different Slow Sampling Frequencies. 379

(D-2.2) Experimental Data and the Theoretical Model (Line) for the Frequency of the Pressure Drop Fluctuations. 384

(D-2.3) Experimental Data and Theoretical Model (Line) for the Amplitude of the Pressure Drop Fluctuations. 386

(D-3) Frequency and Amplitude of the Fluctuations vs. Average Pressure for 100% by Weight Iron and Batch Fluidization. 389

(D-4) Frequency and Amplitude of the Fluctuations vs. Average Pressure for 100% by Weight Iron in Solids and Continuous Solids Throughputs. T_C = 0.256 Seconds. 391

(D-5) The Effect of the Level of Current on Minimum Fluidization Velocities. 394

LIST OF TABLES

Table		Page
(1)	Average Fractions Open and Pressure Drops Across the Stage at Different Working Currents (100% Iron).	89
(2)	Regression Analysis Results for wP_{av} vs. H_s.	97
(3)	Amplitudes and Frequencies Data for 100%.	117
(4)	Amplitudes and Frequencies Data for 50%.	117
(5)	Amplitudes and Frequencies Data for 25%.	118
(6)	Coefficients for the Frequency`s Correlation.	122
(7)	Coefficients for the Amplitude's Correlation.	122
(8)	Results of the Segregations' Studies of the Solids Between the Two Regions for Recycled Feed of Solids.	264
(9)	Results of the Segregations' Studies of the Solids Between the Regions for Fresh Feed of Solids.	265

LIST OF APPENDICES TABLES

Table		Page
(A-1)	Connections to the Inputs of the Timer.	339
(C-1)	Size Distribution of Particles Containing 100% at Various Times.	369
(C-2)	Size Distribution of Particles Containing 50% Iron and 50% by Weight Sand at Various Times.	370
(C-3)	Size Distribution of Particles Containing 25% Iron and 75% by Weight Sand at Various Times.	371
(C-4)	Physical and Geometric Properties of Different Solids in Compositions.	374
(D-3)	Amplitude and Frequency Data Obtained from Spectral Analysis for Batch Fluidization.	388
(D-4)	Amplitude and Frequency Data Obtained from Spectral Analysis for Continuous Solids Throughputs and for T_C = 0.256.	392
(D-5)	Superficial Gas Velocities and the Corresponding Pressure Drops at Different Working Currents.	395

NOMENCLATURE

GREEK SYMBOLS:

ΔP_f	The Filtered Pressure Drop Signal.
ΔP	Pressure Drop Across the Stage.
ΔH	Enthalpy.
ΔP_i	Initial Pressure Drop Across the Stage (psi).
ε	Voidage of the Fixed Bed.
ε_f	The Voidage at the Fluidization Conditions.
ε_{mf}	Voidage at Minimum Fluidization Conditions.
ε_{pb}	Voidage of Closely Packed Bed.
μ	Gas Viscosity.
μ_{eff}	Effective Magnetic Permeability of the Material.
μ_o	Magnetic Permeability of a Vacuum.
θ_i	The Angle Between the Force Acting on a Certain Particle and the Horizontal.
δ	The Thickness of the Layer Close to the Grates.
ρ_g	Density of the Gas
ρ_s	Density of the Solids.

ENGLISH SYMBOLS:

a	Acceleration.
A_{cs}	The Cross-Sectional Area of the Bed.
A_f	Cross-Sectional Area Available for Solids Flow.
A_{fl}	The Amplitude of the Pressure Fluctuations.
$\mathbf{B}$	Magnetic Field Intensity.
d_p	Particle Diameter.
E	The Error Between the Setpoint and Measured Value.
f	The Fundamental Frequency of the Pressure Fluctuations.
FR	Fraction Open (t_{op}/T).
$F(r)$	Magnetic Force Pointing Radially Towards the Grate.
F_d	Drag Force.
F_g	Gravity force.
F_{HT}	Horizontal Component of the Magnetic Force.
F_m	Magnetic Force.
F_{pt1}, F_{pt2}	Tangential Forces to the Magnetic Flux Line.
FR_{outf}	The Final Value of the Fraction Open (Manipulated Variable).
FR_{outi}	The Initial Value of the Fraction Open (Manipulated Variable).
g	The Gravitational Acceleration.
G_{ci}	The Controller's Transfer Function of the ith Stage.
G_d	The Load Transfer Function.
G_f	The Filter Transfer Function.
G_p	The Process Transfer Function.

H	Magnetic Field Strength.
h	Bed Height.
h_f	The Height of the Bed at the Fluidization Conditions.
h_i	Initial Settled Height.
h_{mf}	The Height of the Bed at the Minimum Fluidization Velocity.
h_{pb}	The Height of a Closely Packed Bed.
h_s	Settled Height.
I_{av}	Average Current.
I_h	The Holding Current (No Solids Flow Through the Stage).
I_r	Release Current (Solids Flow Through the Stage is Large).
ISQERR	Integral Square Error of the Pressure Drop Across a Stage.
ISQMAN	Integral Square Error of the Manipulated Variable.
I_w	Working Current.
K_{ci}	The Controller's Gain of ith Stage.
M	The Magnetization of the Particle in a Magnetic Field.
M	Solids Holdup in the Stage.
M_1	Mass of Magnetic and Non-Magnetic Particles in the Region Close to the Valve.
M_2	Mass of Magnetic and Non-Magnetic Particles in the Fluidized Region.
m_i	Solids Flow Rate into the Stage.
m_o	Solids Flow Rate out of the Stage.
M_s	Solids Holdup on a Stage.

M_T	Total Weight of Solids in the Hold System.
N	Dial Setting on the Counter for All Channels.
n	Number of Magnetic Particles.
P_{av}	Average Pressure Drop ($\equiv \Delta P_{av}$).
r	The Radial Distance from the Grate.
R^2	Correlation Coefficient.
T	The Period of the Timer ($t_{cl} + t_{op}$).
T_c	The Sampling Time of the Controller
$\bar{t}$	Resident Time of the Solids in a Stage.
t_{cl}	The Time During Which the Current Flowing Through the Grates Should Be Maximum.
T_{dn}	The Power Supply Response Time to Go from I_w to zero.
τ_f	Filter Time Constant.
t_{op}	The Time During Which the Current Flowing Through the Grate Should Be Zero.
$t_{op\ max}$	The Maximum Time During Which the Current is Zero.
$t_{op\ min}$	The Minimum Time During Which the Current is Zero.
T_{samp}	Sampling Time.
$\bar{t}_T$	Total Pass Time.
T_{up}	The Power Supply Response Time to Go from Zero to I_w.
U_g	Superficial Gas Velocity.
U_s	Superficial Solids Velocity.
U_{ss}	Steady State Value for the Controller.
V_p	Particle Volume.

W_1	Average Weight Fraction of Iron in the Region Close to the Grates.
W_2	Average Weight Fraction of Iron in the Fluidized Region.
ΔW_i	Weight Fraction of Iron in i^{th} Stage.
W_{IA}	Actual Weight Fraction of Iron in the Solids.
W_{IM}	Measured Weight Fraction of Iron in the Solids.
W_m	Weight Fraction of the Main Bed.

MODELING AND CONTROL STUDIES OF A MAGNETICALLY STAGED FLUIDIZED BED

I. INTRODUCTION AND PREVIOUS WORK

I.1 Introduction

Figure (1) shows the behavior of a bed of fine particles when a gas is passed upward through it. At low flow rate,the gas passes through the void space between the stationary particles. As the flow rate increases the bed expands until a certain limit is reached which represents the minimum fluidization conditions. The portion of the curve up to the minimum fluidization conditions (AB) represents the fixed bed. At the minimum fluidization conditions the particles are suspended in the gas. In the case of a gas-solid system, when the flow of the gas increases, large bubbles of gas begin to form and channeling of gas is observed. The portion (CD) of the curve represents this region which is called the bubbling region. The pressure drop increases only slightly in this region and is often considered constant. The bed is called a dense phase fluidized bed. When the flow rate of gas is increased above the terminal velocity of the particles, we have a lean phase fluidized bed with pneumatic transport of solids (curve DE).

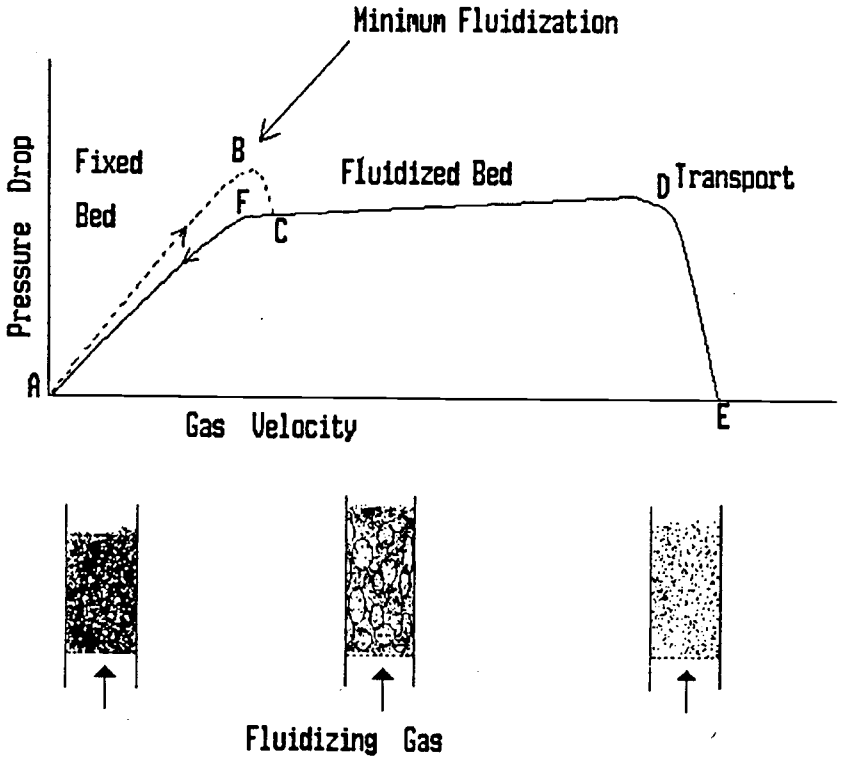

Figure (1) Typical Pressure Drop Versus Gas Velocity Curve.

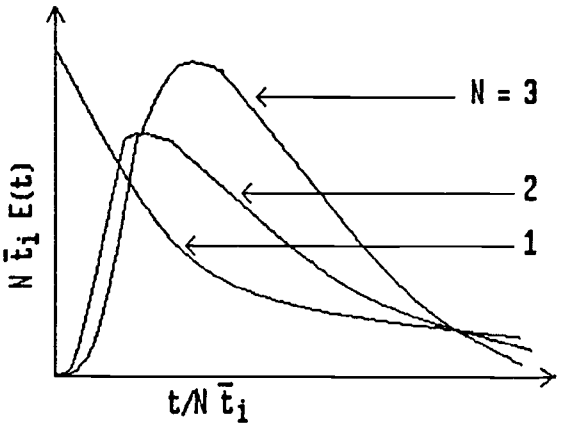

Figure (2) Exit Age Distribution for Single Stage and Multistage Fluidized Beds.

when the velocity of the gas is decreased from a high value corresponding to that at point C to zero, the pressure drop follows a different path (CFA) than the one when the velocity is increased (ABC).

The quality of fluidization is determined by many factors such as the properties of the solids and gasses, bed geometry, gas flow rate and type of gas distributor.

I.1.1 Single Stage Fluidized Bed

A single stage fluidized bed is still the most common type used in industry [26, 27, 67, 105, 122, 133]. Their applications cover a large range of processes such as heat transfer processes, mass transfer processes, gas-solids reactions and others. Some of the main features of the fluidized bed can be summarized as follows: [67, 133]

- Temperature uniformity
- Good contacting between the gas and solids phases
- More efficient and economical for processing large quantities of solids than other methods.

In spite of these attractive features, some problems may appear when a single stage fluidized bed is used. They are summarized as follows: [10, 39, 67, 78, 81, 85, 94, 95, 105]

1) Efficiency is sometimes too low. One example is the heating of solids with high temperature gas where the gases leave the bed still at high temperature, which is a waste of energy.
2) The solids product is not uniform. The sketch of the RTD of the single fluidized bed (Figure 2) confirms this. The RTD is not uniform, so, a single stage bed is not efficient for high conversion in the case of chemical reactions.
3) Bypassing, and channeling have been reported to be a problem in the single stage fluidized bed.

These unattractive features of single stage operations are the motivation for multistage contacting.

I.1.2 Multistage Fluidized Bed

I.1.2.1 Advantages

1) Higher efficiency. [10, 67, 81, 85, 93, 94, 122] This results in reducing the axial mixing of phases which prevents the formation and growth of large bubbles.
2) Reduced bypassing and channeling. [10, 67]
3) Higher capacity. The capacity has been

reported to be several times larger than that of a single stage. [67, 122]

4) Improved RTDs of one, two and three stages are shown in figure (2). As the number of stages increases, the RTD approaches a normal distribution and the product is more uniform. So, a piston flow condition is approached by using a multistage fluidized bed [39, 66, 81, 85, 90, 93, 94, 95, 122].

I.1.2.2 Applications

Multistage fluidized bed adsorbers with activated carbon have been used for the recovery of organic vapors as part of air pollution control (87). A five stage fluidized bed adsorber, 38 feet in diameter was built to recover carbon disulfide from a lean air mixture (.1%) [102]. Avery and Tracy [6] described a similar unit 40 feet in diameter used for the recovery of acetone. They reported [6, 102] that some other solvents such as ethanol, ethyl acetate and mixed hydrocarbons are being recovered by the same method. A multistage fluidized bed was developed to pyrolyze volatile bituminous coals. A multistage fluidized bed was used to activate charcoal [93]. They have been used to collect particles from effluent gases [89]. The efficiency of collection is reported to be very high [89]. Extensive

studies on producing iron and steel from fines of high grade ores by direct reduction with hydrogen using fluidized beds were conducted by Hydro Research Corporation and Bethlehem Steel Company. They found that the optimum conditions, where the conversion and utilization of hydrogen is high, can be achieved by using semi-batch operation with a multistage fluidized bed of ID = 1.7 m and a height of 29 m [67, 102]. Armco used a two stage bed for direct reduction of iron with hydrogen [67]. Multistage fluidized beds are used to recycle heat in the following endothermic reaction in a calcination process [67].

$$CaCO_3 \xrightarrow{1000^oC} CaO + CO_2 \qquad \Delta H = 42.9 \text{ cal/mole} \qquad (1)$$

Both solids and gas leave at 1000°C. The New England Lime Company built the first of these reactors in New England in 1949. A three stage fluidized calcination system with a 5 meter diameter reactor was built by Dorr-Oliver Engineers for upgrading phosphate rock.

Russian engineers built [67] a multistage fluidized bed to efficiently recover heat of the product gases from a rotary kiln treating cement clinkers. Because of their thermal efficiency, multistage fluidized beds are used in a variety of drying applications, such as salt drying [49, 67] and the drying of wet polymer particles [67, 117]. Those

examples show only some of the applications of multistage fluidized bed.

There are two kinds of commercial multistage fluidized beds:

1) Without downcomers, but with perforated plates (Figure 3a).
2) With downcomers and perforated plates (Figure 3b).

Both systems have been studied by many investigators. The studies were done in the areas of design [35, 53, 85, 90, 104, 105, 122], RTD behavior, [67, 85, 94, 95, 114, 122], number of stages necessary for certain operations [67, 91, 94, 95], dynamics of the bed [15, 18, 30, 35, 39, 67, 85, 87, 90, 104, 105, 122], and the effect of many other variables on the behavior of the bed.

I.1.2.3 Operational Problems

However, some problems with multistage fluidized beds have been reported [67, 87, 90, 94, 95].

1) Stability problems. It is reported [35, 67, 95, 104, 105, 122] that sometimes the whole solids suspension collapses to the bottom of the bed. The down flow of solids is hard to control [35] or maintain stable [81, 67]. This will cause poor

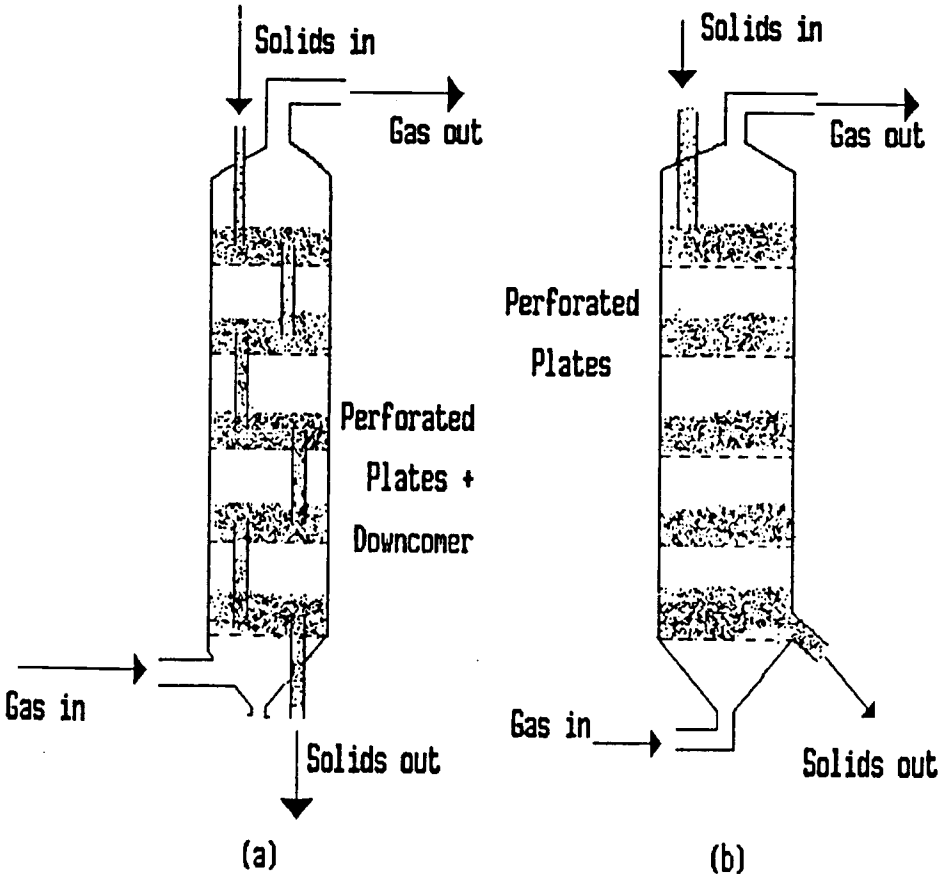

Figure (3) Conventional Multistage Fluidized Bed:
a) Downcomers and Perforated Plates
b) With Perforated Plates Only

distribution of solids among the stages and is the most serious problem in a multistage fluidized bed.

2) Plugging of either the downcomer or the holes in the perforated plates with solids [67, 105, 122].

3) Typical problems of a single stage fluidized bed still exist in the multistage fluidized bed such as shortcircuiting, channeling, bypassing, dead regions and growth of large bubbles [85, 90, 93, 94, 104, 122]

4) The pressure drop across several perforated plates (with or without the downcomer) and the pressure drops cross each bed may contribute to a large pressure drop across the bed and high compression costs. [67, 122]

Some of the problems stated previously can be reduced or eliminated by the use of magnetism either to stabilize the bed in the case of a single fluidized bed or to use it in a more reliable operating distributor-downcomer for the multistaged fluidized bed. Such a distributor-downcomer is the subject of this thesis.

I.2 Previous Work

Previous relevant research can be divided into two main categories. The first is the use of magnetic phenomena for stabilization of a fixed bed of particles. The particles are frozen in place through the use of magnetic field while the gas flows through the voidage homogeneously. These kinds of beds are called magnetically stabilized beds (MSB). The application of magnetic phenomena in other fields like magnetic separators, zeroxing, etc. is similar to this category.

The second category involves the use of the magnetic phenomena to control the flow of particles in a continuous process and the design of the distributors and the downcomers in a multistage fluidized bed. This thesis treats problems of the second category. Previous work in both categories that has influenced this thesis is briefly reviewed in this chapter.

I.2.1 Use of Magnetic Field for Stabilization

The theory of using the magnetic field to stabilize a bed of partially magnetic particles has been studied by many investigators [1, 3, 4 22, 31, 56, 72, 98, 99, 100, 101, 107, 108, 111, 134]

I.2.1.1 Stabilization Diagram

Figure (4) shows a characteristic stabilization diagram. The line which separates the region of bubbling bed and stabilized bed represents the velocity required for minimum fluidization at different field strengths.

In the stabilized region the particles are frozen in place by the action of a magnetic field. As the gas velocity increases the bed expands until the minimum fluidization velocity is reached, after which bubbles begin to appear.

This kind of stabilization is achieved by placing the conductor, which carries the current, around the bed. Different designs exist for the conductor but the most common one is the coil design. Researchers have reported [31, 56, 134] that screens placed inside the bed and below the coil improve the performance and reduce the current needed.

I.2.1.2 Applications

There are three uses for this kind of arrangement:

1) To prevent fluidization by suppressing the bubbles and eliminating turbulence [72, 98, 99, 100]. The particles are held in place by the magnetic field

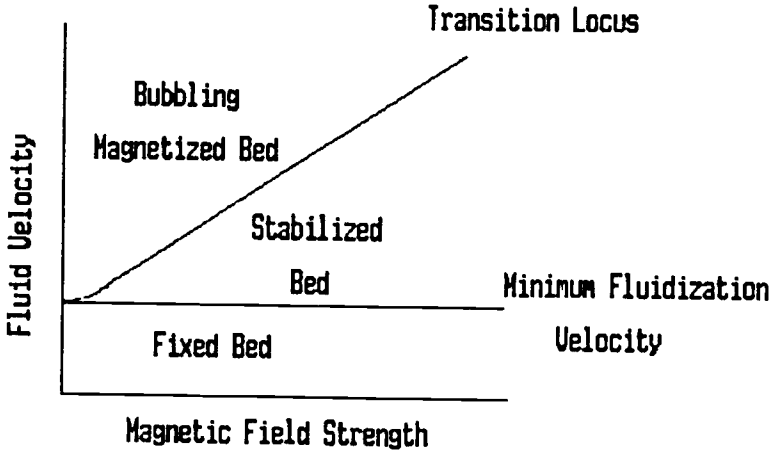

Figure (4) Magnetic Stabilization Diagram.

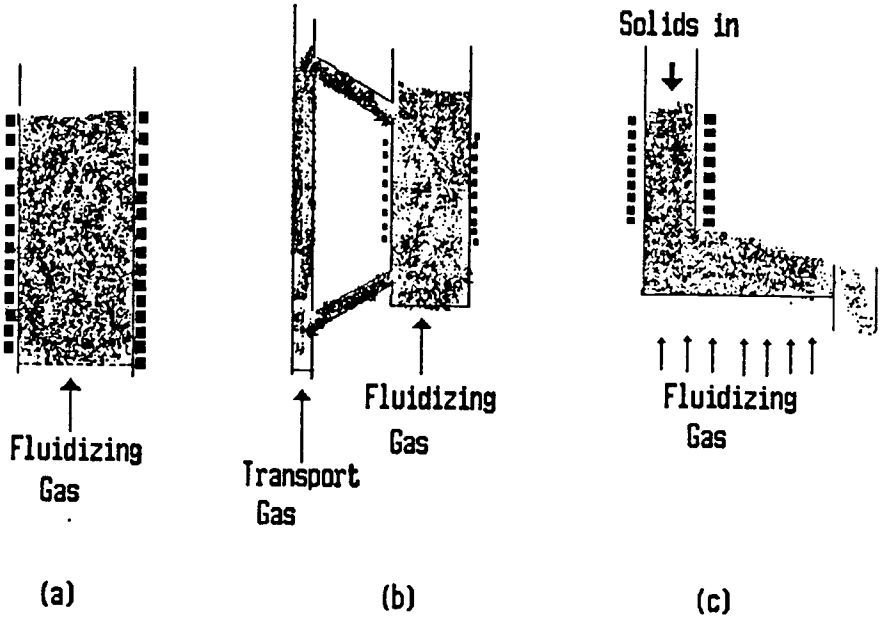

Figure (5) Magnetic Stabilized Beds
a) A No Solids Flow Magnetic Stabilized Beds
b) With Downflow of Solids
c) With Crossflow of Solids

within a stabilized region. The different kinds of operations are shown in figure (5). Continuous downflow [21, 108] as well as crossflow [107, 108] of particles in continuous operations have been reported. The flow rate in either case is controlled by the strength of the magnetic field.

2) To stabilize a fluidized bed. This kind of stabilization promotes uniform fluidization [1, 3, 15, 22, 98, 100, 101, 107, 108]. This is accomplished by designing the magnetic field to prevent the growth of large bubbles [24]. Again, the crossflow magnetically stabilized fluidized bed [22, 107, 108] and the usual downflow magnetically stabilized fluidized bed [3, 21, 98, 100, 101, 108, etc.] have been used in continuous operation. A reliable control of solids flow can be achieved by using the coil design as was the case in controlling the feed of solids into the bed in this work.

The applications of these kinds of beds are reported in the following areas:

- Gas- solid catalytic reactions where good contact is needed [72].
- Chromatography [107, 21].

- The collection of solid particles from gases [1, 72].

Some investigators [4, 72, 134, etc.] reported that beds which consist of mixtures of magnetic and non-magnetic particles can be stabilized in the same way as those which contain only magnetic particles.

I.2.1.3 Associated Problems

However, there are some problems with using magnetic fields with fluidized beds:

1) The air velocities needed for minimum fluidization are higher than those without the presence of a magnetic field. This means high pumping energy cost.
2) In the magnetic stabilized bed, (MSB), the lack of bubbles causes a lack of temperature homogeneity.
3) The controllability of solids flow rate through a large duct is not good, especially with a mixture of magnetic and non-magnetic particles.
4) The existence of a layer of magnetic particles at the inside wall of the bed is another drawback. It results in poor contact between this layer and the gas. This affects the product uniformity.

I.2.1.4 Operation with Mixtures

Some investigators [4, 72, 134, etc.] reported that beds which consist of mixtures of magnetic and non-magnetic particles can be stabilized in the same way as those which contain only magnetic particles. The different methods of making the mixture will be described later in this chapter. According to item (4) above, most of the magnetic particles are attracted to the wall of the bed, thus non-magnetic particles will flow through the center. This makes the control of the solids flow rate through the tube difficult. High current levels (more energy) must then be used to achieve better control over the flow rate of solids. The other problems associated with magnetic solids are still present when operating with the mixtures.

I.2.2 Use of Magnetic Field for Regulating the Flow Rate of Solids and the Design of Distributor and Downcomer

The difficulties which arise in using a magnetic field to stabilize a fluidized bed motivated the building of a bed where an internal grid (instead of the wall) is subjected to the magnetic field [55, 56, 57, 130]. In this design, parallel conductors (the grate) are placed horizontally in the bed as described in chapter two and shown in figure (9).

A copper screen placed under the conductor was found to reduce the current needed for the operation.

This design utilizes the magnetic forces between particles, and serves as:

1) A gas and solids distributor for the bed. The stage valve consists of parallel copper tubes as well as a copper screen placed below it which helps in supporting the solids as well as in distributing them to the next stage. The layer of solids which is attracted to the copper tubes because of the magnetic field, serves as an excellent distributor for the gas entering the bed. The porous nature of the layer helps introduce very small bubbles to the main bed which results in better fluidization.
2) A regulator for the flow of solids down from the stage. This is done by controlling the on-time (on/off operation) or the level ("leaking" valve operation) of the current flowing through the conductor as shown in figure (6).

The design parameters involved can be listed as follows:

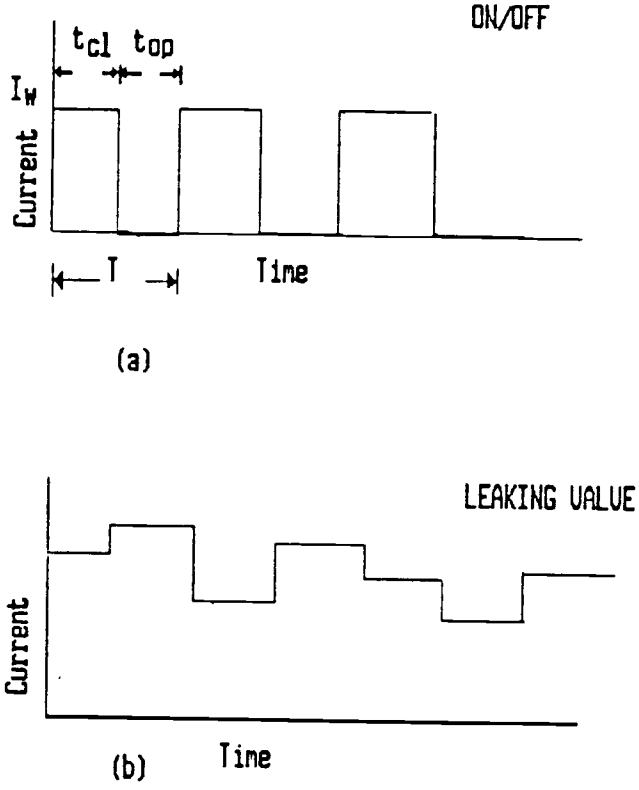

Figure (6) Shape of the Current Signal Flowing Through the Grates:

a) Current Signal Associated with ON/OFF Operation.

b) Current Signal Associated with "Leaking" Valve Operation.

1) Screen aperture
2) Grate spacing
3) Diameter of the grate
4) The distance at which the screen is placed under the grate

Extensive studies have been made on these design parameters [55, 57, 130], but were done for non-fluidization conditions. All previous studies are based on an on/off operation of the bed (pulsed flow). In this type of operation, the current is either equal to zero or equal to the working current (I_W). The corresponding flow of solids is either zero or maximum. In the presence of fluidization, drag forces increase significantly and the holding and release currents are different from those without fluidization. However, previous studies serve as a guide in this work. The design parameters were chosen so that a maximum flow rate, of about 1.6 kg/sec of iron, through the bed could be achieved.

Other studies have been done [55, 57, 130] in non-fluidization conditions on the following:

1) Effect of height of solids in the stage on the mass flow of solids through the bed at fixed on/off-times of the current.

2) Effect of off-time of the current on the mass flux of solids when on-time is held constant.

3) Effect of on-time of current on the mass flux of solids when off-time is held constant.

4) The effect of working current on the mass flux of solids through the bed.

5) The effect of the weight fraction of magnetics in the solids on both the current needed for operation and the mass flux of solid through the bed.

Values of the holding current (I_h) and release current (I_r) have been reported [55, 57, 130] for a non-fluidizing bed which are different than those in the case of fluidization.

The effect of superficial gas velocity on mass flux through the grates is studied [57], where the time the current is "on" is equal to one second and the time the current is "off" is equal to 0.5 second. The effect of the current level on the mass flux of solids through the bed is studied at the same fixed on/off-time of the current and at constant gas velocity of 84 mm/sec. Both of these studies are done at high working currents. These experiments showed the following:

1) The mass flux of the solids decreased linearly with the increase in gas velocity until the minimum fluidization conditions are reached.

After that the mass flux stays almost constant over the range of velocities studied.

2) The mass flux decreases when the current increases. However, the study does not show a strong relation between them.

There is not much said about how the experiments were conducted. The study of geometrical parameters of the bed is the part which was useful to this study . Completely different approaches from those done before in the operation of the bed are undertaken in this thesis.

The multistage operation using the grate valve design is completely new in all its operational aspects. The exact design parameters chosen, the magnetic forces involved and the operation of the bed will be described in subsequent chapters.

I.2.2.1 Applications

The applications of the magnetically staged fluidized bed can include all those mentioned previously. The only requirement is that the solids must contain some magnetic material. Such mixtures can be prepared in two ways:

1) Mix known quantities of magnetic and non-magnetic particles. This is the way the mixtures were prepared in this thesis.

2) Make composite particles where the magnetic material is imbedded in the non-magnetic particles. The cost of making composite particles is high, so these are not used widely.

Depending on the magnetic constituent of the solids to be treated, there are two possible kinds of applications:

1) The particles to be treated in the fluidized bed are themselves partially magnetic. Examples of these are iron ores and some kinds of coal where the percentage of iron is high. Alloys which contain some magnetic metals are another kind of particle that can be used in this kind of operation. A direct application is in gas-solid reactions where the catalyst is iron or another magnetic material. The process of the reduction of iron oxides by hydrogen is most suitably done in this kind of bed. Filtration of particulates from gases is another type of process that can be done. The particulates can be filtered by the beds in different stages and the percentage of particulates in the exit gas is low. The operation can be continuous with the magnetic particles separated from the non-magnetic particles and recycled to the top of the multistage fluidized bed.

2) The particles to be treated are non-magnetic. In this case some magnetic particles have to be added to the non-magnetic particles for satisfactory operation of the bed. The multistage fluidized bed could thus be used in all the applications listed previously for the conventional fluidized bed.

I.2.2.2 Advantages

The following is a summary of the additional advantages of the magnetically multistaged fluidized bed:

1) The flow rates of solids between the stages are completely controllable. The operation of the distributor-downcomer for the fluidized bed is reliable. The layer of solids attracted to the grates serves as an excellent distributor for the gas.
2) No gross bubbling or gas bypassing occurs. There is no dead region of solids detected during the operation of the bed.
3) There are no moving parts required for the operation of this kind of bed.

I.2.3 Organization of the Thesis

Chapter II covers the description of the equipment used in this work. The detailed design of the multistage fluidized bed is discussed in that chapter.

Chapter III covers the open-loop studies done to understand the basic dynamics of the process.

Modeling solids flow rate through the stage valve, comparisons between the "leaking" and on/off operation and the effect of solids holdup in the stage on the solids flow rate out of the stage are discussed in chapter IV.

Chapter V contains detailed studies of the fluctuations of the pressure drop across a stage valve.

The closed-loop control simulations and experiments are covered in chapters VI, VII, and VIII, for solids with iron weight fractions of 100%, 50%, and 25% respectively. Each chapter covers the results for both "leaking" and on/off operations. Chapter VI introduces the overall model for the process and discussion of simulation methods. Detailed studies on the composition of solids on a stage versus time and the related studies are covered in chapter VIII. Chapter IX contains recommendation for future work as well as conclusions of the present study.

II. EXPERIMENTAL EQUIPMENT

The equipment used in this project, shown in figure (7), can be classified as follows:

- The Multistaged Fluidized System
- The Interface

II.1 The Multistage Fluidized System

The multistage fluidized system is the physical process part of the equipment. It consists of the following parts:

- Three stage fluidized bed
- Feed system
- Recycling system

II.1.1 The Three Stage Fluidized Bed

Each stage consists of the following parts:

1) The Bed Chamber:

The bed chamber consists of two Plexiglass tubes of different lengths with the same diameter of 15 cm, as shown in figure (8). The lower tube is 5 cm

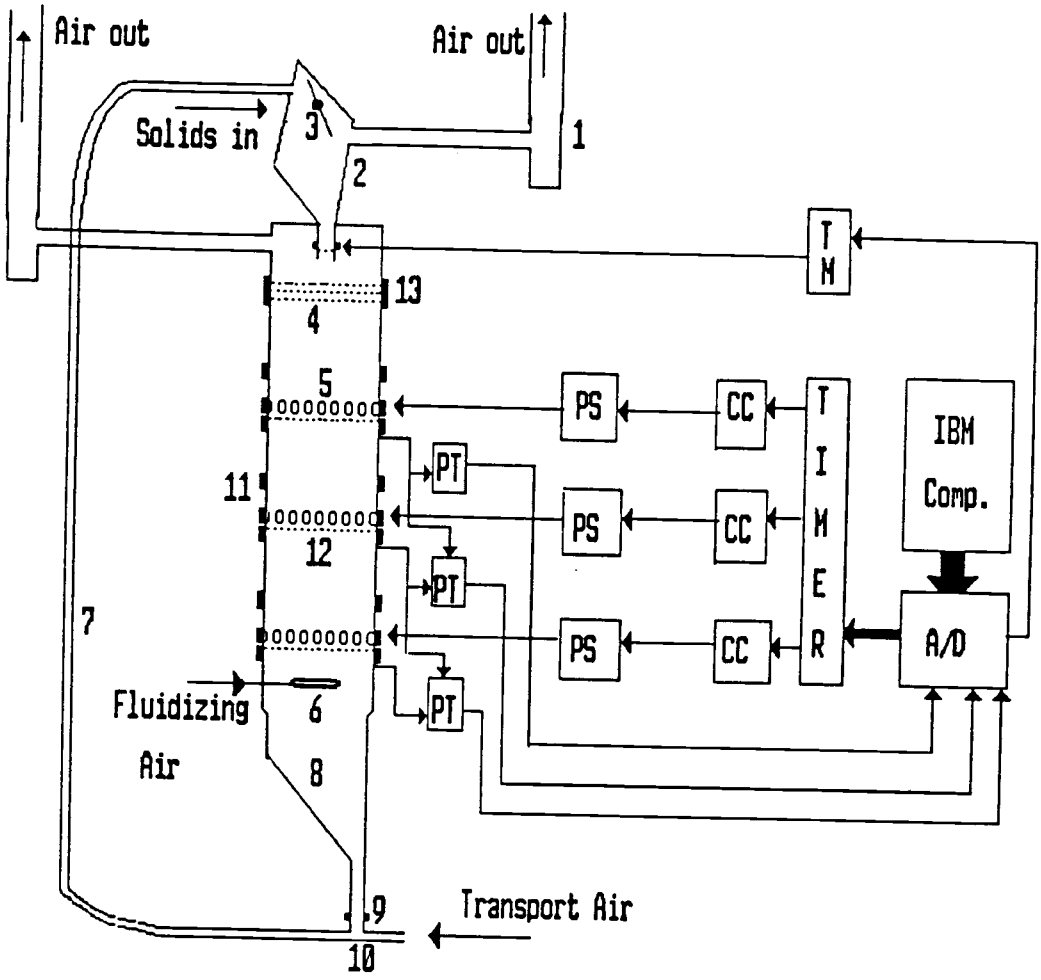

Figure (7) The Complete Layout of the Experimental Equipment:
1) Tube for Ventilation 2) Hopper 3) Metallic Sheet for Solids Impact 4) Three Screens with 1.27 cm Spacing 5) The Grates 6) Gas Distributor 7) The Recycle Tube 8) Plenum Chamber for Solids Holdup 9) Copper Coil 10) Recycle System 11) The Square Plexiglass Sheets 12) A Copper Screen 13) Four Plexiglass Square Sheets to Hold the Screens.

high and is embedded at both ends into a square sheet of plexiglass (22.2 cm in side length and 1.27 cm in thickness) with a circular opening of 15 cm drilled in the middle. The lower end has the grids embedded in it and the upper end is connected to the other tube through the square sheet. The height of the upper part of the chamber is 28 cm. Also, it is embedded at both ends into similar square plexiglass sheets as is the lower tube. The total length of the lower part including the square ends is 7.62 cm and that of the upper part is 30.48 cm. The square ends are designed for flexibility in changing the height of the upper part while the lower part's height is kept constant. The square ends have four small holes in the corners to connect the tubes to the other parts of the bed by means of screws. The pressure and sampling taps are also shown in figure (8).

2) Magnetic Valves:

Figure (9) shows the details of the stage valve. Each magnetic valve consists of a current carrying copper tube (6.5 mm I.D.). This tube is embedded in the square end of the lower tube. The tube is run across the square plexiglass sheet length then bent and run again across the square sheet.

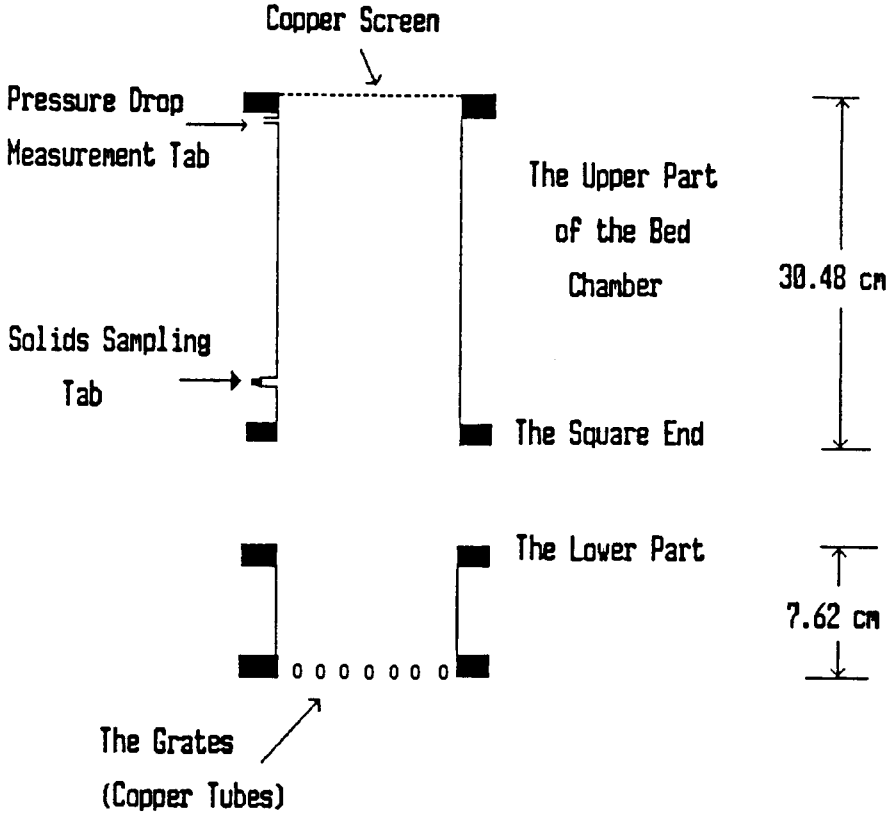

Figure (8) Details of the Bed Chamber.

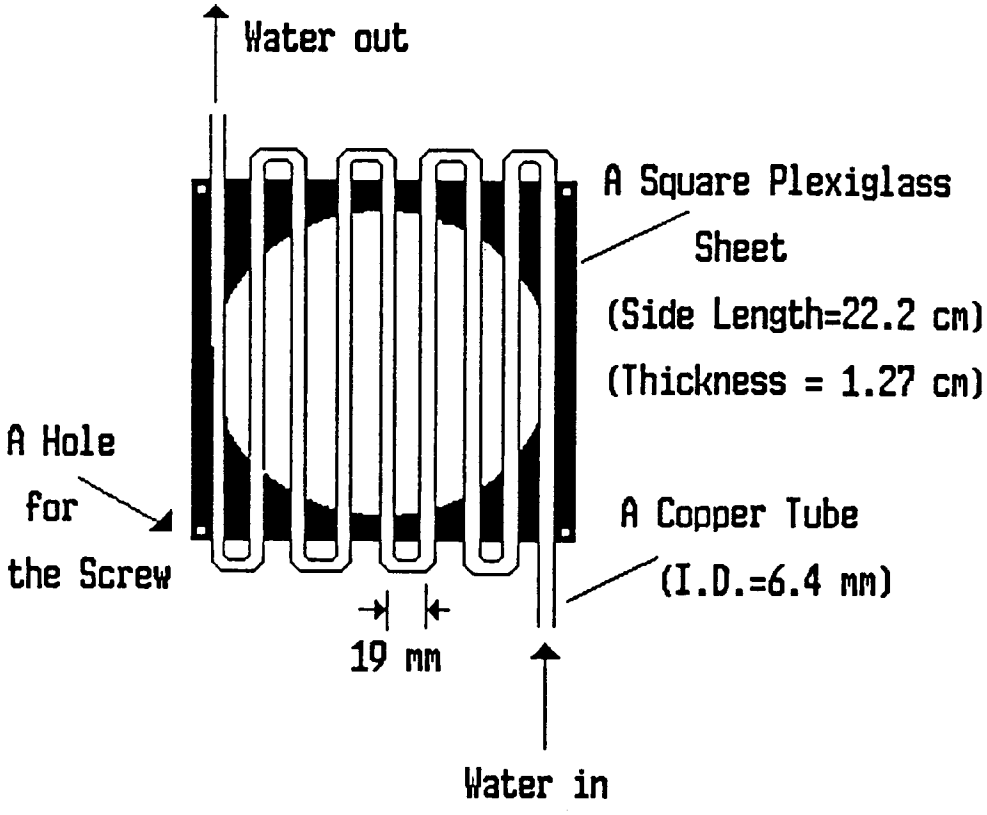

Figure (9) The Stage Valve with the Grates.

This is continued until the cross section of the circular opening in the square sheet is covered with tubes with 19.00 mm center-to-center spacing. A circular copper screen 16.25 cm in diameter with an aperture of 6.4 mm is placed under the copper tubes. A 3 mm thick circular rubber seal with an inside diameter of 15.0 cm and an outside diameter of 16.25 cm is placed between the copper tubes and the screen to prevent direct contact between them.

II.1.2 Feed System

Figure (10) shows the various parts of the hopper. The body is made from 38 cm I.D. PVC cut at an angle of 23° and capped. The outlet is put at the longest point, so that when the pipe is vertical all the solids can be drained. A pipe of 3.5 cm I.D. and 10 cm in length is attached to the bottom of the hopper. The tube is attached so that when it is in the vertical position the rest of the hopper makes an angle of 73° with the horizontal. This is to ensure a rapid draining of solids from the hopper. A 500-turn copper coil is positioned around the tube at a distance of 7 cm below the hopper. A 3.8 cm I.D. screen with 6.4 mm square apertures is placed inside the tube directly under the coil to help reduce the current needed to control the flow rate of solids. Three 16.5 cm I.D. screens with 6.4 mm apertures

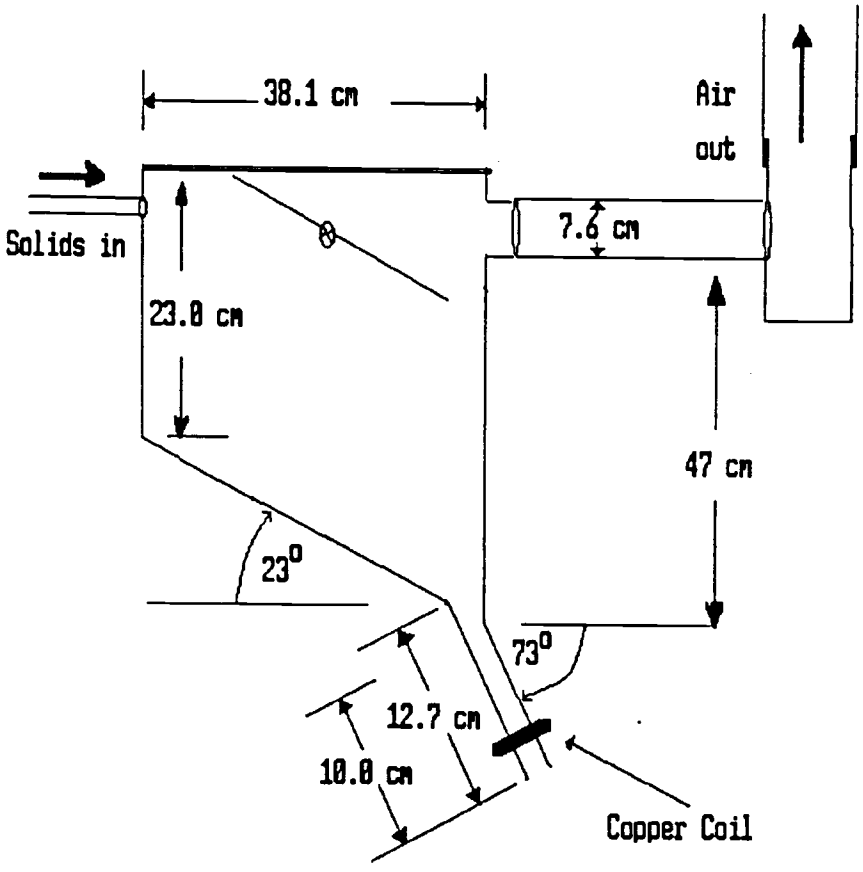

Figure (10) The Hopper.

are placed 4.45 cm below the discharge end of the tube and 1.27 cm apart to help disperse the solids entering the top stage.

II.1.3 The Recycle Solids System

The recycle solids system consists of a SCH 80 TEE tube as shown in figure (11). The solids flow through the vertical opening via a 3.8 cm I.D. tube which is connected permanently to a larger tube of 13.75 cm I.D. which is cut at an angle of 45 degrees to allow complete draining of solids. This tube is connected to the plenum chamber via a rubber seal 7.6 cm high. A 500-turn copper coil is positioned around the bottom part of the 3.8 cm tube to allow the control of the solids level in the plenum chamber. The current in the coil is manipulated by an on/off controller which uses an optical device embedded in the wall of the plenum chamber to regulate solids level.

Figure (12) shows the air supply system. Air supplied by a Sutorbilt 3 HV-B blower is first passed through a water cooled 1-2 shell and tube heat exchanger. Part of it is then passed through a 1.9 cm PVC tube fitted with a nozzle end. The tube is positioned in the center of one of the horizontal openings of the "T" tube. This part of the air is used to recirculate solids through the other horizontal

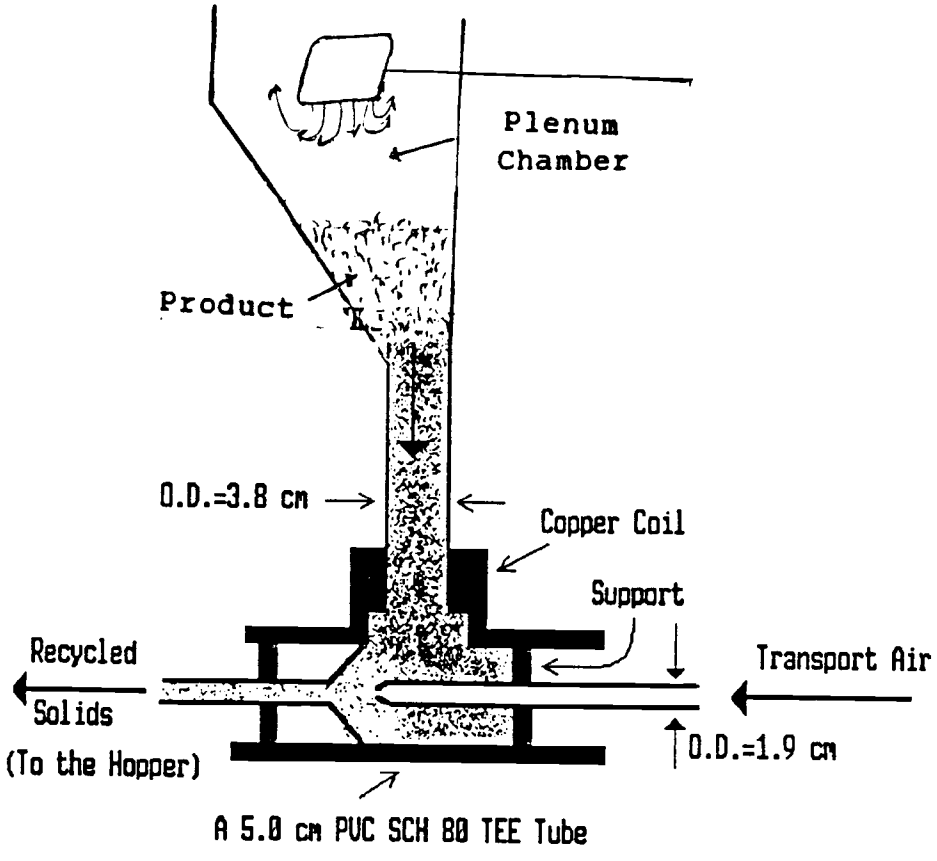

Figure (11) The Recycle System.

opening with 1.9 cm I.D. duct positioned in the center which leads to the hopper 2.83 meters above.

The other part of the air is fed via one of the two calibrated rotameters to the plenum chamber located below the bottom stage. The air is introduced to the chamber via a square gas distributor pointing downward.

The air exits through two openings located on the top part of the walls of the multistage fluidized bed and the hopper respectively, as shown in figure (7). The air is then vented to the atmosphere via a system which recovers elutriated solids.

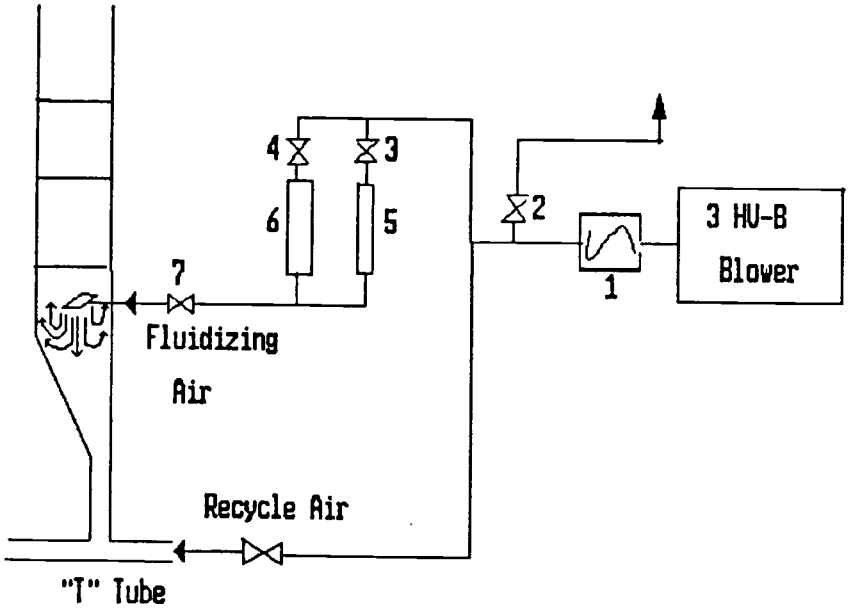

1) Heat Exchanger 2) Bypass Valve 3) Valve to the Lower Range Flowmeter (5) 4) Valve to the Larger Range Flowmeter (6) 7) Valve to Air Distributor 8) Valve to Recycling System.

Figure (12) Air Supply System

II.2 The Interface

Figure (13) shows the main components of the interface. The interface consists of the following parts:

1) IBM data acquisition and control adapter
2) The timer
3) The current control card
4) The differential pressure cell

II.2.1 IBM Data Acquisition and Control Adapter:

The data acquisition and control adapter manual gives all of the information required for the operation of the board. A 640 KB IBM-XT computer was used for data acquisition and control. The second and third parts of the interface are described briefly.

II.2.2 The Timer:

The timer has three channels for inputs and three corresponding outputs. The input to each channel is an eight digit binary number from the computer representing the time during which the current flowing through the stage valve is "off". The corresponding output for each channel is a square wave with the high voltage limit equal to 5.0

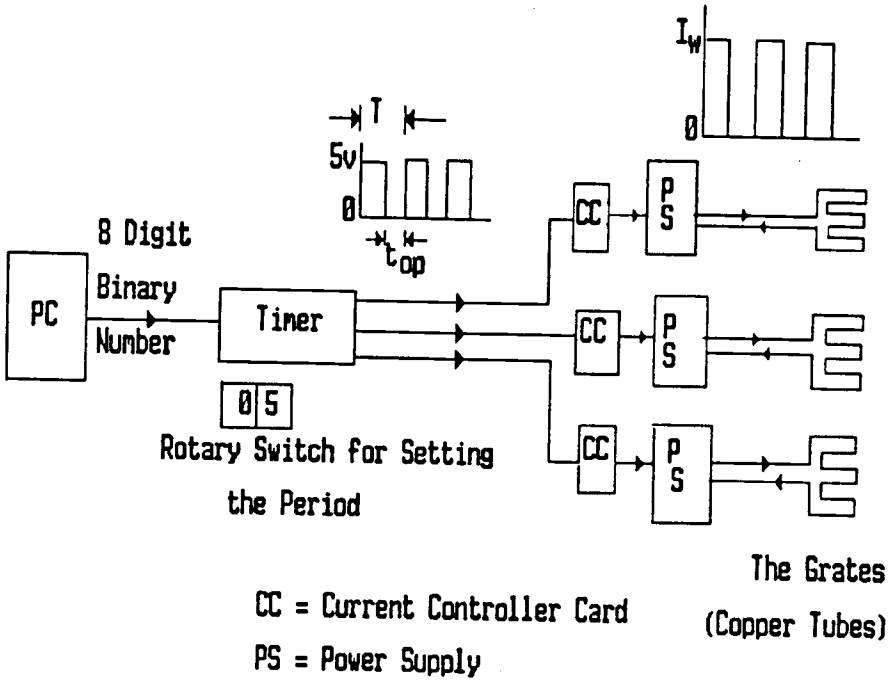

Figure (13) The Main Components of the Interface.

volts and the lower limit equal to 0 volt. These levels result in the current through a grate to be "on" or "off" respectively. The period of oscillation (T) can be adjusted by setting a rotary switch located in the front of the timer. This switch runs from 1 to 99 with each count representing 25.6 milliseconds.

The eight digit binary number for each stage valve is sent consequently to the corresponding channel by sending an additional three signals via the computer to the timer, two of which are for the channel selection. The status (high or low) of both signals specify the channel to be selected. The third signal has to be set low then high at the beginning and the end of transmission of the binary number to the chosen channel. The output will continue to oscillate until another number is sent again. The conversions involved can be summarized as follows:

N = dial setting on the counter for all channels

$T = N * 25.6$ msec

$T = \text{period} = t_{op} + t_{cl}$

where t_{op} = control action or manipulated variable

$0 \leq t_{op} \leq T$

$$t_{cl} = T - t_{op}$$

$$t_{op} = \frac{T - \text{binary number}}{255} \quad (\text{ms}) \qquad (1)$$

A similar timer with a single channel was used to control the flow rate of solids from the feed hopper to the bed.

Both of these timers can be operated manually or automatically. The choice is made via a three position switch located on the timer. The voltage output of the timer is zero or 5 volts for the switch at the upper or the lower position respectively. The middle position is for automatic operation. More information about the two timers is supplied in appendix (A-1).

II.2.3 <u>The Current Control Circuit Card</u>:

Three auxiliary circuit cards were used in this project to control currents. They are used either to control the current level of the power supply, ("leaking" valve), or to send a square signal to the power supply. In the second case, the current output of the power supply is either on or off depending on the high and the low limits of the square wave.

Each circuit card has two input channels and one output. The first input channel is connected to the timer.

When the input to the channel is less than 2 volts, the output of the card is 5 volts, which corresponds to no current output by the power supply. When the input is greater than 2, the output of the card is zero volts, which corresponds to a current output of the power supply equal to the working current, I_W. This input channel was used for the on/off operation.

The second input channel is used to vary the current level of the power supply when in the automatic mode. The input to the channel is a continuous voltage supplied by the computer. The output current of the power supply varies linearly between 0 and 200 amps as the input voltage to the second input channel changes between 0 and 5 volts. This channel is used for "leaking" valve operation.

Alternatively, the output current can be adjusted manually by a potentiometer located in the front panel. A three position switch on the front panel allows a choice of operating the card in manual or automatic mode. More information about the circuit card is given in appendix (A-3).

II.2.4 <u>The Differential Pressure Cell:</u>

The cell converts the pressure drop across the stage linearly to a continuous voltage. More details about the cell will be presented in appendix (A-4).

III. DYNAMIC BEHAVIOR OF THE PROCESS

The following studies were done on the process without feedback control in order to study the dynamic behavior of the process.

III.1 Definitions of Input/Output Disturbances

Input Load Disturbance:

An input disturbance can be made by introducing a step change in the flow rate of solids out of the hopper to the top stage. The step change in the solids flow rate can be achieved by increasing or decreasing the fraction open of period during which the current flowing through the coil is off via the computer and a timer. Increasing the fraction open results in increasing the flow rate (positive step change) while decreasing the fraction open results in decreasing the flow rate (negative step change).

Output Disturbance:

The output disturbance results from changing the fraction open of period during which the current flowing through the copper grates is off. Increasing

the fraction open results in an increase in the flow rate of solids through the stage valve while decreasing the fraction open results in a decrease in the flow of solids through the stage valve. The change in the fraction open can be achieved through the use of a computer, the three channels, current control circuit, and the power supply.

III.2 Operation at Different Values of Fraction Open with Constant Period

Procedures:

1) The bed is first filled with solids to the desired height, h_i.
2) The data acquisition program is then started. After about half a minute, the gas flow rate is started. The process is run for a minute with no solids flow through the stage.
3) The flow rate of the solids (m_i) into the stage is set to 62.14 gm/sec and the outlet flow rate is started by the program. The process is run for another eight minutes.

This experiment is repeated for different values of the fraction open of period the valve is open, (different solids flow rates out of the valve), and for different initial solids inventory in the bed.

For the same initial bed inventory of solids, the pressure drop either increased, decreased, or remained nearly constant, depending on the fraction open of period the valve was open. Figures (14) and (15) show the histories of pressure drop in the bed for different initial heights of 5 inches and 7 inches respectively. The frequency of pressure fluctuations are less in figure (14), h_i = 7"

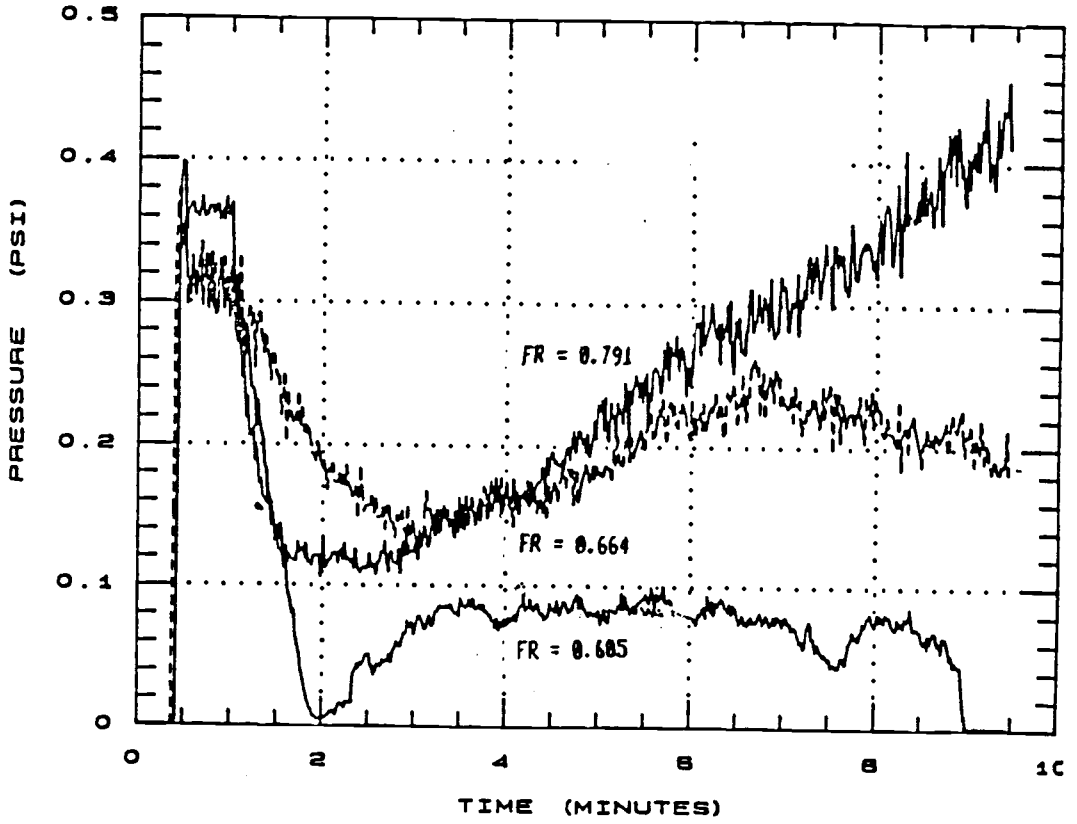

Figure (14) Histories of Pressure Drop Across the Bed at Different Fractions open.
m_i = 62.14 gm/sec and h_i = 5"

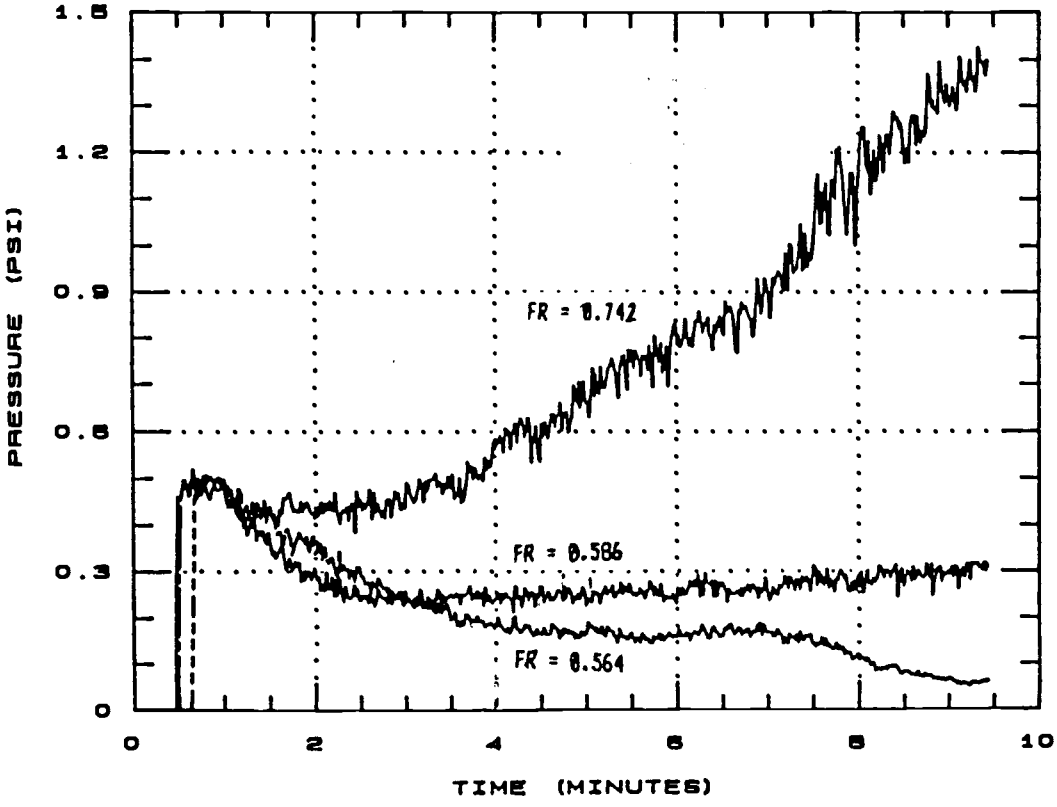

Figure (15) Histories of Pressure Drop Across the Bed at Different Fractions open.
m_i = 62.17 gm/sec and h_i = 7"

, than in figure (15), h_i = 5", and the change of pressure with time is more gradual.

The other conclusion that can be drawn from this experiment is that the value, if there is any, of the fraction open required for steady state is near the value of 0.549. This result is used later in other open-loop studies.

Other experiments were done under different conditions than those above and for longer durations. Figure (16) shows pressure drop histories when the flow rate of solids into the bed was 80. gm/sec and the fraction open of the valve was equal to 0.588. The process appears to have multiple steady states and the plots for two similar experiments done under the same measured conditions can be completely different.

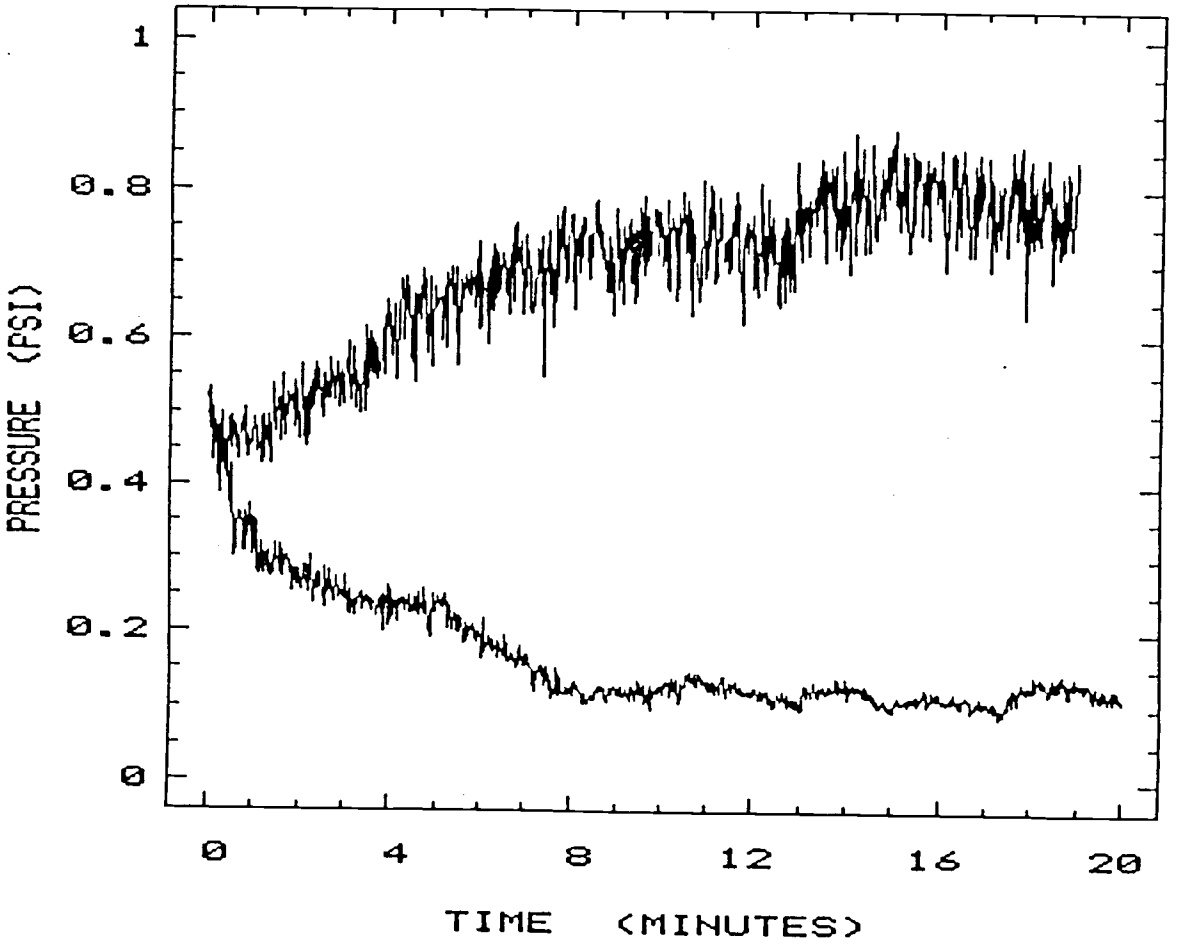

Figure (16) Histories of Pressure Drop Across the Bed.
m_i = 80 gm/sec and Fraction Open = 0.588

III.3 Step Change in the Flow Rate of Solids into the Bed

Procedures:

1) The bed is filled with solids to the desired level. The gas flow rate is started. The process is operated for five minutes.
2) The flow rate of the solids in and out of the valve is started from within the data acquisition program and the process is run for about one minute. The fraction open of the stage valve is chosen as 0.549 so that the the input and output flow rates are approximately equal .
3) The step change in the flow rate of solids into the bed is implemented by the program by changing FR_{in} and the operation is continued for two minutes.

Figure (17) shows the plots of pressure drop with time. As expected, the height increases when ΔFR_{in} is negative, but decreases when ΔFR_{in} is positive, where :

$$\Delta FR_{in} = \text{new } FR_{in} - \text{old } FR_{in}$$

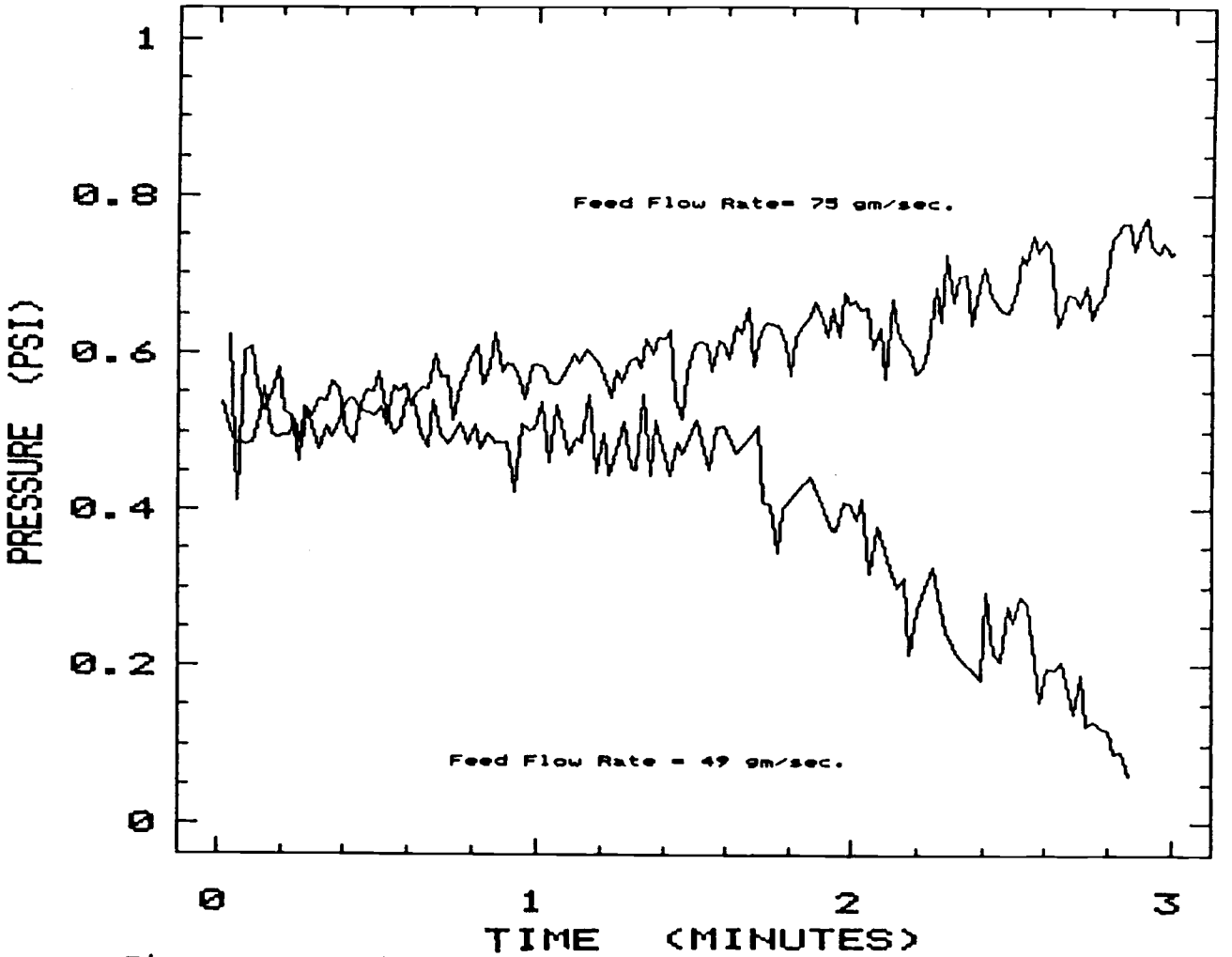

Figure (17) Histories of Pressure Across the Bed for a Step Change of the Flow of Solids into the Bed. Δm_{in} = 12.56 gm/sec; Fraction Open of Stage = 0.549

III.4 Step Change in the Flow Rate Out of the Bed

Procedures:

1) The stage is filled with the solids to the desired level. Then the gas flow rate is started for fluidization.
2) The flow of solids into and out of the stage is started by the data acquisition program. The corresponding fraction of the period the valve is open is again 0.549, because then the bed height dosn't change rapidly during the time of operation.
3) A step change in the fraction of period open (FR_{out}) of the stage valve is introduced and the bed is operated for 4.65 minutes. The flow rate of solids into the bed is kept constant at 62.14 gm/second. The steps are made in two directions:

   A. Step up where

   $\Delta FR_{out} > 0$

   B. Step down where

   $\Delta FR_{out} < 0$

   where ΔFR_{out} = new FR_{out} - old FR_{out}

The results are shown in figure (18). As expected, the pressure drop in the bed increases with time for the negative step in FR_{out}, while it decreases for the positive step.

III.5 Conclusions

The following conclusions can be drawn from the previous experiments:

1) The process is not open-loop stable in the bounded input/bounded output sense. The use of some kind of controller to stabilize it is necessary for its operation.
2) Initially, with no solids flow, the pressure drop is nearly constant across the fluidized bed. When the flow rate of solids starts, the operation is greatly disturbed. This can be observed from the large decrease in the pressure drop with time. The pressure then increases, decreases, or doesn't change that much with time.
3) The rate of change of the pressure in the bed is the same for positive or negative steps in the flow rate of solids through the stage valve as long as the pressure drop across the bed is greater than 0.20 psi. When the pressure drop

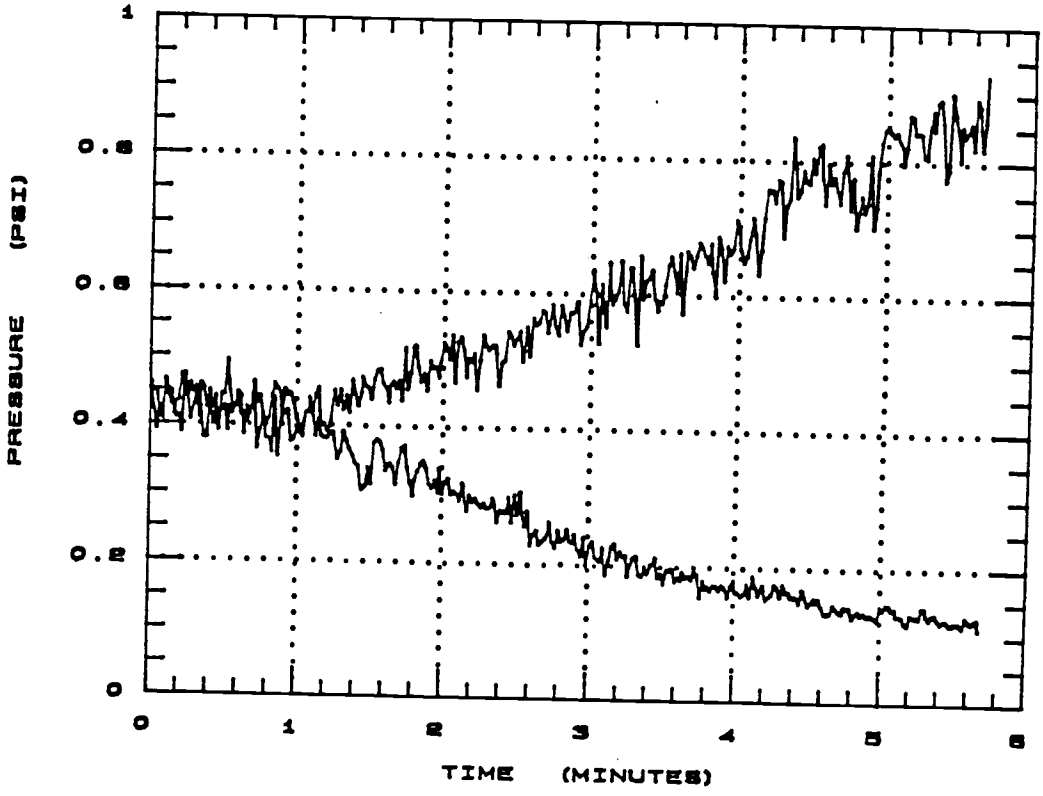

Figure (18) Histories of the Pressure Drop Across the Bed. m_i = 62.17 gm/sec; ΔFR_{out} = -.078 for Upper Curve; Step at t = 1.0 Minutes; wFR_{out} = 0.078 for the Lower Curve.

is below 0.2 psi, its behavior with time is not predictable. It might increase again, decrease or stay constant for some time and then change.

4) The rate of change of pressure with time is more gradual when the pressure drop is greater than 0.2 psi. For longer operations of the process more than one steady state can occur.

5) For the same measured operating conditions the pressure drop may follow different trajectories.

6) The previous discussion of the experimental results indicates strongly that the process has integrator type characteristics. The modelling and simulations in the subsequent chapters will be based on this conclusion.

The pressure fluctuations associated with the fluidized bed as well as the change of the geometry of the solids layer attracted to the conductor will affect the flow of air as well as the flow of solids from the stage. These effects may be responsible for conclusions (2) and (5).

IV. MODELING SOLIDS FLOW THROUGH A STAGE

IV.1 Simple Fundamental Model

The following simple fundamental material balance around a single stage can be made:

accumulation = input - output

$$\frac{d\Delta M}{dt} = m_i - m_o \qquad (2)$$

M = solids holdup in the stage

m_i = solids flow rate into the stage

m_o = solids flow rate out of the stage

Which can be expressed also as:

$$\frac{d\Delta P}{dt} = \frac{g}{A_{cs}\ g_c}\ (m_i - m_o) \qquad (3)$$

where $A_{cs} * \Delta P = M * \frac{g}{g_c}$

ΔP = pressure drop across the stage

The following two cases depend on m_i and m_o:

case 1:

$$m_i = m_o, \text{ then } \frac{d\Delta P}{dt} = 0 \quad \text{then } \Delta P = \text{constant}$$

Using the initial condition at $t = 0$, $\Delta P = \Delta P_i$ gives

$$\Delta P(t) = \Delta P_i, \text{ a constant} \tag{4}$$

Case 2:

$$m_i \neq m_o, \text{ then } \frac{d\Delta P}{dt} = (m_i - m_o)\frac{g}{g_c}$$

by integration it becomes:

$$\Delta P = \frac{g}{g_c}(m_i - m_o) + \Delta P_i \tag{5}$$

a) $m_i > m_o$ the pressure will increase with time without bound or until physical constraints are active.

b) $m_i < m_o$ the pressure will decrease with time until it reaches zero.

Figure (19) is a sketch of the pressure behavior for these two cases and shows the characteristics of an integrator type process. This model is an idealized model and does not take into account the pressure fluctuations or spatial dependence of some variables involved. However, it does describe the behavior of the bed as a function of the solid flow rate in and out of the bed.

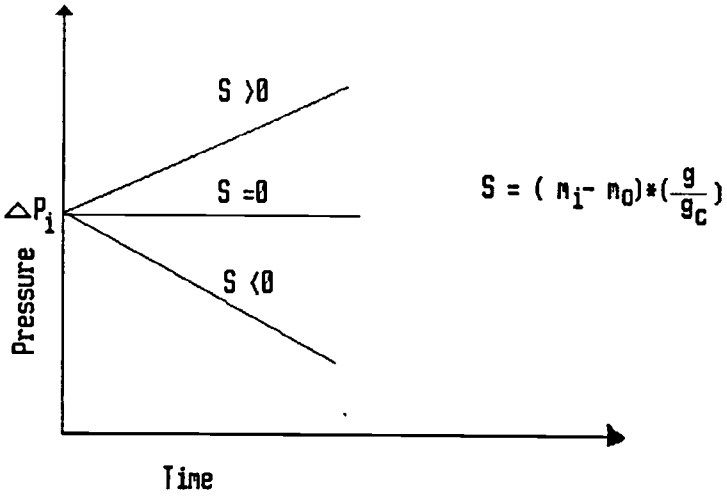

Figure (19) Behavior of the Pressure Drop for Different Values of m_i and m_o in the Simple Fundamental Model.

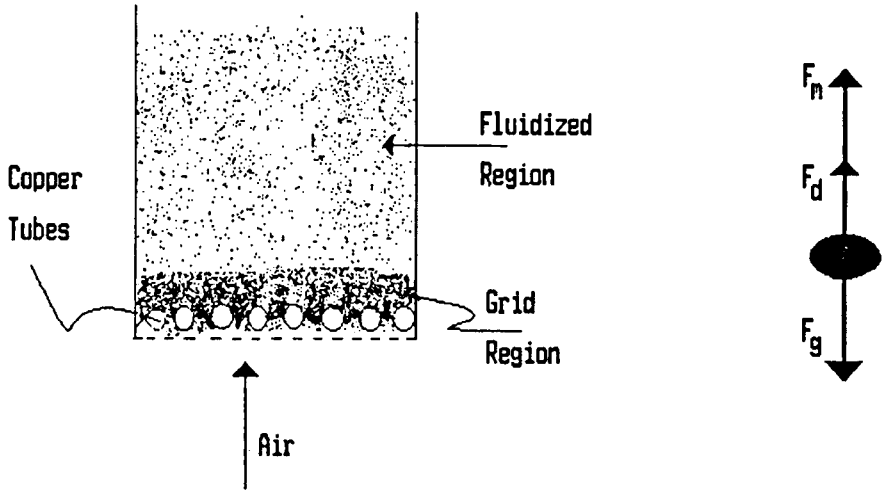

Figure (20) Regions Inside the Stage Valve.

IV.2 Regions Inside the Stage Valve

The bed chamber is divided into two regions, figure (20), in order to model the flow rate of solids out of a stage.

IV.2.1 Fluidized Region

This region is so far away from the magnetic grid that the effects of magnetic forces are negligible. This region is fluidized by air so that the solids are well-mixed in this region. Making a force balance around this region gives: [67]

$$\left[\begin{array}{l}\text{drag force by upward}\\ \text{moving gas}\end{array}\right] = \left[\text{weight of particles}\right]$$

$$\Delta P * A_{cs} = F_g = (1 - \epsilon_f)\ [(\rho_s - \rho_g)]\ \left(\frac{g}{g_c}\right) * A_{cs} * h$$

$$\frac{\Delta P}{h_f} = (1 - \epsilon_f)\ [(\rho_s - \rho_g)]\ \left(\frac{g}{g_c}\right) \qquad (6)$$

where: ϵ_f = the voidage at the fluidization conditions

ρ_s = density of the solids

ρ_g = density of the gas

A_{sc} = the cross-sectional area of the bed

h_f = the height of the bed at the fluidization conditions

IV.2.2 The Non-Fluidized Region Close to the Magnetic Valve Grid

In this region, magnetic forces play an important role. Because of these forces the solids are not fluidized and behave like a moving packed bed. This region is similar to a magnetically stabilized bed in which an external coil around a tube with the current flowing through it is used to hold a certain amount of solids in place. To fluidize this region, the air velocity has to be much higher than the velocity range used in this thesis. In this region the Ergun equation, which is used to describe the drag forces in packed beds, can be used. It is assumed that the average width of this region is constant and equal to δ. A force balance can be made around this region. The sheer stress between the solids and the bed wall is negligible due to the small thickness of the layer δ.

$$F_g + F_d + F_m = 0 \tag{7}$$

F_m = The total force resulting from the magnetic field acting on the region

F_d = drag forces resulting from upward flow of air

F_g = combined gravity forces on all particles in the region

The drag and gravity forces are well known, so only a brief discussion of them will be given.

IV.2.2.1 Gravity Forces (F_g)

$$F_g = \begin{bmatrix}\text{volume of the} \\ \text{fixed region}\end{bmatrix} * \begin{bmatrix}\text{fraction of space} \\ \text{occupied by the} \\ \text{solids}\end{bmatrix} * \begin{bmatrix}\text{specific weight} \\ \text{of solids}\end{bmatrix}$$

$$F_g = (A_{cs} * \delta) * (1 - \epsilon) * \rho_s \qquad (8)$$

Some solids also exist between the grates and between the grates and the copper screen. It is assumed that the volume of the solids between the bottom of the grate and the copper screen is equal to the volume of the grates. Therefore, δ is measured from the bottom of the grate.

IV.2.2.2 The Drag Forces

The Ergun equation [67]which describes the drag force for a fixed bed has the following form:

$$F_d = \frac{150\ (1 - \epsilon)^2\ \mu\ \Delta U\ \delta}{g_c\ \epsilon^3\ d_p^2\ \rho_g} + \frac{1.75\ (1 - \epsilon)\ (\Delta U)^2\ \delta}{g_c\ \epsilon^3\ d_p} \qquad (9)$$

In our case the solid particles are small and the ranges of the flow rates of solids and gas are not high. Therefore, the second term of equation (9) can be omitted without appreciable error. For counter-current gas-solid flow:

$$\Delta U = U_g - (-U_s)$$

$$\Delta U = U_g + U_s$$

U_g = magnitude of time averaged superficial velocity of the gas > 0

U_s = magnitude of time averaged superficial velocity of the solids > 0

μ = gas viscosity

ϵ = voidage of layer close to the grid

d_p = particle diameter

Equation (9) can be reduced to the following form:

$$F_d = \frac{150\ (1 - \epsilon)^2\ \mu\ \ U * \delta}{g_c\ \epsilon^3\ d_p^2\ \rho_g} \qquad (10)$$

Let $$A_1 = \frac{150\ (1 - \epsilon)^2\ \mu * \delta}{g_c * \epsilon^3 * d_p^2 * \rho_g}$$

Equation (10) can then be written as:

$$F_d = A_1 U_g + A_1 U_s$$

since: $m_o = \rho_s A_f U_s$, $\quad U_s = \dfrac{m_o}{\rho_s A_f}$

Therefore, the final equation has the following form:

$$F_d = A_1 U_g + \frac{A_1}{A_f \rho_s} m_o \tag{11}$$

Where: m_o = time averaged solids flow rate out of the stage valve

A_f = maximum cross-sectional area available for solids flow

A_f = A_{cs} - (the projected area of the grates)

IV.2.2.3 Magnetic Forces

The magnetic forces acting within this region are not well understood and many different theories to explain them have been suggested since 1819, when Oersted first observed the magnetic effect of a current carrying wire. The following explanation is extracted from many theories published in books and papers and is believed to describe the magnetic stage adequately. [3, 4, 11, 12, 20, 22, 32, 33, 34, 38, 40, 48, 52, 54, 55, 57, 60, 62, 64, 65, 86, 98, 100, 101, 107, 108, 111, 112, 115, 131, 133].

When ferromagnetic particles are placed in a magnetic field they become magnets and can be considered as a collection of elementary dipoles. As a result they align along the field flux lines and form chains. The length and

stiffness of the chains depend upon the magnetic forces on the particles. A rigorous calculation of the magnetic forces from the solution of the Maxwell equations that describe forces involved in magnetic fields is extremely complex and may be impossible for a complicated boundary like a chain of particles. If more than one chain are involved, which is the case in magnetic valves, the exact solution of Maxwell's equation is impossible. The following description and analysis are therefore greatly simplified.

The magnetic flux lines around the conductor carrying the current are curved (figure 21-a). The following assumptions are made:

- The field is uniform (if it is not uniform the chains will not form in the first place).
- The particles are spherical in shape. Each particle will have its own magnetic field since it is considered to be a magnet.

For simplification, only magnetic forces between neighboring particles aligning in a single chain will be considered. The interparticle forces (figure 21-b) can be resolved into two kinds of forces:

1) Tangential forces to the magnetic flux lines
2) Normal forces to the magnetic flux lines

The tangential forces (F_{pt1}, F_{pt2}, in figure 21-c) on any single particle are assumed to cancel. The normal force (F(r) in figure 21-c) points always towards the region of higher flux density which is towards the conductor. This force can be resolved into horizontal and vertical component with respect to the stage valve. As will be discussed later, the horizontal forces are used for regulating the flow rate of solids flowing through the valve. The vertical component will point either downward or upwards depending on the position of the particle with respect to the conductor. In the lower half of the conductor, it helps hold the solids in place while in the upper half, it helps attract the magnetic solids to the conductor. It is observed during the operation that the particles do not form perfect chains. Instead, they form clumps which follow the magnetic lines.

The intensity and flux of the magnetic field increase as the conductor is approached. Therefore, the vertical and horizontal forces follow the same behavior. The variation of the magnetic field within a particle diameter is assumed to be negligible.

The flux lines of the magnetic field around the copper tubes (the grates) are represented in Figure (22-a).

In the case of the stage valve, the magnetic material is introduced to one side of the grates carrying the current.

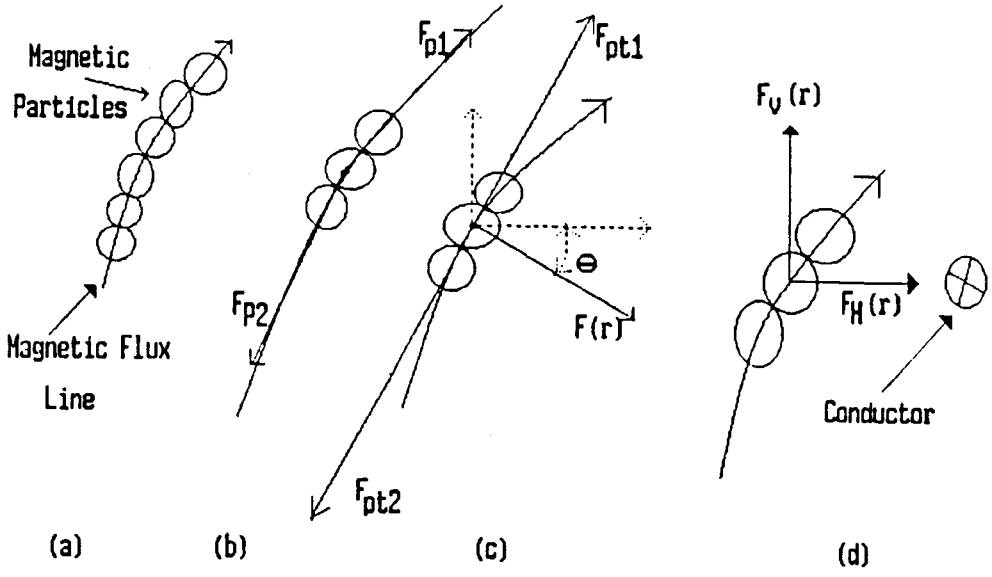

Figure (21) Orientation of the Magnetic Particles in the Magnetic Field and the Various Forces Involved.

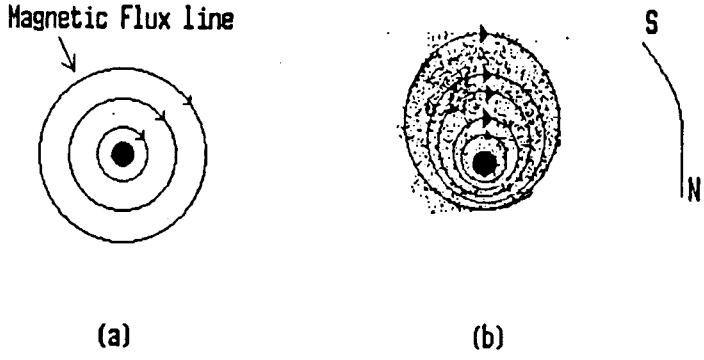

Figure (22) Magnetic Field Flux Lines Around the Copper Tubes:
a) Without the Presence of Magnetic Material
b) With the Presence of the Magnetic Materials.

Generally the introduction of magnetic material increases the magnetic flux intensity by a factor μ_r, where μ_r is the material magnetic permeability. This is a result of the magnetization of the particles which produces an additional current called an amperian current. The overall current is thus increased to an effective value called I_{eff}. The result of this is a stronger and larger region of magnetic flux on the side of the grate containing magnetic material. A sketch of the magnetic flux lines in the presence of magnetic material is shown in Figure (22-b).

IV.2.2.3.1 Derivation of the Magnetic Force Equation

The general expression of the magnetic force on a particle F_m in vacuo is given by :

$$F_m = \tfrac{1}{2} \int \Delta M * H \, dV_p \qquad (12)$$

where M is the magnetization of the particle in a magnetic field of strength H and dV_p = differential particle volume.

For a particle in a medium, neither the magnetization of the particle nor that of the medium is large compared to H. The direction considered to be important is the radial direction pointing towards the conductor, figure (21). The variation of the field across the particle is also assumed to be negligible. Thus equation (12) reduces to:

$$F(r) = \frac{V_p}{2} M(r) \left[\frac{-dH(r)}{dr} \right] \quad (13)$$

$$M(r) = \frac{B(r)}{\mu_o} - H \quad \text{(ampere/meter)} \quad (14)$$

$$B(r) = \mu_{eff} * H \quad (\text{Web/m}^2) \quad (15)$$

$F(r) \equiv$ magnetic force pointing radially towards the grate

μ_o = magnetic permeability of a vacuum (Web/amp m)

r = the distance from the grate (m)

$\mu_{eff} \equiv$ effective permeability at that particular field strength. Figure (24) shows the plots of B versus H and a procedure to calculate μ_{eff}. For high H, as is the case in this work, μ_{eff} is inversely proportional to H which results in a constant B.

Therefore:

$$\frac{B}{\mu_o} = K_m$$

Equation (13) can then be rewritten in the following form:

$$F(r) = (K_m - H) \frac{V_p}{2} \left[\frac{dH(r)}{dr} \right] \quad (16)$$

The field strength H at a distance (r) away from a straight line conductor carrying a current (I) is given by:

$$H = \frac{I}{2\pi r} \quad (17)$$

$$\frac{dH}{dr} = \frac{I}{2\pi r^2}$$

So the equation becomes:

$$F(r) = -\frac{V_p}{2}\left[K_m - \frac{I}{2\pi r}\right] * \left[-\frac{I}{2\pi r^2}\right]$$

$$F(r) = -\frac{V_p}{8\pi^2 r^3}(K^* - I)\ I \qquad (18)$$

where $K^* = 2\pi r k_m$

It was noted previously that it is the horizontal component of this force that is effective in blocking the flow channel of the bed due to friction between the facing particles. There are many of those forces (as many as the number of particles). The effective combined resultant force can be approximated as :

$$F_{HT} = \frac{1}{8\pi^2}(K^* - I) * \sum_{i=1}^{n} V_{pi} \frac{\cos \theta i}{r^3 i}$$

where: F_{HT} ≡ the total horizontal component of the magnetic force in the non-fluidiized region

n ≡ number of particles in the non-fluidized region

θ_i is the angle an individual particle makes with a horizontal plane and r_i is the distance which separates an individual particle and the conductor. The resultant

friction force between the particles is assumed to be proportional to F_{HT}. The following equation represents the final expression for the resultant force which is due to magnetic field.

$$F_m = K\ F_{HT} = \frac{1}{8\pi^2}\ (K^* - I) * \sum_{i=1}^{n} V_{pi}\ \frac{\cos \theta i}{r^3 i}$$

Further, it is assumed that the overall orientation and position of the particles with respect to the conductor is constant so that:

$$K_1 = \sum_{i=1}^{n} \bar{V}_{pi}\ \frac{\cos \theta i}{r^3 i} \tag{20}$$

Also, it is assumed that $V_{pi} = V_p$ = constant so that:

$$F_m = \frac{\bar{V}_p\ K_2}{8\pi^2}\ (K^* - I) \tag{21}$$

where: $K_2 = K1 * K$

IV.2.2.4 <u>Ferromagnetic Material Hysteresis</u>

The magnetization curve for ferromagnetic materials exhibits hysteresis behavior. A typical curve is shown in figure 23. The curve (oa) shows that as H increases, B also increases. The path can be reversed up to point L, after

which the path is not reversible. When H decreases from its value, which corresponds to point a, the curve (ac) is followed. (oc) represents the residual magnetization in the material and indicates the possibility to create a permanent magnet, which is called remanence. The area closed by the region (oab) represents the total absorbed energy while the area (cab) represents the restored energy. The difference between them, which is the area (oac), represents lost energy. To demagnetize the material a negative field equal to (od) must be applied to the material. Because of the curve symmetry around the x-axis, half (negative B) of the curve is the same but opposite in sign to that of the first half. Since we are using DC current, only the plot in the first quadrant is of importance to us which is shown in figure (24). [20, 112, 33]

When H is less than that at point (a), the effective material permeability, μ_{eff}, in equation (15), is constant and equal to the slope of the tangential line to the curve at the point of inflection. For H greater than that at point (a), B is essentially constant, but μ_{eff} is variable and equal to the slope of the line connecting the origin to the point at which the μ_{eff} value is desired. In this region μ_{eff} is inversely proportional to H.

The residual magnetism actually improves the response of the valve. When the valve opens in the on/off operation,

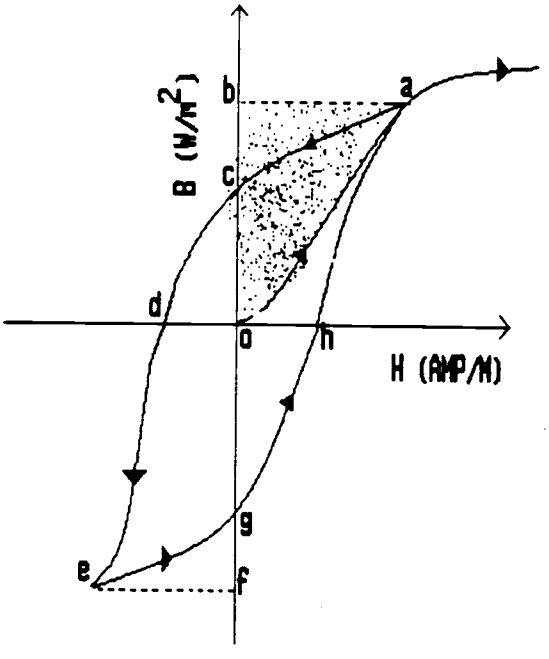

Figure (23) Typical Curve of Magnetization Curve for Ferromagnetic Materials with Hysteresis.

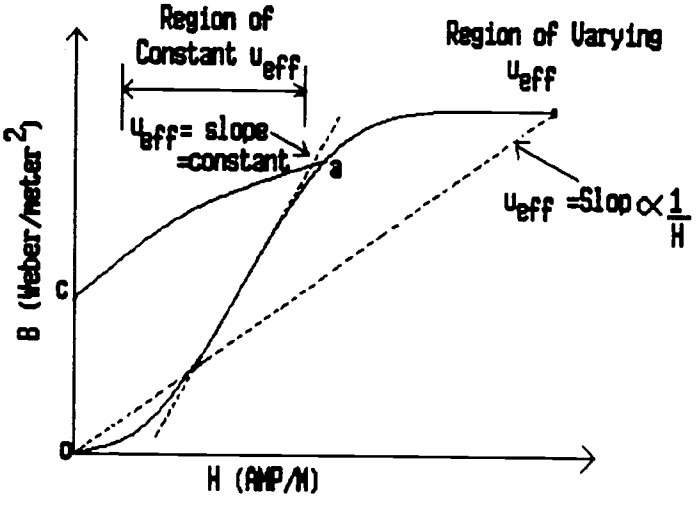

Figure (24) Magnetization Curve of Magnetic Materials when Using a D. C. Current.

H goes to zero but B, the magnetization in the particle, does not. When the circuit is closed again, the time needed to close the valve is small since the change in B from point c to b is smaller than the change in B from o to b. The residual magnetization (oc) may become larger when a screen of magnetic material is used. Such a screen further constrains the flow rate of solids. The screen also has a residual magnetism which, when combined with the particle's residual magnetism, blocks the flow channel. In fact, it has been observed that some solids will stay in the stage valve after the current is completely turned off. For low flow rate operations, a magnetic screen may be useful. The screen used in this project is made of non-magnetic material (copper), since a moderate flow rate of solids is desired. More information can be found in references [38, 33, 112, 20, 130].

The operation of the "leaking" valve lies on the curve where H is greater than that at point a. Although, the current goes to zero in the on/off operation, the average H is greater than that at point a. Therefore, the average magnetization (B) is assumed to be constant. Figure (25) shows a plot of B versus H obtained experimentally [38]. The lowest average current in this project was equal to 22 amps which gave 350 amps/meter as a value of H. The figure shows that B is constant even for this low current.

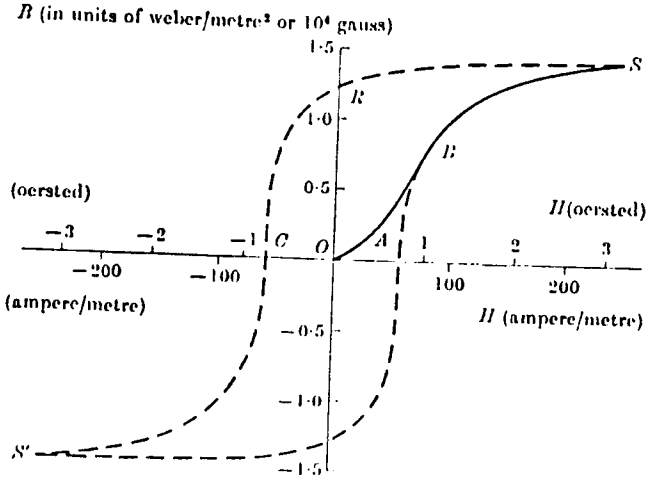

Figure (25) Magnetization Curve (Full Line OABS) and Hysteresis Loop (Broken Line) for Iron.

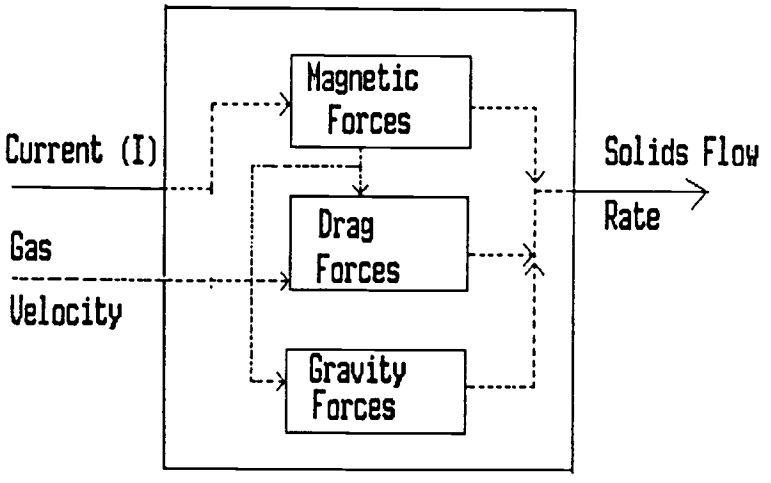

Figure (26) Graphical Presentation of the Forces Acting on Solids Close to the Grates.

IV.2.2.5 Mechanism of Valve Operation

The flow of solids through the stage valve is assumed to be continuous. This is because of the short periods used in this research. During on/off operation with short periods, the current would not step immediately to zero because the response time of the power supply is close to t_{op}. (For more details see section IV.3). When the particles are moving downward between the grates, the horizontal component of the magnetic force causes friction between the neighboring particles which increases as they get closer to the grate due to the increase in the horizontal magnetic forces. Therefore, the flow rate of solids decreases as the distance from the grate decreases. Actually, it is observed experimentally that a layer of magnetic particles remains continuously around the conductor. The layer's outside radius is a strong function of t_{op} (I_{avg}) and period (t_{cl} + t_{op}). The radius of the layer was found to vary between zero and one half the distance between the neighboring grates, depending on t_{op}.

The direction of the friction force between the particles is upward since the particles are moving downward with varying speeds which approach zero as the grate is approached. The friction force is assumed to be proportional to the magnetic force in this research.

The other forces, i.e. the drag force caused by the flow of gas which is in the direction of the friction force

and the gravity force which points downward, are constant in this work. Therefore, the flow is regulated by changing the friction force (magnetic force) by either changing t_{op} (I_{av}) in the on/off operation or changing the current directly in the "leaking" valve operation.

A similar mechanism also applies in the "leaking" valve operation. The radius of the layer surrounding each grate is strongly affected by the current. The existence of an opening between two neighboring grates has been observed experimentally. The width of the opening depends on the level of the current through the grates. Therefore, the flow through the valve is regulated by adjusting the width of the opening and by the magnetic force (which decreases as the distance from the grate increases) which affects the solids flowing through the opening.

The discussion above shows that the flow through the valve varies across the area and also with time. Therefore time averaged values of the flow and all the other variables associated with it are used throughout this work.

IV.2.2.6 Model Equations for Solids Flow Rate

Figure (26) shows the whole process (the big box). This box can be partioned into three small boxes which describe the process adequately. The current and solids flow rate, as well as the gas flow rate, can be measured

flow rate, as well as the gas flow rate, can be measured experimentally. However, there are some lumped parameters in the previous expressions for the forces such as K_2, K_* and δ. Those parameters are hard to measure directly and are believed to vary with the current. The strategy is thus to determine the unknown lumped parameters from available experimental data. Combining all the force expressions gives:

$$\frac{V_p\ K_2}{8\ \pi^2} *(K^*-I)I+ A_1\ U_g + \frac{A_1\ m_o}{A_f\ \rho_S} = (A_{cs}*\delta)*(1 - \epsilon) * \rho_s$$

Let $$\frac{V_p\ K_2}{8\ \pi^2} = K_3{}^* \tag{22}$$

$$-K_3{}^*\ I^2 + K_3{}^* K\ I + A_1\ U_g + \frac{A_1\ m_o}{A_f\ \rho_S} = (A_{cs} * \delta)*(1 - \epsilon)* \rho_s$$

which can be written in the following form:

$$K_3\ I^2 - K_4\ I + K_5 = m_o \tag{23}$$

$$K_5 = \frac{\rho_s\ A_f}{A_1}\ (A_{cs} * \delta) * (1 - \epsilon)\ \rho_s - A_1\ U_g)$$

$$K_4 = K^3\ K^* \qquad\qquad K_3 = K_3{}^*\ \frac{\rho_s\ A_f}{A_1}$$

By fitting the data to the form of the above equation the constants K_3, K_4, K_5, can be obtained from which the

parameters K^*, K_2, δ, can be substituted into equation (22) which can then be used for simulation and analysis.

When mixtures of magnetic and non-magnetic solids are used, the model would still be valid if the assumption is made that essentially all the material in the fixed region is magnetic material (ie, $W_{iron} = 1$). During the operation with 25% iron and 75% sand, two separate layers in each bed are observed:

1) A very dark region close to the copper tubes
2) A light colored region away from the copper tube. This layer is completely fluidized.

There are still some traces of non-magnetic particles among the magnetic particles as a result of sheer forces between the particles. The effect of the non-magnetic particles on the other parameters will be assumed to be negligible. However, the thickness of this layer(δ) will depend on the intensity of the current through the copper tubes(I), the weight fraction of the magnetic particles in the second region (main bed), (W_m), and the gas flow rate (U_g).

$$\delta = F\ (I,\ W_m,\ U_g) \tag{24}$$

The trend is that δ increases with an increase in the weight fraction of the magnetic material in the fluidized region or with an increase in the current and decreases with an increase in the gas flow rate. A complete study of this

region done with 25% magnetic particles will be presented in chapter VIII.

IV.3 On/Off Valve Operation vs. "Leaking" Valve Operation

There are two ways in which the stage valve can be operated:

- on/off operation
- "leaking" valve operation

Figure (7) is a sketch of the current which flows through the stage valve for both kinds of operation. This figure presents the ideal situation of perfect square waves.

IV.3.1 On/off Operation

In this kind of operation, the flow of solids through the valve is regulated by controlling the on/off time of the current flowing in the copper grids.

When the current is on, the solids line up along the magnetic flux lines, hence, blocking the flow of solids. For stable operation, the level of the current has to be greater than the holding current (I_h). The actual current used is called the working current (I_w). When the current is less than the release current (I_r), the solids will flow

through the valve at a flow rate which is greatest when the current is zero.

IV.3.1.1 Characterization of the Operation

There are three types of flow of solids through the stage valve:

1) glob flow
2) continuous flow
3) pulsed flow

Figure (27) shows the regions of each of the above flow types. The boundaries between the regions shown in figure (27) were based on the following:

a) visual inspection of the flow of solids from the stage valve.
b) Measurements of the minimum and maximum current actually achieved by the power supply and the fraction open of the period, if any, during which the current is equal to zero. The data were taken at different periods and at fixed working current (I_W) of 148 amps.

The procedures above involve some error, but will give an approximate diagram for the different regions of

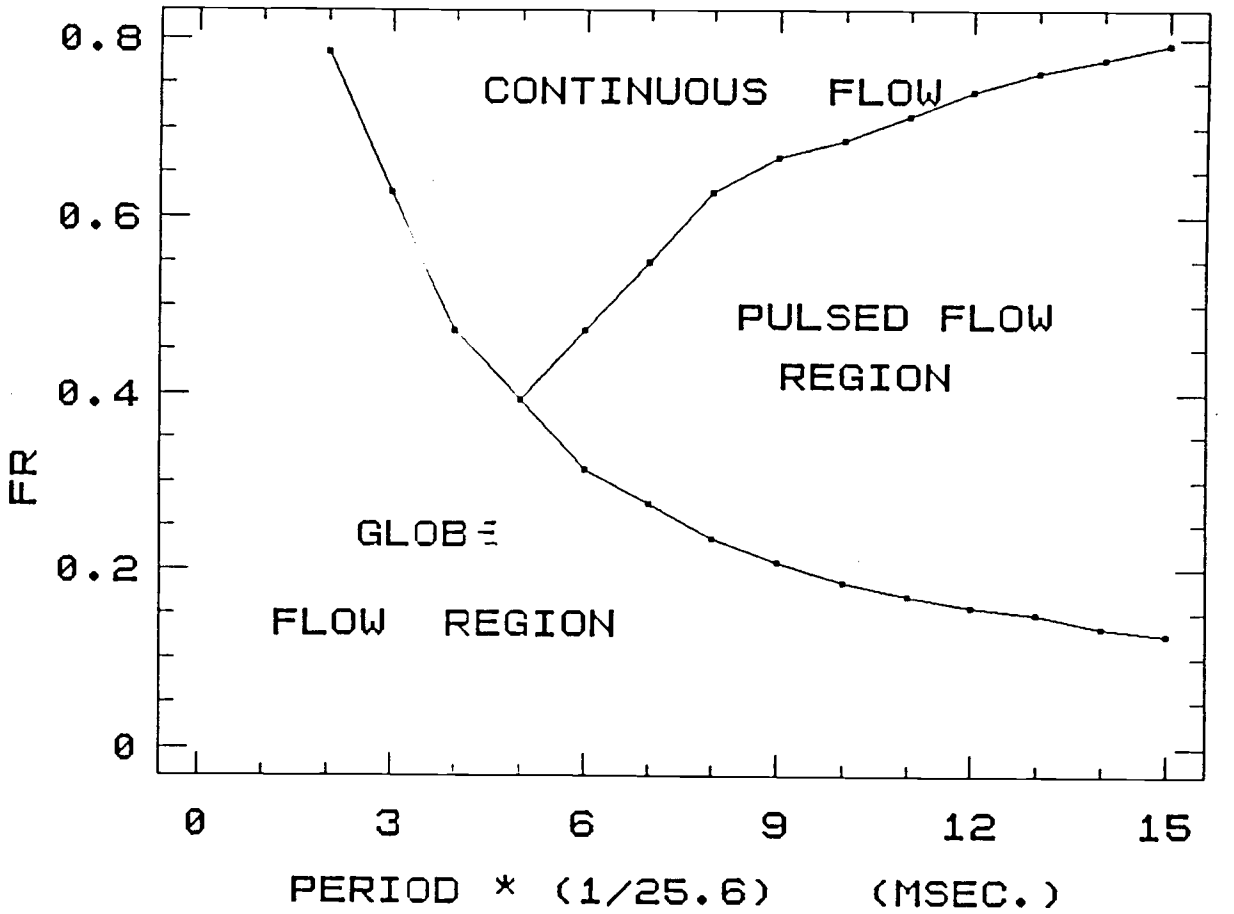

Figure (27) Flow regions of solids flow through the stage valve. I_w = 148 amps.

operations. The following parameters are important in explaining the existence of the different regions:

T_{up} = Time needed for the power supply output to change from 0 to I_w

T_{dn} = Time needed for the output of the power supply to change from I_w to 0

For the power supplies used in this project and I_w of 148 amps,the constants were found to be:

T_{up} = 41.5 milliseconds

T_{dn} = 40.6 milliseconds

Depending on T_{up} and T_{dn} the following cases can arise:

case 1)

$t_{op} < T_{dn}$; $t_{cl} \geq T_{up}$

The current oscillates between some lower limit current I_{LL} and I_w.

$$I_{LL} \leq I \leq I_w$$

case 2)

$t_{op} \geq T_{dn}$; $t_{cl} < T_{up}$

The current oscillates between zero and some upper limit current I_{UL}.

$$0 \leq I \leq I_{UL}$$

case 3)

$$t_{op} = T_{dn}; \quad t_{cl} = T_{up}; \quad T = T_{up} + T_{dn}$$

The current oscillates continuously between zero and I_w.

$$0 < I \leq I_w$$

The oscillation is sinusoidal with amplitude equal $\frac{I_w}{2}$ and frequency equal $\frac{1}{T}$.

case 4)

$$t_{op} < T_{dn}; \quad t_{cl} < T_{up}$$

The current oscillates between an upper limit and a lower limit:

$$I_{ll} < I < I_{ul}$$

case 5)

$$t_{op} > T_{dn}; \quad t_{cl} > T_{up}$$

The following two subcases occur:

5a) The t_{op} and t_{cl} are large enough so that T_{up} and T_{dn} can be neglected. In this case the current oscillates between 0 and I_w in a square wave fashion.

$$I \begin{cases} = I_w \text{ during } t_{cl} \\ = 0 \text{ during } t_{op} \end{cases}$$

5b) The t_{op} and t_{cl} are about 1 - 3 times as large as T_{up} and T_{dn} respectively. The current decreases gradually to zero where it stays for a short time then it increases gradually to I_w.

IV.3.1.2 <u>Glob Flow Region</u>

The solids are detached from the stage valve at different locations in clumps. The solids rain from the stage valve continuously. This type of flow is observed for small opening time of the stage valve.

This region is represented by case (1), (3), and (4). Case (4) represents this region if $t_{cl} > t_{op}$ and $I`_{LL} \leq I_r$ (i.e. the release current). In this region, the current never goes to zero. Small periods (T < 81 milliseconds) and small fractions open of larger periods, as shown in figure

(27), result in this kind of flow. This kind of operation is not suitable for large flow rates of solids.

IV.3.1.3 Continuous Flow Region

The region representing this type of flow arises from cases (2) and (5b). In case (5b) the flow is observed to be continuous over a large range of fraction open of period which are bounded by: $85 < T < 205$ milliseconds. Case (2) represents continuous flow over all the periods. The flow of solids in case (5b) is moderate while it is high in case (2). A period of 5 counts (128 milliseconds) was used in subsequent experiments for two reasons:

1) The flow is observed to be more continuous than with larger periods.
2) A wide range of flow rate can be achieved.

The boundary between the glob and the continuous regions is drawn for completeness. Those regions are nearly indistinguishable except at very small opening times, t_o.

IV.3.1.4 Pulsed Flow Region

This region arises for case (5a) and occurs for long periods ($T > 209$ milliseconds). In this kind of operation the solids flow rate through the valve switches between zero and maximum flow. The current through the valve is close to

a square wave with values fluctuating between zero and the working current (I_w).

$$F \begin{cases} = 0 & \text{when } I = I_w \quad \text{during } t_{cl} \\ = F_{max} & \text{when } I = 0 \quad \text{during } t_{op} \end{cases}$$

The periodicity of the flow rate of solids from the stage valve adds an additional undesirable oscillation which can cause control problems. At high flow rate of solids the pressure drop across the valve exhibits large low frequency oscillations which are a result of solids flowing onto the stage during the closing time of the valve.

This kind of operation would not be suitable in a multi-stage fluidized bed since the output flow of each valve is the input to the stage below it. The following problems are characteristic of this flow regime:

1) Serious bed vibration.

2) Mixing from fluidization is reduced during long periods of maximum flow. The layer attracted to the stage valve is released at the beginning of each period. This layer serves as a good distributor for the fluidizing air. Losing it will cause a large disturbance to the fluidizing air and will cause the formation of large bubbles which tend to shift the fluidization towards the slugging regime and will increase elutriation

of the fine particles. Product non-uniformity will be the result of all of the above reasons.

Figure (28) shows the actual current through the stage valve at four different fraction open values. Figure (28-a) represents the glob flow region while figure (28-b) is the transition between glob and continuous flows. Figures (28-c) and (28-d) represent the continuous flow region. The period was 128 milliseconds and working current was 148 amps.

Similar experimental data were taken for the same fraction open but with different periods. The data are shown in figures (29-a, 29-b, and 29-c) for glob, continuous, and pulsed flows respectively. A fraction open of 0.55 was used and the working current was again 148 amperes.

IV.3.1.5 Calculation of Average Current from a Fraction Open Specification

Equation (23) for leaking valve is expressed in terms of current, so obtaining the flow as a function of average current is needed for comparison. The output of the power supply is recorded at a sampling rate of 1000 samples/second for several values of the fraction open. The fraction open

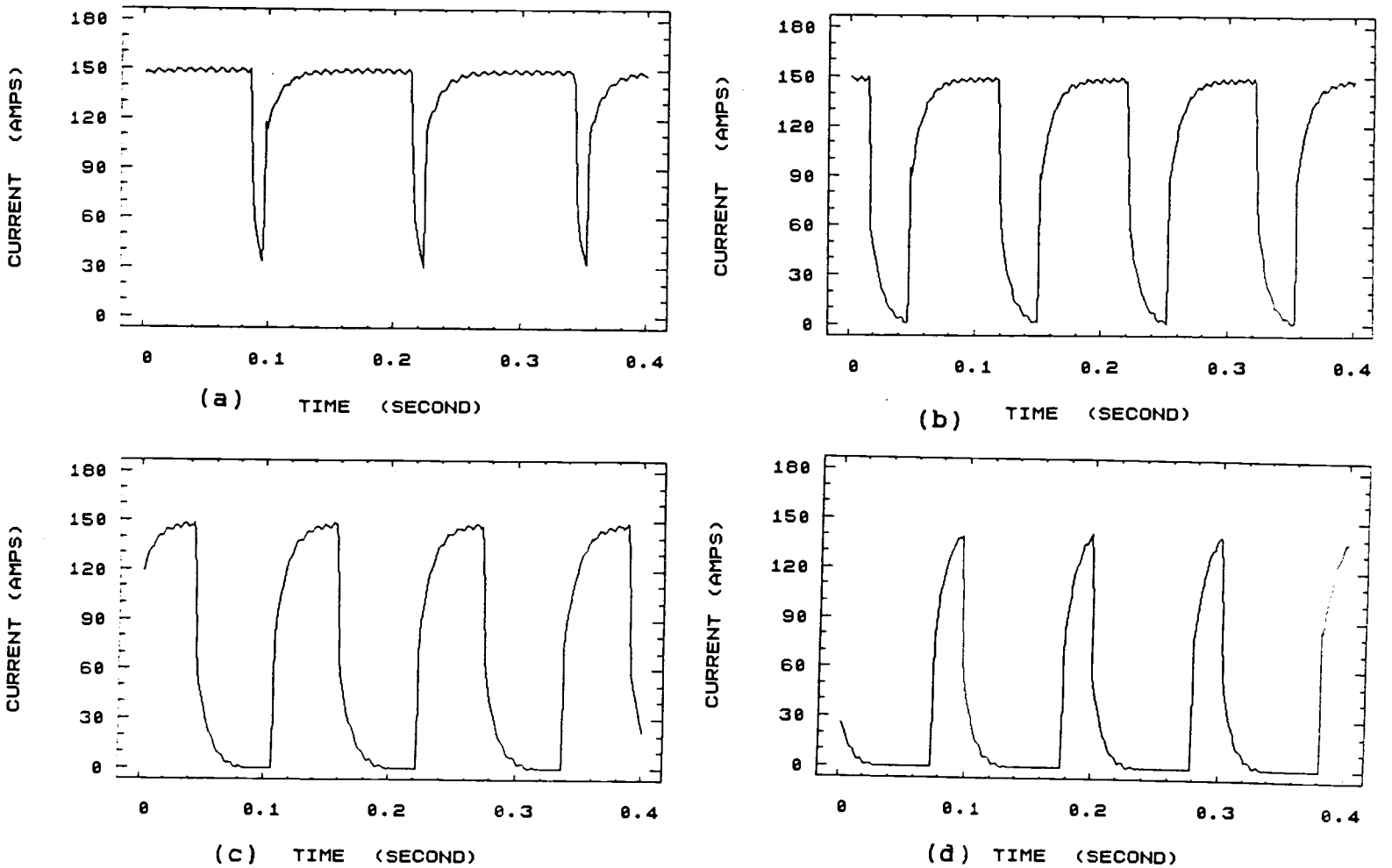

Figure (28) Actual Signal of Current Flowing Through the Valve at Different Fraction open.a) FR = 0.781; b) FR = 0.3125;
c) FR = 0.5469; d) FR = .7812)

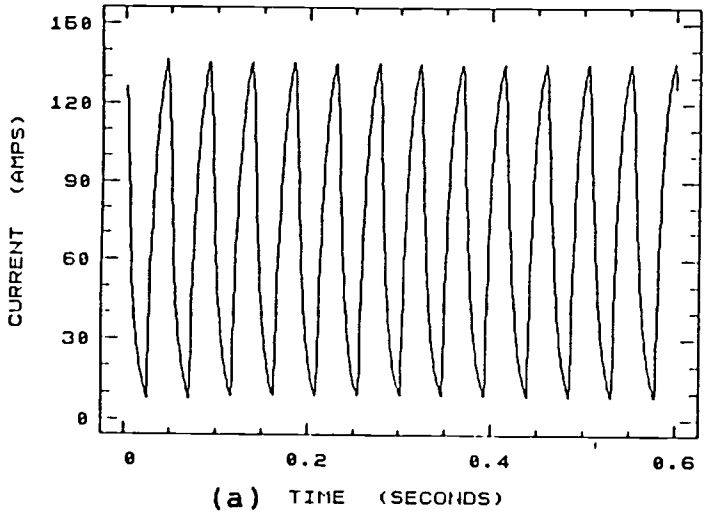

(a)

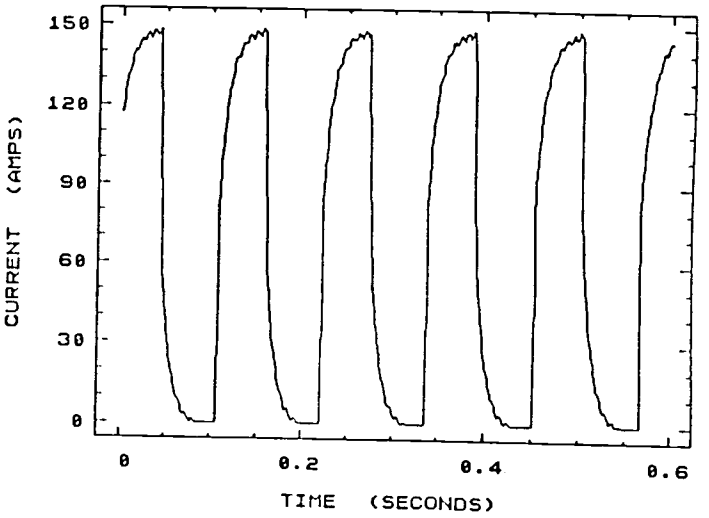

(b)

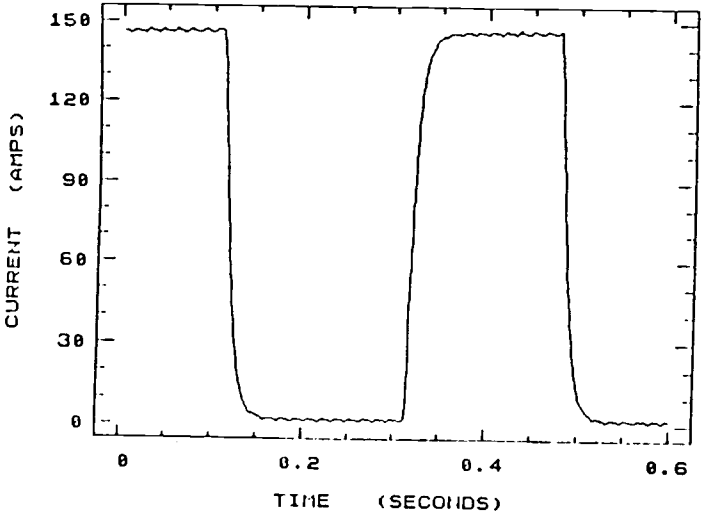

(c)

Figure (29)

Actual signal of the current Through the Valve at Different Periods.
a) T = 51.2 ms; b) T = 128 ms; c) T = 409.6 ms.

The fraction open is varied between zero and one, while the working current (I_W) is fixed. The same data is obtained for other working currents. The time average current is then plotted versus the fraction open for different working currents and a linear relationship was found to represent the data:

$$I_{avg} = I_W \ (1 - FR) \tag{25}$$

The correlation is based on linear regression. The correlation coefficient is found to be 0.999 indicating a very good fit. Figure (30) shows the plots of fitted lines as well as the experimental data at different levels of working currents (I_W). Since equation (23), which predicts flow of solids out of the stage, depend only on the current, the flow of solids out of the stage during on/off operations should depend only on average current. To obtain the desired fraction open for a given average current , one goes horizontally along the desired average current and intersects a line representing the working current. The fraction open needed for a certain average current increases as the working current increases. Therefore, since the average current is the same there is no saving of the amount of energy by choosing a lower working current level.

The above conjecture was verified by running the process (closed-loop) at different working currents. The

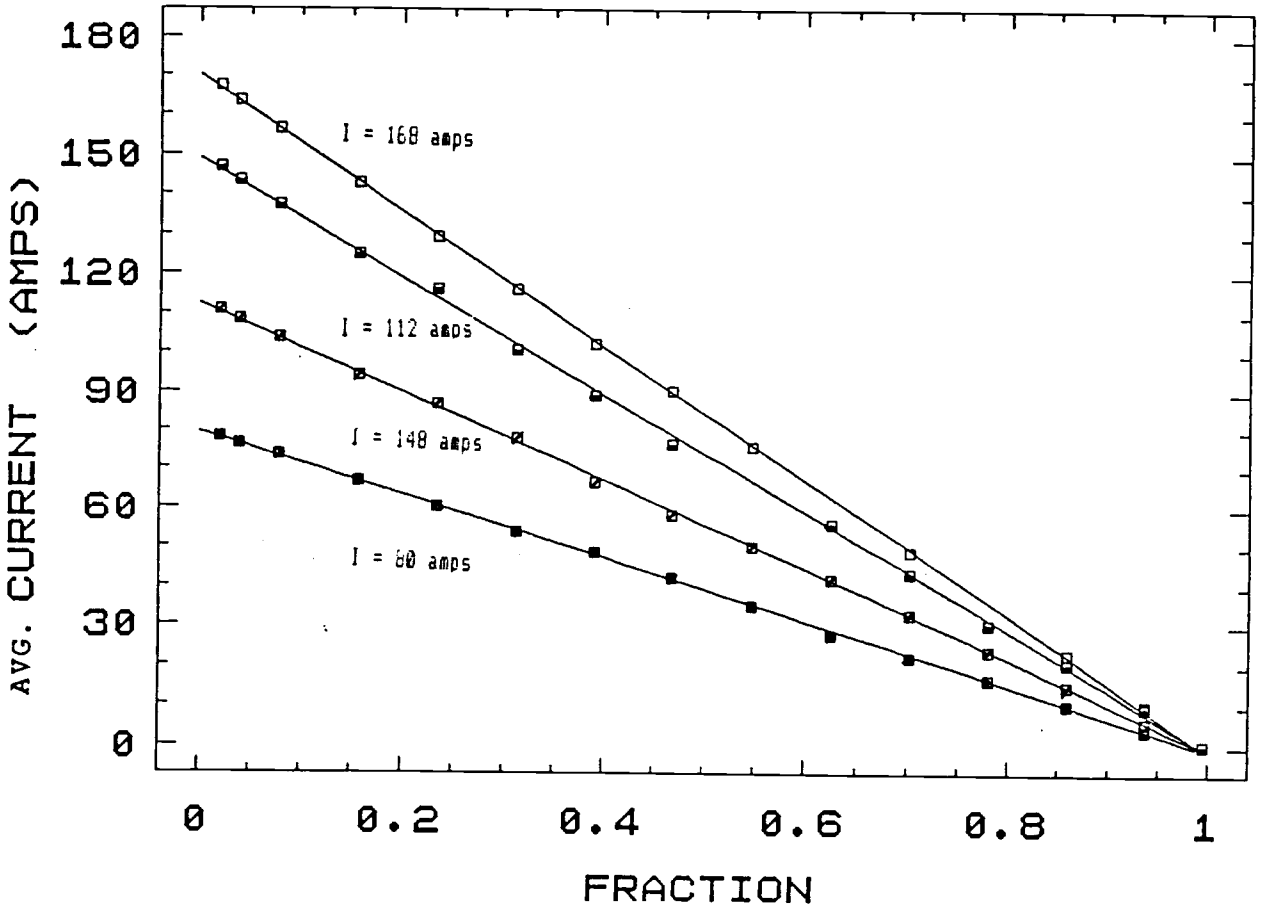

Figure (30) Average Current Versus Fraction Open for Different Working Currents.

average fractions open, as well as the average pressure, of each experiment are calculated. Their values, as well as the standard deviation, are listed in table (1). It can be concluded from table (1) that the average current shown in the last column yielded the same closed-loop steady state using different combinations of working current and fraction open. This confirms the previous statement about the absence of energy savings by simply operating at low working current level. However, the response of the stage valve is much faster and more reliable when a high current is used.

Table (1) Average Fractions Open and Pressure Drops Across the Stage at Different Working Currents (100% Iron).

I_w (Amps)	P_{av} (psi)	St. Dev. (psi)	Fraction Open	St. Dev.	I_{av} (Amps)
148	0.495	0.02	0.52	0.02	71.0
148	0.492	0.03	0.53	0.02	69.5
148	0.498	0.02	0.54	0.02	68.1
112	0.497	0.01	0.37	0.01	70.6
112	0.495	0.01	0.38	0.01	69.4
80	0.497	0.007	0.13	0.009	69.6
80	0.510	0.011	0.14	0.01	68.8

An expression of the flow rate of solids out of the stage in terms of fraction open can be obtained by sub-

stituting equation (25) which expresses the average current as a function of the fraction open, into equation (23). The following equation is the result:

$$m_o = K_3 I_w^2 FR^2 - (2 K_3 I_w^2 - K_4 I_w) FR + K_3 I_w^2 + K_5 \quad (26)$$

However, the average current in on/off operation has a much larger standard deviation than that of the "leaking" valve operation. Therefore, the values of the coefficients in the above equation are not as certain as those predicted by the "leaking" valve operation. Also, in on/off operation, the assumptions made to derive the flow expressions in section IV.2.2.3 are not as convincing as in the "leaking" valve operation.

IV.3.2 "Leaking" Valve Operation

In this operation the flow rate of solids through the stage valve is manipulated by adjusting the power supply output current. The current level must be between the holding current (I_h) and the release current (I_r). In this range of currents, the solids can be considered leaking between the grates, thus, the valve is called a "leaking" valve. The operation of the valve is reliable as long as no large positive step in error for solids level occurs. For example, a negative setpoint change in the operation of the

valve shows hysteresis behavior, figure (31). To achieve the new lower setpoint, the current goes down to a value at C that is equal to or below the release current where the flow of solids is large. However, to go back to normal operation, the current has to be raised to a value larger than the holding current through a different path (i.e. ca), then decreased to the steady-state value on the curve (ab). The hysteresis behavior becomes stronger as weight fractions of magnetic particles in the solids decreases. The gap between the holding current and release current, figure (31), increases as the weight fraction of magnetic particles on the stage decreases.

Figure (32) shows the plot of the release and the holding current versus the weight fraction of magnetic particles in the bed. At lower weight fractions ($W < .25$) the current needed for satisfactory operation is higher and the hysteresis behavior becomes worse. For low fraction of magnetic particles in the solids, the steady-state operation might be acceptable. It has been found that steady-state operation for solids with irons weight fraction of 0.25 is acceptable with some special type of control strategy. The details are discussed in chapters VI to VIII in this thesis.

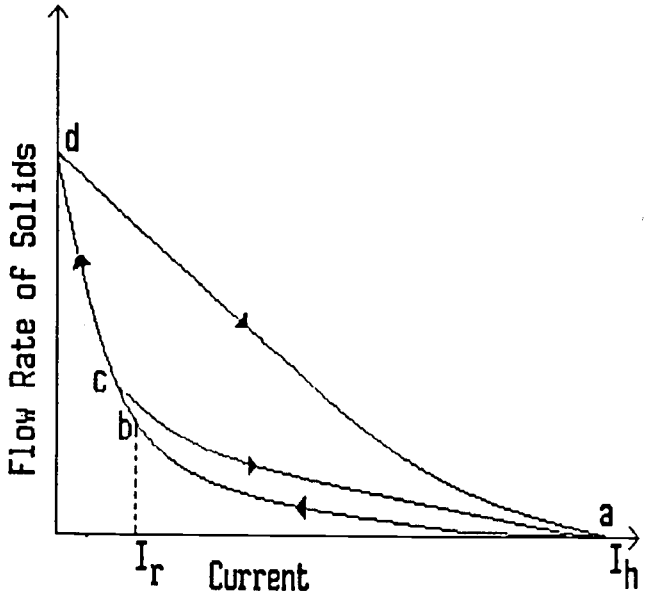

Figure (31) Hysteresis Associated with "Leaking" Valve Operation.

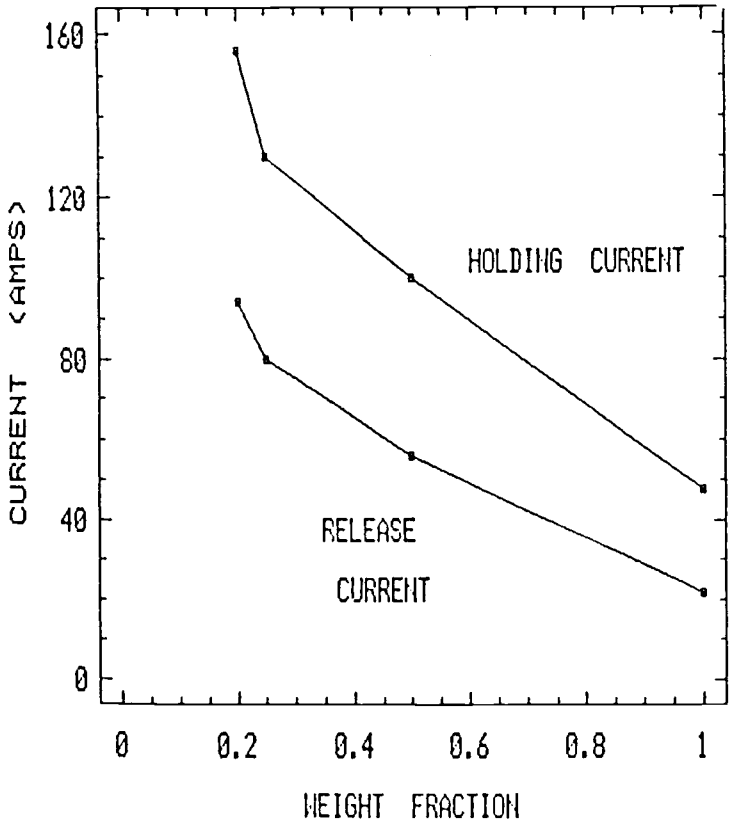

Figure (32) Release and Holding Currents for Different Weight Fractions of Magnetic Particles.

IV.4 Effect of Solids Holdup on the Flow Rate of Solids Out of the Stage Valve

The analysis which was done previously did not take into account the effect of solids holdup on solids flow rate out of the stage valve. However, some experiments were done to investigate that effect. The solids flow rate into the stage is kept constant and the holdup is varied by changing the pressure setpoints during the closed-loop operation. The controller gain is chosen so that the fluctuations of the control signal (fraction open or current), as well as the pressure drop across the stage, are small. Under this condition the operation is steady and the time average values of the pressure drop across the bed (i.e. solids holdup) and the controller output are obtained.

Figure (33) shows the plot of fraction open for on/off operation versus the average pressure drop across the bed while figure (34) shows the plot of current for leaking valve operation versus the pressure drop across the bed. The flow rate of solids (62.17 gm/sec) into the stage valve is the same in both figures. From the figures, the fraction open of period the valve is open and the current are constant when the pressure drop is greater than 0.2 psi. When the pressure is less than 0.2 psi, the fraction open increases linearly with decreasing pressure drop . In the

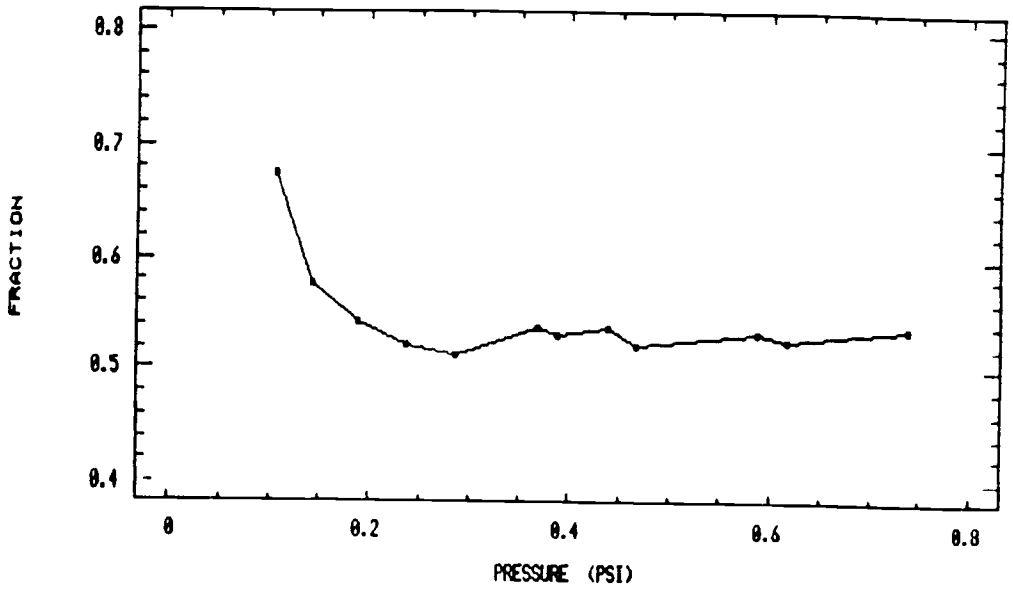

Figure (33) Effect of the Pressure Drop Across the Stage on the Fraction.

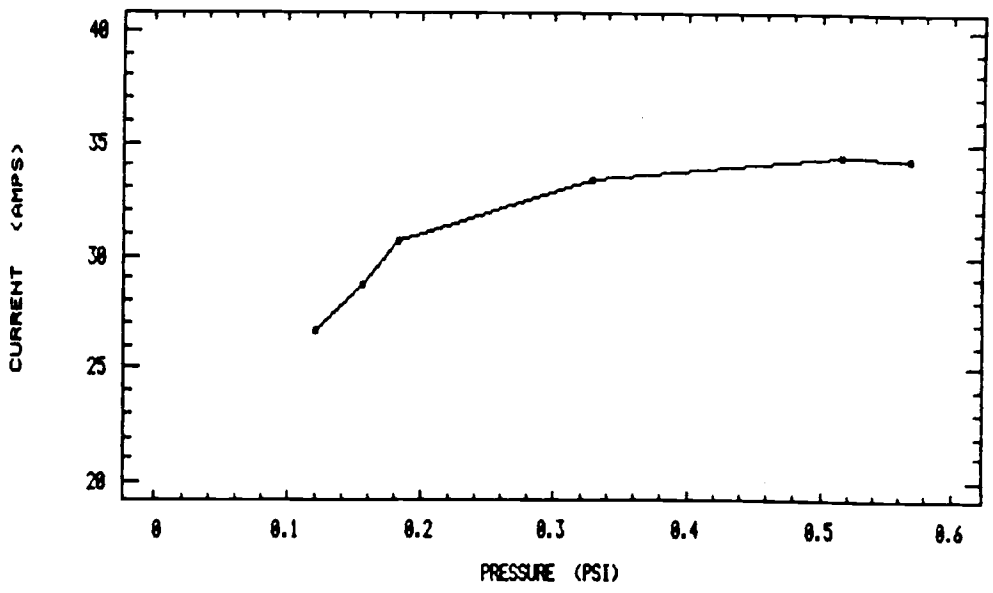

Figure (34) Effect of the Pressure Drop Across the Stage on the Current.

case of "leaking" valve operation, the current decreases linearly with decreasing pressure drop.

At low pressure drop (i.e. solids holdup) the whole bed is shifted to the fixed bed region although the surface of the bed is spouting. When the surface of the bed is spouting, the average thickness of the fixed region is larger than that of uniform fluidization (wP > 0.2 psi). As a result, the number of particles facing each other is larger which requires less current (larger fraction open) to maintain the same solids flow rate. Also, the amperian current is larger because the amount of magnetic materials is larger. When the bed is completely fixed, the drag and gravity forces decrease linearly with the decrease in the fixed layer thickness. Accordingly, the magnetic forces should decrease linearly. The smaller number of particles, as well as the decrease in current, contribute to the decrease of magnetic force. From the previous analysis, (IV.2) the layer thickness increases as the current increases so the current needed for certain thickness is adjusted by the controller to meet this requirement.

For P > 0.2 psi, the layer thickness is assumed to be constant. The whole analysis in this project is done for wP > 0.2 psi since this is the region of interest in most of the applications.

V. PROCESS MEASUREMENT

V.I Relation Between Bed Height and Pressure Drop

Figure (35) is an illustration of the pressure measurement locations with respect to that stage valve. The general equation for pressure drop across the fluidized bed ($P_3 - P_2$) is given by the following equation:

$$P_2 - P_3 = (1 - \epsilon_f)\ (\rho_s - \rho_g)\frac{g * h_f}{g_c}$$

and,

$$h_f = \alpha^* h_s \tag{27}$$

$$P_2 - P_3 = S_1 * h_s$$

Where $S_1 = (1 - \epsilon_f)\ (\rho_s - \rho_g)\ \frac{g}{g_c} * \alpha^*$

Measurement of the height of the fluidized bed (h_f) is very difficult. So h_f will be assumed to be proportional to the settled height (h_s). Also, the voidage of the fluidized bed changes very little from the one at the minimum fluidization condition (ϵ_{mf}). Therefore, it will be assumed to remain constant.

The total pressure drop between point (1) and (3) is given by:

$$P_1 - P_3 = (P_1 - P_2) + (P_2 - P_3) = \Delta P_T \tag{28}$$

$$\Delta P_T = \Delta P_s + S_1 * h_s \tag{29}$$

ΔP_T = Total pressure drop.

ΔP_s = The pressure drop across the stage valve.

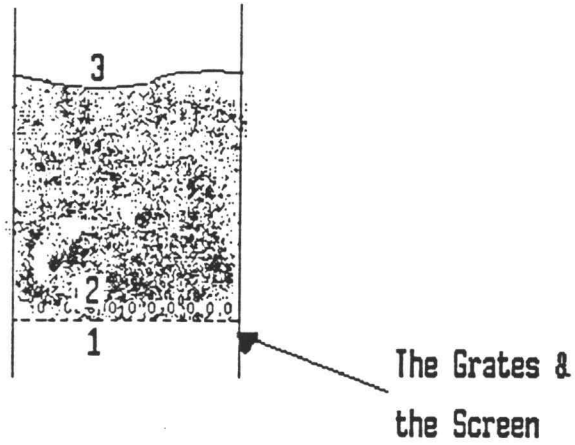

Figure (35) Illustration of the Pressure Measurement Locations in Equation (27).

Table (2) Regression Analysis Result for P_{avg} vs. H_s.

% of Iron in Solids	ΔP_s (PSI)	K (PSI/FT)	R^2
100	0.012	0.8461	0.9780
50	0.008	0.6922	0.9697
25	0.008	0.6427	0.9664

Thus, the plot of the total average pressure drop (ΔP_T) versus the settled height (h_s) should be a straight line with slope equal to k and intercept corresponding to ΔP_s. Figure (36), shows this kind of plot for beds which consist of 100%, 50%, and 25% by weight iron where the remaining percentages are sand particles. The data is obtained by measuring the pressure drop across the total bed at different settled heights. Table (2) contains the best slope and intercept for the straight line through the data which is obtained by linear regression. Table (2) shows that the slope of the fitted straight line decreases as the weight fraction of iron particles in solids decreases. This is due to the decrease in the effective density of the mixtures as the weight fraction of iron decreases. From the table and the plots, the pressure drop across the stage (ΔP_s) is so small that neglecting it would not cause significant error. Therefore, the final correlation between the average pressure and settled height can be written in the following form:

$$\Delta P_{av} = K * h_s \qquad (30)$$

This equation can be used for conversion of pressure data, to settled height values (ie. weight of the solids).

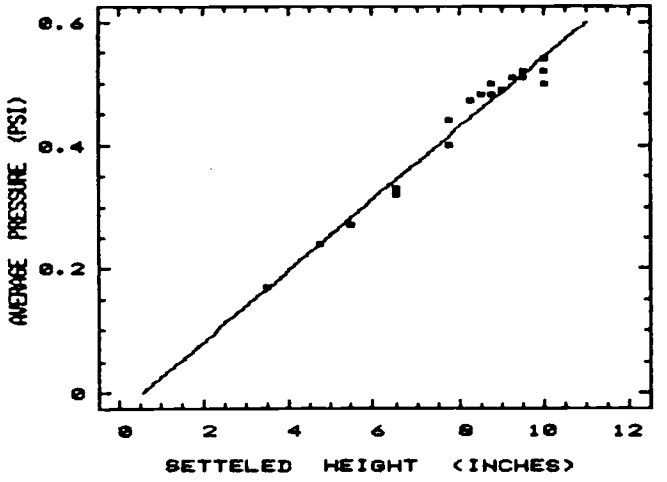

(a)

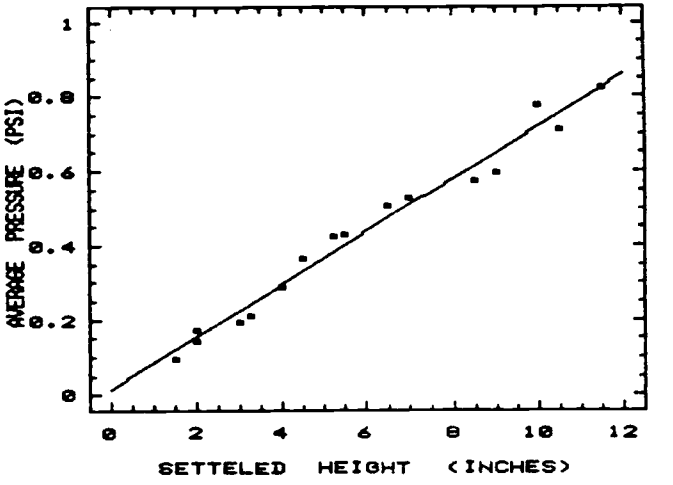

(b)

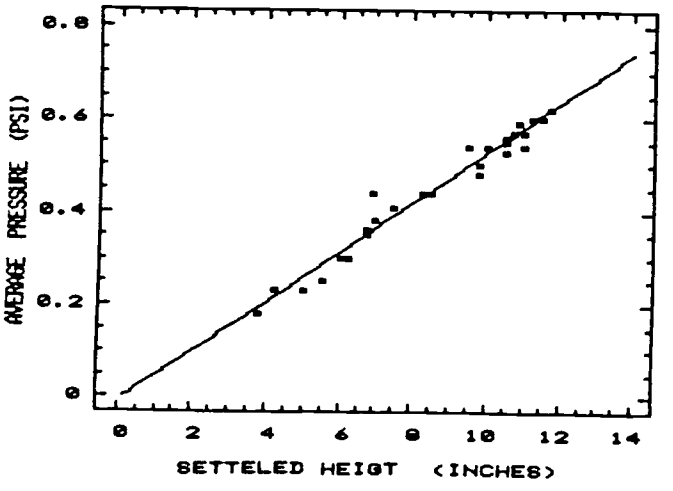

(c)

Figure (36)

Average Pressure Drops vs. Settled Height for Solids Consisting of 100%, 50%, and 25% by Weight Iron.

V.2 Pressure Fluctuations

V.2.1 Motivation for Characterization of Pressure Fluctuations

V.2.1.1 Fluidization Quality

The frequency of pressure fluctuations can be used to determine fluidization quality which is interpreted as a measurement of the bubble size. The following correlations are often used for the calculations of the bubble sizes.

a) Tamarin's equation [72]:

$$\bar{D}_B = \frac{8.3 * D_p^{1.5}}{f} * \frac{[U - U_{mf}]^{0.275}}{U_{mf}} \qquad (31)$$

b) Kunii and Levenspiel [67]:

$$\bar{D}_B = \frac{1.5}{f} \quad (U - U_{mf}) \qquad (32)$$

f = the frequency of the fluctuations (cycles/second)

U = gas velocity (cm/second)

U_{mf} = gas velocity at minimum fluidization (cm/second)

D_p = particle diameter (cm)

$\bar{D}_B$ = average size of the bubble (cm)

V.2.1.2 Influence on the Choice of Sampling Frequency for the Controller

From the discussion presented previously, the fastest sampling frequency for continuous throughputs of solids we can achieve with the experimental equipment is equal to 7.8 samples/second. To eliminate aliasing problems, the following relation has to satisfy (Nyguist criterion from the Shannon sampling theorem, Astrom and Wittenmark [5]).

$$f_s > 2f \tag{33}$$

f_s = sampling frequency

f = pressure fluctuation frequency

Generally, the above maximum possible sampling frequency imposes the following limit on the continuous process because of the frequency of pressure fluctuations:

$$\Delta P_{avg} \geq 0.18 \text{ psi} \tag{34}$$

This results in a lower limit on solids holdup in the stage which can be adequately controlled.

V.2.1.3 Determining the Filter Time Constant

There are two types of dynamics of the pressure drop during the continuous process.

1) Slow dynamics:

   These changes are related to the time averaged holdup of solids on the stage. Changes in the average flow of solids into and out of the stage result in changes of solids inventory. These kinds of disturbances can be controlled.

2) Very fast dynamics:

   These changes are the result of fluctuations due to bubbles formation which are periodic in nature. The eruption of gas bubbles at the surface of the fluidized bed is the prime reason for the occurring fluctuations. These dynamics are hard to model, since many variables play important roles. The control of the average pressure drop would be impossible without some form of filtering of these effects.

The strategy is to attenuate the fast dynamics as much as possible without affecting the slow dynamics. The following equation represents the effect of the filter time constant and the amplitude of the fast fluctuations:

$$\tau_f \frac{d\,Y_f\,(t)}{dt} + Y_f\,(t) = X(t) \tag{35}$$

where:

τ_f = the filter time constant (seconds)

$X(t)$ = the unfiltered pressure fluctuations = $A \sin(\omega * t)$ (psi)

A = the amplitude of the pressure fluctuations (psi)

Y_f = the filtered pressure fluctuations (psi)

Solving the above equation by first taking the Laplace transform, then taking the inverse Laplace transform, the following equation for Y_f can be obtained:

$$Y_f\,(t) = \frac{A_{fl}}{\sqrt{\tau_f^2\,\omega^2 + 1}}\,\mathrm{SIN}\,(\omega t + \phi)$$

$$\frac{\text{output amplitude}}{\text{input amplitude}} = \frac{1}{\sqrt{\tau_f^2\,\omega^2 + 1}} \tag{36}$$

The ratio A_f/A is desired to be as small as possible without affecting the response of the slow dynamics. In the

subsequent chapters, the slow dynamics restriction on the choice of the filter time constant will be discussed.

V.2.2 Previous Work in Gas Flow Systems

Many investigators have studied the pressure fluctuations in a fluidized bed. Some of those [50, 51, 123], have proposed detailed models to describe the pressure fluctuations in a fluidized bed. Some of these models [50, 51], are difficult to apply and are mathematically complicated. Nevertheless, their predictions of the pressure fluctuation may be inaccurate. Other investigators [7, 9, 17, 71, 123, 129] were mainly concerned with the experimental determination of the characteristics of pressure fluctuations in the bed even in the absence of external disturbances. Still, others [7, 129] have compared the pressure fluctuations at the bottom and in the plenum of a fluidized bed with imposed changes in the inlet gas flow rate. The majority of the investigators agreed upon the existence of a fundamental frequency of fluctuation. This fundamental frequency has been shown to be related to the emergence of gas bubbles at the surface of the bed. Verloop et al. [123], reported that pressure fluctuations in shallow fluidized beds are sinusoidal. Broadhurst et al. [17] and Baskakov et al. [9] proposed correlations for predicting the amplitude and frequency of the pressure fluctuations. Their analysis is

based on the spectral analysis of the pressure signal from the fluidized bed. Some of the previous investigators confirmed the strong relationship between the pressure fluctuations and the fluidized bed height. Others did not find such a relationship and attribute pressure fluctuations to changes in gas flow rate and porosity in the dense phase of the bed caused by the action of bubbles.

All of these previous studies were done for the batch fluidization process. No studies were found of the case when continuous solids throughput was taking place. Because of the absence of data on pressure fluctuations during the continuous process and conflicting previous results, a study of pressure fluctuations was performed.

V.2.3 Sampling

Tracking the pressure fluctuations in a batch fluidized process was not a problem because the equipment used could measure 20,000 samples/second. However, the situation is different in the case of the continuous solids throughput process. As shown previously, this process is not open loop stable, therefore, some kind of controller to stabilize it is necessary. This means that some time will be taken by the computer to do the computations required for the controller parameters. From experiments, it is found that the minimum time required for these computations is 115

milliseconds. However, the period settings on the timer can be set only as a multiple of 25.6 milliseconds. This imposes the use of a period of 128 milliseconds which makes the use of two IBM-PC computers at the same time with two different sampling frequencies necessary. The first computer is used for controlling the process with a sampling frequency of 7.8 samples/second, while the other one is used to sample the pressure fluctuations with sampling frequency of 100 samples/second. This sampling rate was found to be rapid enough to fully capture the pressure fluctuations in the fluidized bed. This conclusion was reached by conducting a series of experiments during which the sampling frequency is varied from 20,000 samples/second to 100 sample/second. More information is presented in appendix D-1. At least 1000 data points (78 cycles) were collected at each value of solids holdup. The experiments were repeated at various solids holdups to study its effect on the amplitude and frequency of the pressure fluctuations.

V.2.4 Spectral Analysis Fluctuation Data Sets

The statistical properties of the pressure fluctuations were analyzed. The two most important properties are:

1) Autocorrelation
2) Power Spectrum

The first is a measure of the degree of correlation between neighboring values of the pressure fluctuations, while the second is a measure of the distribution of energy versus frequency. The studies are conducted for the following cases:

1) Without solids throughput
2) With solids throughput at two different controller sampling frequencies of 7.8 samples per second and 3.9 samples/second. The fast sampling frequency is the same in both cases and is equal to 100 samples/second.

Figure (37-a) shows the plot of the pressure signal versus time for the case where there are no solids throughput. Figure (37-b) shows that the autocorrelation functions damp to zero almost immediately, indicating a low degree of correlation between neighboring values of pressure fluctuations. This behavior is characteristic of a random time series. The resulting spectrum [figure (37-c)] is almost flat indicating a uniform energy distribution with frequency. In this type of operation, a large number of small bubbles are bursting in a completely random fashion at the

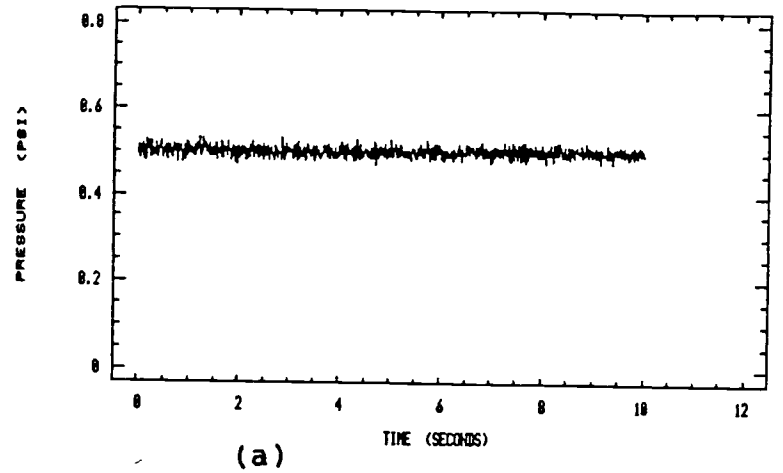

(a)

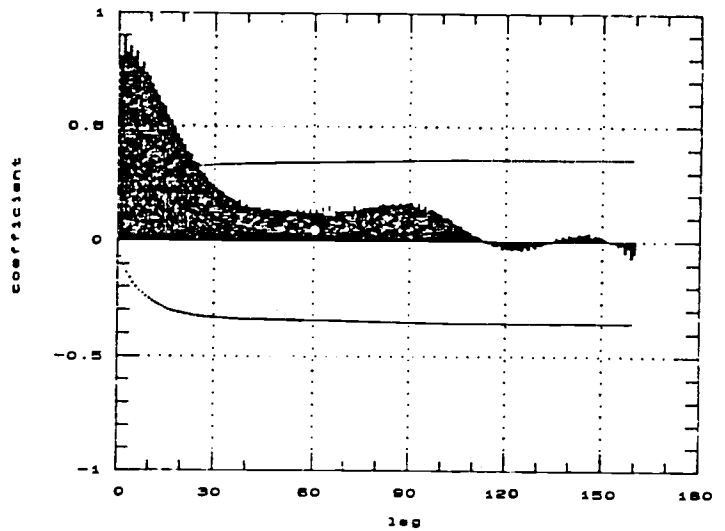

(b)

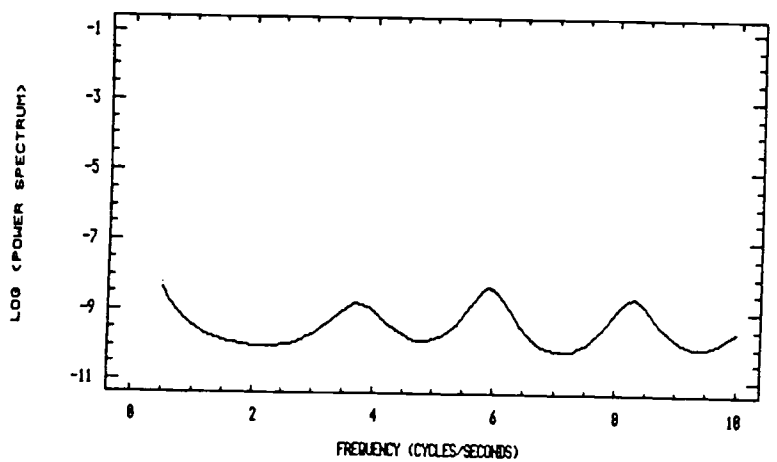

(c)

Figure (37)

Pressure Drop Signal's Plots for Uniform Batch Fluidization.
a) Pressure Signal
b) Autocorrelation Functions
c) Power Spectrum

bed surface which results in very smooth fluidization. However, for gas solids fluidization, the smooth regime is hard to achieve. Figure (38) shows another plot of pressure versus time without solids throughput at various solids holdups. In this case, the autocorrelations plots in figure (39) have a pronounced slow oscillation indicated by the peak in the spectrum plots in figure (40). In this kind of experiment the random small bubbles have coalesced to form a small number of large bubbles which is sufficient to remove the gas in excess of that required for incipient fluidization. The large bubbles burst at the bed surface with frequency equal to that at which a peak in the spectrum plot occurs. Similar plots are shown in figures (41), (42), (43) for continuous solids throughput and for control sampling frequency of 7.8 samples/second (T = 128 milliseconds). It is found that if the settled height of the bed or gas velocity is increased above certain limits, the slugging regime is approached. This can be deduced from figure (38-c) which is for a settled bed height of 11.5 inches. The pressure fluctuations are non-stationary (the time average is not constant) indicating the approach of the slugging fluidization region.

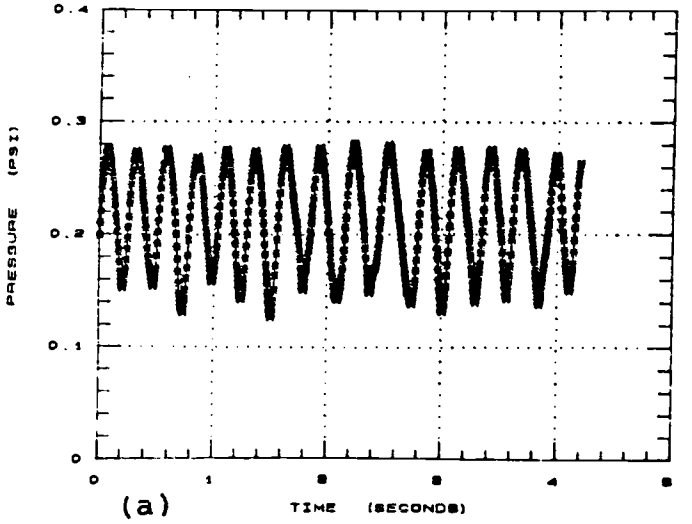

(a)

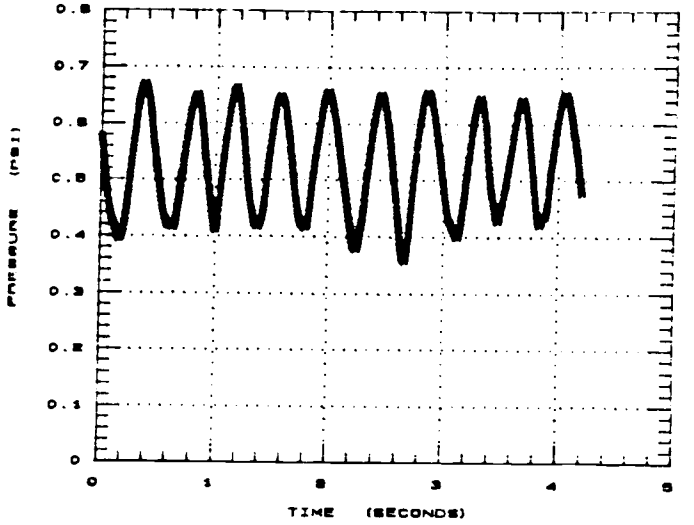

(b)

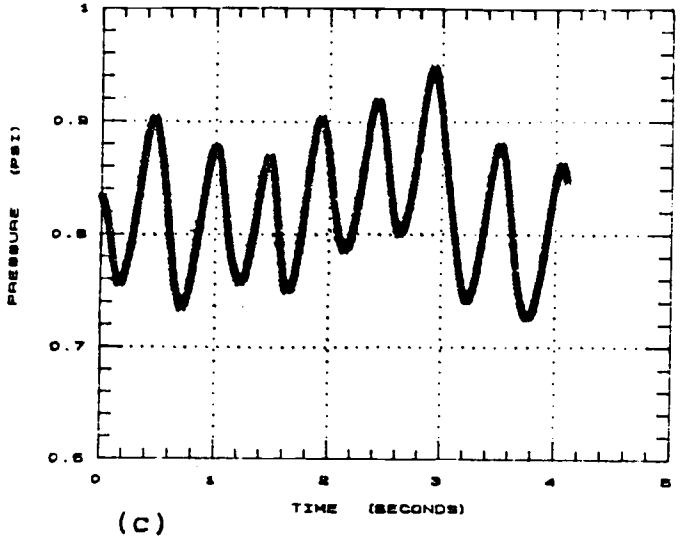

(c)

Figure (38)

Pressure Drop Signal's Plots for Batch Fluidization.
a) P_{av} = 0.23 psi
b) P_{av} = 0.49 psi
c) P_{av} = 0.81 psi

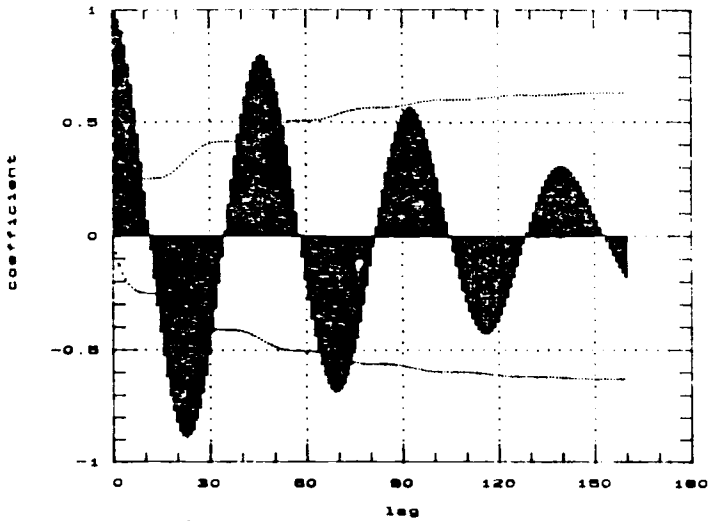

(a)

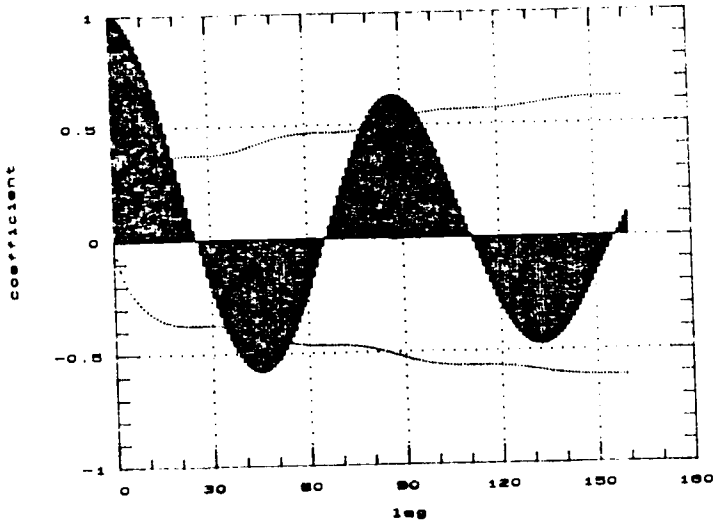

(b)

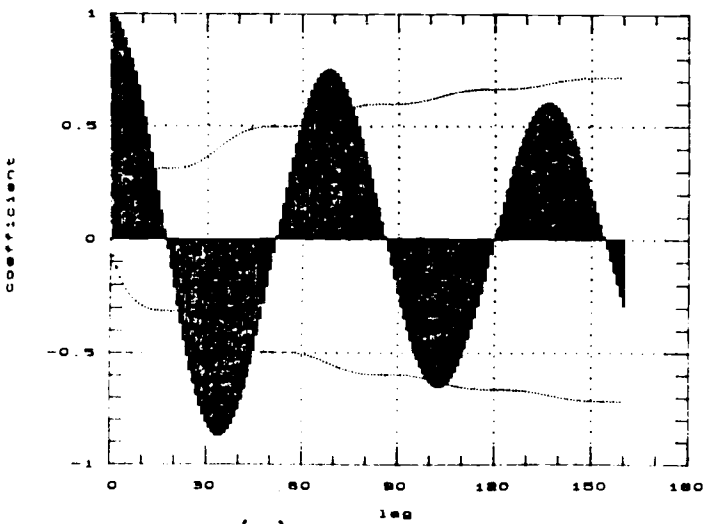

(c)

Figure (39)

Autocorrelation Coefficient Plots of Pressure Drop for Batch Fluidization.
a) P_{av} = 0.23 psi
b) P_{av} = 0.49 psi
c) P_{av} = 0.81 psi

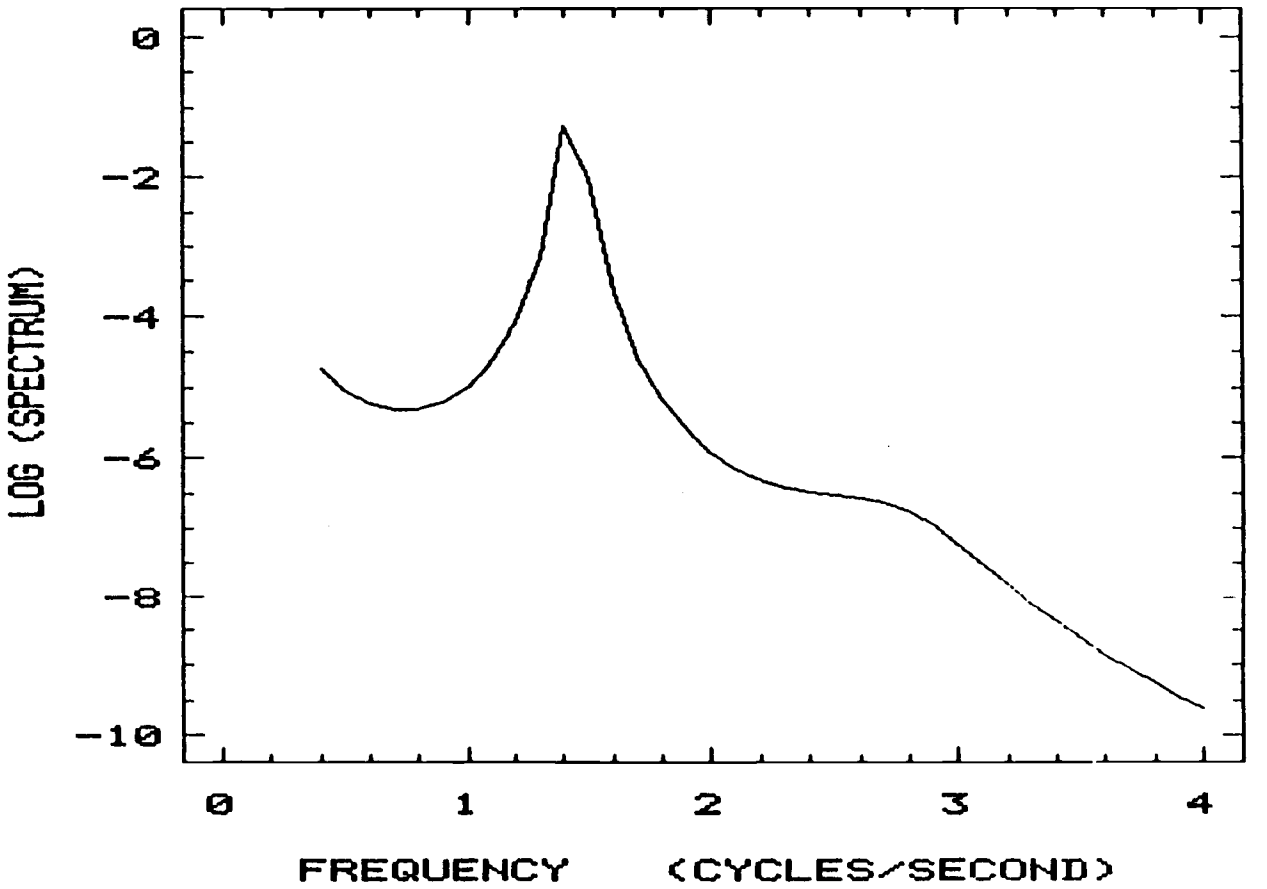

Figure (40) Power Spectrum Plots of Pressure Drop for Batch Fluidization for P_{av} = 0.81 psi.

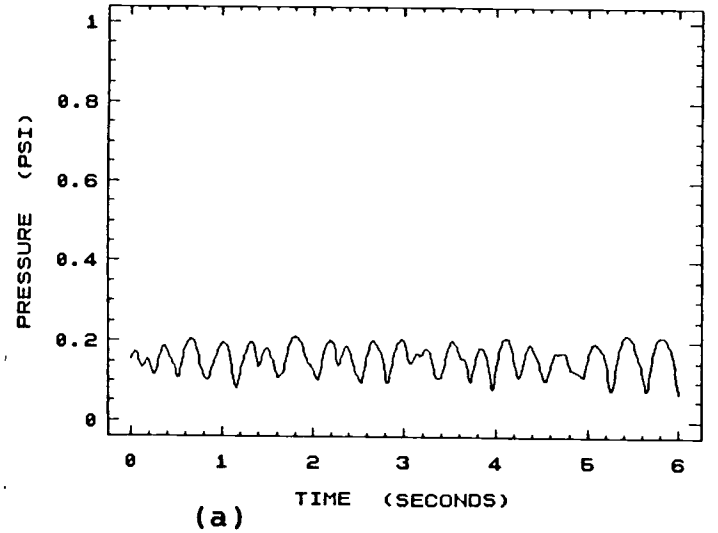

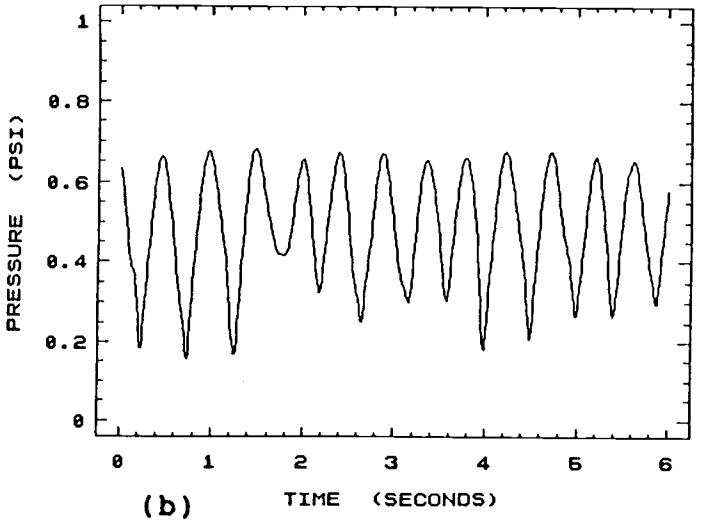

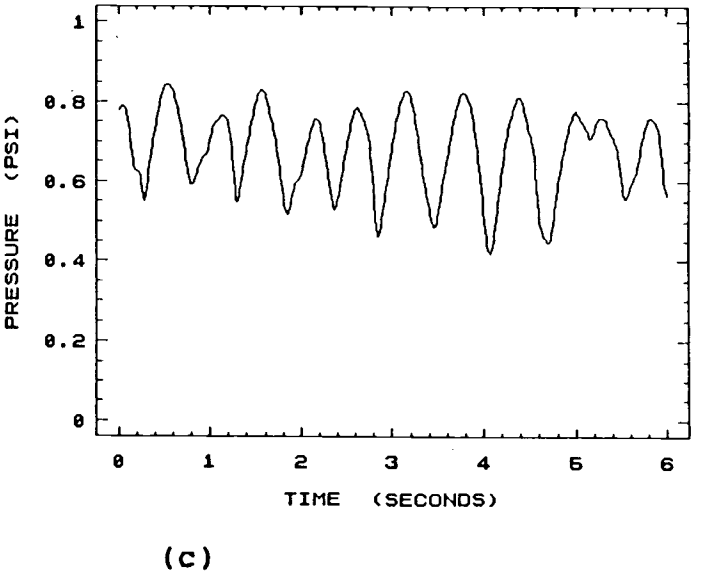

Figure (41)

Pressure Drop Signal's Plots for Continuous Solids Throughputs at Different Average Pressures.
a) P_{av} = .144 psi
b) P_{av} = 0.41 psi
c) P_{av} = 0.68 psi

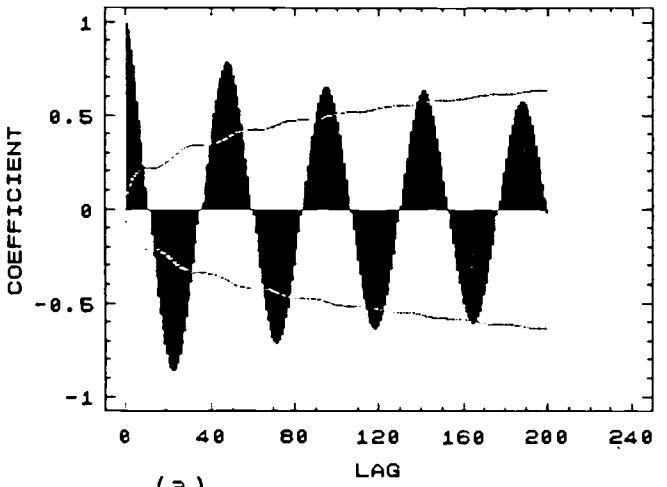

(a)

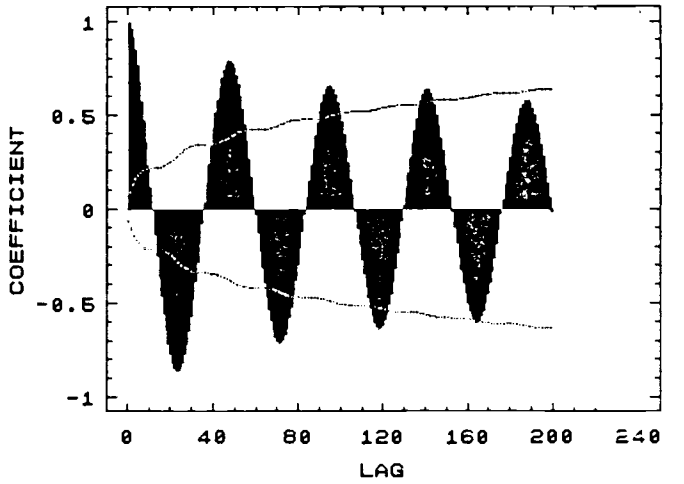

(b)

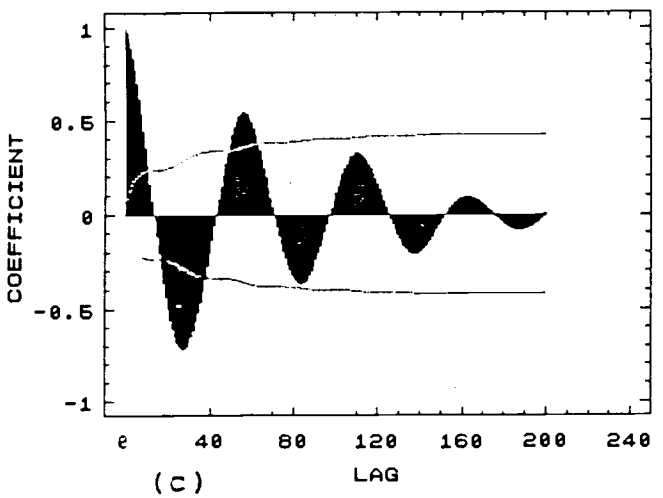

(c)

Figure (42)

Autocorrelation Coefficient of Pressure Drop for Continuous Solids Throughputs vs. Lag at Different Average Pressures.
a) P_{av} = .144 psi
b) P_{av} = .41 psi
c) P_{av} = .68 psi

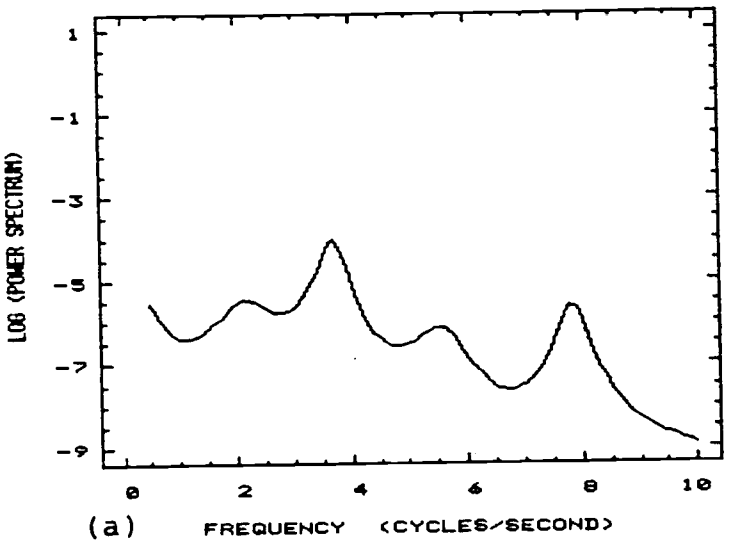

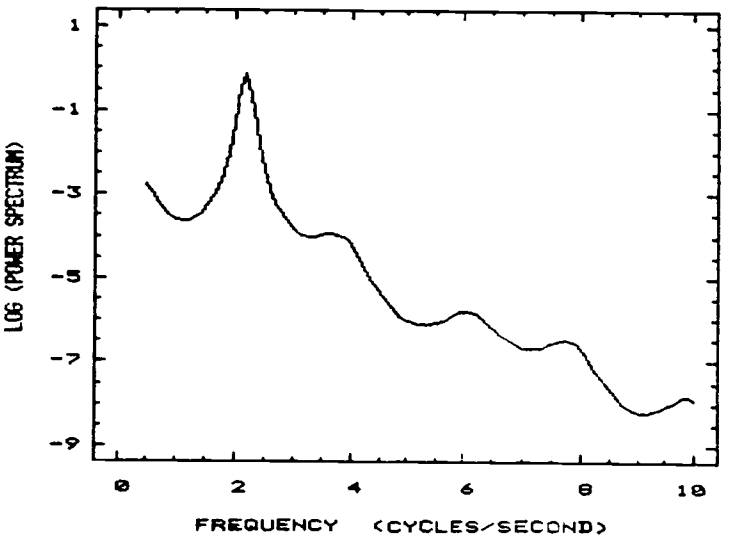

(b)

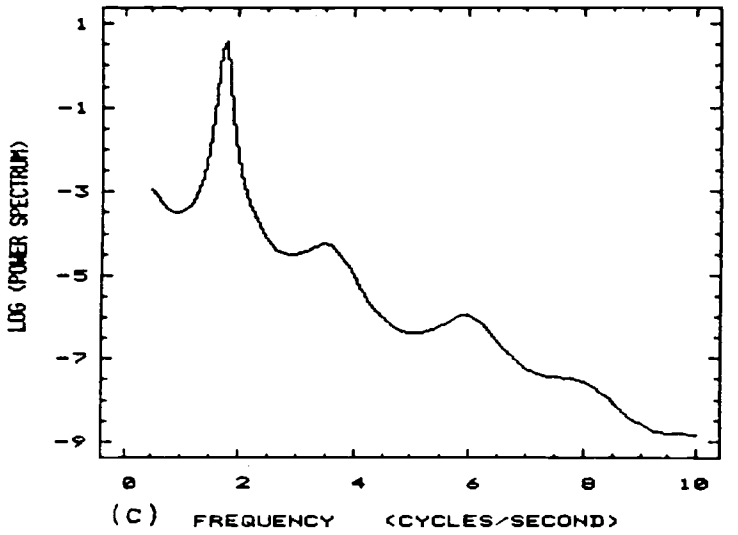

Figure (43)

Power Spectrum of Pressure Drop for Continuous Solids Throughputs.
a) P_{av} = 0.144 psi;
b) P_{av} = 0.41 psi;
c) P_{av} = 0.68 psi.

V.2.5 Determination of Dominant Amplitude and Frequency of Fluctuation Data Sets

The computational procedure for the autocorrelation coefficients and the pressure power spectrum are described in references [58] and [92]. The amplitude (A_{fl}) and frequency (f) of the pressure fluctuations are determined from the pressure spectrum. The amplitude is related to the peak height while the frequency is equal to the peak frequency. Measurment of the average pressure fluctuation's amplitude and frequency was also done by plotting all experimental data versus time then counting the cycles and determining the average amplitude to check those determined from the spectral analysis. The values were found to be nearly identical.

Tables [3] through [5] show values of the fundamental frequencies and amplitudes of the pressure fluctuations for different solids composition. The frequency of the pressure fluctuations is nearly constant and the amplitude slightly increases as the weight fraction of magnetic particles is varied from 1 to .25.

Table (3) Amplitudes and Frequencies Data Obtained From Spectral Analysis for 100% Iron.

Average Pressure Drop (PSI)	Amplitude (PSI)	Frequency (Cycles/sec.)
0.144	0.068	3.526
0.160	0.071	2.867
0.319	0.100	2.324
0.363	0.107	2.693
0.411	0.114	2.276
0.481	0.123	2.102
0.589	0.136	1.858
0.684	0.147	1.792

Table (4) Amplitudes and Frequencies Data Obtained from Spectral Analysis for 50% Iron.

Average Pressure Drop (PSI)	Amplitude (PSI)	Frequency (Cycles/sec.)
0.141	0.075	3.925
0.176	0.082	3.312
0.264	0.100	2.931
0.331	0.119	2.541
0.404	0.125	2.246
0.498	0.139	2.096
0.586	0.151	1.779

Table (5) Amplitudes and Frequencies Data from Spectral Analysis for 25% Iron.

Average Pressure (PSI)	Amplitude (PSI)	Frequency (Cycles/sec.)
0.120	0.073	4.55
0.170	0.088	3.57
0.250	0.106	3.12
0.330	0.122	2.41
0.390	0.132	2.13
0.500	0.150	2.02
0.560	0.158	1.83

V.2.6 Correlating Dominant Amplitude and Frequency Measurements With the Average Pressure Drop Across the Stage

Correlations for frequency and amplitude of the pressure fluctuations in the fluidized bed were obtained at different solids compositions (i.e. different densities) using linear regression after taking the log of each side of the equation. The correlations chosen have the following standard form used by other investigators: [9, 17 ,123]

1) frequency:

$$f = C_1 \, P_{avg}^{N_1} \tag{37}$$

2) amplitude:

$$A_{fl} = C_2 \, P_{avg}^{N_2} \tag{38}$$

values of C_1 and N_1 are shown in table (6) while those of C_2 and N_2 are shown in table (7).

Plots of the experimental data as well as the estimated model for the frequency of the pressure fluctuations versus the average pressure drop are shown in figures 45-a, b, and c, for magnetic weight fractions of 1, 0.5, and 0.25, respectively. Similar plots for the amplitude are shown in figures 46-a, b, and c. The correlations are obtained for the continuous solids throughput case at a controller

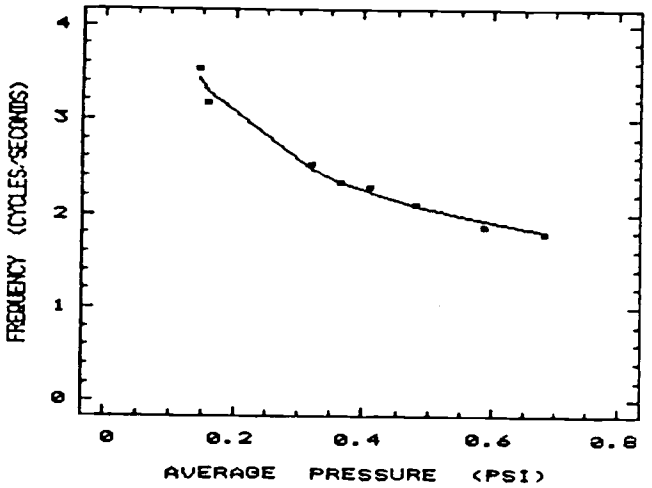

(a)

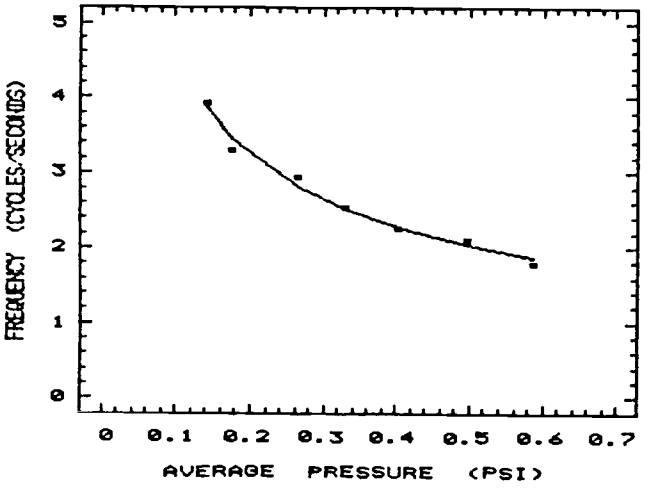

(b)

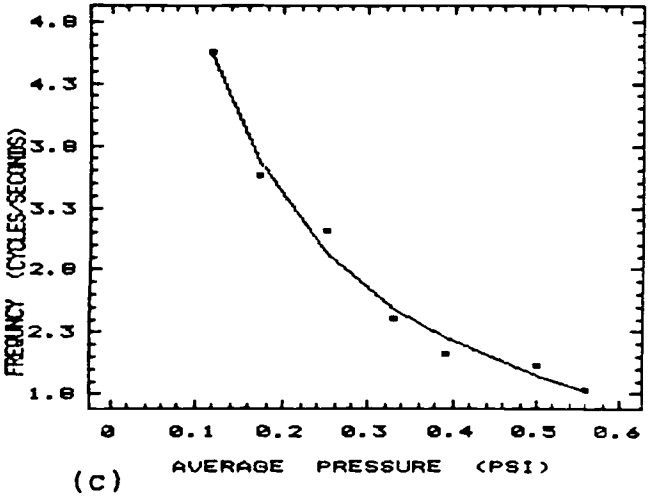

(c)

Figure (44)

Frequency vs. Average Pressure for.
a) 100% Iron; b) 50% Iron;
c) 25% Iron.

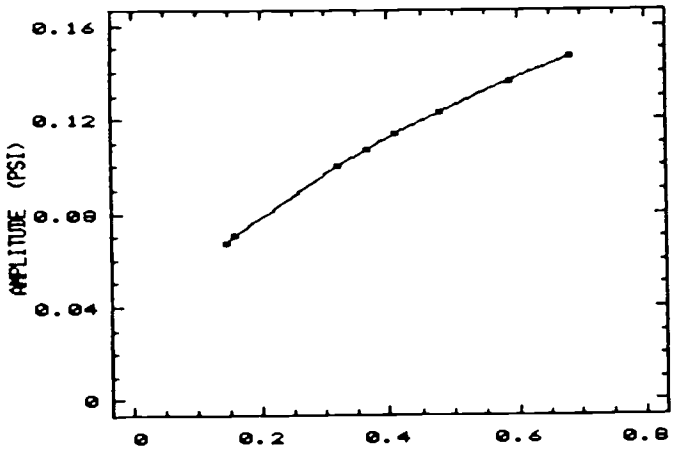

(a)

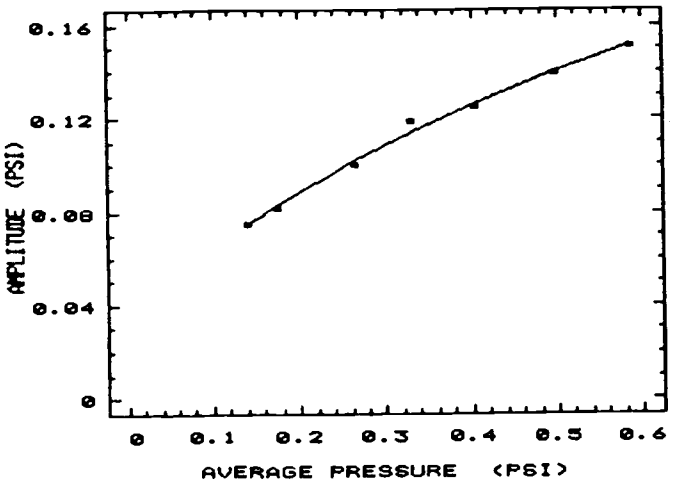

(b)

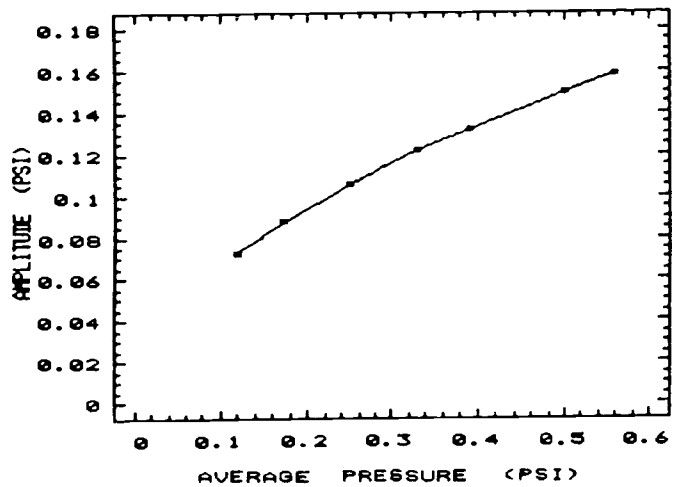

(c)

Figure (45)

Amplitude v.s. Average Pressure for.
a) 100% Iron; b) 50% Iron;
c) 25% Iron.

Table (6) Coefficients for Equation (37) at Various Weight Fractions of Iron in Solids.

Weight Fraction	C_2	N_2	R^2
1.0	1.538	-0.415	0.988
0.5	1.429	-0.509	0.984
0.25	1.291	-0.591	0.987

Table (7) Coefficients for Equation (38) at Various Weight Fractions of Iron in Solids.

Weight Fraction	C_2	N_2	R^2
1.0	0.178	0.500	1.00
0.5	0.197	0.496	0.99
0.25	0.211	0.498	1.00

sampling rate of 7.8 samples/second. Similar results at a controller sampling rate of 3.9 samples/second, as well as for the batch case, are presented in appendix D-4 and D-3, respectively. A comparison between these experimental frequencies and amplitudes to the theoretical values developed from a model is presented in appendix D-2. Also, the effect of gas velocity and the solids density on the pressure fluctuations are discussed in appendix D-2.

Figure (38) shows that the pressure fluctuations are actually unmodelled dynamics of the fluidized bed. If it is only noise then the curve wouldn't be smooth; instead some disturbances which are characteristic of the noise will appear along the curve. However, some noise, which is very small compared to the fluctuations, exists. That may be the reason of the fluctuations of the amplitude of the signal. The reproducibility of the pressure fluctuations over a large number of runs is further evidence of its dynamic characteristics, since if it were only random noise , the reproducibility would be very bad.

Modeling pressure fluctuations is not an easy task. It involves complicated mathematical procedures and even then may not describe the pressure fluctuations successfully. A very simple model of the pressure fluctuations is presented in appendix (D). In this model the pressure fluctuations are assumed to be sinusoidal. The frequencies and amplitu-

des calculated before are used to describe the fluctuations as follows:

$$P = P_{avg} + A_{fl} * COS(\omega * t) \tag{39}$$

where P = simulated pressure signal and

P_{av} = average pressure drop

ω = frequency (radians/second)

The model does not describe individual pressure fluctuations, however for controller design the model is adequate. The model has been used in simulations for estimating the filter time constant and other control parameters.

VI. SIMULATION PRELIMINARIES AND CLOSED-LOOP STUDIES FOR 100% IRON

VI.1. Introduction:

Most of the work in this thesis is done with pure magnetic solids. The dynamic behavior of the process and the other related variables (chapters III and IV) were studied using pure magnetic solids. The qualitative results are applied to the operation with mixtures (chapters VII and VIII).

The first part of this chapter will be a discussion on the control related topics such as the interactions among the stages and the various control parameters. The results and discussion of this section could be applied to mixtures (chapters VII and VIII). However, some minor differences exist and will be noted in the proper chapter.

The second part of this chapter is about the controller design, the performance simulation and the experimental performance. This part is for 100% iron only.

VI.1.1 Preliminary Studies for the Closed-Loop Simulation

Possible Problems:

From the previous studies, the following possible problems arose:

- The process is open-loop unstable
- The existence of the interaction among the stages
- Input (manipulated variables) constraints leading to non-linear behavior

Results:

- The choice of manipulated variable, filtering of process measurement, discrete time sampling system and control algorithm were found to give stable steady-state operation of the staged fluidized bed.
- Step disturbances in solids feed flow to the staged fluidized bed and setpoint changes to individual stages were found to require different actions depending on the direction of the change. Interactions in the worst case required coordination of the controllers on all three stages controllers.

- The worst case upsets to the staged fluidized bed were determined and incorporate non-linear control elements were incorporated to compensate for input constraints.

VI.1.2 The Equations Used in the Simulation

Material balance:

Top stage

$$\frac{d\ \Delta P_{av}\ (1)}{dt} = \alpha\ (m_i - m_o\ (1)\ ) \tag{40}$$

Middle stage

$$\frac{d\Delta P_{av}\ (2)}{dt} = \alpha\ (m_o\ (1) - m_o\ (2)) \tag{41}$$

Bottom stage

$$\frac{d\Delta P_{av}\ (3)}{dt} = \alpha\ (m_o\ (2) - m_o\ (3) \tag{42}$$

where:

$$\alpha = \frac{g}{A_{cs}\ g_c}$$

m_i = solids flow rate from the hopper into the top stage

$m_{o(i)}$ = solids flow rate from i^{th} stage

m_o has the following general forms:

In terms of fraction open:

$$m_o = C^*_1 + C^*_2 * FR + C^*_3 * FR^2 \tag{43}$$

In terms of current:

$$m_o = K_3 I^2 - K_4 I + K_5 \tag{44}$$

The constants K_3, K_4, K_5, C^*_1, C^*_2, and C^*_3 are determined by linear fitting of the experimental data. Those constants are functions of the solids' physical and magnetic properties, the fluidizing fluid's physical properties, etc. The different expressions with the determined constants will be presented in the subsequent chapters.

- The relations between the pressure drop across the bed and the settled height (h_s).

$$\Delta P = S_1 * H_s \tag{45}$$

where S_1 is determined experimentally . It has different values for different weight fractions of magnetic particles.

- The simulated pressure signal

$$P = P_{av} + A_{fl} * COS\ (Wt) \tag{46}$$

This signal is to be filtered then used for calculating the controller output which is either the fraction open or current depending on the type of manipulated variable. The controller output is then used in the expression for the flow rate of solids from the stage valve (m_o). The mass balance equations are integrated to give an average value of the pressure drop across the stage.

- The frequency and amplitude of the pressure fluctuations are calculated using equations that have the following general forms as discussed in chapter V.

$$A = C1 * \Delta P_{av}^{N1}$$

$$f = C2 * \Delta P_{av}^{N2} \tag{47}$$

The constants N_1, N_2, C1 and C2 are calculated by non-linear curve fitting to experimental data.

VI.1.3 Interactions Between the Stages

Equations (40), (41), and (42) can be rewritten in the following form:

$$\underset{\sim}{P}_{av} = \alpha \underset{\sim}{A} \underset{\sim}{m}_o + \alpha \underset{\sim}{B} \underset{\sim}{m}_i \tag{48}$$

Where :

$$\underset{\sim}{A} = \begin{bmatrix} -1 & 0 & 0 \\ 1 & -1 & 0 \\ 0 & 1 & -1 \end{bmatrix} ; \qquad \underset{\sim}{B} = \begin{bmatrix} 1 \\ 0 \\ 0 \end{bmatrix}$$

$$\underset{\sim}{P}_{av} = \begin{bmatrix} \dfrac{d\ P_{av}\ (1)}{dt} \\ \dfrac{d\ P_{av}\ (2)}{dt} \\ \dfrac{d\ P_{av}\ (3)}{dt} \end{bmatrix} ; \qquad \underset{\sim}{m}o = \begin{bmatrix} m_o\ (1) \\ m_o\ (2) \\ m_o\ (3) \end{bmatrix} ; \qquad \underset{\sim}{m}_i = \begin{bmatrix} m_i\ (1) \\ m_i\ (2) \\ m_i\ (3) \end{bmatrix}$$

The structure of the matrix A shows a one-way interaction between the stages. Figure (46) is the closed loop block diagram and clearly shows the one way interaction.

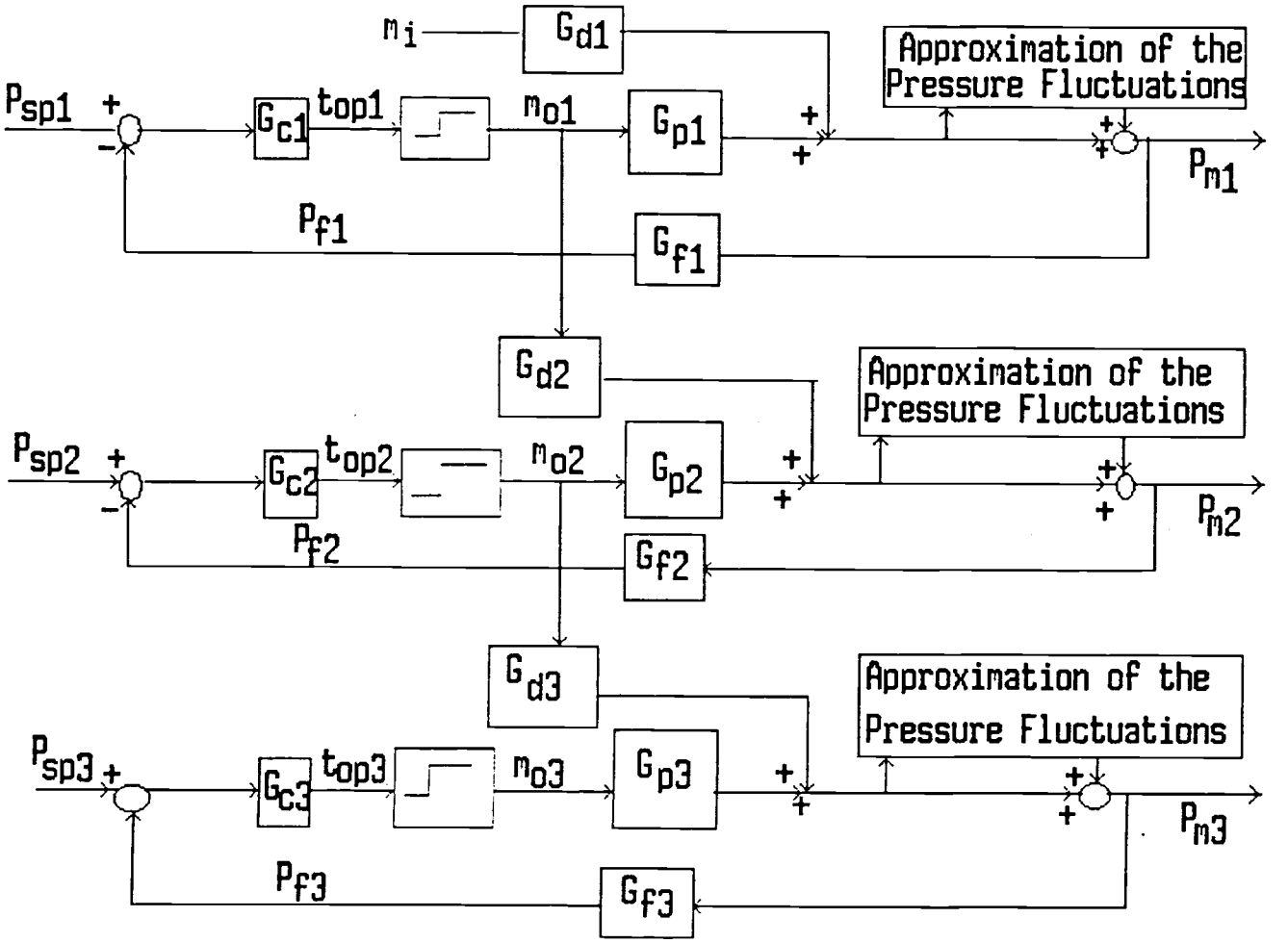

Figure (46) The Closed-loop Block Diagram of the Multi-Staged Fluidized Bed.

$$G_p = \text{process transfer function} = -\frac{\alpha}{s} \tag{49}$$

$$G_d = \frac{\alpha}{s} \tag{50}$$

$$G_f = \frac{1}{\tau_f s + 1} \tag{51}$$

s = Laplace transform variable

According to control theory, a proportional controller can control an integrator type process adequately and requires the least amount of calculation. It was mentioned previously that the sample time for the controller should be as small as possible. The objective was to determine the simplest controller in order that a minimum sampling time could be used to control the process adequately. Proportional control, when augmented with some simple logic statements, was found to be adequate to control the average pressure drop (ΔP_{av}) values of the staged fluidized bed.

Therefore:

$G_{ci} = K_{ci} = K_i$, the same gain for all three controllers.

Interactions between the stages were found to be worse when a large setpoint change or large disturbance in the feed flow rate of solids onto the top stage is made. A negative change in the setpoint in the top stage causes nearly a sharp pulse disturbance to the middle and bottom stages. The height and width of the pulse depends on how large the change is in the top stage's setpoint. The negative change in the setpoint of the middle stage similarly upsets the bottom stage, but, has little effect on the top stage. Positive change in any setpoint could be done without significant interactions using only proportional controllers.

VI.1.4 Decoupling

In order to further reduce the interactions observed between the stages, a logic-based decoupler was developed. The conventional analysis based on relative gain array (RGA) does not apply in this work because the process is open-loop unstable.

The decoupler performs a feed forward-like function. A stage is considered to be critical whenever the error on that stage is negative and larger than a certain size. The decoupler then overrides controllers on stages below the critical stage and attempts to match all outlet flow rates to the outlet flow rate from the critical stage. Ideally,

this would prevent the upset to the critical stage from affecting any others. In practice, this override was found to be needed only when the critical error is large. Once that error is reduced, individual controllers again provide good control.

From equations (40), (41), and (42), the average pressure drop across the bed can be kept constant at the setpoint value by setting the derivative to zero.

$$\frac{d\Delta P_{av}(1)}{dt} = \frac{d\Delta P_{av}(2)}{dt} = \frac{d\Delta P_{av}(3)}{dt} = 0 \qquad (52)$$

This gives the following equations:

$$\begin{aligned} m_o(1) &= m_i \\ m_o(2) &= m_o(1) \\ m_o(3) &= m_o(1) \end{aligned} \qquad (53)$$

In the absence of large positive errors, each stage is controlled individually for the following reasons:

- All of the modeling is done on the basis of the average values of all the variables involved. However, with fluidization taking place, the actual

process, the flow rate of solids out of the stage, the average pressure drop across the bed, the flow rate of solids into the top stage, and the flow of air into the bed are not constant but fluctuate with time. In addition, the air flow profile along the cross section of the bed is not uniform. It changes when the flow rate of solids changes and it may be different from one stage to another.

- Dependency of the frequency and amplitude of the pressure drop fluctuations on the average pressure drop across the bed.
- The desire to be able to manipulate the pressure drop across each individual stage independently.

Load and setpoint changes to each stage were investigated. It was found that the most difficult situations to control were the following:

- Negative setpoint change in top stage

Set

$m_o\ (2) = m_o\ (1)$

$$\text{when} \quad P_{av}|_{sp} - P_{av}|_{m} < -0.05 \qquad (54)$$

$m_o\ (3) = m_o\ (1)$

- Negative setpoint change in the middle stage

Set

$$m_o\ (3) = m_o\ (2) \qquad \text{when} \qquad P_{av}|_{sp} - P_{av}|_m < -0.05 \qquad (55)$$

Values of the limit greater than -.05 psi were found to cause undershoot while values smaller than -.05 did not promote adequate decoupling.

While the decoupler was found to work well in all situations with pure magnetic particles, additional problems with mixtures of low magnetic particles content required further modification of the control algorithm. The discussion of these problems and controller modifications are in chapter VIII.

A simple analogy can be made of an individual stage with the liquid level control of a tank when the outlet flow is manipulated by a constant displacement pump (figure 47). The level of the liquid in the tank will be maintained at a certain value as long as $F_o = F_i$. However, if a small change in the flow rate of the liquid into the tank is introduced the level will either go down to zero or increase until the tank is flooded.

The open loop studies done in chapter III exhibit such an open-loop behavior. Therefore, control of each stage is necessary to maintain constant solids inventories.The closed-loop block diagram is shown in figure (47). The closed-loop transfer functions have the following forms:

$$\frac{y}{y_{sp}} = \frac{K_c\ K_p}{s + K_c\ K_p} \tag{56}$$

$$\frac{y}{d} = \frac{K_d}{s + K_c\ K_p} \qquad K_p = K_d \tag{57}$$

For a unit step change in the set point

$$y = \frac{K_c\ K_p}{s + K_c\ K_p} * \frac{1}{s}$$

From the final value theorem:

$$\lim_{s \to 0} s\ y = 1$$

Therefore, the offset = y_{sp} - Lim sy = 1 - 1 = 0

For a load unit step change

$$y = \frac{K_d}{s + K_c\ K_p} * \frac{1}{s}$$

and $$\lim_{s \to 0} s\ y = \frac{K_d}{K_c\ K_p} = \frac{1}{K_c}$$

Therefore, offset = $0 - \frac{1}{K_c} = \frac{-1}{K_c} \# 0$

The last analysis indicates that the pressure drop across each stage can be controlled effectively with proportional control for changes in the set point. For load changes, the offset $1/k_c$ may be acceptable for some K_c. To eliminate the offset completely:

$$K_c = \frac{K_d}{K_p} \tag{58}$$

but values of K_d and K_p were not estimated for the process of this thesis because the process is open-loop unstable and non-linear.

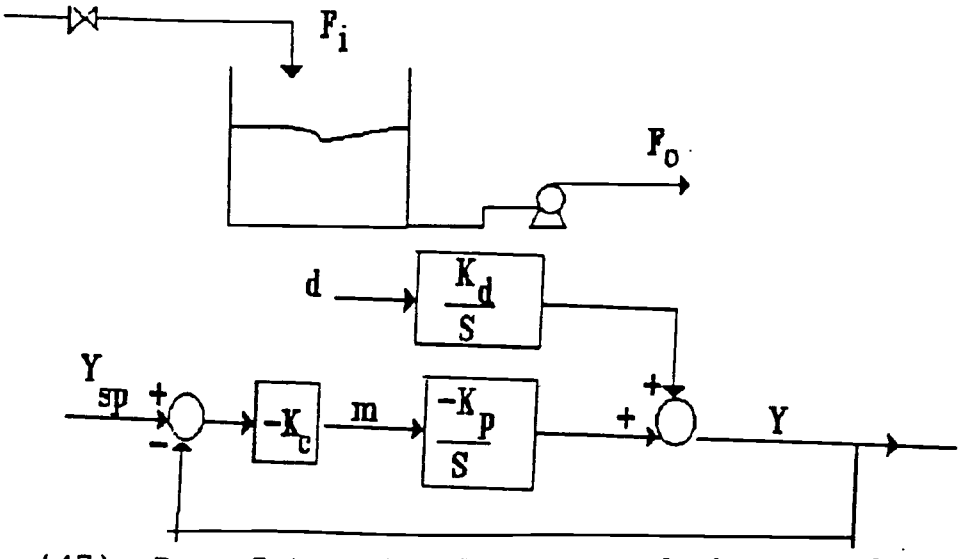

Figure (47) Pure Integrator Process and the Corredponding Closed-loop Block Diagram.

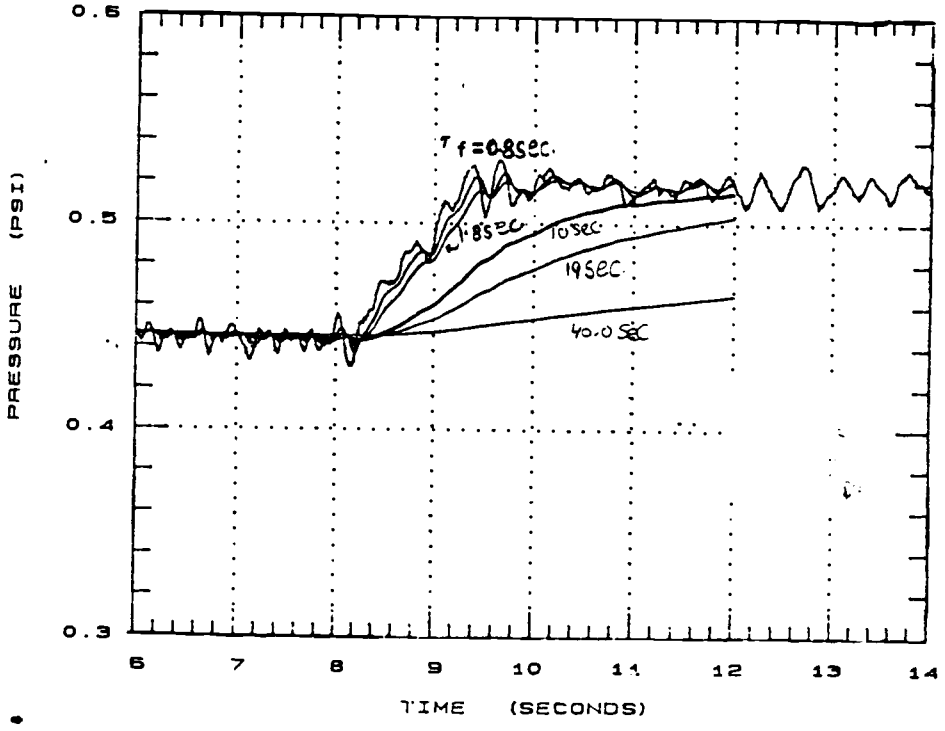

Figure (48) Average Pressure Drop Across a Stage v.s. Time for Different Values of Filter Time Constants.

VI.1.5 Design of Control System Parameters via Simulation

The following control system parameters are determined through the use of simulation:

1) On/off Operation:

- K_c The controller gain which is the same for all the stages (psi/millisecond)
- τ_f Filter time constant (seconds)
- $t_{op\ max}$ The upper limit on the manipulated variable (the time during which the current should be zero, milliseconds)
- $t_{op\ min}$ The lower limit on the manipulated variable (milliseconds)

2) "Leaking" Valve Operation

- K_c The controller gain which is the same for all the controllers (psi/ampere).
- τ_f Filter time constant (seconds).
- I_h The upper limit on the manipulated variable (the current flowing through the valve, amperes).

I_r The lower limit on the manipulated variables (amperes).

A negative step change in the setpoint of -0.2 psi was introduced to the top stage and caused disturbances to the middle and bottom stages which can be assumed to have sharp pulse characteristics.

A series of simulations each of which has a simulation time of 4.1 minutes, which was found to be adequate to reach a new steady state, were made. One of the control parameter was changed by an increment in going from one simulation to another, while keeping the others constant. The integral square error of the pressure drop across the stage (ISQERR) and the integral square error of the manipulated variable (current or t_{op}, ISQMAN) were calculated for each simulation. At the beginning of this work, none of the control variables were known. Therefore, the value of T_f of 1.8 seconds used in the simulation is based on preliminary studies, figure (48). The upper and lower limit values of the manipulated variables were chosen to be equal to 128 and zero milliseconds for the on/off operation and I_h and I_r for the "leaking" valve operation. K_c was the first parameter incremented.

Figure (49) shows a block diagram of the simulation program used for the closed-loop performance and the calculations of ISQERR and ISQMAN versus control system parameters.

Figure (50) shows the plots of ISQERR and ISQMAN versus time. The area under each curve represents one point on the plot of ISQERR or ISQMAN versus the control parameter. ISQERR and ISQMAN are calculated according to the following equations:

$$ISQERR = \int E^2 \, dt \tag{59}$$

$$ISQMAN = \int (U - U_s^2) \, dt \tag{60}$$

Which can be rewritten in the following discrete form:

$$ISQERR = ISQERR + E^2 * T_{samp} \tag{61}$$

$$ISQMAN = ISQMAN + (U - U_{ss})^2 * T_{samp} \tag{62}$$

T_{samp} = Sampling time

ΔP_f = filtered pressure signal

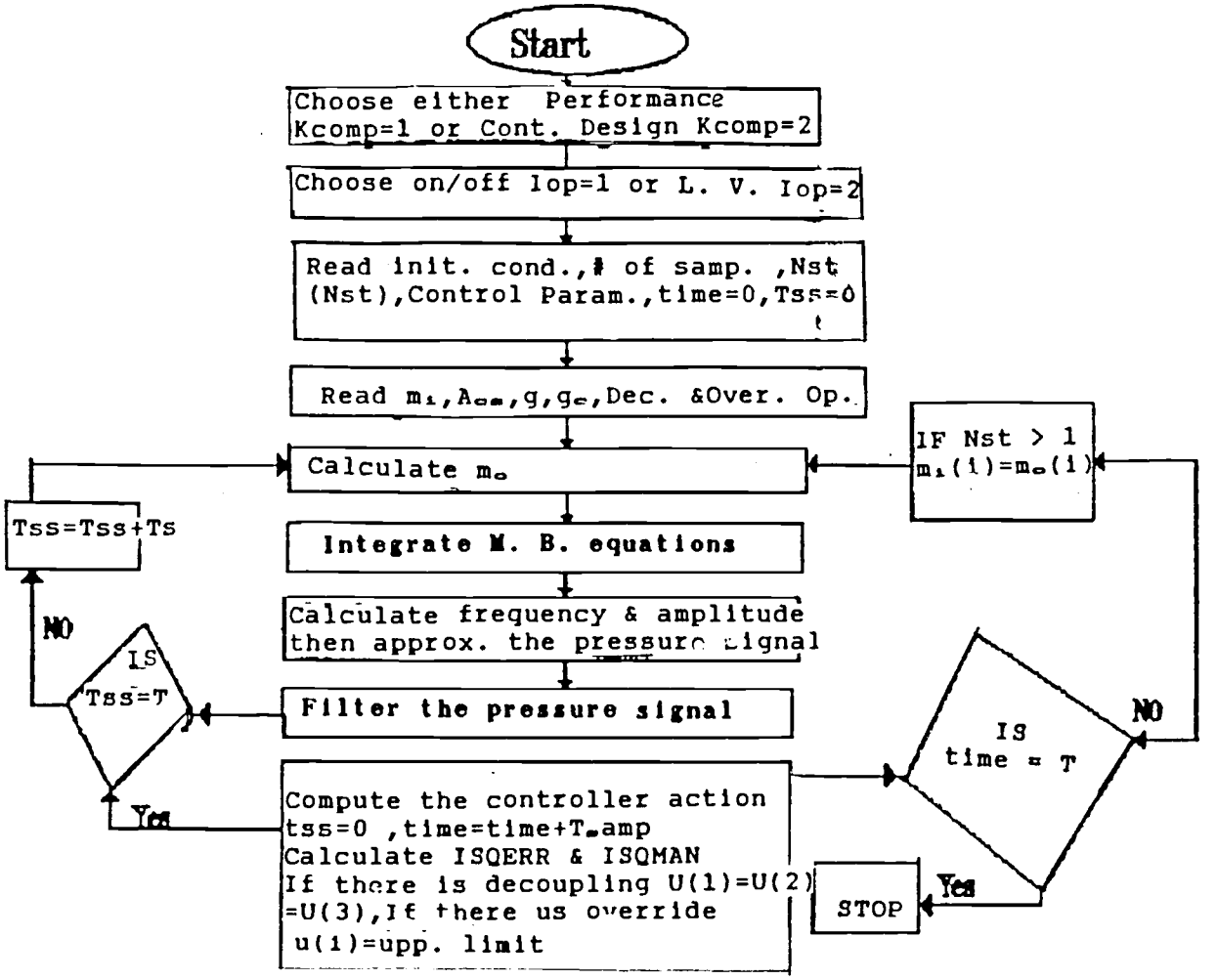

Figure (49) The block diagram for the simulation.

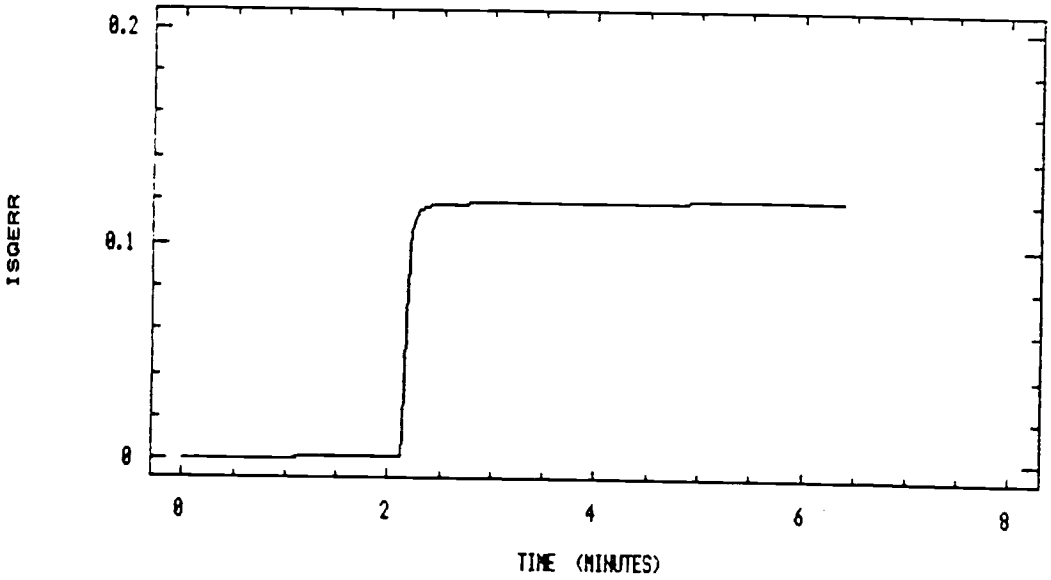

Setpoint Change at t=2 minutes

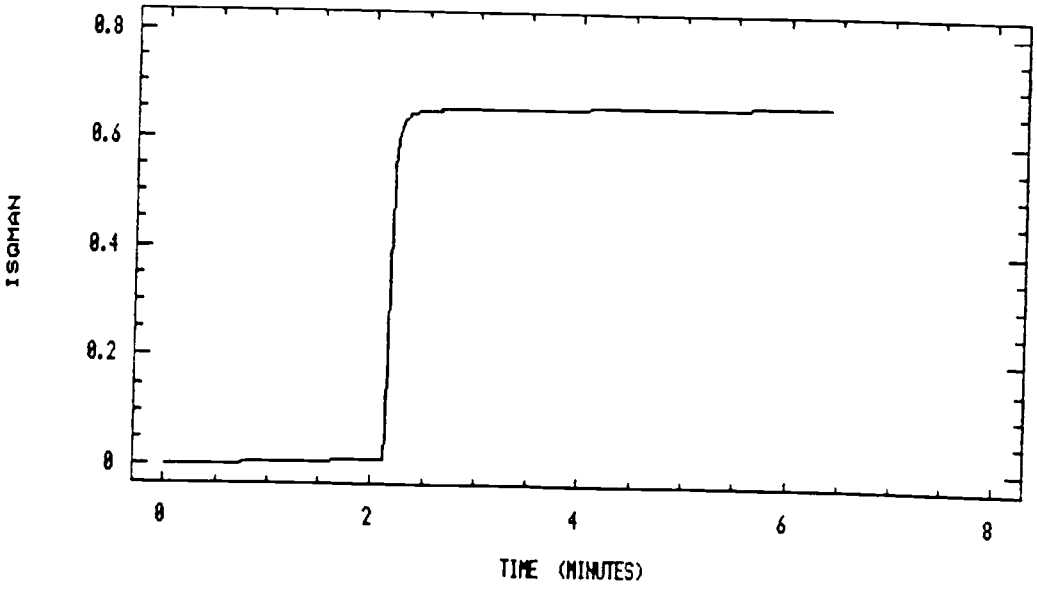

Figure (50) Plots of ISQERR and ISQMAN vs. Time.

U_{ss} = The value of the controller output at the initial steady state value which can be calculated from equations (43), (44), by setting $m_o = m_i$ and solving the quadratic equation.

The values of the previously mentioned control parameters were determined based on a trade-off between the performances of the process and the required input which is the controller output. The process input (controller output) is considered in the trade-off for the following reasons:

- The non-linear behavior of the process becomes stronger as the ($|U - U_{ss}|$) increases. The on/off control is approached as ($U - U_{ss}$) increases. Accordingly, the undesired pulse flow regime is approached.
- For mixtures that have low fraction of magnetic particles, the process might become unstable for large ($U - U_{ss}$). Large ($U - U_{ss}$) will cause the release of the solids layer attracted to the grates. The replacement of this layer is very slow because of the low weight fraction of the magnetic particles in the main bed.

- The wear-out of the power supply is more likely to happen for large $(U - U_{SS})$.

First, linear combinations of ISQERR and ISQMAN were considered, but the computations for any linear combination was found to have equivalent multiple local minimums. Therefore, the determination of the control system parameters was based on the careful inspection of plots and data of ISQERR and ISQMAN versus the control parameter in hand. The control parameter was selected so that the pressure performance (ISQERR) does not improve significantly by an increase/decrease of the control parameter. ISQMAN affected the decision on how improved the ISQERR was.

VI.2 Closed-Loop Studies for 100% Iron

Figure (51) shows the experimental data as well as the theoretical model obtained. The constants in the model of the solids flow rate through the valve written in terms of fraction open were first determined by linear regression of the experiment data to the form suggested by the fundamental model of section IV.3.1.5 (equation [26]). The following equation is the result of the fitting:

$$m_o = 1.39 - 5.81 * FR + 6.20 * FR^2 \qquad (63)$$

$$R^2 = 0.93$$

Comparing the above equation to the flow rate model out of the stage (equation [26]) results in the following:

$K_3 * I^2_W = 6.20$ $\quad K_3 = 2.83 * 10^{-4}$ $\quad (I_W = 148$ amps)

$2\ K_3\ I_{2W} - K_4\ I_W = 5.81$ $\quad K_4 = 0.0445$

$K_3 I^2_W - K_4\ I_W + K_5 = 1.39$ $\quad K_5 = 1.78$

The values of the constants are substituted in the expression relating them with the different parameters of the solids, the gas, and the bed.

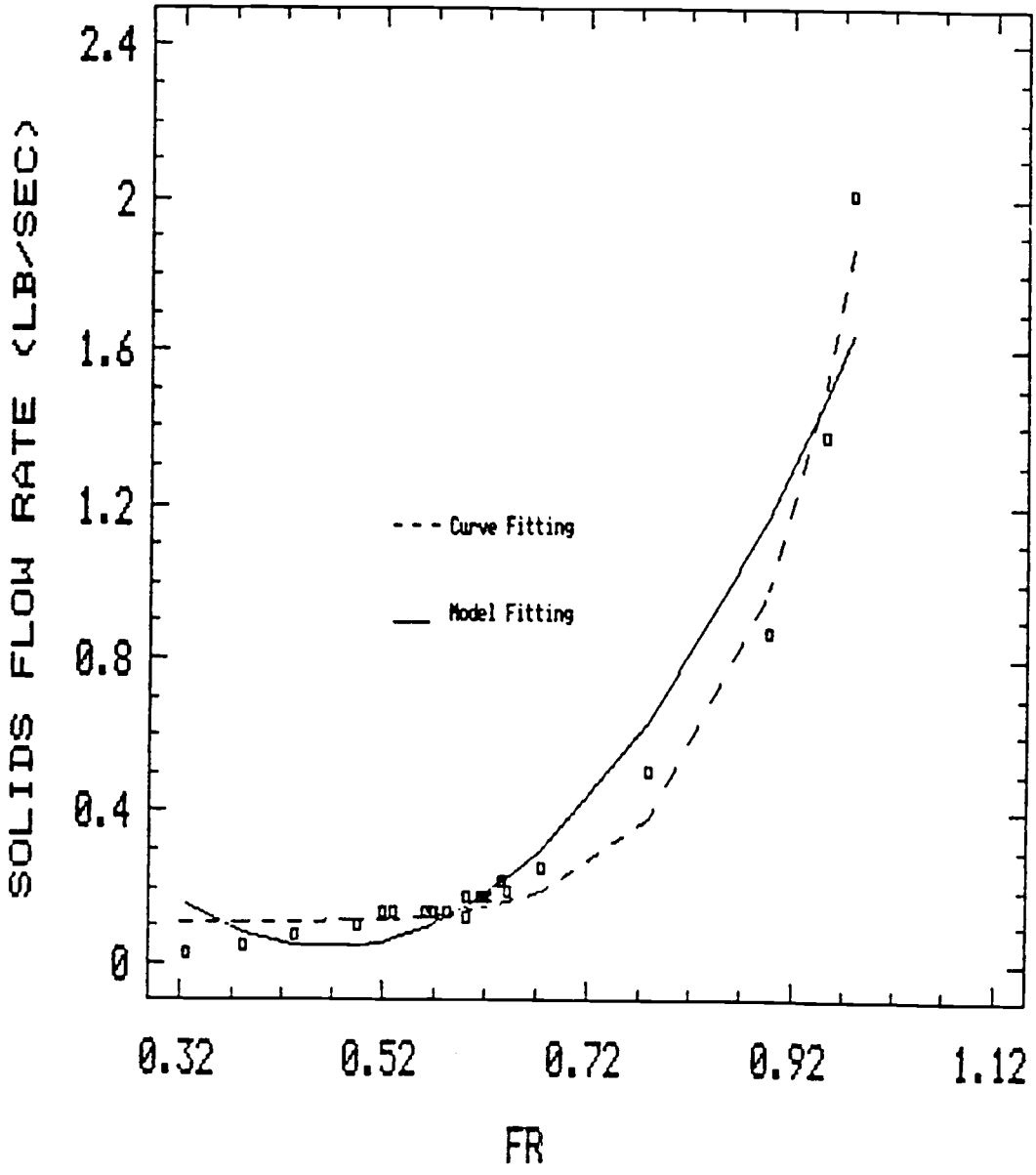

Figure (51) The Plots of the Flow Rate of Solids vs. Fraction Open for Experimental Data (points), the Fit to the Fundamental Model and the Curve Fitted Model.

The following are expressions after the substitution of the constants:

$$\frac{\bar{v}_p K_2}{8 \pi^2} \quad \frac{(\rho_s A_f)}{A_1} = 2.83*10^{-4}$$

$$K_3 K^* = 0.0445$$

$$\frac{\rho_s A_f}{A_1} [(A_{cs} \delta) (1 - \epsilon) \rho_s - A_1 U_g] = 1.78$$

By doing some algabriac substitutions and manipulations the following equations can be obtained:

$$\frac{(V_p K_2) * (\rho_s A_f)}{A_1} = 0.0223 \tag{64}$$

$$\frac{r B}{\mu_o} = 25.03 \tag{65}$$

$$\frac{\rho_s A_f}{A_1} = [(A_{cs} \delta) (1 - \epsilon) \rho_s - A_1 U_g] = 1.78 \tag{66}$$

A_f = the average cross-sectional area of the opening through which the solids flow

The fit of experimental data to the model is not particularly good ($R^2 = 0.92$). Therefore, the above results may have appreciable error and serve only as an order of magnitude estimate. Also, in the on/off operation, the

above value is an average value with a large standard deviation.

The following model for the solids flow rate through the stage is obtained by curve fitting of the experimental data using non-linear regression. The model is used in the simulation program for evaluation of controller parameters and simulation of the pressure and controller output performances.

$$M_o = 0.119 + 2.096 * FR^{8.503} \quad (67)$$

$$R^2 = 0.98 \text{ and,}$$

$$FR \geq 0.32$$

VI.2.1 Design of the Control System Parameters via Simulation

VI.2.1.1 Controller Gain

Figure (52) shows the plots ISQERR and ISQMAN versus the controller gain for the top, middle and bottom stages respectively. Each plot has two curves representing the error in pressure drop across the fluidized bed and the process input (fraction open).

The plots of ISQERR of the pressure drop versus the control gain are similar to each other for the three stages. For K_C greater than -200 ms/psi, ISQERR decreases rapidly

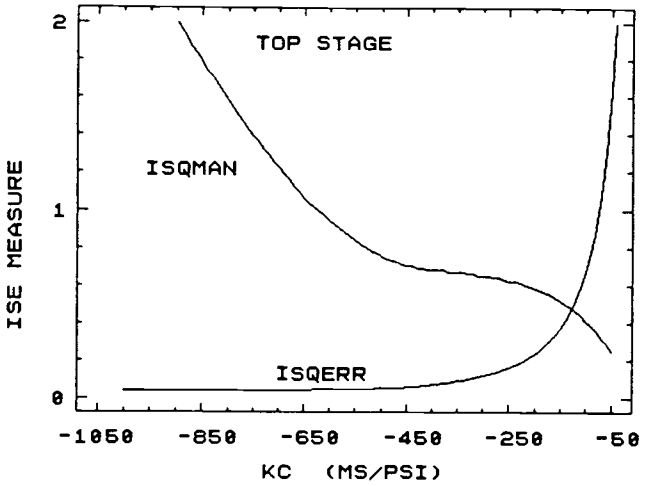

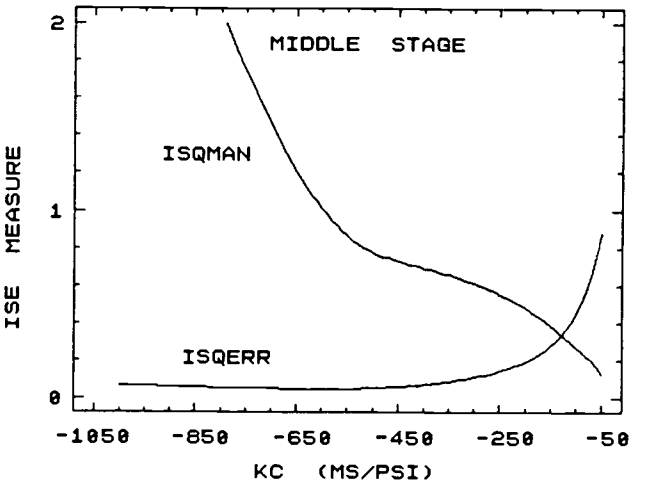

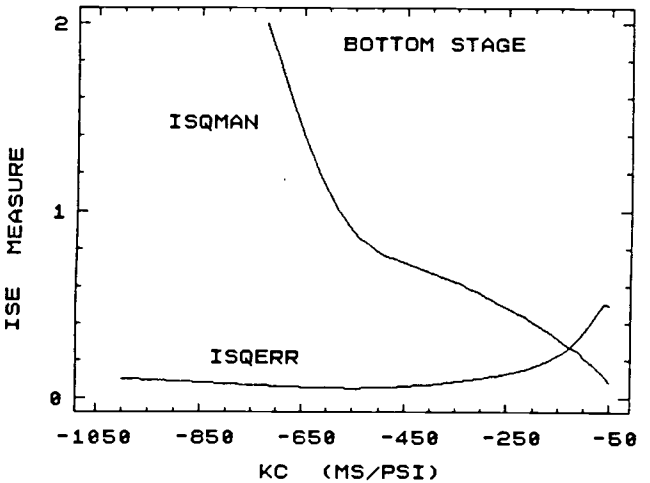

Figure (52)

Plots of ISQERR and ISQMAN for the Three Stages vs. the Controller Gain.

with decreasing controller gain. Then, ISQERR decreases slowly as K_C increases until a value of K_C reaches -450 ms/psi after which the decrease of ISQERR with K_C is negligible. The plots for the middle and bottom stages show a minimum at a value of k_C of -550 ms/psi.The corresponding curves for the required controller output (fraction open) shows an inflection point at a K_C value of-500 ms/psi. The change of ISQERR with respect to K_C decreases as K_C decreases until it reaches zero at the inflection point after which the rate of change increases rapidly. The rate of change of ISQERR for the top stage stays almost constant for K_C between -250 ms/psi and -500 ms/psi.

The choice of the controller gain was based on a tradeoff between the performance of the controller and process inputs as discussed in section VI.1.4. Based on this criteria, a value of -300 ms/psi was chosen to be used in both the closed loop simulation and the real process control.

VI.2.1.2 Filter Time Constant

Figure (53) shows the plots of ISQERR and ISQMAN versus the filter time constant. All the plots exhibit a minimum at filter time constant value of 1.8 seconds. The curves for the plots of ISQERR are smoother than those corresponding to the ISQMAN because of the wider range over which the controller output oscillates which is maximum when the setpoint change is introduced. Figure (48) shows the

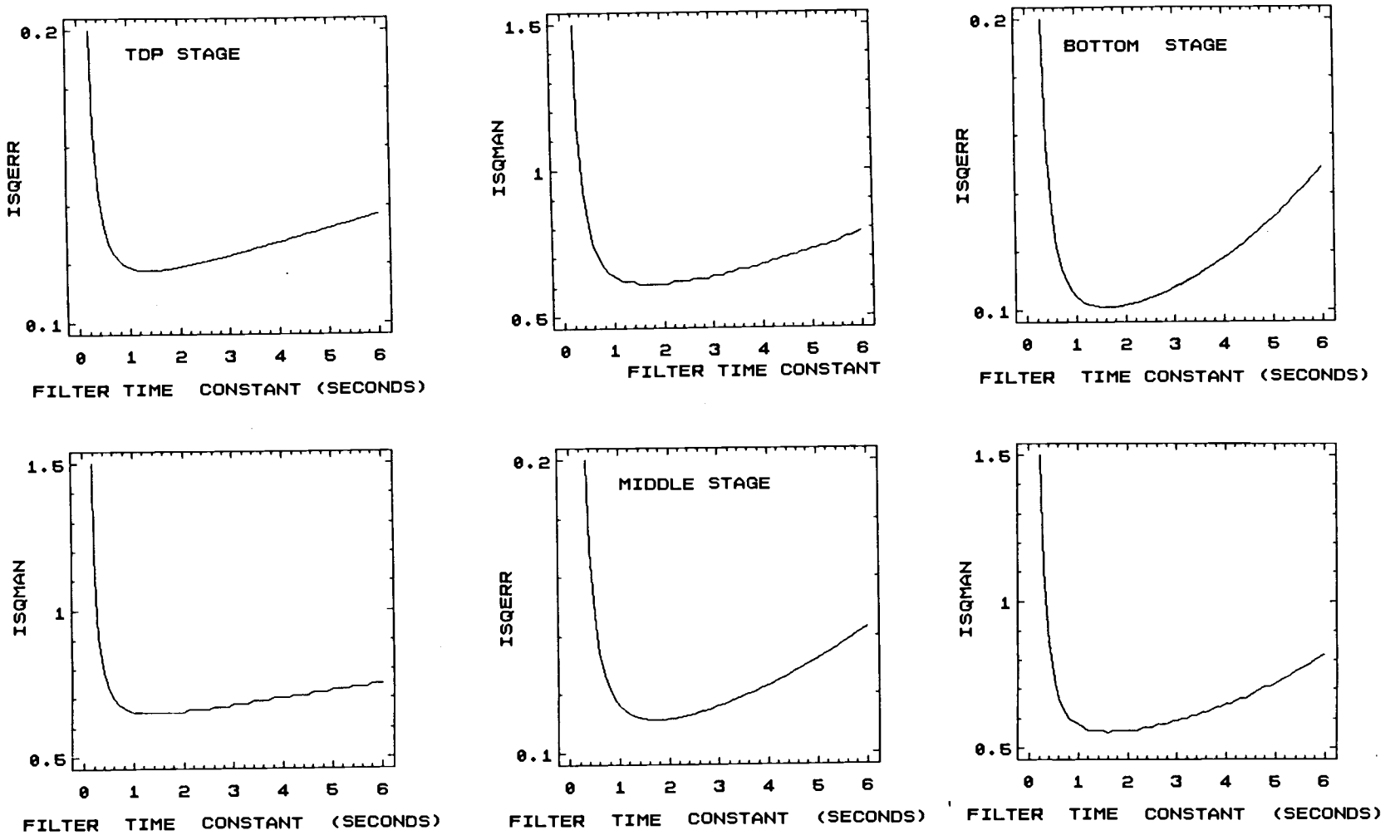

Figure (53) Plots of ISQERR and ISQMAN for the Three Stages vs. Filter Time Constant.

experimental plots of the pressure versus time for different values of the filter time constant. It shows that as the value of the filter time constant increases the response of the control system becomes more sluggish and the filter dynamics dominate. It shows that a choice of 1.8 seconds for the filter constant is effectively an optimal value. Substituting this value in equation (36) for the attenuation of pressure fluctuations gives:

$$\frac{A_{fl}}{A} = 0.01$$

Thus, the attenuation is satisfactory and a value of 1.8 seconds was chosen for the filter time constant.

VI.2.1.2 Input Constraints

Figure (54) shows the plots of ISQERR and ISQMAN versus the upper limit of the time during which the current is off (t_{opmax}). ISQERR for the top stage decreases gradually as the upper limit of t_{op} increases. The rate of change of ISQERR with respect to the $t_{op\ max}$ is large until $t_{op\ max}$ reaches a value of 106 milliseconds. The rate then decreases until a value of 116 ms, after which the ISQERR stays essentially constant.

The plots for the middle and bottom stages show different trends. However, the value of ISQERR and ISQMAN in

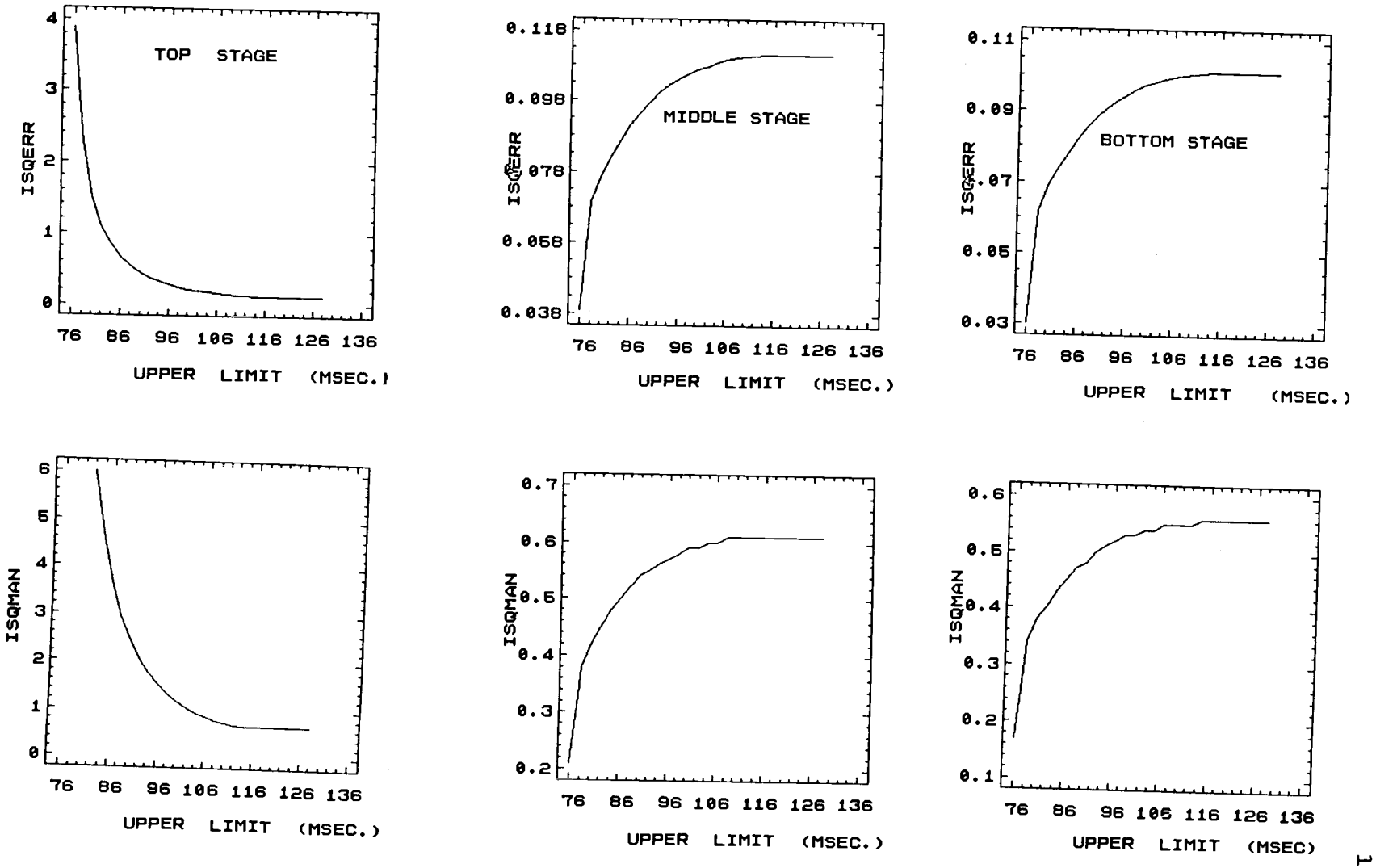

Figure (54) Plots of ISQERR and ISQMAN for the Three Stages vs. the Upper Limit.

those plots are small compared to that of the top stage. The ISQERR and ISQMAN both increase monotomically with increase in $t_{op\ max}$. The rate at which ISQERR increases is high until $t_{op\ max}$ reaches a value of 96 ms, then the rate decreases until it reaches zero at t_{opmax} = 112 ms. Therefore, the selection of the upper constraint of t_{op} will be based on the top stage. A value of 128 ms (FR = 1) was thus chosen as the upper constraint. This value was used in the closed-loop simulations and the experiments. The behaviors of the plots of the middle and the bottom stages are due to the interactions between the stages. The disturbances to the middle and bottom stages are pulses whose duration increases as $t_{op\ max}$ increases. This causes the ISQERR and ISQMAN of the middle and bottom stages to increase as t_{opmax} increases. Figure (55) shows simillar plots for t_{opmin} for three stages. The lower constraint does not affect the performance of either the controller or the pressure drop except at $t_{op\ min}$ less than 2 msec., where the ISQERRS increases very slightly. The figures show that ISQERR and ISQMAN decrease in going from the top stage to the bottom stage. This is further evidence that $t_{op\ min}$ has little effect on the performances of the controller and the pressure drop. The values of ISQERR and ISQMAN shown in figure (55) reflect those that would have been obtained without the existence of the lower constraint. Therefore, a value of 30 ms (which corresponds to zero flow of solids

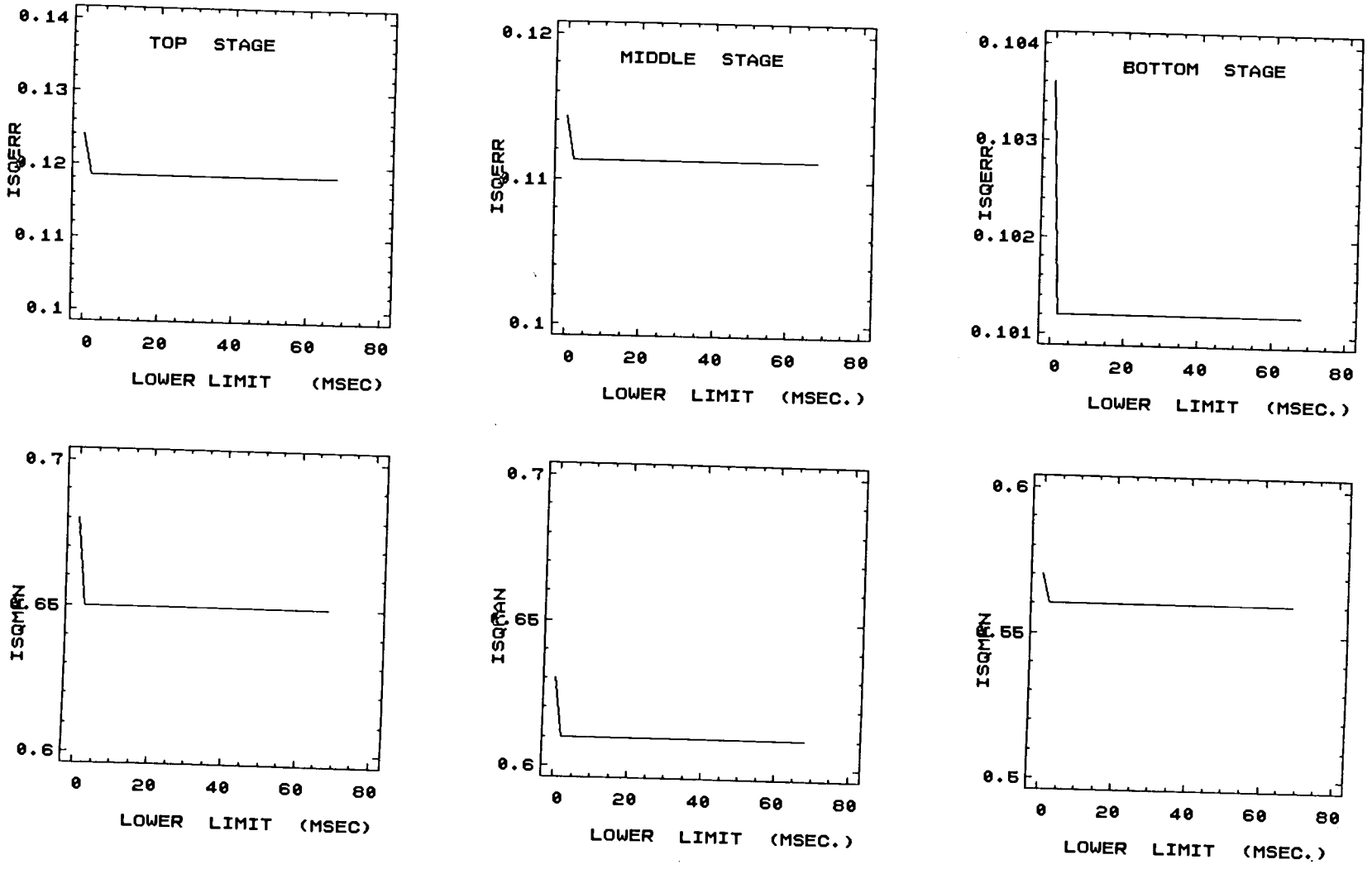

Figure (55) Plots of ISQERR and ISQMAN for the Three Stages vs. the Lower Limit.

of the stage valve) was taken to be the lower constraint of t_{op}.

VI.2.2 Simulated Closed-Loop Performance

VI.2.2.1 Negative Setpoint Change in the Pressure Drop Across a Stage

Figure (56) shows the simulated closed loop performance of the three stages. A negative setpoint change ($\Delta(\Delta P)_{sp}$ =-.20 psi) is introduced in the top stage. The control parameters used in the simulation are those determined previously and no decoupling was used. The pressure drop in the middle stage jumps from the setpoint value of 0.5 psi to a value of 0.64 psi. The disturbance to the pressure on the lower two stages can be assumed to be pulses. The pulse duration in the bottom stage is larger than that of the middle stage (sluggish behavior). The response of the pressure drop to the setpoint change in the top stage is very fast. The manipulated variables (fraction open) shown in the bottom part of the figure have pulse characteristics similar to those for the pressure. The valve is completely opened for the top stage when the step is introduced. Fraction open reaches a maximum value of 0.83 and 0.77 for the middle and the bottom stages respectively. The frequencies of the oscillations in the manipulated variables are similar to that of the pressure, but with larger amplitudes since the control enlarges them by a factor equal to the controller gain. Figure (57) shows the result of the simulation with

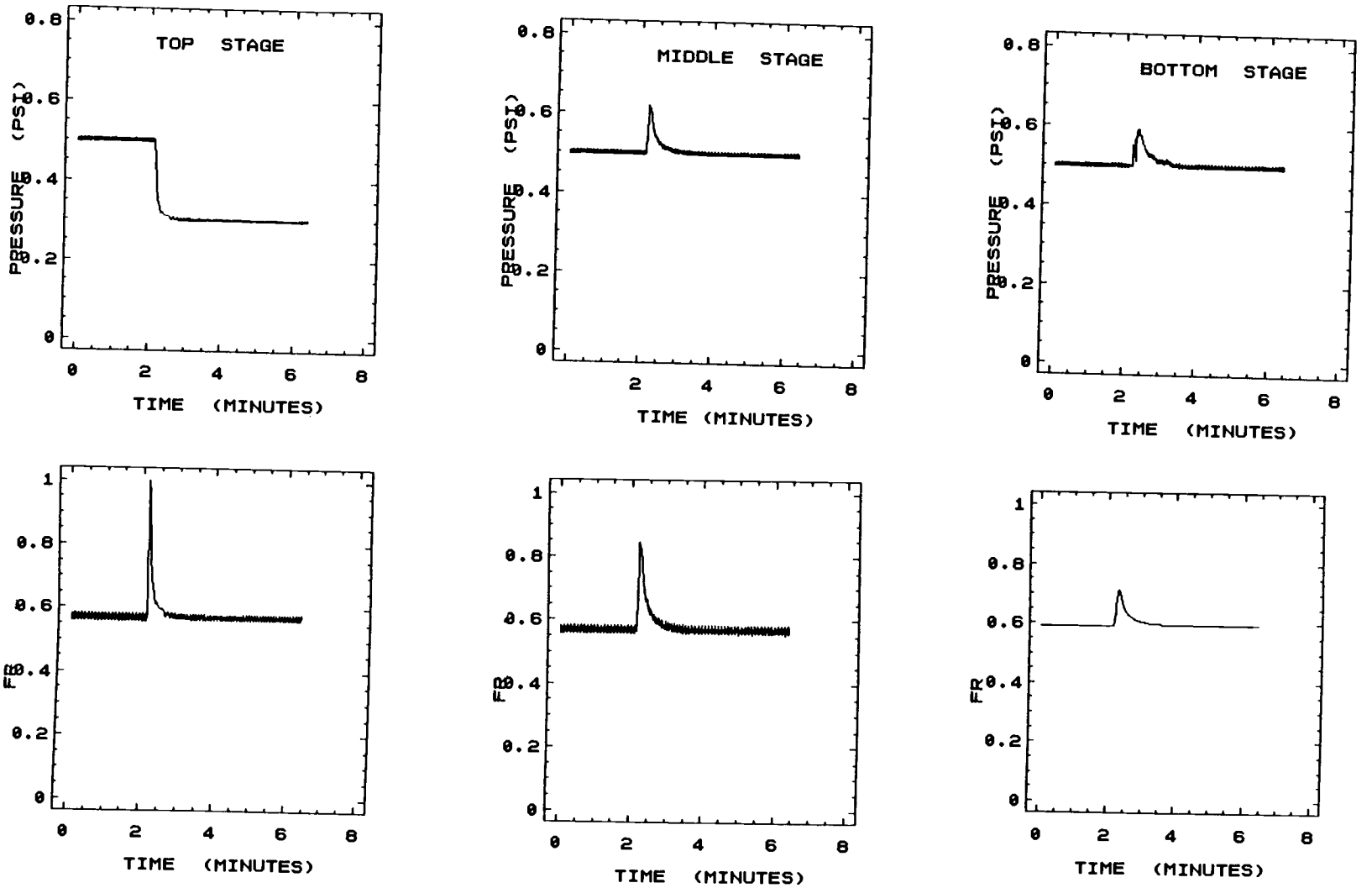

Figure (56) Simulated Closed-loop Performances for a -.20 psi Setpoint Change in the Top Stage without Decoupling.

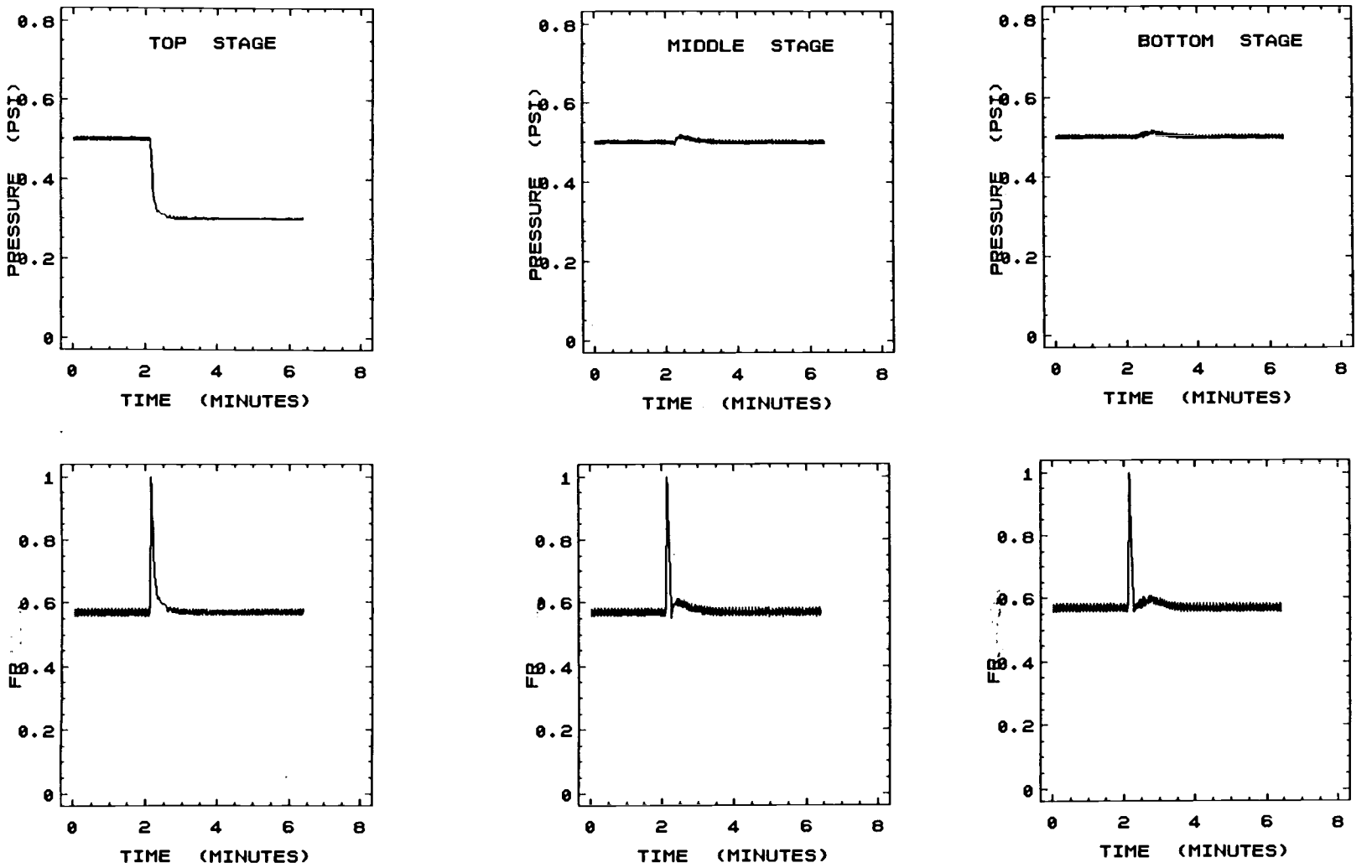

Figure (57) Simulated Closed-loop Performances for a -0.20 psi Setpoint Change in the Top Stage with Decoupling.

the same operating conditions as the last case except with decoupling implemented. The pressure performances for all the stages are excellent. The pressure in the middle and bottom stages is never more than 0.52 psi. Similar plots are shown in figure (58), when the negative setpoint change is introduced to the middle stage. The performance for the middle and the bottom stages are excellent. The performance for the top stage is not affected by the changes in the middle and bottom stages, as expected from the one-way interactions.

VI.2.2.2 Positive Step Change in the Feed Flow Rate of Solids

Figure (59) shows the closed loop performance when a positive step change in the feed flow rate (a disturbance) is introduced to the top stage. The pressure upset reaches a maximum value of -0.04 psi. According to the analysis done in section IV.1.3, some offset will result from the load changes. The amount of the offset predicted by the analysis is 0.12 psi. The simulated results show that the offset never exceeds 0.04 psi and it actually decreases very slowly with time with an offset of .03 at the end of the simulation.

It was mentioned previously that the steady-state value for the controller output can be determined by using

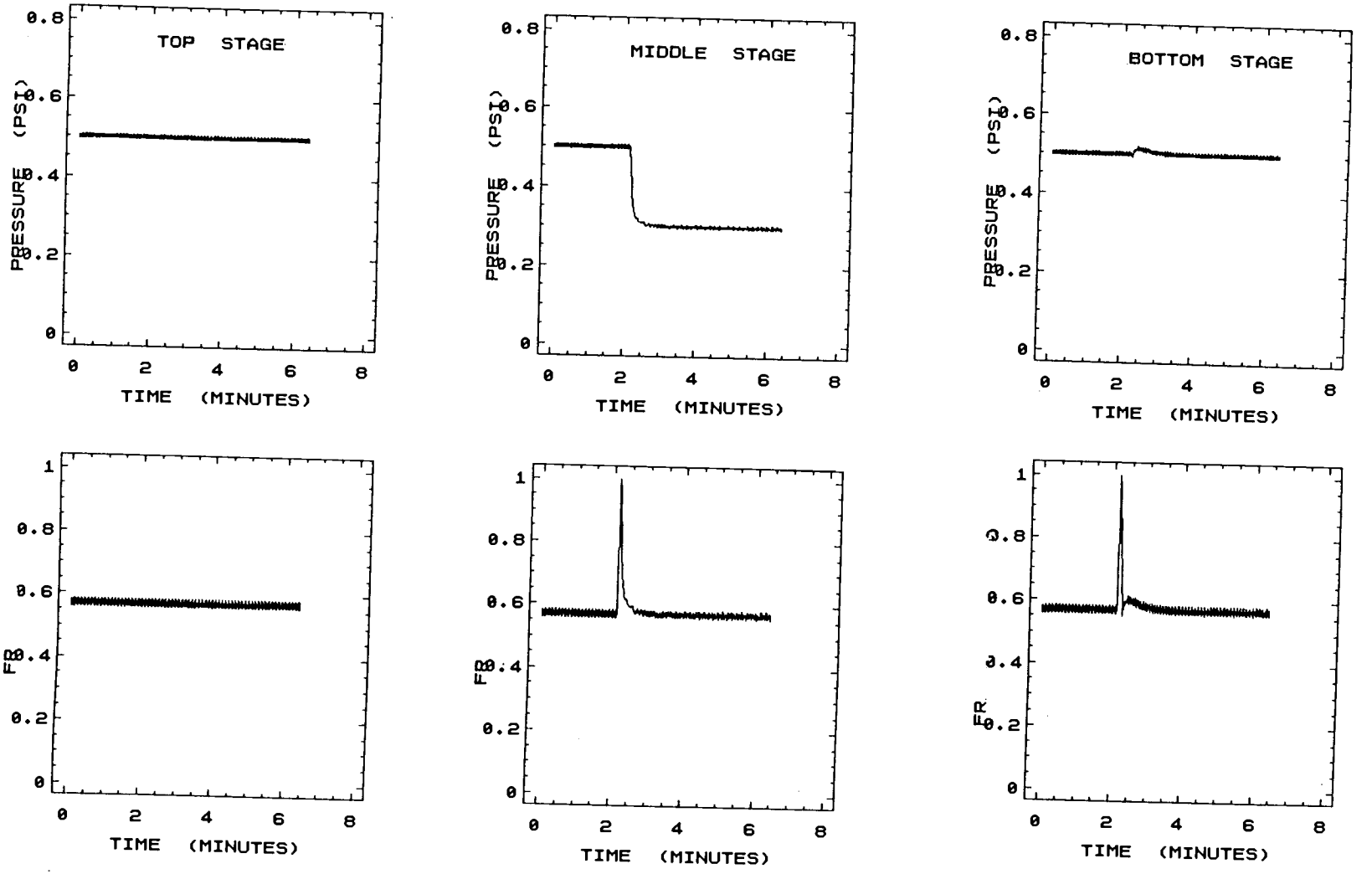

Figure (58) Simulated Closed-loop Performances for a -.2 psi Setpoint Change in the Middle Stage with Decoupling.

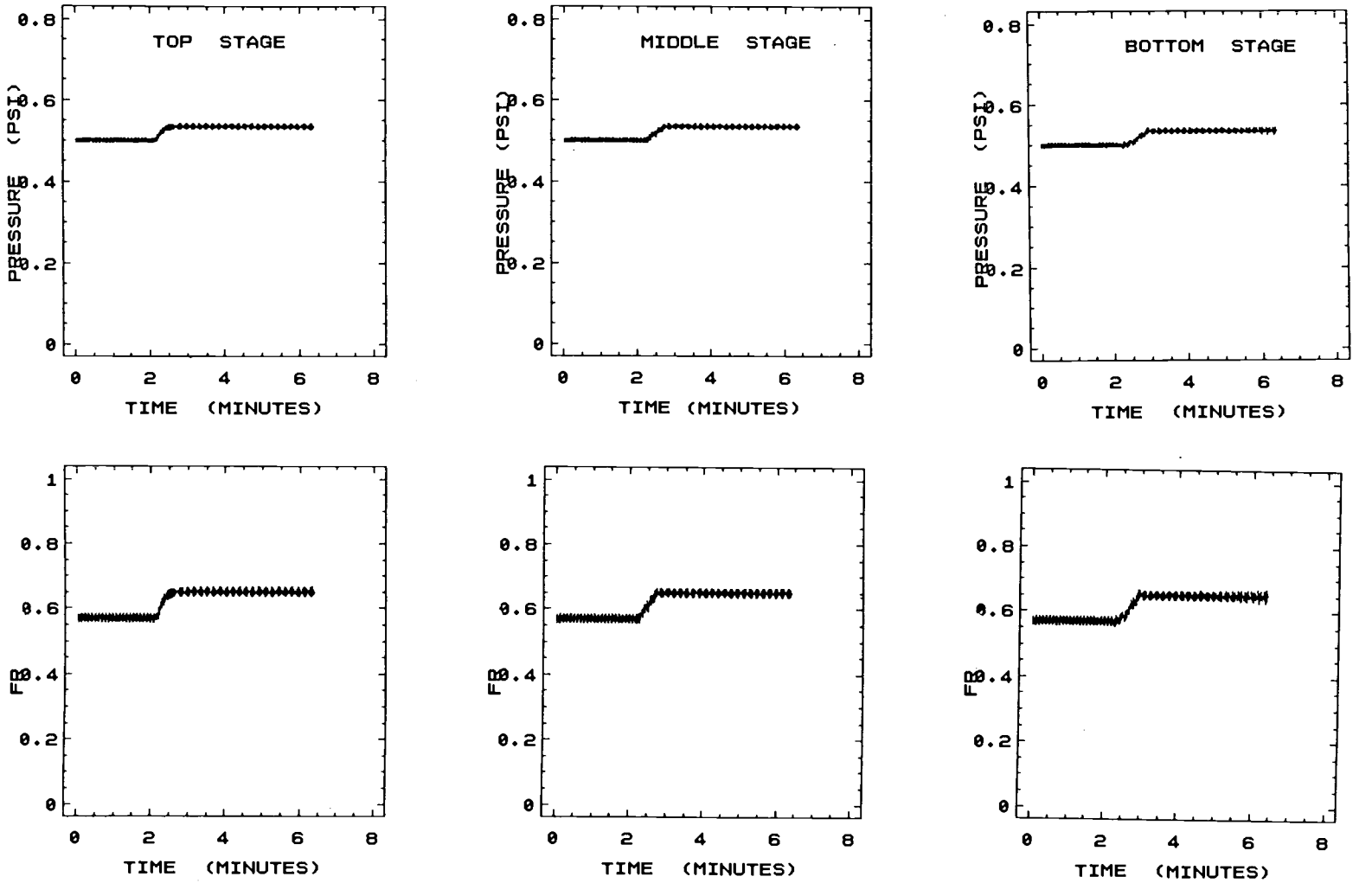

Figure (59) Simulated Closed-loop Performances for a 35 gm/second Step Change in the Flow Rate of Solids into the Top Stage.

equation (67) with $m_o = m_i$. The values of the steady-state controller action before and after the step disturbance is introduced are:

$U_{ss}|t < t_s = 0.57$ old steady state

$U_{ss}|\ t \geq t_s = 0.65$ new steady state

t_s = the time at which the step change is started

= 2 minutes

This suggests the change of U_{ss} to the new steady-state value using the model of the solids flow rate.

VI.2.3 Closed-Loop Experiments

VI.2.3.1 Negative Step Change in the Pressure Drop Across a Stage

Figure (60) shows the experimental closed loop performances using the same control parameters as those used for the simulation part without decoupling. The experiment was similar to that of simulation, figure (56). The pressure drop across the middle stage has a maximum value of 0.68 psi, while that of the middle stage has a value of 0.72 psi.

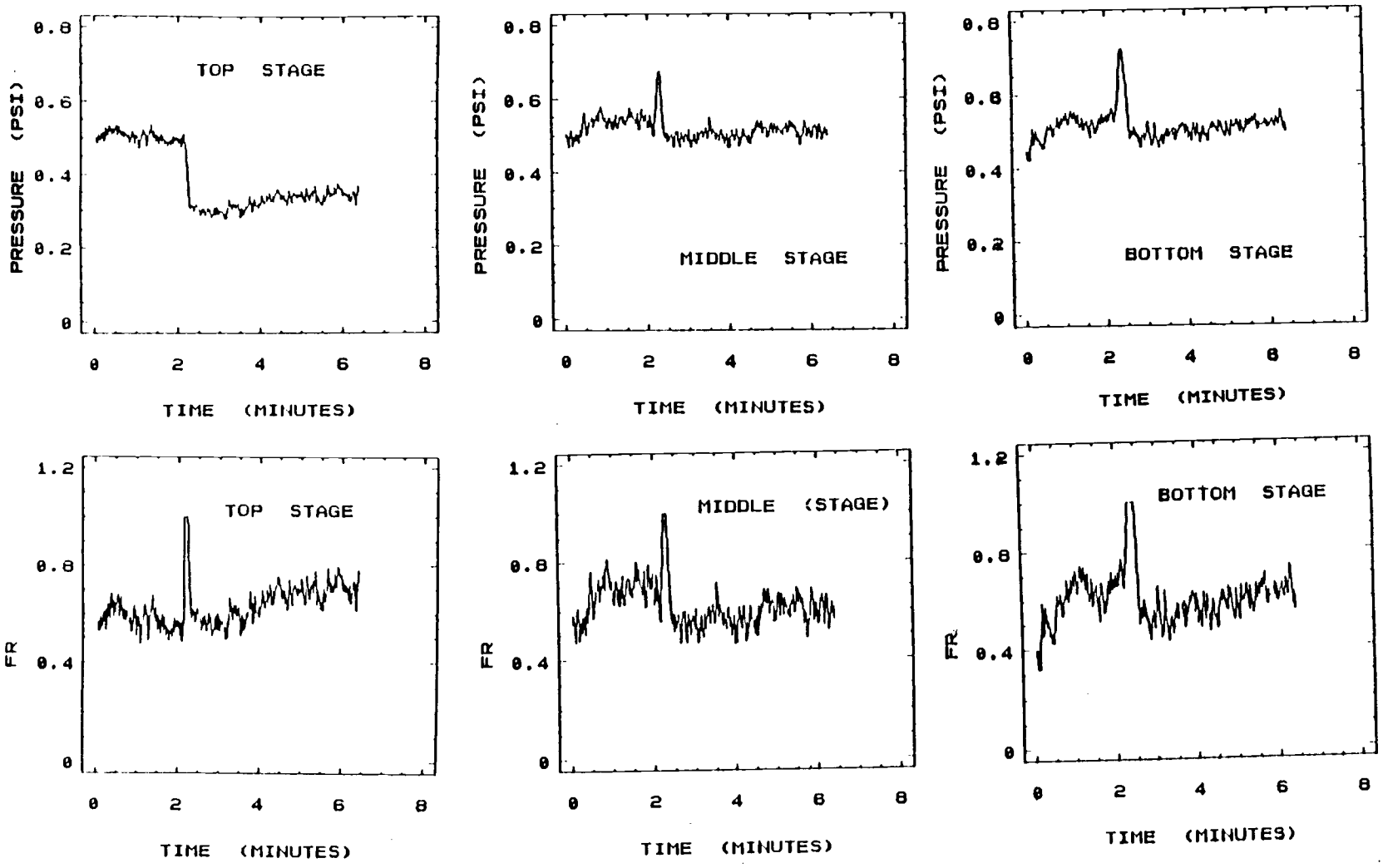

Figure (60) Experimental Closed-loop Performances for a -0.20 psi Setpoint Change in the Top Stage Without Decoupling.

The disturbance to the middle stage is nearly a pulse while the disturbance to the bottom stage is similar but, is wider and larger in height.

Figure (61) shows the experimental results with decoupling. The disturbances in the pressure drop of the middle and bottom stages are significantly reduced and the controller outputs have less fluctuation than the case without the decoupler. Figure (62) shows the experimental results when the setpoint is introduced in the second stage with decoupling. The pressure performances are good for all three stages. The pulse upset in the pressure drop across the bottom stage is significantly decreased. The performance of the top stage, as expected, is not influenced by the change of the pressure drop of the middle stage.

VI.2.3.2 Positive Step Change in the Feed Flow Rate

Figure (63) shows the experimental results for the closed-loop experiments when a step in the feed rate (ΔP = 30 gm/sec) is introduced in the top stage after two minutes of operation. The response of the pressure drop across each stage is a broad pulse. The response is more sluggish in going from the top to the bottom but in all the stages, the pressure eventually reaches the setpoint. No offset was noticed for a time greater than four minutes. It is also noticed that the disturbances caused by the step in the flow

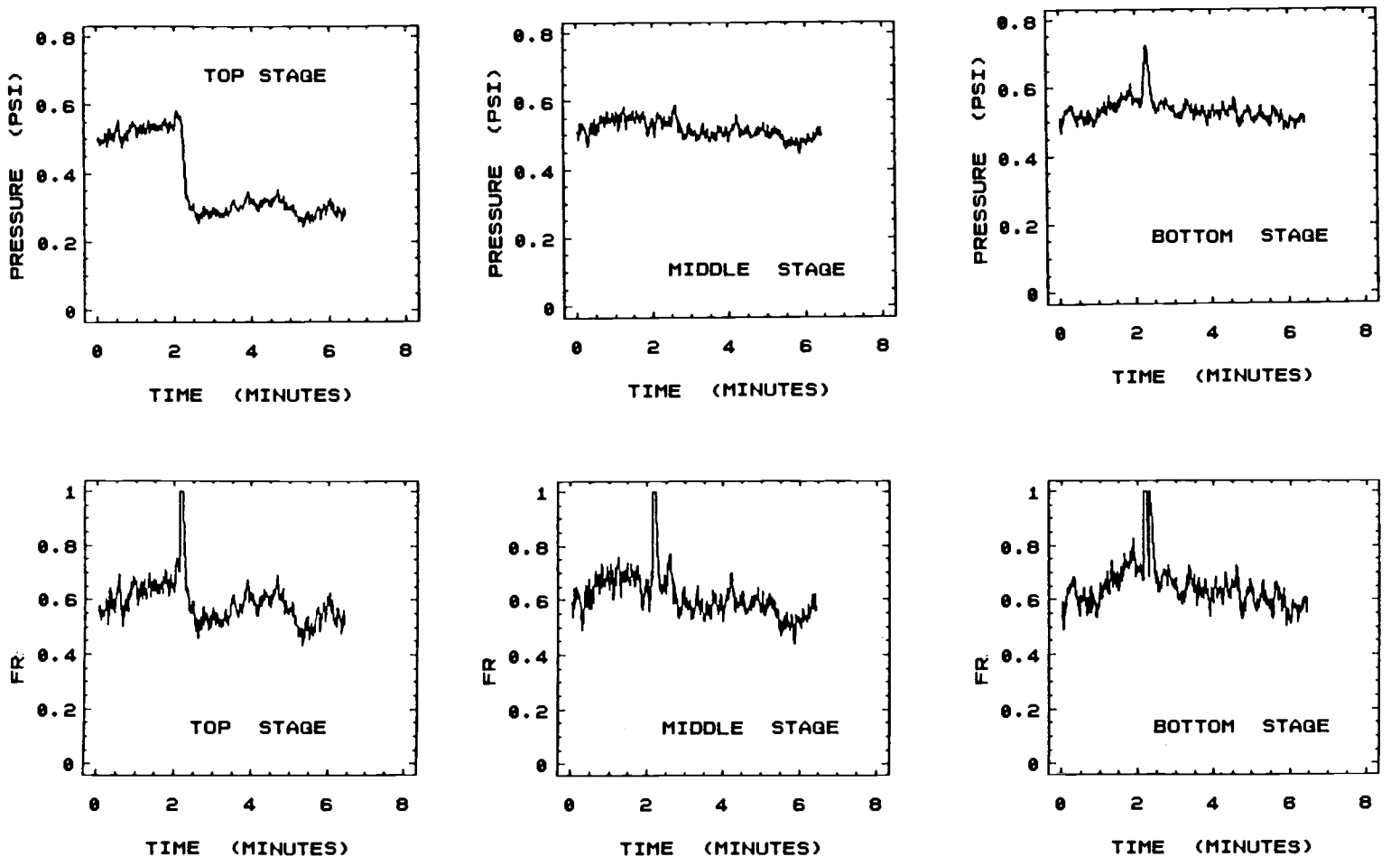

Figure (61) Experimental Closed-loop Performances for a -0.20 psi Setpoint Change in the Top Stage with Decoupling.

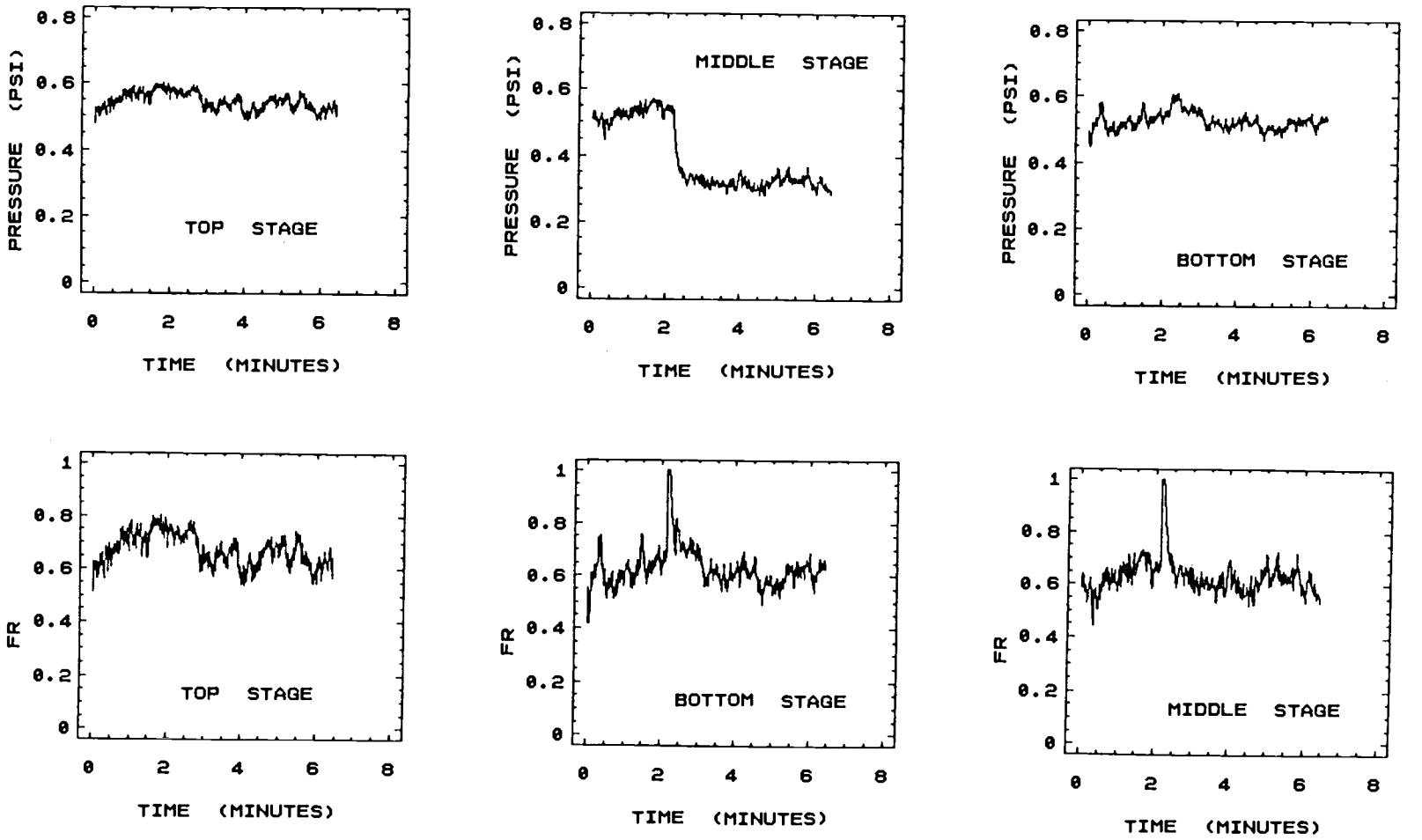

Figure (62) Experimental Closed-loop Performances for a -0.20 psi Setpoint Change in the Middle Stage with Decoupling.

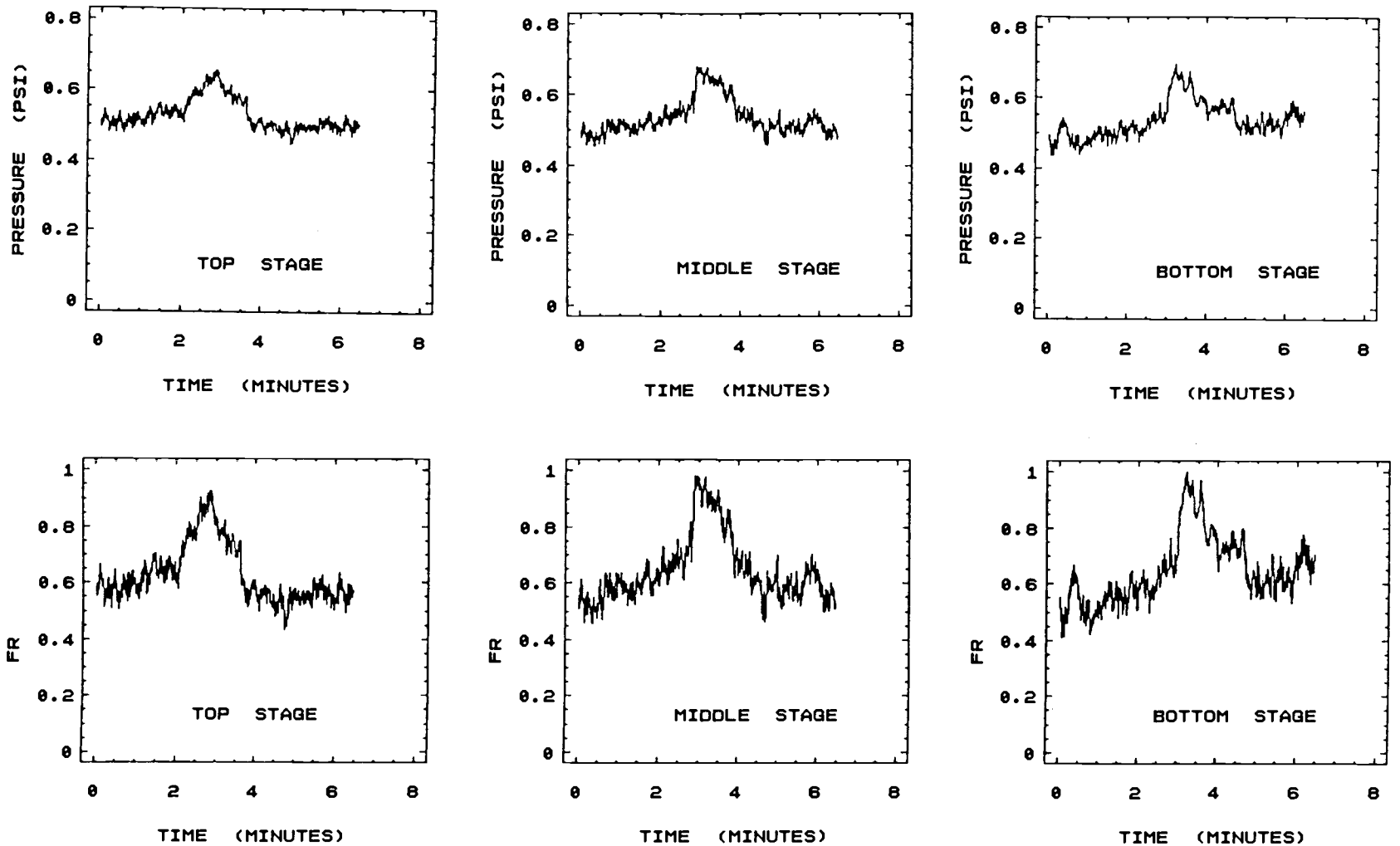

Figure (63) Experimental Closed-loop Performances for a 35 gm/sec Step Change in the Flow Rate of Solids into the Top Stage.

of solids into the bed is delayed in going from the top to the bottom stages.

VI.2.4 Comparison Between Experimental and Simulated Performances

The previous two sections demonstrated good agreement between the experimental and the simulated performances. However, the simulated pressure performance does not show the slow oscillation of the experimental pressure drop. The proposed model contains many assumptions and simplifications which may affect its accuracy. The flow of air through the stages is assumed to be uniform in the model when actually it is not. The flow of air through the stage valve and its effect on the flow rate of solids out of the stage may be the prime reasons for the slow fluctuations in the pressure drop performance. In the actual process, there are many sources of noise that are not included in the model. Also, the pressure fluctuations are modeled as sinusoidal oscillations while the experimental data shows them as non-stationary time series which have a fundamental frequency.

In spite of all the assumptions, the model does predict the interactions between the stages as well as the pulse heights, widths, attenuation and the progressively more sluggish performance from the top to the bottom stages.

The controller handled the positive setpoint change in the flow rate of solids into the top stage much better than that of the simulation. The offset due to the step in the load approaches zero in the experimental pressure performance while that of the simulation shows an offset of -0.03 psi. The difference between the two performances could be due to the same reasons mentioned at the beginning of this section.

VI.3 "Leaking" Valve Operation

VI.3.1 Design of the Control System Parameters via Simulations

The following equation is obtained from the model for the flow rate of solids for the "leaking" valve operation ad described in chapter IV. The constants have been determined through the use of linear regression:

$$m_o = 3.16 - 0.14\ I + 0.0016\ I^2 \tag{68}$$

$$R^2 = 0.974$$

Going through the same calculations as in section V.2, the following equations result:

$$\frac{(\bar{V}_p\ K_2) * (\rho_s\ A_f)}{A_1} = 0.13 \tag{69}$$

$$\frac{r * B}{\mu_0} = 13.93 \tag{70}$$

$$\frac{(\rho_s\ A_f)}{A_1}\ [\ (A_{cs}\ \delta)\ (1-\epsilon)\ \rho_s - A_1\ u_g\ ] = 3.16 \tag{71}$$

Figure (64) shows the plots of the experimental flow data along with the theoretical model. The fit of experimental data was very good (R^2 = 0.974). The relations between the various gas and solid properties and the bed geometry, and the determined model constants is more

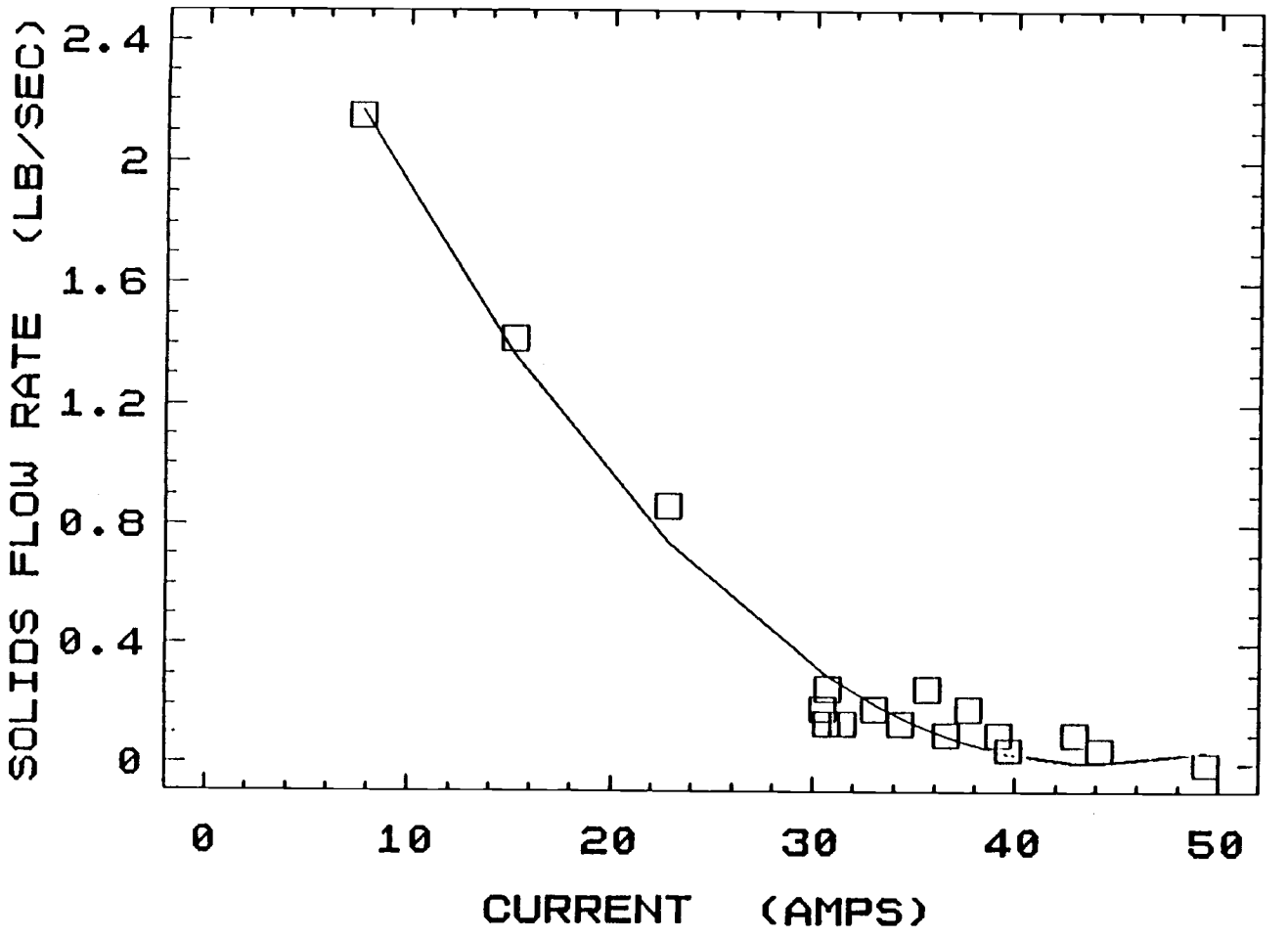

Figure (64) The Plots of Solids Flow Rate Out of the Stage vs. Average Current.

reliable than those in the on/off operation. The standard deviation of the measured current has a maximum value of 4 amps. This tight distribution in the current justifies some of the assumptions made in chapter IV to derive the flow expression.

VI.3.1.1 Controller Gain

Figure (65) contains plots similar to those for the on/off operation, however, the behavior of the curves are different. The ISQERRS for the pressure decrease monotomically with K_c and reach a constant value for K_c = 250 amps/psi. The curves for the middle and the bottom stages show some fluctuation for values of K_c > 260 amps/psi. The fluctuations are more pronounced for the ISQMAN. At high K_c value, the control becomes an on/off control and the pressure undershoots, which causes more fluctuations in the controller output. The ISQMAN has a nearly linear dependence on K_c for values of K_c less than 260 amps/psi. A value of 228 amps/psi was chosen for K_c based on the performance ISQERR, which does not improve appreciably for greater K_c values.

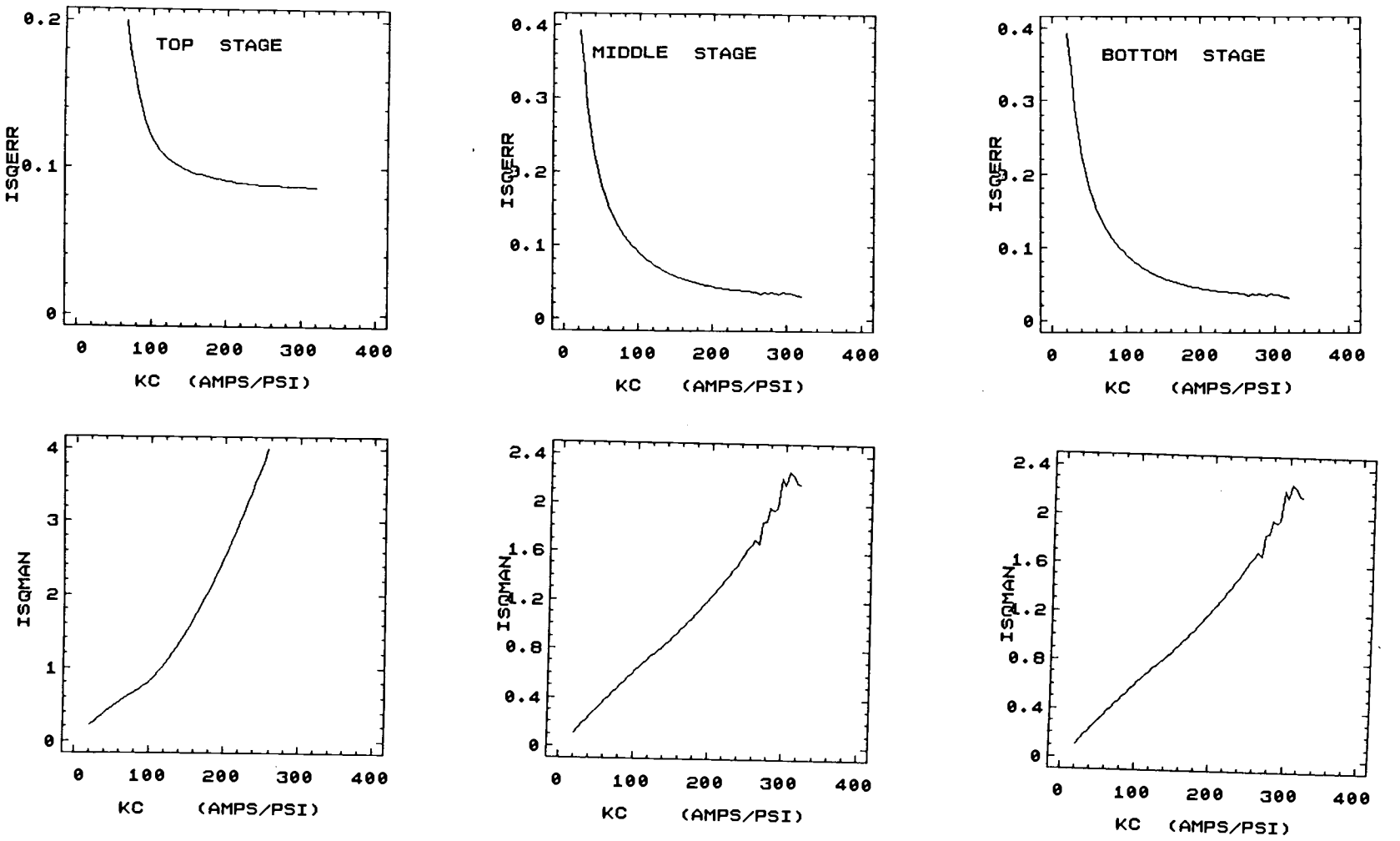

Figure (65) ISQERR and ISQMAN for Three Stages vs. the Controller Gain.

VI.3.1.2 Filter Time Constant

Figure (66) shows the plots of ISQERR and ISQMAN as a function of the filter time constant for the three stages. The plots exhibit a similar behavior to that in the on/off operation Figure (53). The minimum for the curve of the top stage, however, does not occur at $T_f = 1.8$ seconds, as found in the on/off operation but at a larger (about four seconds) filter time constant not shown in the plot. However, the rate of change of ISQERR is very small for $T_f > 1.8$ seconds.

A value of 1.8 seconds was thus chosen for the closed-loop experiments simulations using the "leaking" valve operation.

VI.3.1.3 Input Constraints

In the "leaking" valve operation, the input constraint is determined by the holding current for the upper constraint and the release current for the lower input constraint. The corresponding values are 49 amps and 22 amps. These values will give the best performance and reduce the energy consumption. Figure (67) shows the plots of ISQERRS and ISQMANS. The plots of the top stage show that the ISQERRS drops quickly as the lower limit decreases to 22 amps (I_r). ISQERR decreases slightly for a lower limit less

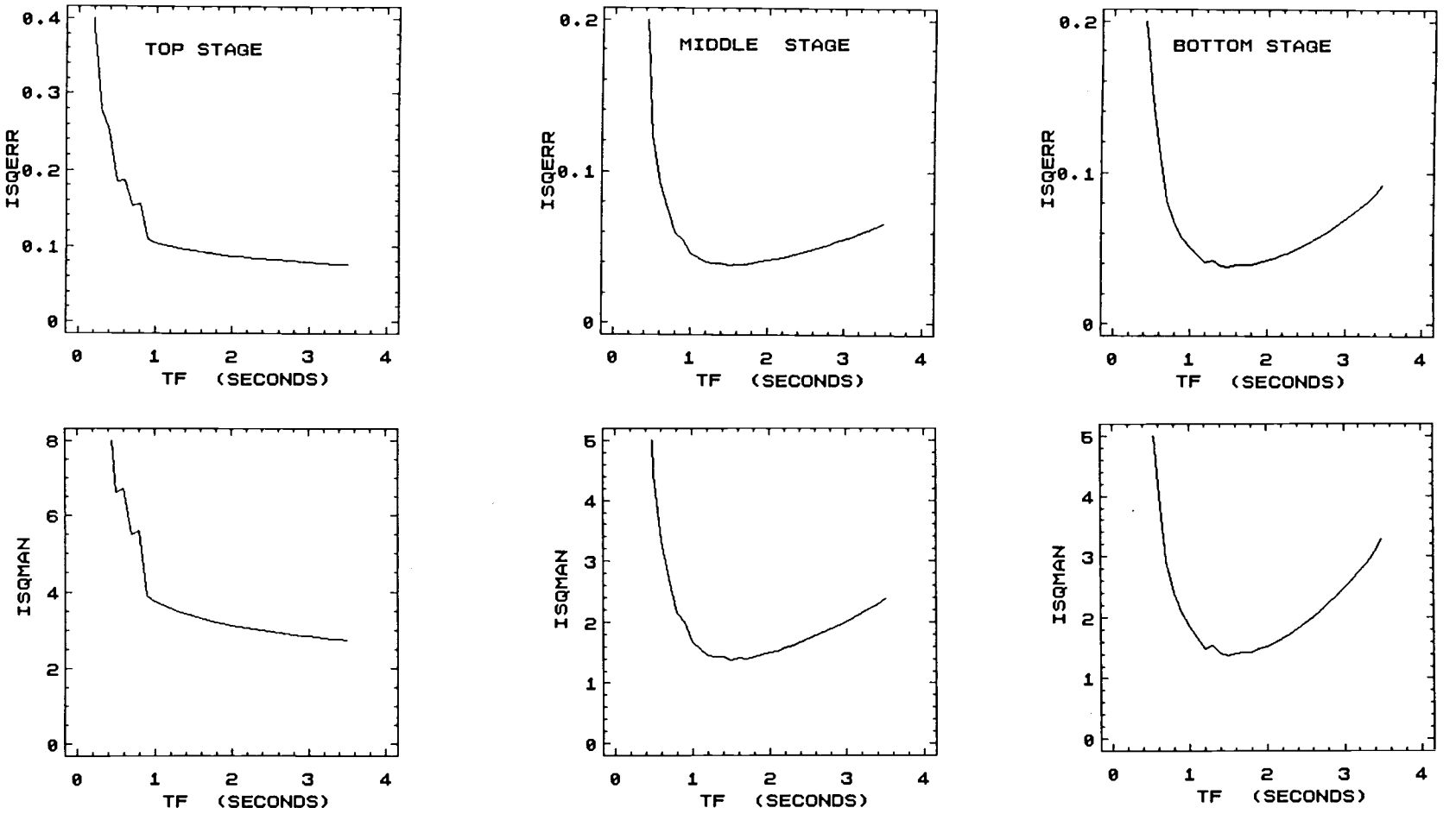

Figure (66) ISQERR and ISQMAN for Three Stages vs. the Filter Time Constant.

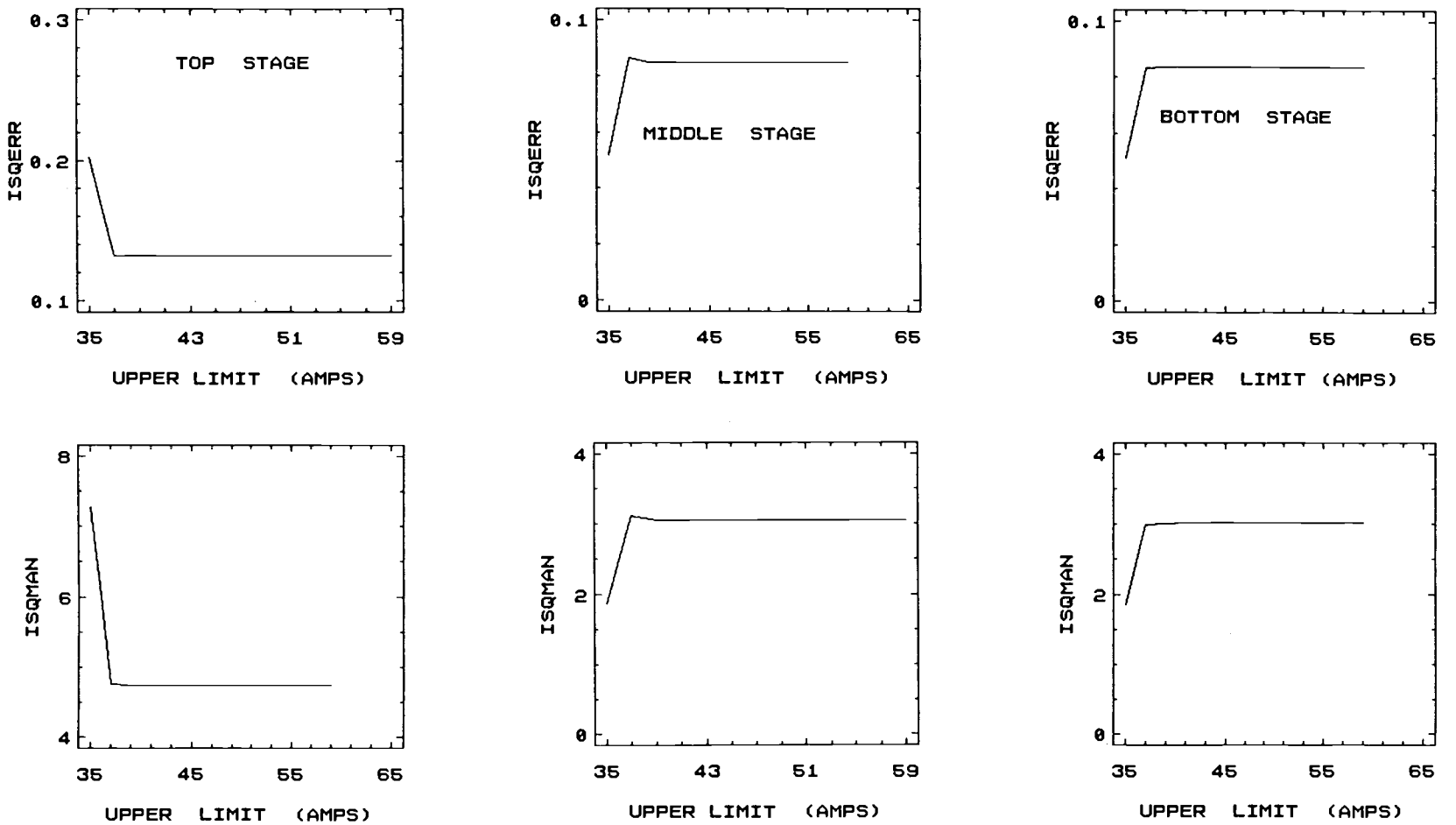

Figure (67) ISQERR and ISQMAN for Three Stages vs. the Upper Limit on Input.

than (I_r). This suggests the use of zero current would be possible as the lower constraint. However, as the lower constraint is decreased, the pressure drop response remains fast, but undershoots. The undershoot is very large and upsets the lower stages considerably. Therefore, the lower constraint was chosen as 22 amps. The corresponding plots for the upper constraint of ISQMAN is shown in figure (68). The ISQMAN for the top stage is constant for controller output upper constraints greater than 49 amps. The plots for the other stages show constant ISQERR for all values of the controller output upper limit greater than 39 amps.

VI.3.2 Simulated Closed-loop Performances

VI.3.2.1 Negative Setpoint Change in the Pressure Drop Across a Stage

Figure (69) shows the closed-loop response to a negative setpoint change $\Delta(\Delta P)_{sp} = -0.2$ psi) in the pressure drop across the top stage without decoupling. The pressure performances show the same behavior as those for on/off operation. However, the pressure response as well as the controller output show oscillatory behavior. The oscillation has a slower frequency (≈ 6 cycles/minute) than the pressure fluctuation (≈ 110 cycles/minute). The frequency became higher at low pressure drop (≈ ΔP = 0.3 psi)

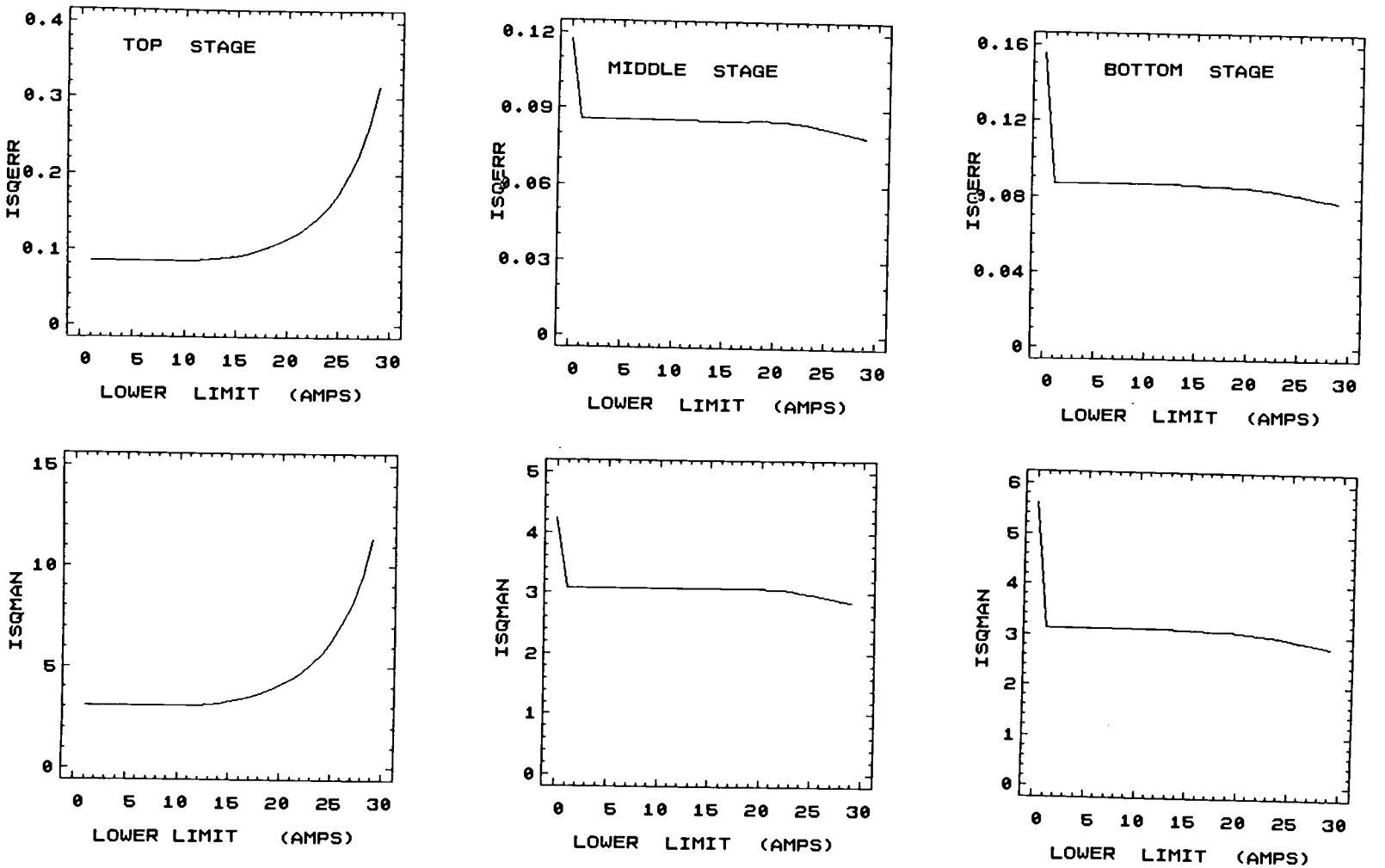

Figure (68) ISQERR and ISQMAN for Three Stages vs. the Lower Input Constraint.

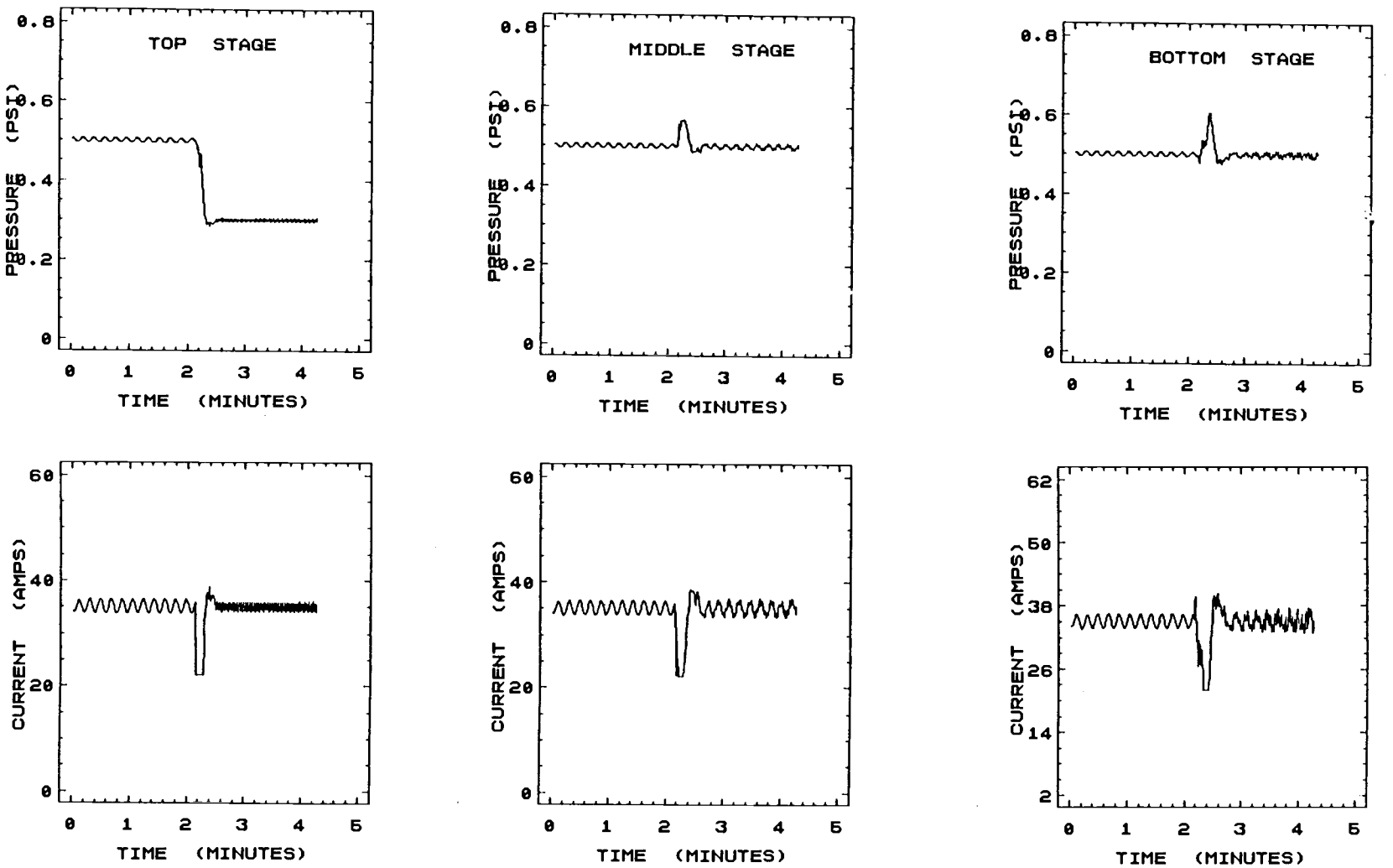

Figure (69) Simulated Closed-loop Performances for -0.20 psi Setpoint Change in the Top without Decoupling in "Leaking" Valve Operation.

while the amplitude has a constant value of 0.01 psi for the pressure and 1.5 amps for the controller. Increased disturbance attenuation and sluggishness going from the top stage to the bottom stage is also observed. The pressure drop across the top stage undershoots the desired value (ΔP_{sp} = 0.3 psi) by 0.03 psi. The pressure drops across the middle and bottom stages undershoot the desired value ($\approx P_{sp}$ = .5 psi) by the same amount at the end of the disturbance.

Figure (70) shows the results of a similar simulation when decoupling is taking place. The effect of the disturbance to the middle and bottom stages are effectively eliminated. The undershoot in the middle stage is about 0.04 psi and that of the bottom stage is about 0.02 psi. The undershoot in the middle stage happens only for a very short time. Hence, it does not cause a serious problem to the controlled process. The oscillatory behavior is also noticed here.

Figure (71) shows a similar simulation result to the last one with the step introduced in the middle stage. The pressure drop across the top stage is not affected by the changes introduced to the other stages. The pressure drop of the middle stage undershoots to a lower value (0.25 psi) than the last two cases. This is because the flow rate of solids into the top stage has a constant value 62.14 gm/seconds while the flow of solids into the middle stage is the same as that out of the top stage, which is fluctuating.

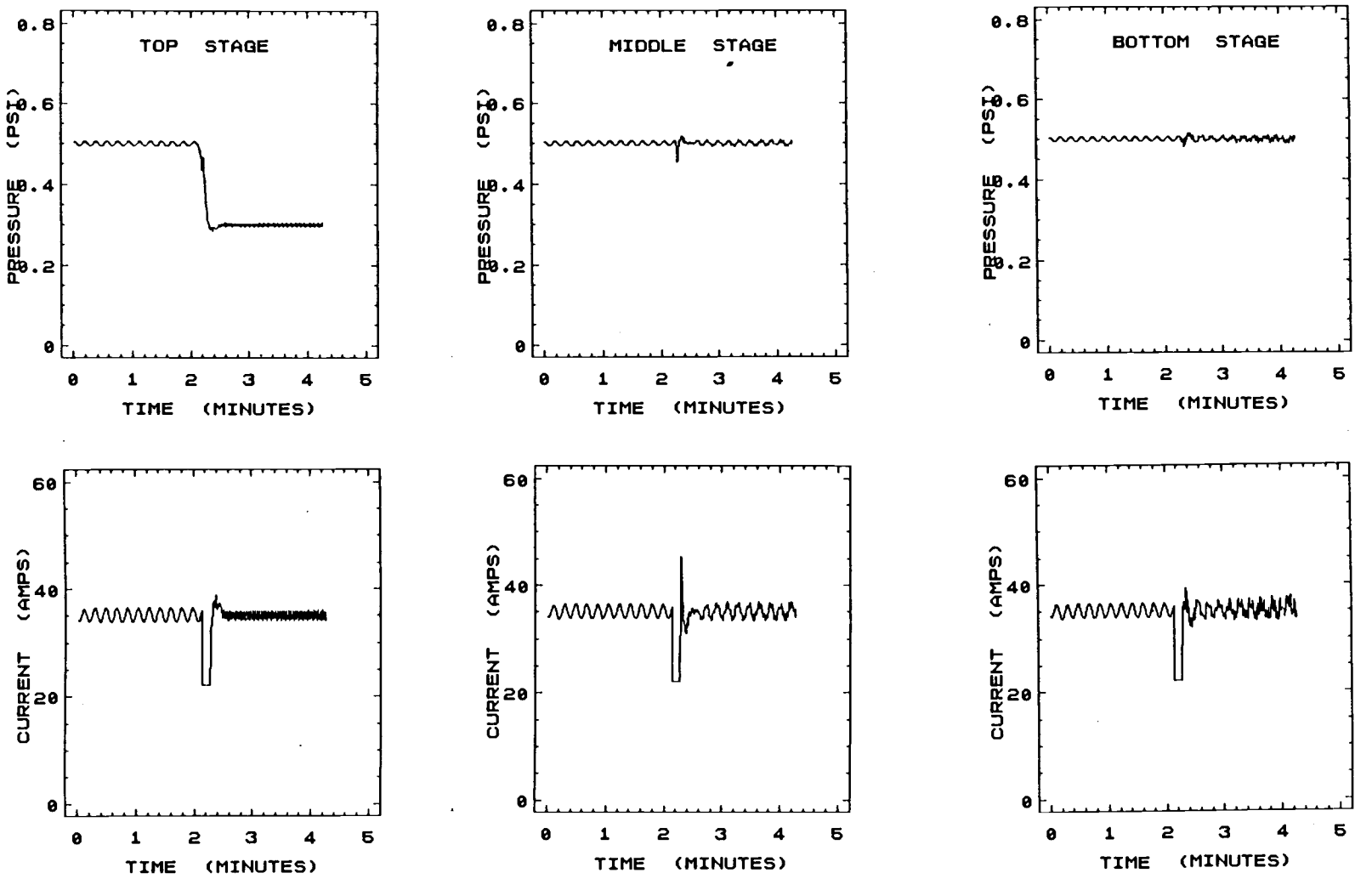

Figure (70) Simulated Closed-loop Performances for -0.20 psi Setpoint Change in the Top Stage with Decoupling.

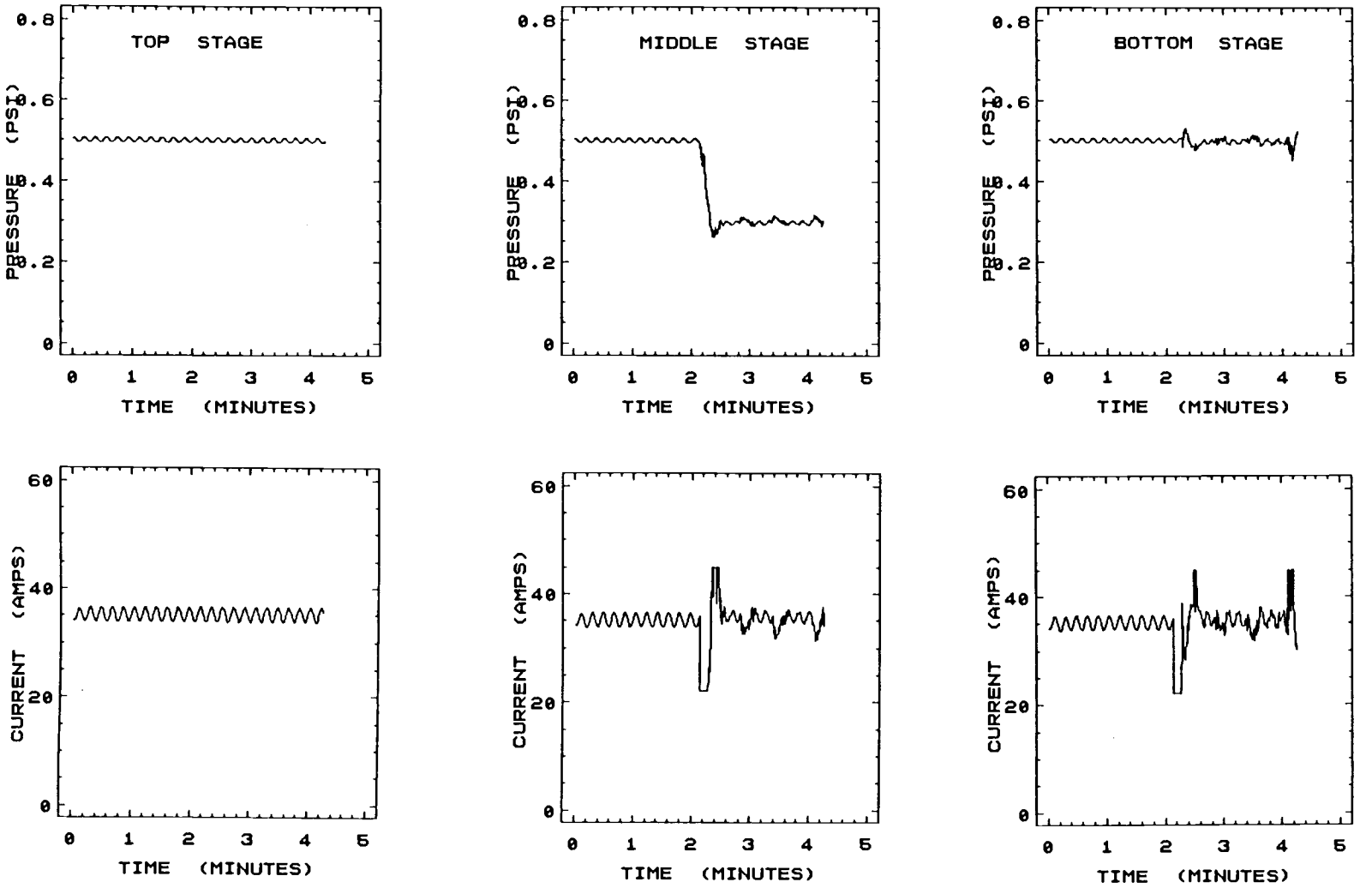

Figure (71) Simulated Closed-loop Performances for -0.20 psi Setpoint Change in the Middle Stage with Decoupling.

There is a good possibility that the flow rate of the top stage is at its lowest value at the time when the setpoint change is introduced. The controller parameters used in all the simulations are those found in the last section.

The controller output hit the lower constraint (I = 22 amps) in all the previous cases, then it hit the upper constraint (I = 47 amps) as a result of the undershoot. In some other cases it does not hit the upper limit, instead it reaches an intermediate value between the steady state and the upper limit.

VI.3.2.2 Positive Step Change in the Feed Flow Rate of Solids

Figure (72) shows the pressure drop and the controller output performance when a step change in the feed rate (ΔF = 35 gm/seconds) is introduced to the top stage. The effect on the pressure drop is negligible and the controller handled the disturbance well. The maximum offset happened at t = 2 minutes and was equal to 0.01 psi. The slow oscillations are not observed in this case which is due to the low pressure drop across the stages (0.32 psi) where the frequency of the oscillations are much faster and the amplitude is smaller. The disturbances to the pressure drop response was delayed in going from the top to the bottom stages.

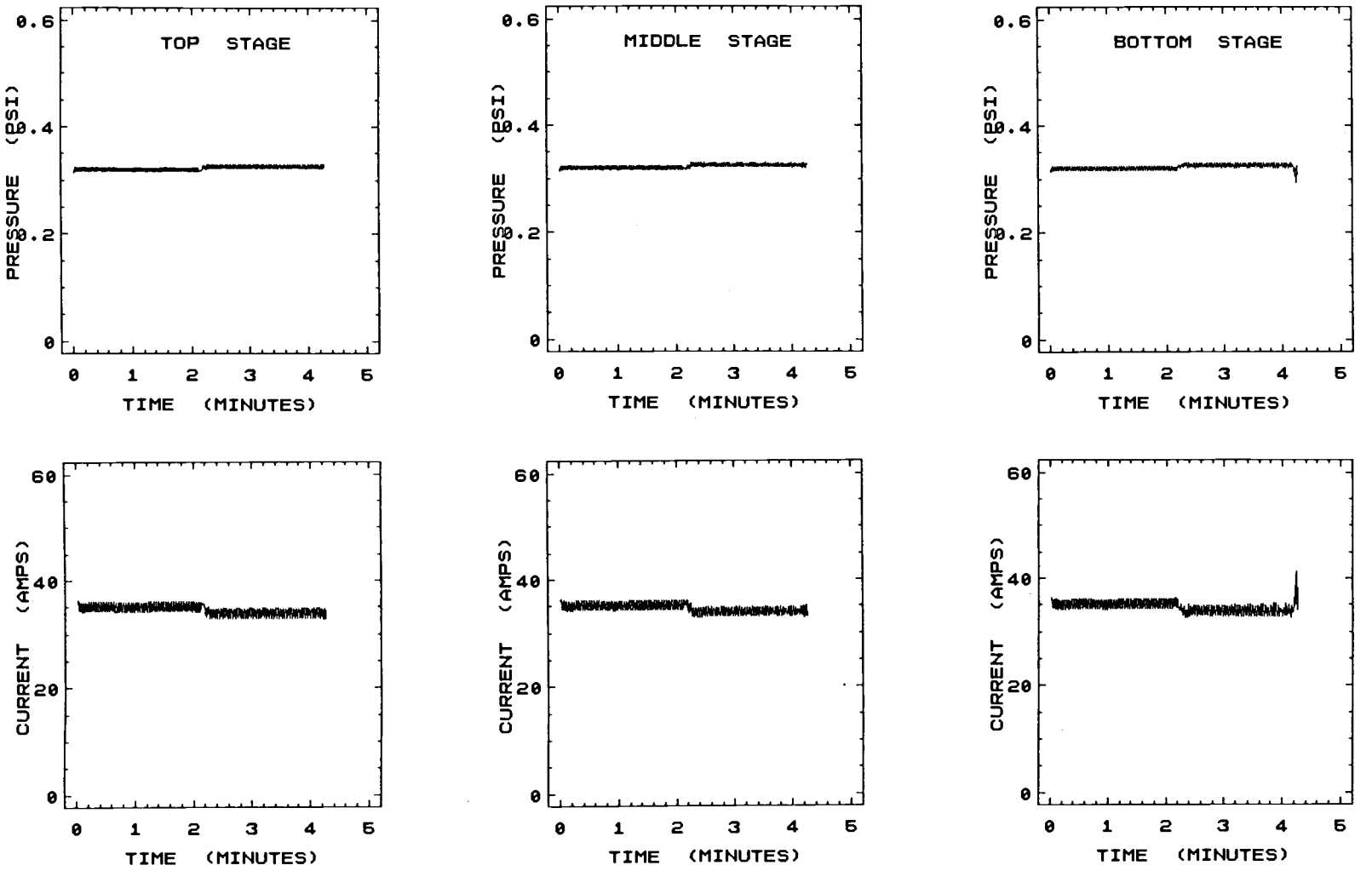

Figure (72) Simulated Closed-loop Performances for 35 (gm/second) Step Change in the Feed Flow Rate of Solids.

VI.3.3 Closed-Loop Experiments

VI.3.3.1 Negative Setpoint Change in the Pressure Drop Across a Stage

Figures (73), (74), (75), show similar cases to those shown in section VI.2.3.

Figure (73) shows the case without a decoupler. The pressure drop shows slow fluctuations around the setpoint. The average amplitude of the pressure fluctuations has a standard deviation of .03 psi. The undershoot of the pressure drop is observed in all the stages. Its value ranges from .03 psi in the top stage to 0.07 psi in the bottom stage. The pressure performance for the top stage is good. The slow fluctuation's amplitude increases in going from the top stage (.02 psi) to the bottom stage (0.05 psi). Therefore, the performance gets worse especially after the step in the setpoint change in going from the top to the bottom stages but the average pressures in all the three stages have the same value as the setpoint.

The disturbances in the pressure drops of the middle and the bottom stages show similar behaviors to those of the simulation.

The controller output performance differs from that of the simulation. It hits the lower constraint (I_r = 22 amps) when the setpoint is introduced and it hits the upper

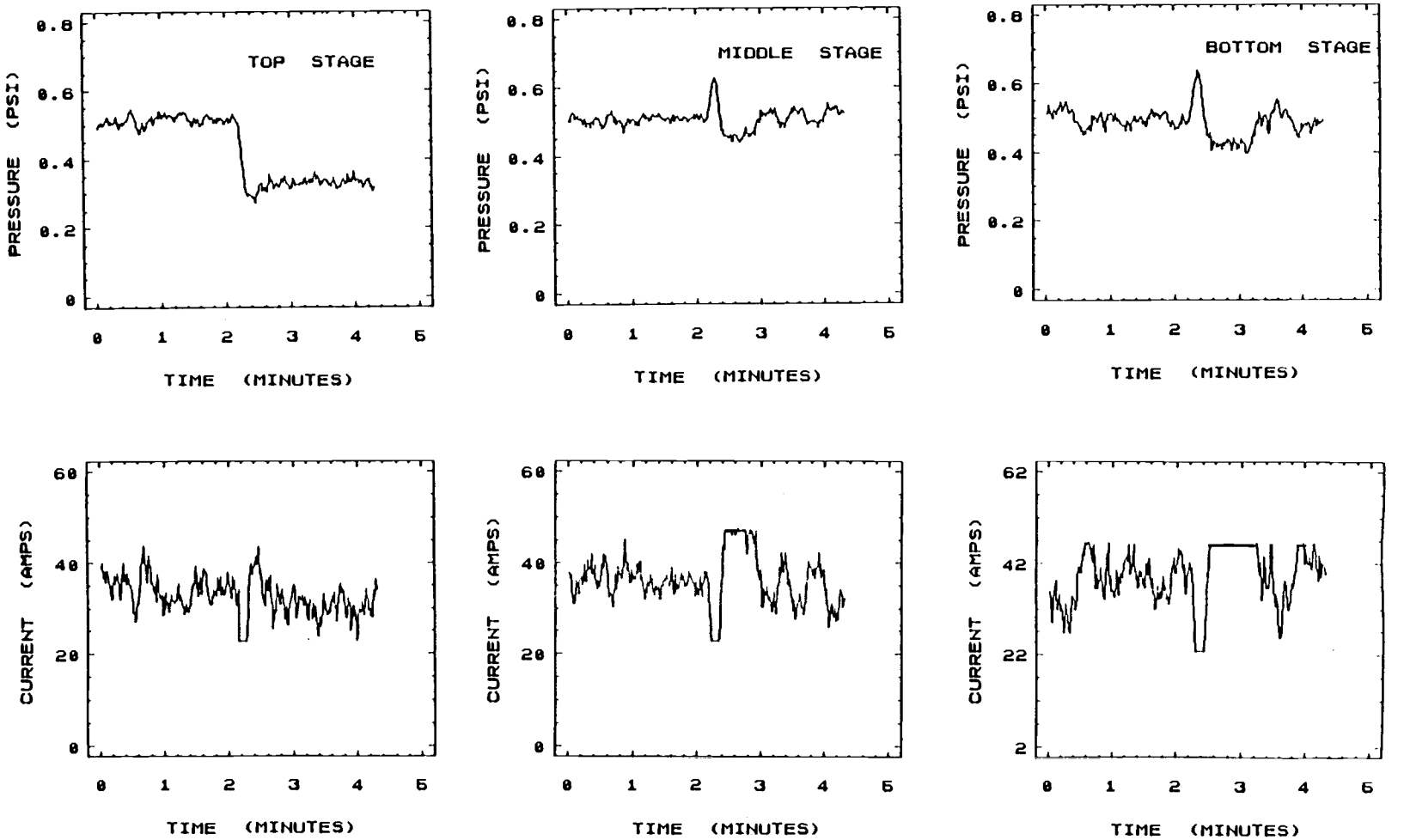

Figure (73) Experimental Closed-loop Performances for -0.20 psi in Setpoint Change in the Top Stage without Decoupling.

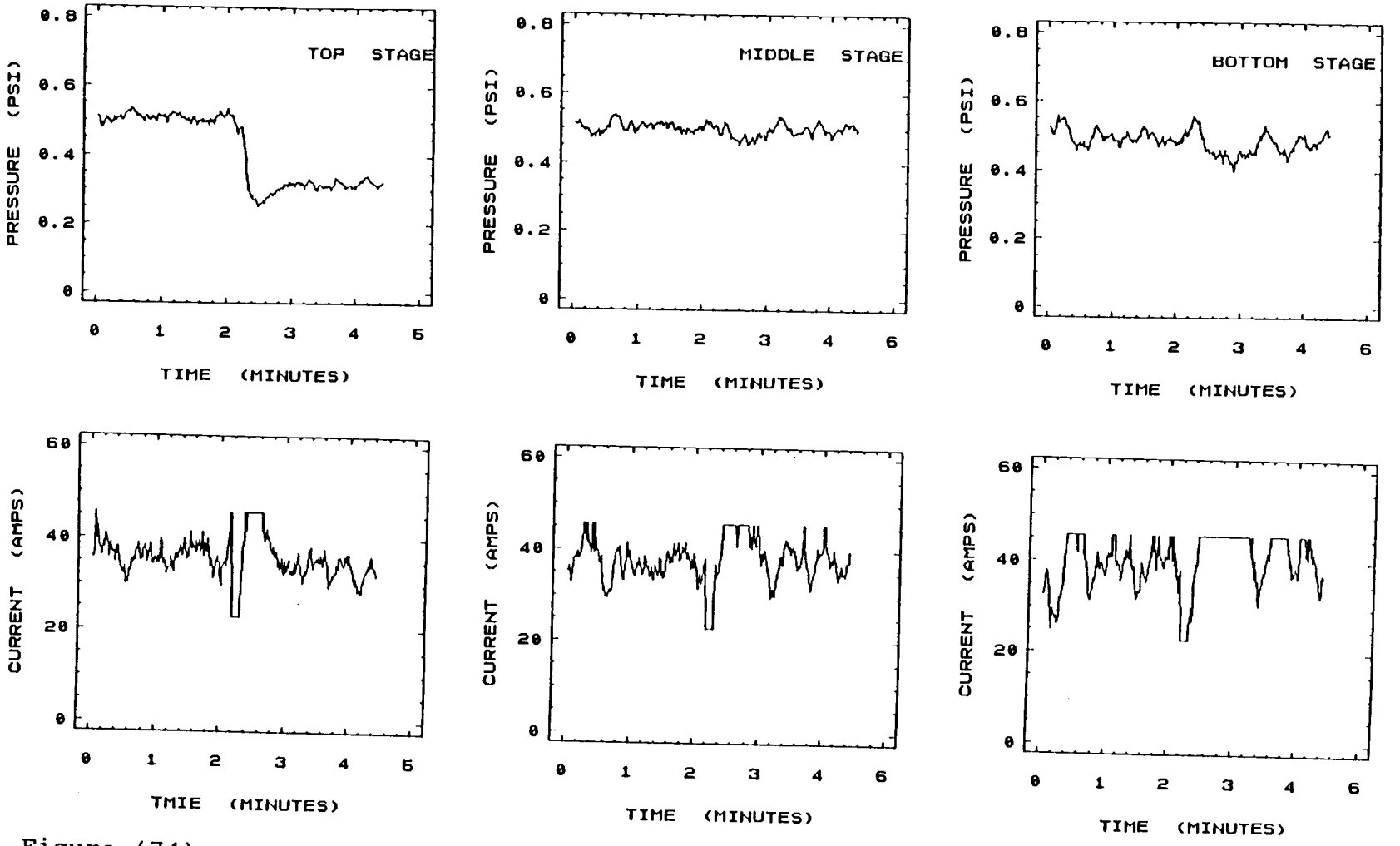

Figure (74) Experimental Closed-loop Performances for a -0.20 psi in the Setpoint in the Top Stage with Decoupling.

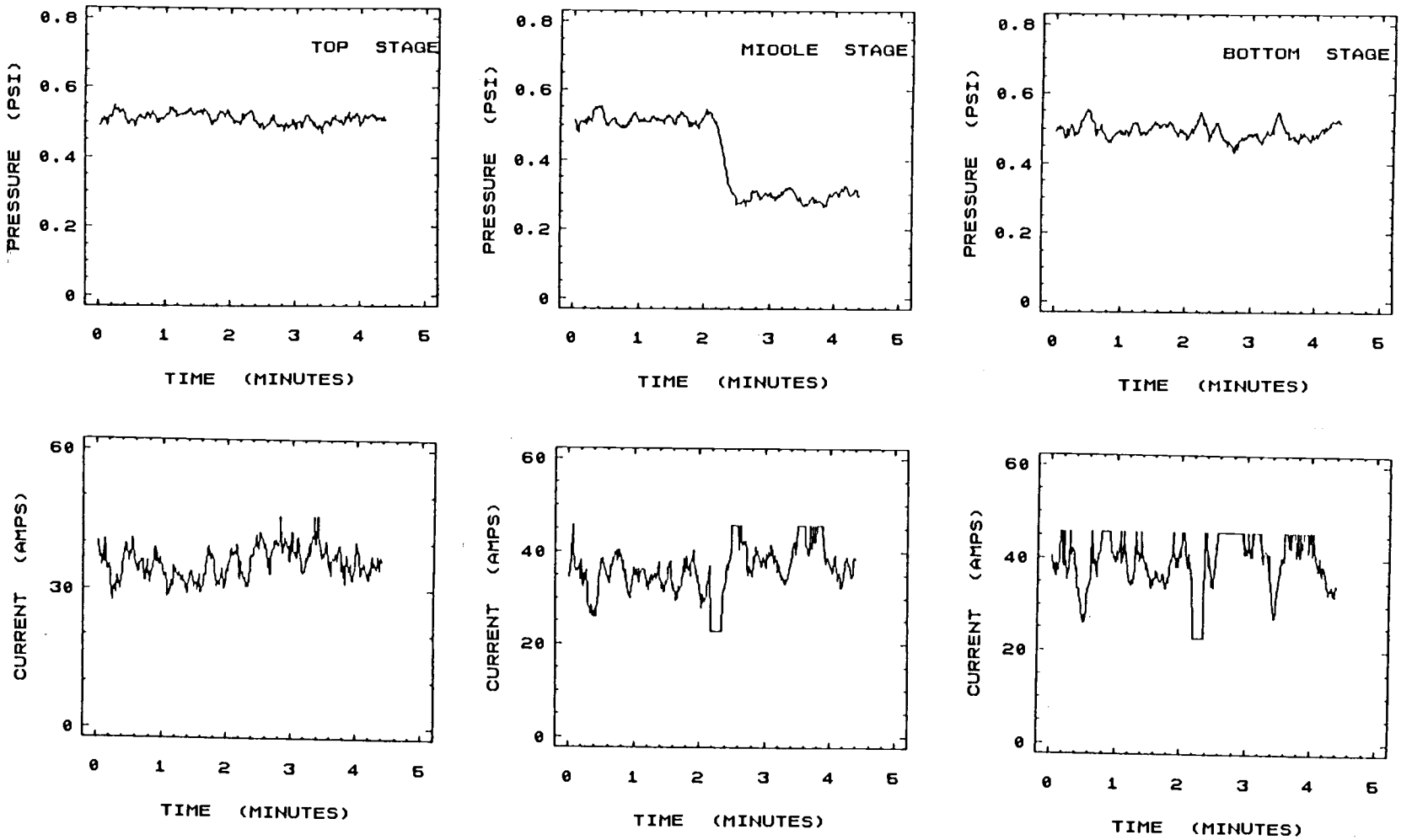

Figure (75) Experimental Closed-loop Performance for a -0.2 psi in the Setpoint of the Middle Stage with Decoupling.

constraint (I_h = 47 amps) many times as a result of large pressure fluctuations.

Figure (74) shows the case where decoupling is implemented. The responses of all the stages have less fluctuations than the non-decoupling case. The undershoot in the top stage (≈ 0.05 psi) is larger than that of the last experiment while it has the same value as for the other stages. Similar controller output behavior is observed as in the last case.

Figure (75) shows a similar case to the last figure when the setpoint is introduced to the middle stage. The performances of all three stages are good. Similar types of fluctuations are observed as in the last experiment. The top stage performance is very good with the fluctuations looking very similar to those of the simulation. The pressure undershoots in the middle and bottom stage are the same as those for non-decoupling experiments. The controller output performance is similar to the last two cases.

VI.3.3.2 Positive Step Change in the Feed Flow Rate of Solids

Figure (76) shows the pressure performance for a step change in the feed flow of solids of 35 gm/seconds. The pressure drop shows a slight increase (0.01 psi) after the step is introduced. The desired pressure value (0.32 psi)

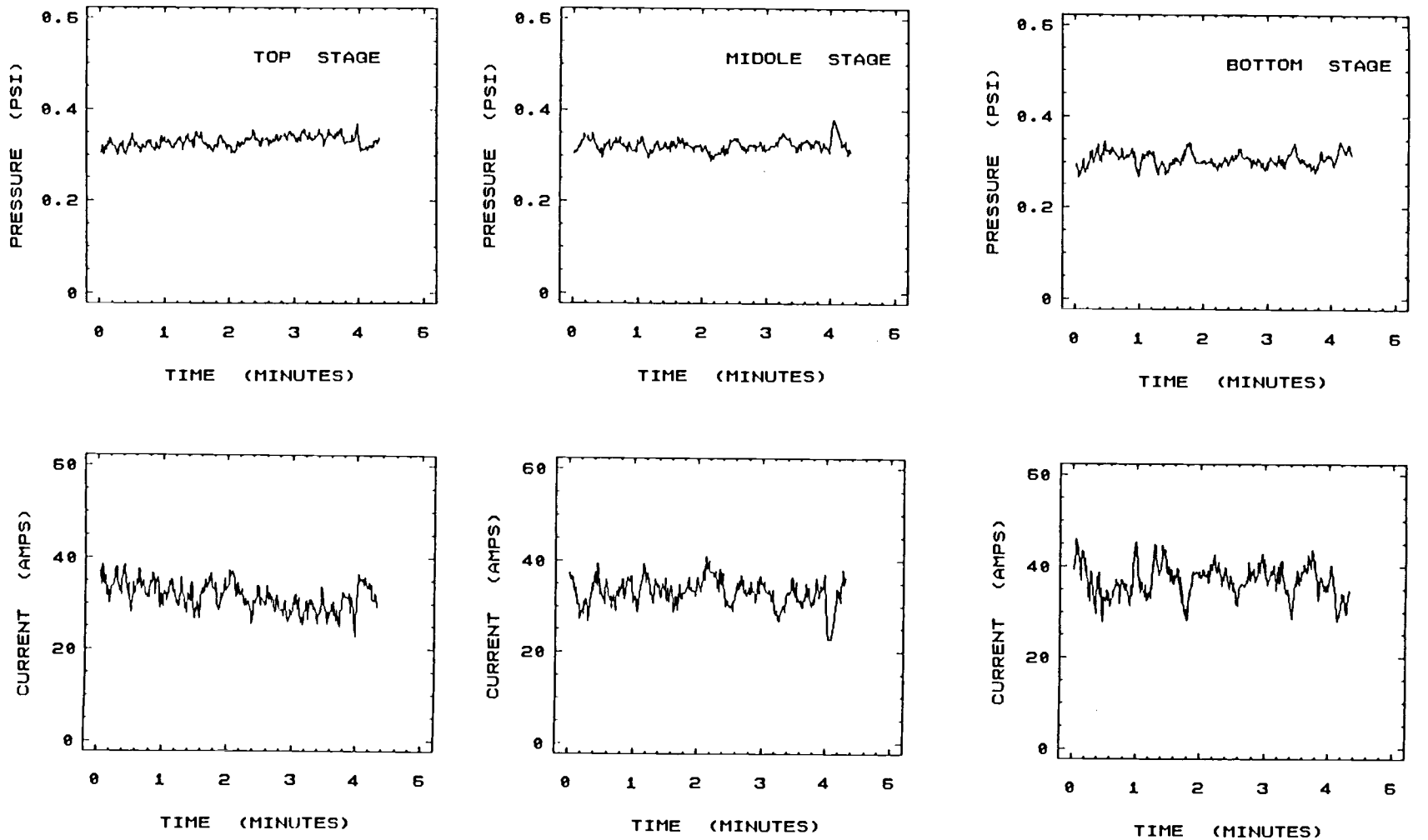

Figure (76) Experimental Closed-loop Performances for a 35 (gm/second) Step Change in Solids Flow Rate.

is attained in less than half a minute. The offset was eliminated after half a minute which did not agree with the analysis of section VI.1. The performance of the pressure drop looks very good in all the stages and the manipulated current did not hit either constraint.

VI.3.4 Comparison Between the Simulated and Experimental Performances

The results of the last sections show that the simulations using the proposed model predict some of the real process' behavior. They predict the occurrence of the undershoot, the disturbance in pressure drop as a result of the setpoint change, and the pressure fluctuations around the desired value. However, the simulations show the fluctuations are sinusoidal oscillations while the real process fluctuations are more complex. The differences between those two types of fluctuations is due to the fact that the fast pressure fluctuations are modelled as sinusoidal oscillations. The same reasons mentioned previously in the on/off operation (sec. 6.2.4) contribute to the difference observed between the experimental and simulated performances in the "leaking" valve operation. The controller outputs hit both of the constraints more frequently in the experimental results than the simulation results because

of the larger fluctuations observed in the experimental response of the pressure drop.

The greatest differences between experimental and simulated pressure drop responses are for the non-decoupled cases and especially for the stage/stages which lie below the stage at which the setpoint change is introduced. The other cases show good agreement with the simulated results.

The simulation and experimental results show a very good agreement in handling the disturbances which result from a change in the feed flow rate of solids.

The above observations indicate that the proposed model, with few restrictions, is adequate for designing the controller and predicting the responses of the pressure drop across each stage to both disturbances and setpoint changes.

VI.4 Comparison Between On/Off and "Leaking" Valve Operations

Figure (77) shows the plots of the solids flow rates versus the calculated average current for the on/off operation and "leaking" valve operations. From the figure, "leaking" valve operation is more efficient than on/off operation when the solids flow rate is less than 0.85 (lb/seconds), (386 gm/seconds). For larger flow rates, the efficiency is about the same for both operations.

The general behavior of the pressure responses are similar in both cases. The slow fluctuations associated with the "leaking" valve operation have larger amplitude than those for on/off operation. Sometimes, a small undershoot occurs when a change in the setpoint of the pressure drop across the stage is introduced in the "leaking" valve operation. This is due to the low level of current used in the operation ($I \approx 35$ amps) and to the hysteresis characteristics of the "leaking" valve operation (section V.3.2). The pressure fluctuations associated with the pressure during the on/off operation have a higher frequency than that for the "leaking" valve operation. This is because on/off operation adds some fluctuations to the pressure response which results from the fluctuation in the solids and gas flow rates. The magnetization of the solids during the on/off operation is larger than that for

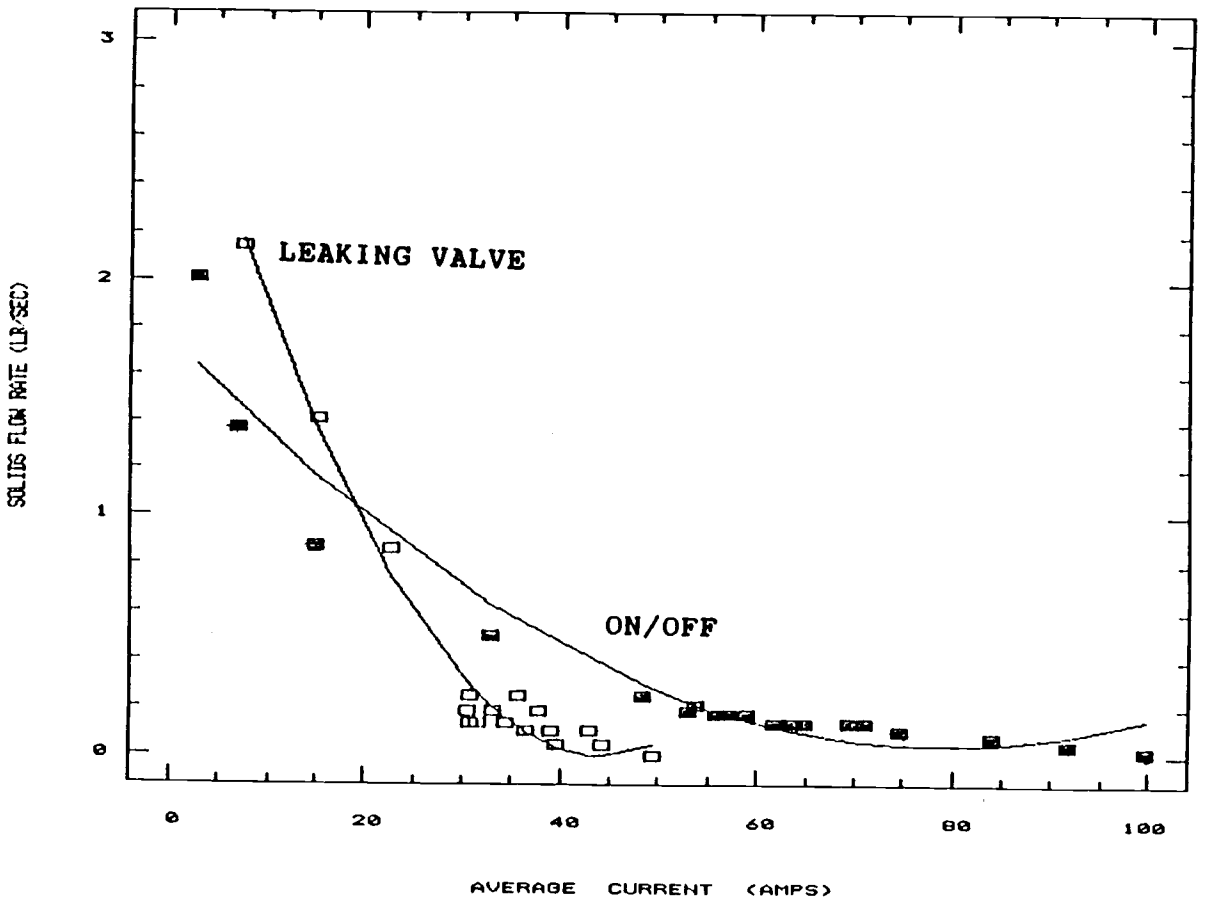

Figure (77) Comparison Between the ON/OFF and the "Leaking" Valve Operations.

"leaking" valve operation because of the difference in the average currents used in each operation (I_{av} [on/off] = 66 amps, I_{av} [leaking] = 35 amps. This reason could be used to explain the sluggish response of the pressure drop to a step in the feed flow associated with on/off operation. The corresponding one for "leaking" valve operation is very fast.

Generally, the pressure performances are similar for both of the operations. The "leaking" valve operation is preferred because the energy consumption is lower and failure of the power supply is less likely to occur because of the relatively smaller changes required in the power.

VII. CLOSED-LOOP STUDIES FOR SOLIDS CONTAINING 50% IRON

This chapter will also be divided into two main parts. The first part will cover the studies related to the on/off operation while the second part will cover those related to the "leaking" valve operation. The design of control system parameters, the closed-loop simulations and experimental results, and the comparison between them will be covered in each part. Comparison between on/off operation and "leaking" valve operation will be presented at the end of the chapter.

The analysis done in section VI.1 will be applied in this chapter. The modeling and control studies done in this chapter are believed to be more accurate and better than those done for other solids' weight fractions. This may be due to the weight fraction (.5) used in this operation. Very high weight fraction causes residual magnetism problems while low weight fraction causes strong valve hysteresis.

VII.1 On/Off Operation

Figure (78) shows the experimental data as well as the theoretical model obtained. The following equation is obtained by fitting the proposed model of chapter IV to the experimental data via linear regression:

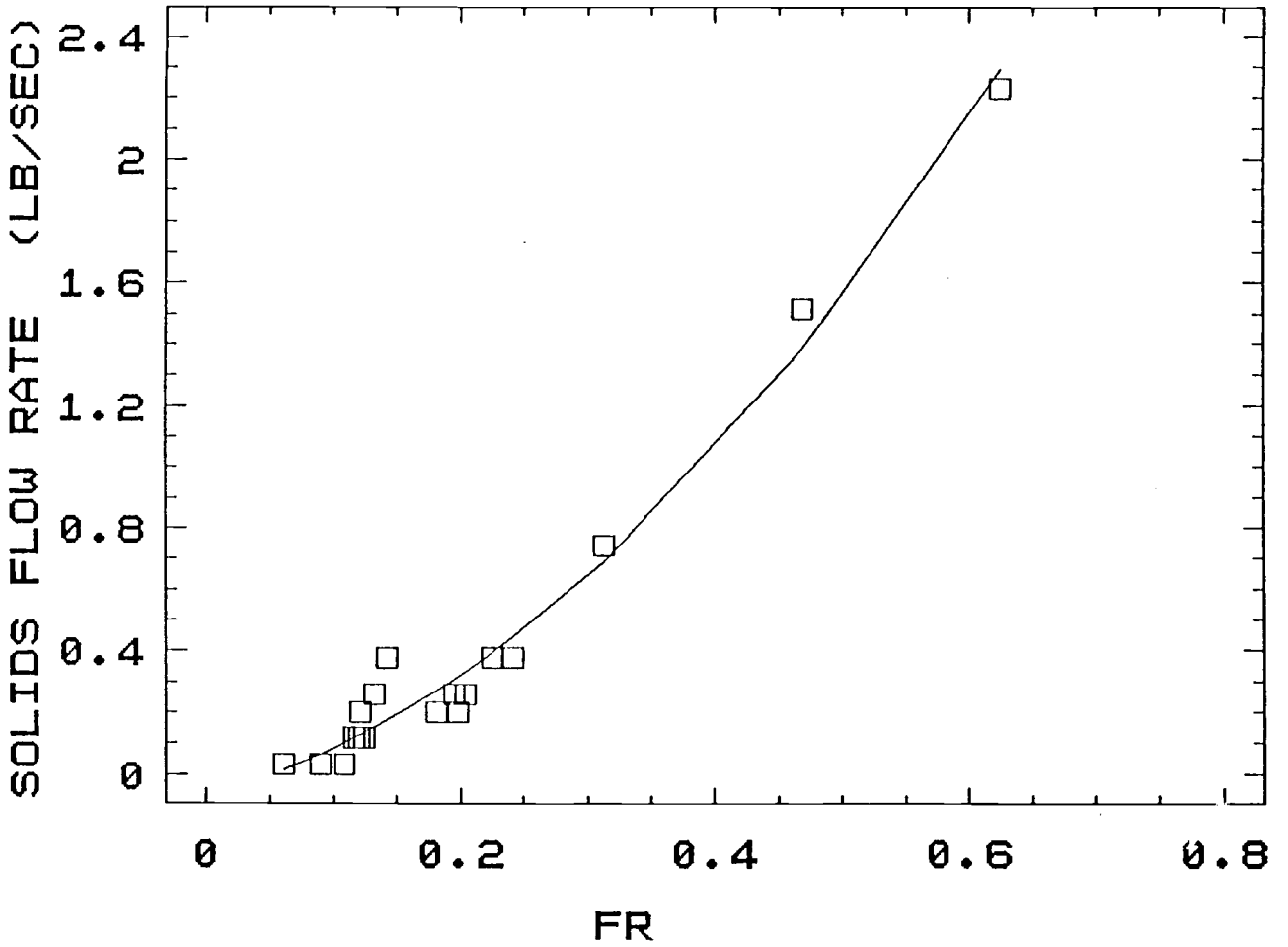

Figure (78) Plots of Experimental Data and Theoretical Models's Prediction (solid line) vs. Fraction.

$$m_o = 0.0327 + 0.555 * FR + 4.909 * FR^2 \quad (72)$$

$$R^2 = 0.992$$

$$FR > 0.043 \quad (t_{op} = 5.5 \text{ ms} << T_{dn})$$

It is found experimentally that the flow rate is very small (≈ 0) when the t_{op} is less than 5.5 ms. The following equations are obtained by following the same procedures described in IV.2.1.

$$\frac{(\bar{V}_p K_2) * (\rho_s A_f)}{A_1} = 0.018 \quad (73)$$

$$\frac{r * B}{\mu_0} = 49.77 \quad (74)$$

$$\frac{(\rho_s A_f)}{A_1} [(A_{cs} \delta) (1 - \epsilon) \rho_s - A_1 u_g] = 5.431 \quad (75)$$

The working current used in this operation is the same as that used in the operation with 100% solids (I_w = 148 a).

VII.1.1 Design of the Control System Parameters via Simulation

The various controller parameters are determined in a similar way to those of 100% iron (Chapter VI.).

VII.1.1.1 Controller Gain

Figure (79) shows the plots of ISQERR and ISQMAN versus the controller gain (K_C). The plots of the two variables follow different trends where ISQERR increases when the controller gain increases while ISQMAN decreases when the gain increases. The rate of the change in the former with K_C is much higher than the later one.

A value of -100 ms/psi is chosen for the proportional gain. The value is chosen on the basis of the criteria discussed in section IV.1.4.

VII.1.1.2 Filter Time Constant

Figure (80) shows the plots for ISQERR and ISQMAN versus the filter time constant for all three stages. All the plots show minimums around a filter time constant of 1.8 seconds. The minimums are more clearer for the plots of the middle and second stages than that for the top stage. Similar reasons to those given in section VI.2.1.2.2 could be used to explain the occurrence of the minimums.

VII.1.1.3 Input Constraints

Figure (81) shows similar plots of ISQERR and ISQMAN versus the upper limit constraint of $t_{op\ max}$ as those

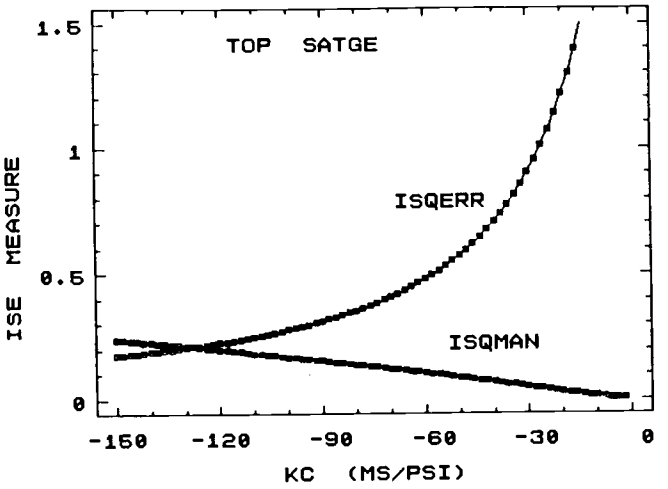

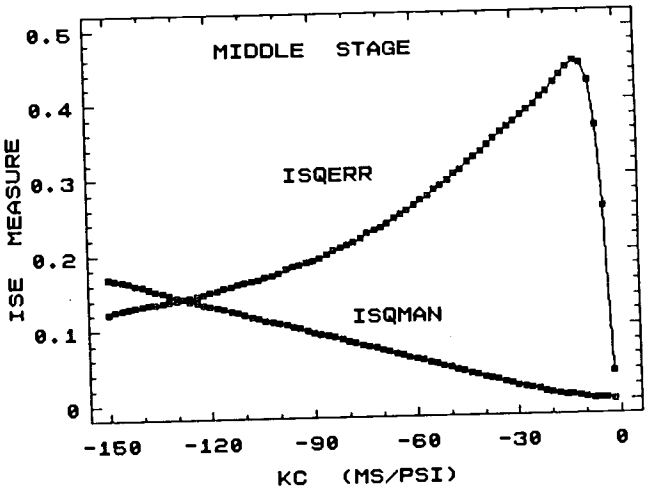

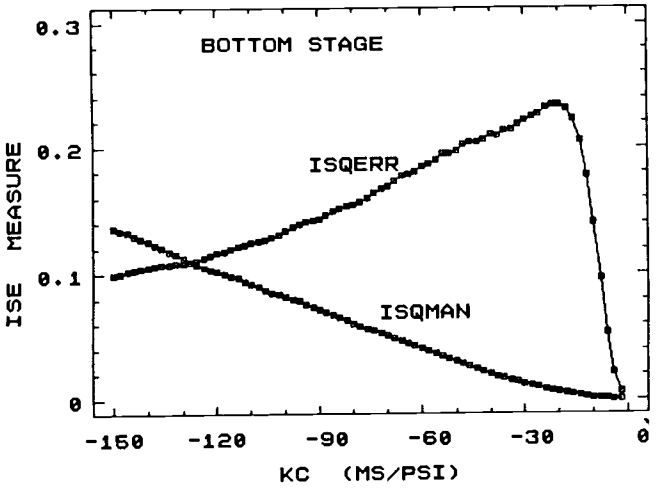

Figure (79)

ISQERR and ISQMAN for the Three Stages vs. the Control Gain for ON/OFF Operation (50% iron).

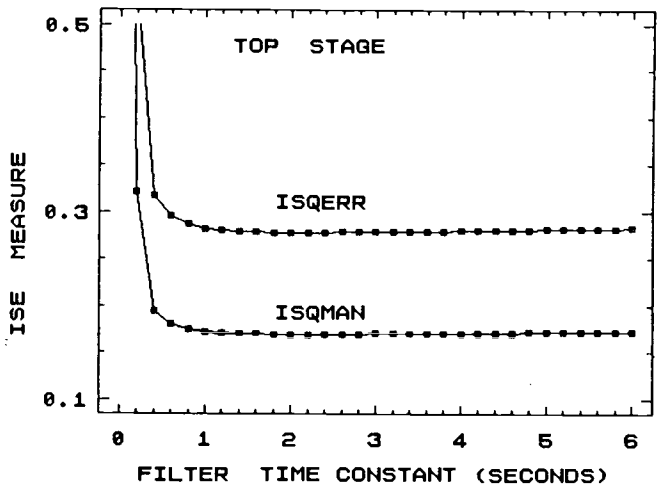

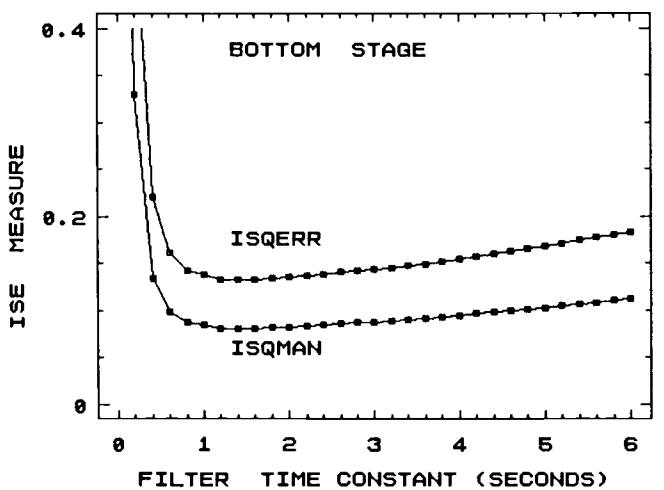

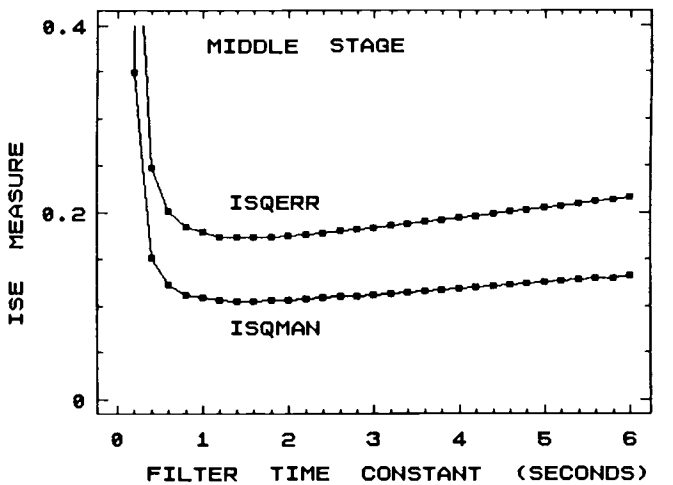

Figure (80)

ISQERR and ISQMAN for the Three Stages vs. Filter Time Constant for ON/OFF Operation (50% iron).

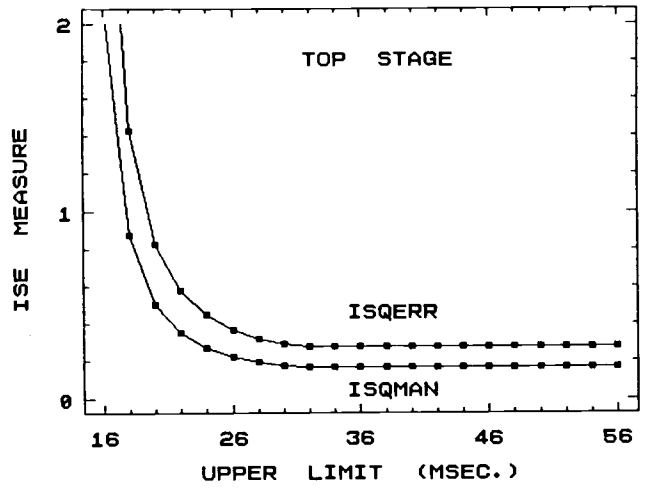

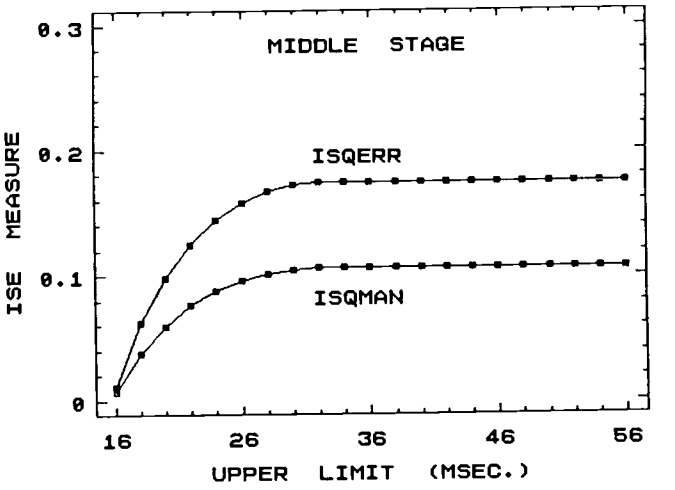

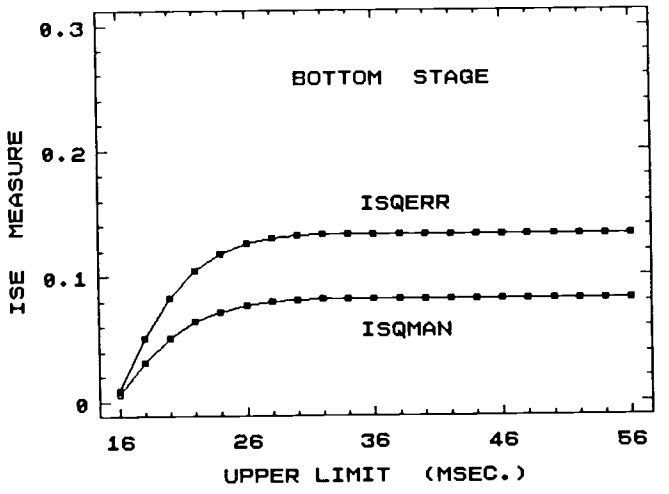

Figure (81)

ISQERR and ISQMAN for the Three Stages vs. the Upper Limit on Input Constraint for ON/OFF Operation (50% iron).

presented for 100% iron (figure 54). ISQERR for the top stage decreases with increasing upper limit of $t_{op\ max}$ until it reaches a constant value at $t_{op\ max}$ = 36 ms while that of the middle and bottom stages increase with the upper constraint on t_{op} until they reach a constant value at $t_{op\ max}$ = 32 ms. Therefore, a value of the upper limit of $t_{op\ max}$ is chosen to be equal to 36 ms.

The choice is mainly based on the results of the top stage, since the ISQERR and ISQMAN for this stage are much larger and more sensitive to the changes in the upper limit of $t_{op\ max}$ than the other stages. The explanation for the behaviors of the other stages is similar to that given in section VI.2.1.1.3

Figure (82) shows similar plots to the last one when the lower limit (constraint) of $t_{op\ max}$ is varied. The plots show that ISQERR and ISQMAN are not affected by changing the lower limit of $t_{op\ max}$ when $t_{op\ max}$ is less than 14 ms. Therefore, a value of zero is chosen to be the lower limit on $t_{op\ max}$.

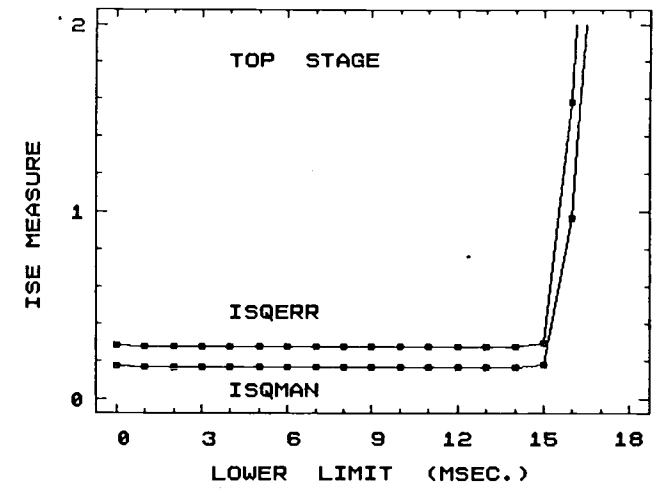

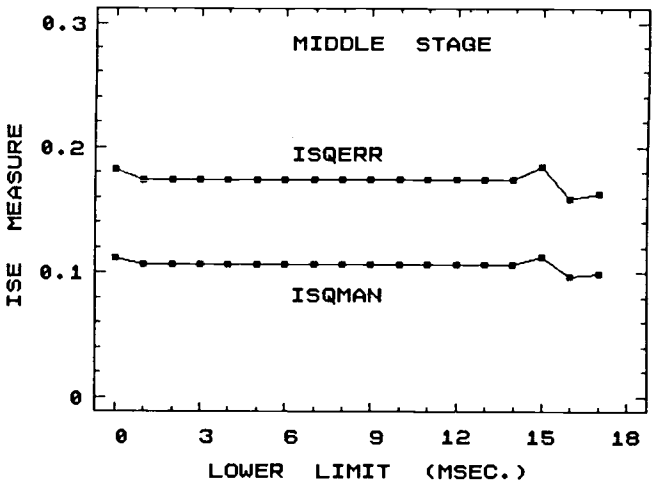

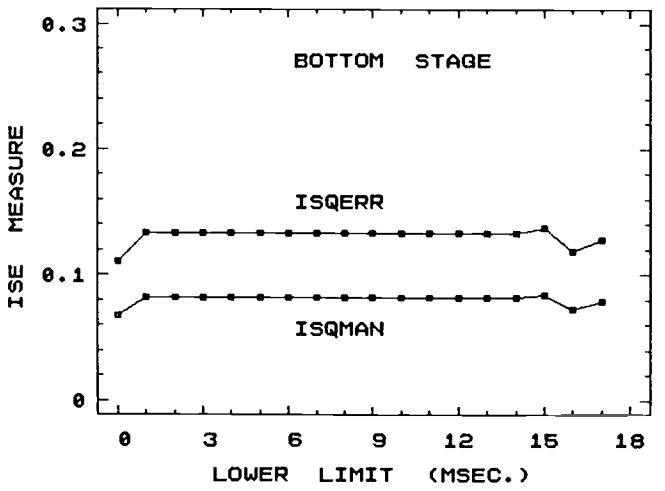

Figure (82)

ISQERR and ISQMAN for the Three Stages vs. the Lower Limit on Input Constraint for ON/OFF Operation (50% iron).

VII.1.2 Simulated Closed-Loop Performance

VII.1.2.1 Negative Step Change in the Pressure Drop Across the Stage

Figure (83) shows the pressure drop and the fraction open (controller output) responses for the three stages when a step change of -0.2 psi is made in the pressure drop of the top stage. The disturbances, which are due to the setpoint change in the top stage, in the pressure drops of the middle and bottom stages show irregular behavior when the change is introduced. The pressure drops fluctuate before the pulse occurrence. The duration of the disturbance increases from the middle to the bottom. The attenuation in the disturbances' height in negligible. The response of the top stage to a step in the setpoint is not as fast as those in chapter VI (figure 56). This is due to the lower value of K_c used in this chapter. The fractions open (controllers outputs) have much lower values than those in chapter VI. They never hit the constraints (FR_{up} = 0.28, FR_{dn} = 0). This low fraction open is due to the fact that solids flow rate through the stage is a strong function of the fraction open when partially magnetic solids are used (50% by weight). The setpoint in this case is equal to 0.5 psi. Similar plots are shown in figure (84) when decoupling is implemented. The fluctuations as well as the disturbances are greatly reduced. The disturbances in the pressure

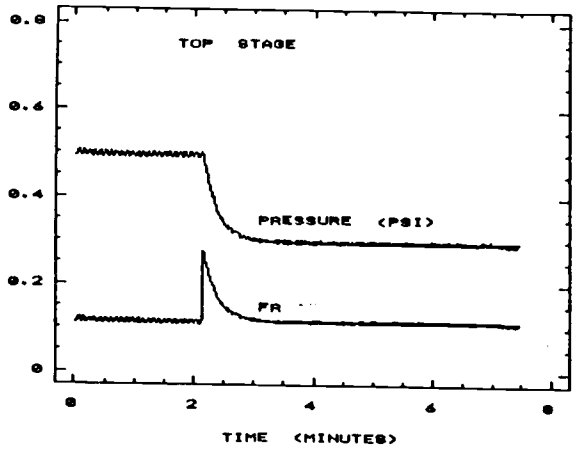

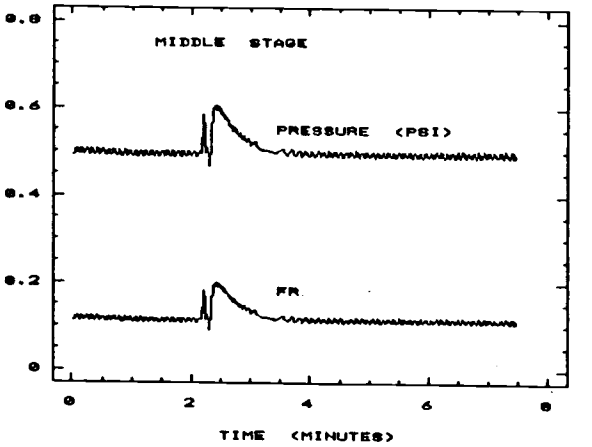

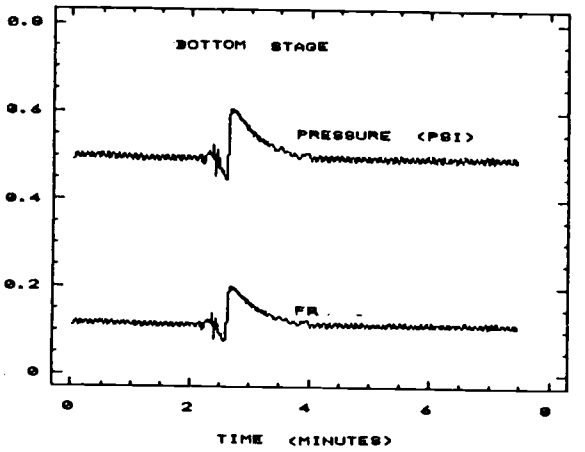

Figure (83)

Simulated Closed-loop Performances for a -0.2 psi Setpoint Change in the Top Stage without Decoupling (ON/OFF Operation and 50% Iron).

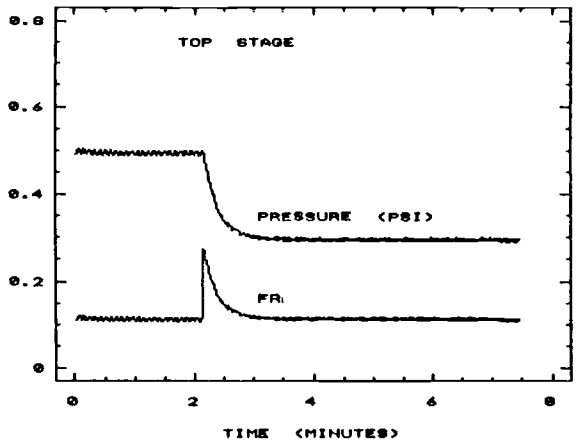

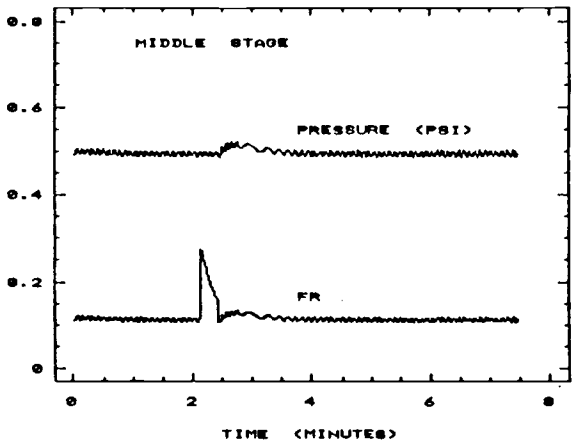

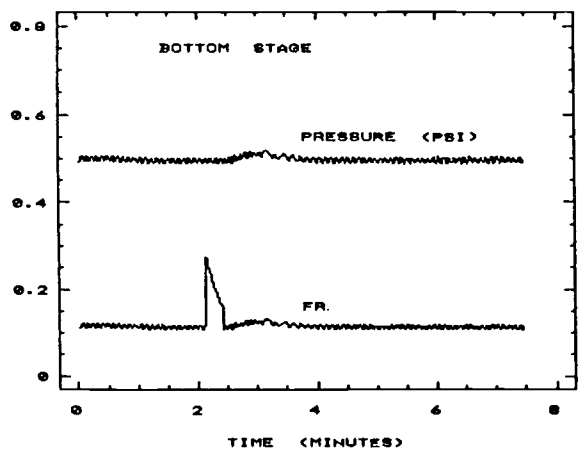

Figure (84)

Simulated Closed-loop Performances for a -0.2 psi Setpoint Change in the Top Stage with Decoupling (ON/OFF Operation and 50% Iron).

drop of the middle and bottom stages have maximum values of 0.53 psi and 0.52 psi respectively. The values of the fractions open of the middle and bottom stages, when the setpoint change is made, are equal to that of the top stage (FR = 0.28).

Figure (85) shows the results of a similar simulation with the setpoint change introduced to the middle stage. The height of the pressure drop disturbance across the bottom stage has a maximum value of 0.53 psi which can be considered as a good decoupling (ΔP_{max} = 0.61 for non-decoupling case). The pressure drop response across the top stage is not affected by the pressure drop levels or disturbances across the stages located below.

VII.1.2.2 Positive Step Change in the Feed Flow of Solids

Figure (86) shows the plots of pressure drop across the stage and controller output performances when a step in the feed rate of solids (ΔF = 32.3 gm/second) is introduced to the top stage at t = 1.5 minutes. The offset in the pressure drop has an average value of -0.03 psi as discussed in section VI.1.4. The response to the setpoint is more sluggish in going from the top stage to the bottom stage. Also, the response to the change is delayed from the top to the bottom stages.

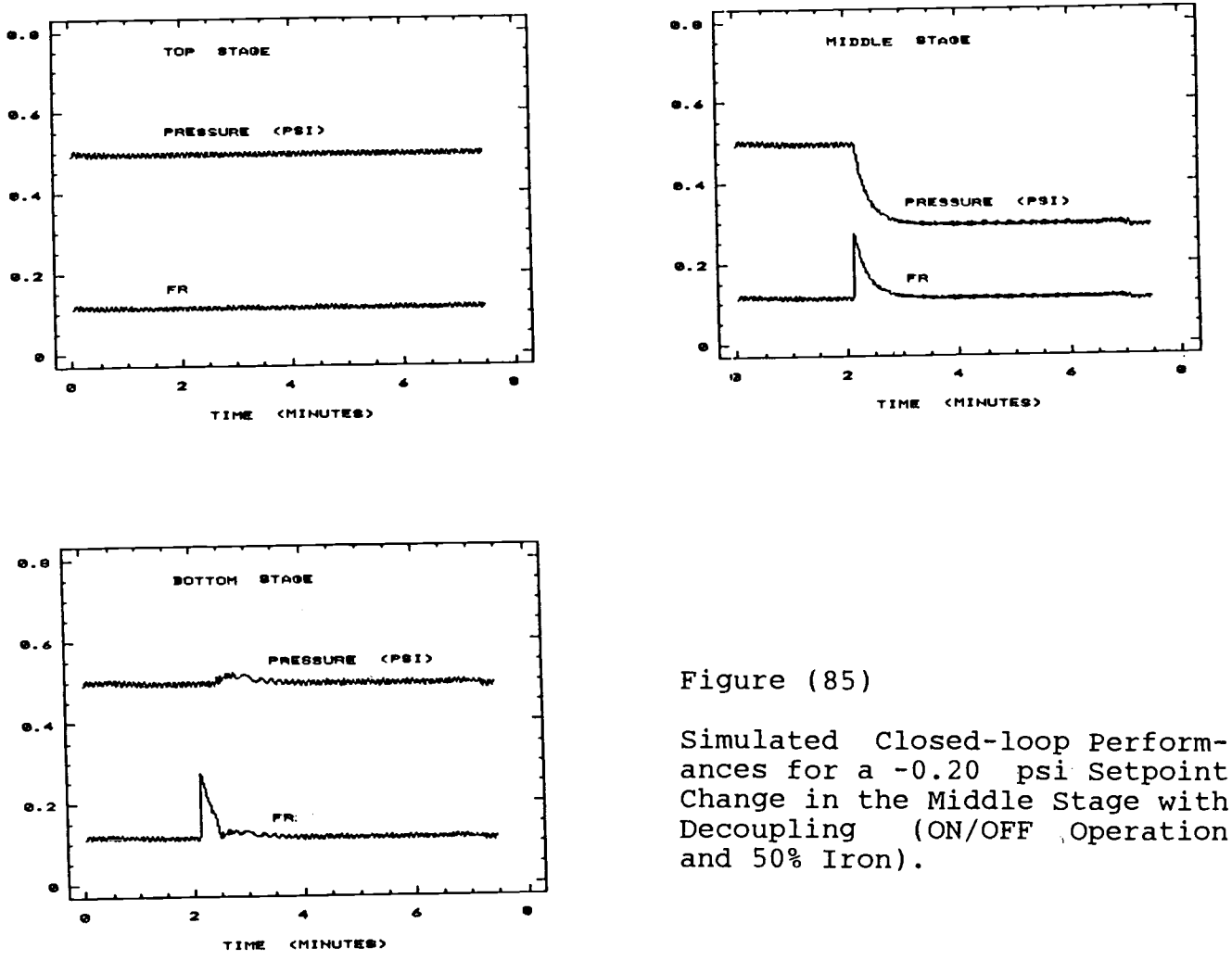

Figure (85)

Simulated Closed-loop Performances for a -0.20 psi Setpoint Change in the Middle Stage with Decoupling (ON/OFF Operation and 50% Iron).

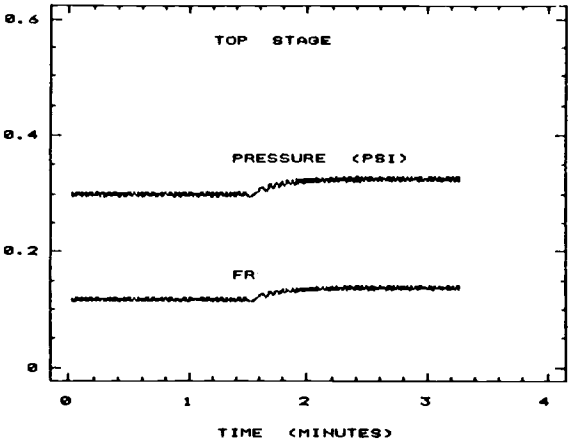

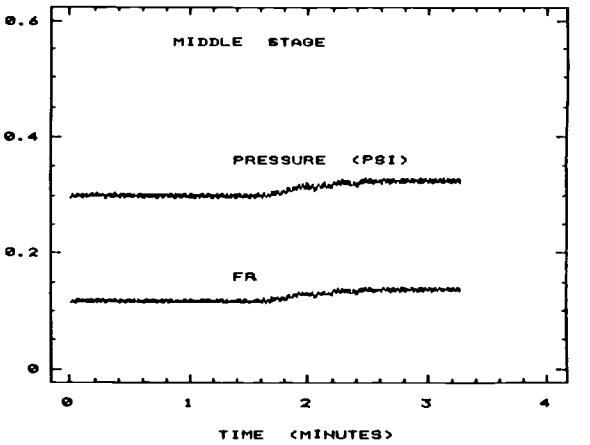

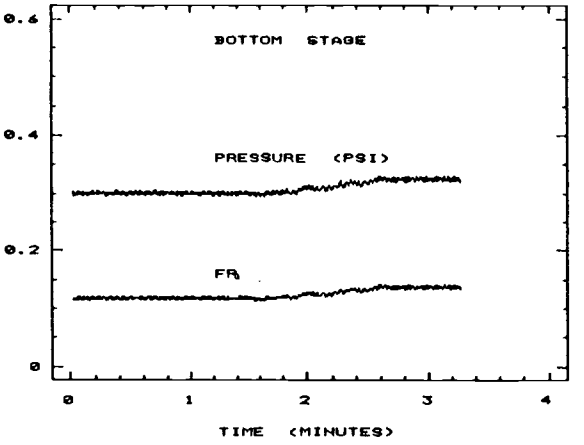

Figure (86)

Simulated Closed-Loop Performances for a 35 gm/second Step Change in the Feed Flow of Solids into the Top Stage (ON/OFF Operation and 50% Iron)

VII.1.3 Closed-Loop Experiments

VII.1.3.1 Negative Setpoint Change in the Pressure Drop Across a Stage

Figure (87) shows the experimental results corresponding to that of the last section (figure 83). The performances of the pressure drop and the controller output are very good and are similar to those of the simulation (figure 83). There is no undershoot in any of the stages. However, the disturbances in the pressure drops of both the middle and the bottom stages have maximum values of 0.67 psi and 0.62 psi respectively. The disturbance for the bottom stage has wider distribution than that for the middle stage. The controller outputs of all the stages did not hit any of the constraints.

Figure (88) shows similar plots with decoupling. Again, the performance of the pressure drops across each stage is very good. The disturbances in the pressure drops across the middle and bottom stages are reduced to values of 0.6 psi and 0.57 psi respectively.

Figure (89) shows the results of a similar experiment to the last one with the setpoint change introduced to the middle stage. Good pressure drops and controller output performances are observed. The disturbance in the pressure drop across the middle stage is completely eliminated.

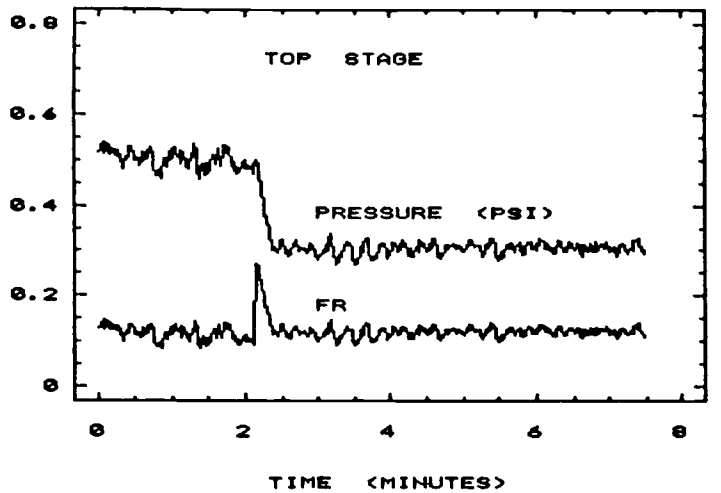

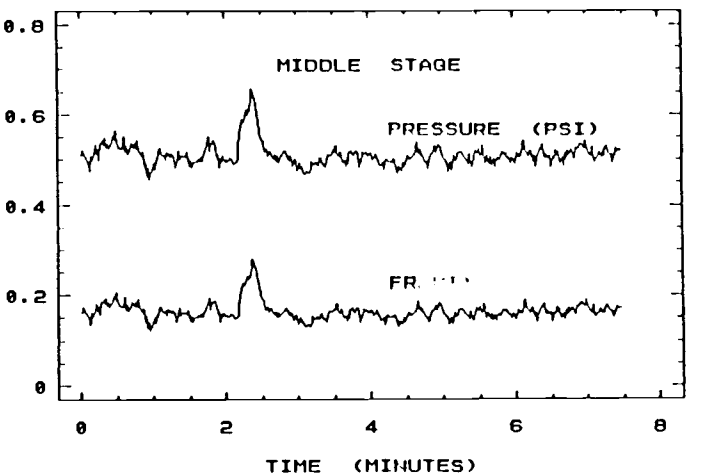

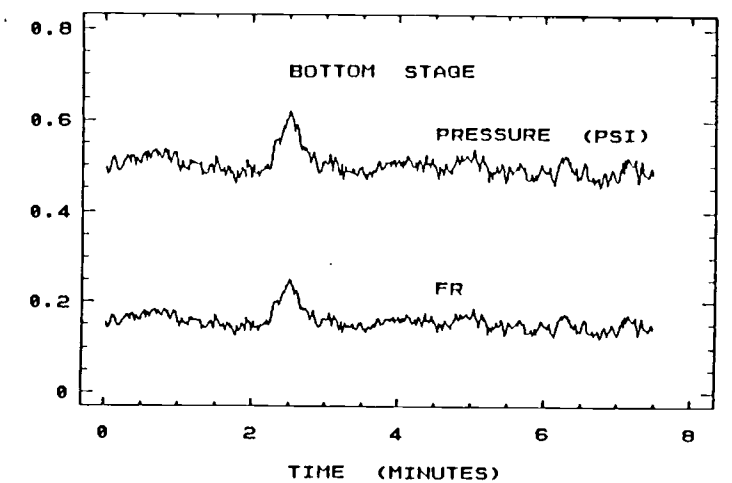

Figure (87)

Experimental Closed-loop Performances for a -0.20 psi Setpoint Change in the Top Stage without Decoupling (ON/OFF Operation and 50% Iron).

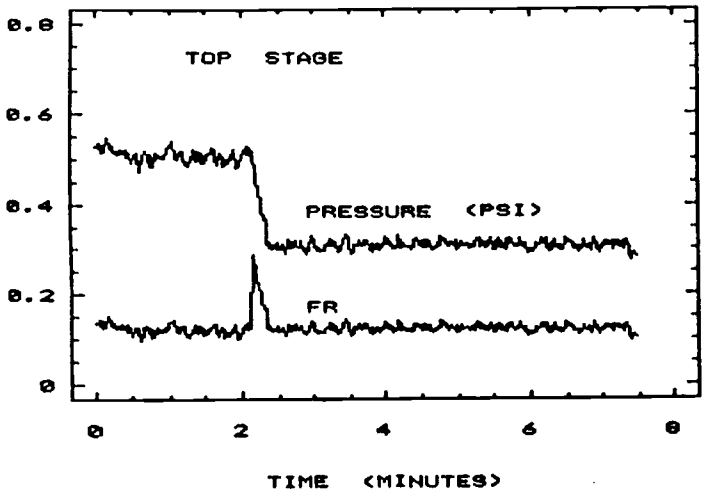

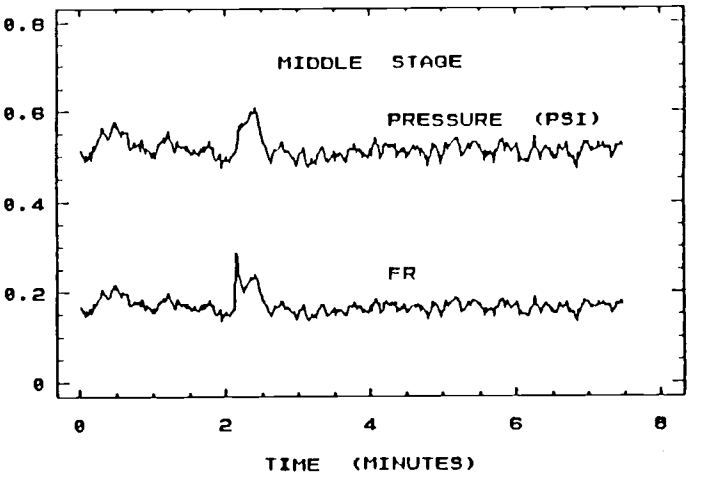

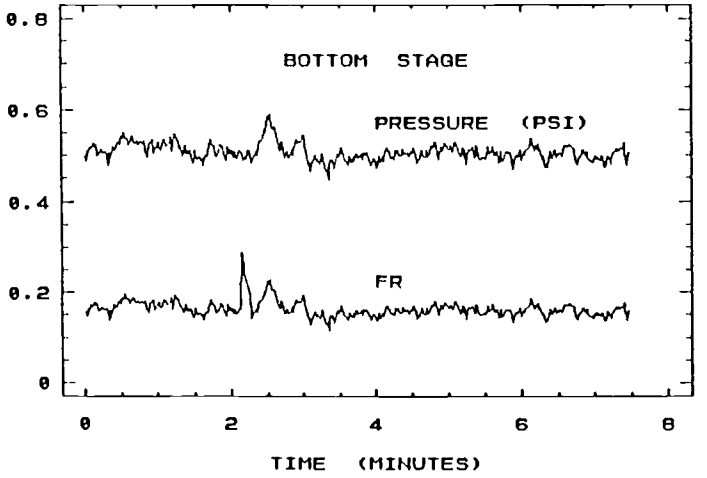

Figure (88)

Experimental Closed-loop Performances for a -.20 psi Setpoint Change in the Top Stage with Decoupling (ON/OFF Operation and 50% Iron).

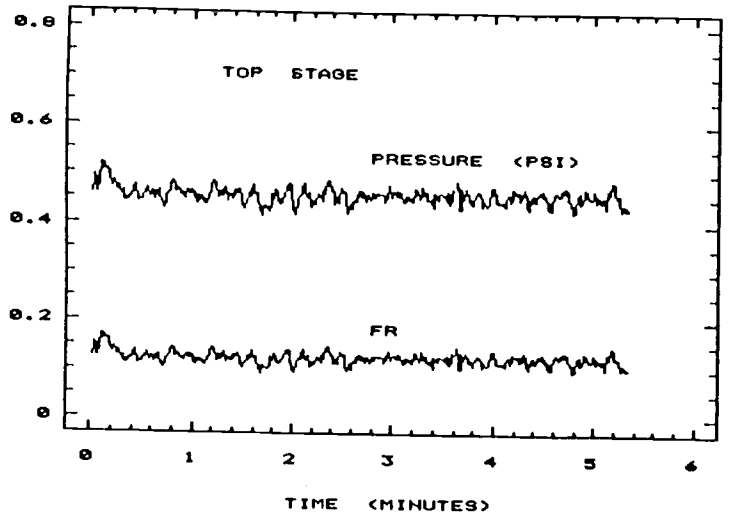

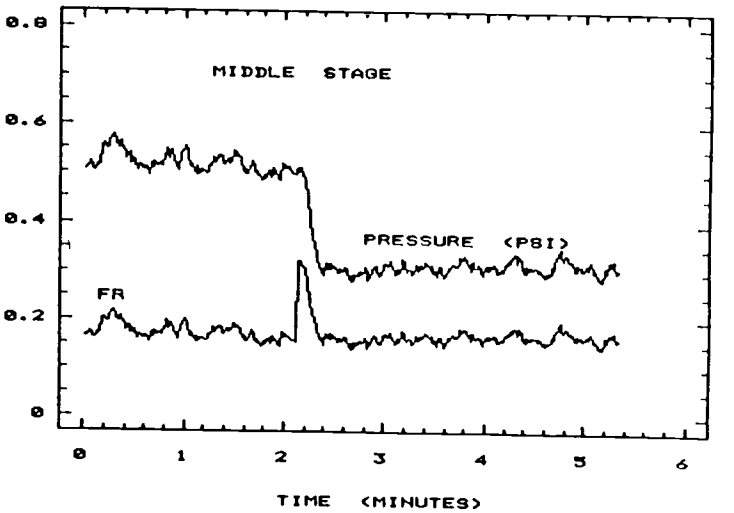

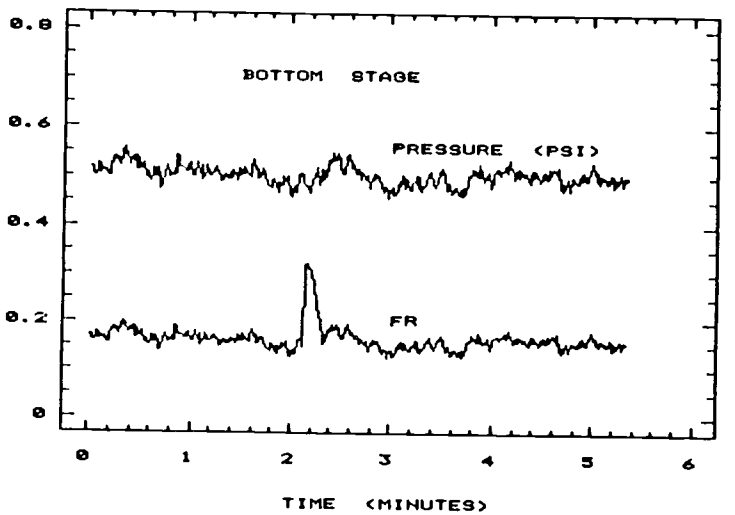

Figure (89)

Experimental Closed-loop Performances for a -0.20 psi Setpoint Change in the Middle Stage with Decoupling (ON/OFF Operation and 50% Iron).

eliminated. From the figures, the setpoint change in the pressure drop of the middle stage (changing the solids inventory) does not affect the performance of the top stage. The value of the controller outputs (fraction open) for the middle and bottom stages, when the step is introduced, is higher than the last case. This is due to the fluctuations in the flow rate of solids into the middle stage where the change in pressure drop setpoint is introduced.

VII.1.3.2 Positive Step Change in Feed Flow Rate of Solids

Figure (90) shows plots corresponding plots to those of section VII.1.2.2. The pressure drop across each stage rises to a value of 0.33 psi then slowly comes back to the desired value 0.3 psi in less than half a minute. This shows that the changes in the feed of solids to the column don not impose a serious control problem on the performance of the process.

VII.1.4 Comparison Between the Simulated and Experimental Performances

The response of the real process was close to the response obtained by the simulation using the proposed model.

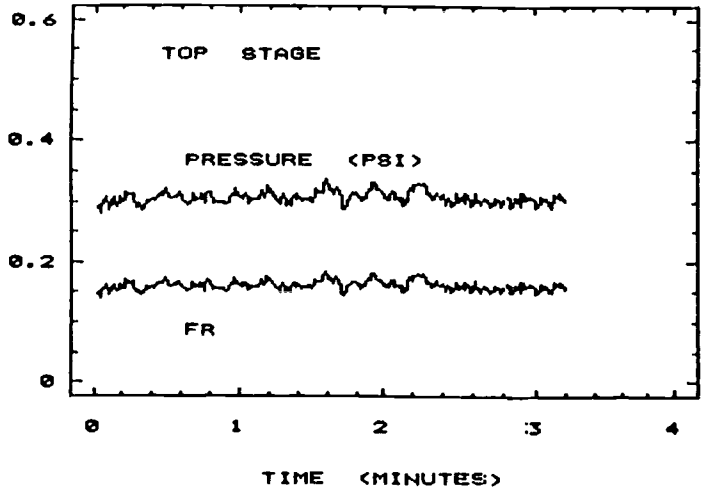

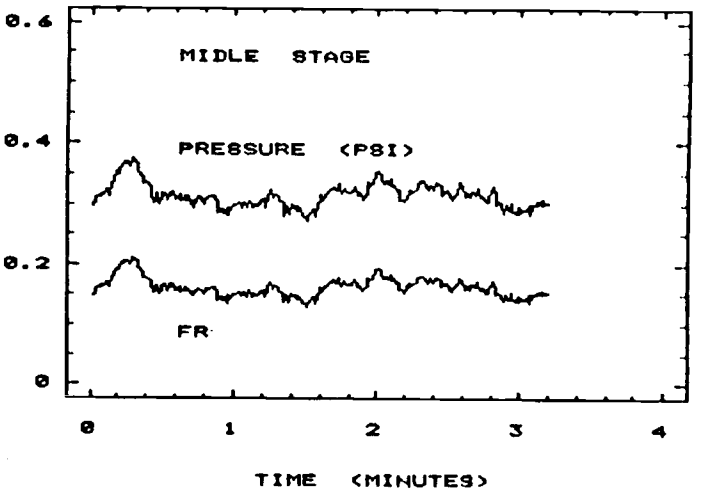

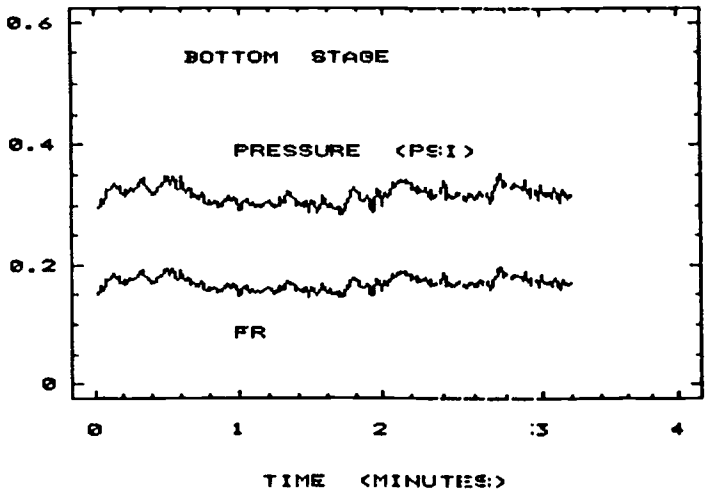

Figure (90)

Experimental Closed-Loop Performances for a 35 gm/second Step Change in the Feed Flow of Solids into the Top Stage (ON/OFF Operation and 50% Iron)

The heights of the disturbances in the experimental responses of the pressure drop across the middle and bottom stages are larger than those of the simulation. This is due to the faster experimental response of the pressure drop across the stage to the setpoint change. The pressure drop across the stage to which the step is introduced comes to the desired value in about 25 seconds for the experimental response and in about 35 seconds for the simulation response. The model for the flow rate of solids through the valve is based on the data taken for closed-loop steady-state operation which has a very good performance. The model does not properly describe the flow exactly during the transition from one pressure drop setpoint to another. The use of mixtures of magnetic and non-magnetic solids is one reason for this discrepancy between the simulation and experimental results. For large positive errors, the thickness of the layer close to the grate becomes very small and the flow of solids is large. Accordingly, the efficiency of the decoupling decreases. The simulation predictions were in very good agreement with the experimental results when the setpoint change is introduced to the middle stage and when decoupling is implemented. The response of the simulated closed-loop to a step change in the feed flow rate shows, as expected, an offset of about -0.03 psi. However, the experimental response to the same change in the flow rate is a pulse-like disturbance where the pressure drop

across each stage rises slightly then comes back to the desired value in a short time. The slow fluctuations of the experimental pressure drop across the stages differ from those in the simulation. The former are slower, more irregular, and less in amplitude than the latter. Similar reasoning, as those mentioned in the beginning of this section, as well as those mentioned in section VI.2.4 could be used to describe the discrepancy between the simulated and experimental results.

Generally, the agreement between the experimental and simulated pressure drop performance are good and better than that observed for 100% iron. No undershoot is observed in the simulated and experimental responses. This is partially a result of the use of the proper upper constraint predicted by the model.

VII.2 "Leaking" Valve Operation

The following correlation is obtained in a similar way to those in chapter VI.2.2.

$$m_o = 6.844 - 0.140 * I + 0.00071 * I^2 \qquad (76)$$

$$R^2 = 0.981$$

The following relations are obtained by the same procedure described previously for 100% iron.

$$\frac{(\bar{V}_p K_2)\ (\rho_s A_f)}{A_1} = 0.0561 \qquad (77)$$

$$\frac{r\ B}{\mu_0} = 31.38 \qquad (78)$$

$$\frac{(\rho_s A_f)}{A_1}\ [\ (A_{cs}\ \delta)\ (1-\epsilon)\ \rho_s - A_f\ u_g\ ] = 6.844 \qquad (79)$$

Figure (91) shows the plot of flow rate of solids through the stage and experimental data along with the theoretical line obtained by the non-linear regression.

VII.2.1 Evaluation of the Control System Parameters via Simulation

The control system parameters can be determined by following the previous procedures described in chapter VI.1.4.

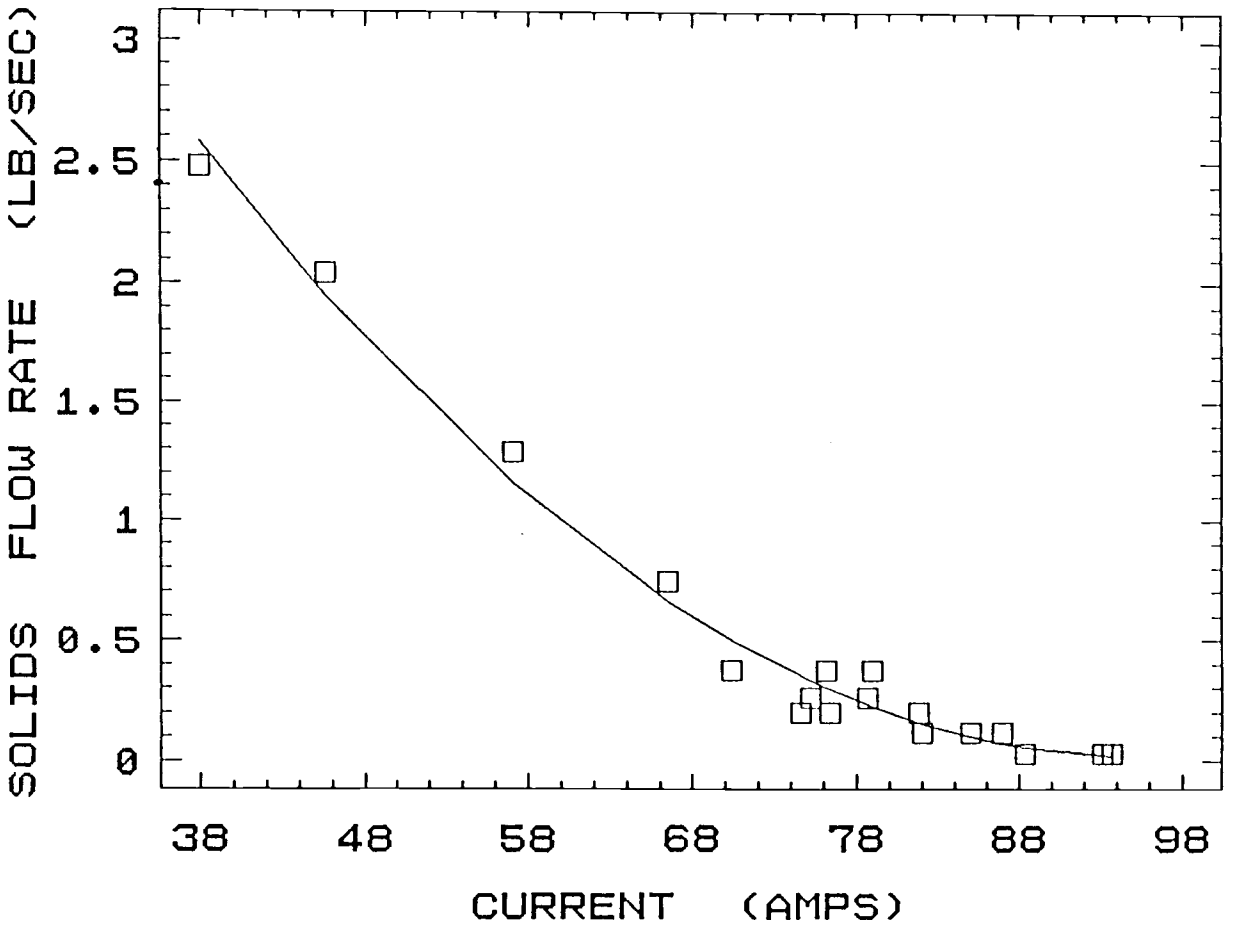

Figure (91) Plots of Solids Flow Rate out of the Stage vs. the Average Current (leaking valve operaion and 50% solids).

VII.2.1.1 Controller Gain

Figure (92) shows similar plots of ISQERR and ISQMAN versus K_C (amps/psi) to that of section VI.2.3.1.1 (figure 52). The ISQERR for each stage increases sharply for values of K_C less than 190 (amps/psi). The increase in ISQERR for K_C > 190 (amps/psi) is small. ISQERRS of the controller outputs increase linearly and have relatively large slopes (≈ .01 volts^2 * psi/amps = 14.44 amps/psi). As K_C increases, the controller behaves similarly to an on/off controller which has larger ISQERR. A value of 190 (amps/psi) is chosen for K_C. The choice of the proportional gain is based mainly on the results of the ISQERRS of the pressure drop across each stages following the same guidelines as those of section VI.1.4.

VII.2.1.2 Filter Time Constraint

Figure (93) shows the corresponding plots for T_F (filter time constant) for all the stages. The plots show minimums of ISQERR and ISQMAN for each stage at a filter time constant of 1.8 seconds. Therefore, a value of 1.8 seconds is chosen for the filter time constant.

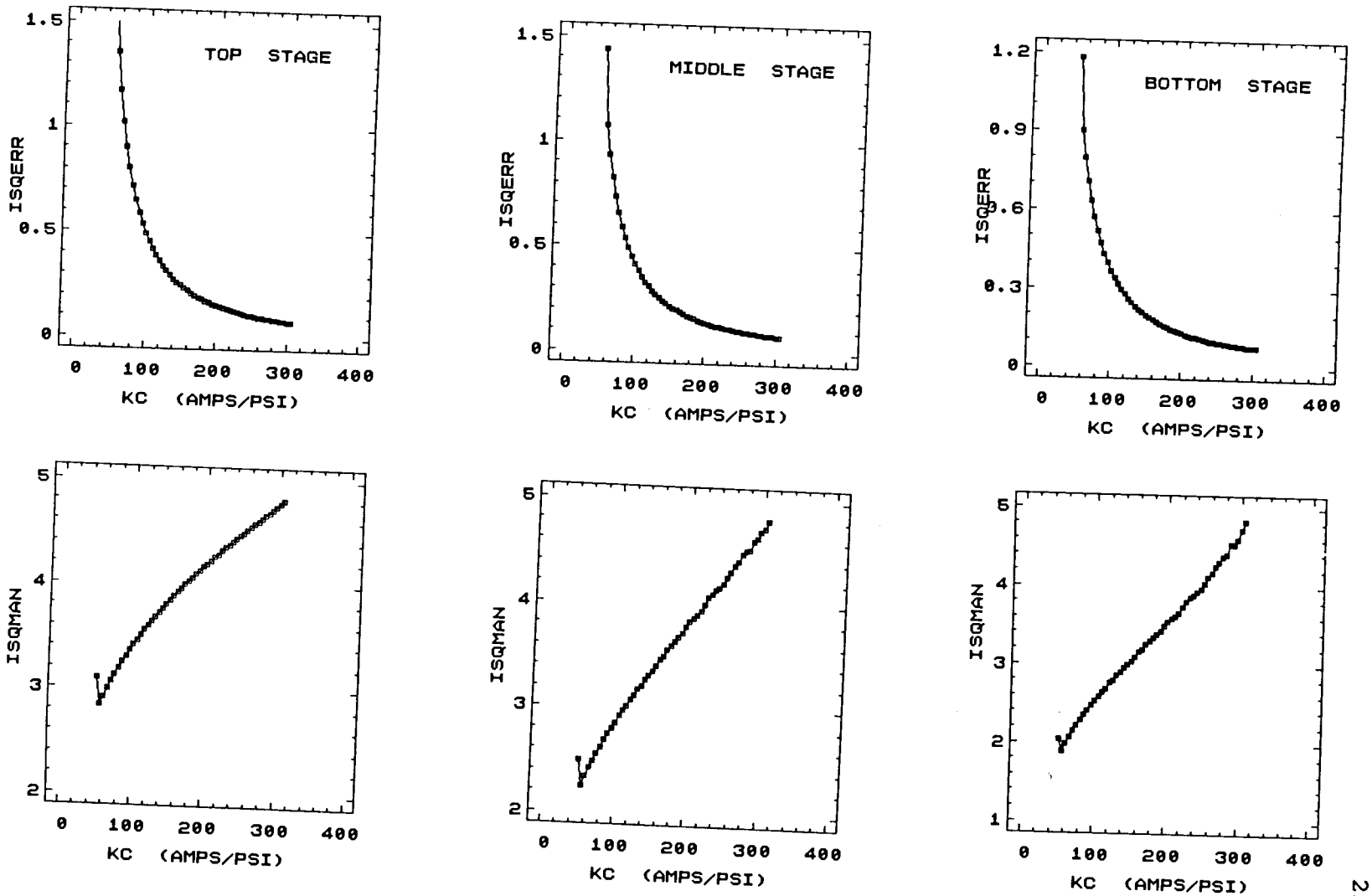

Figure (92) ISQERR an ISQMAN for the Three Stages vs. the Controller Gain.

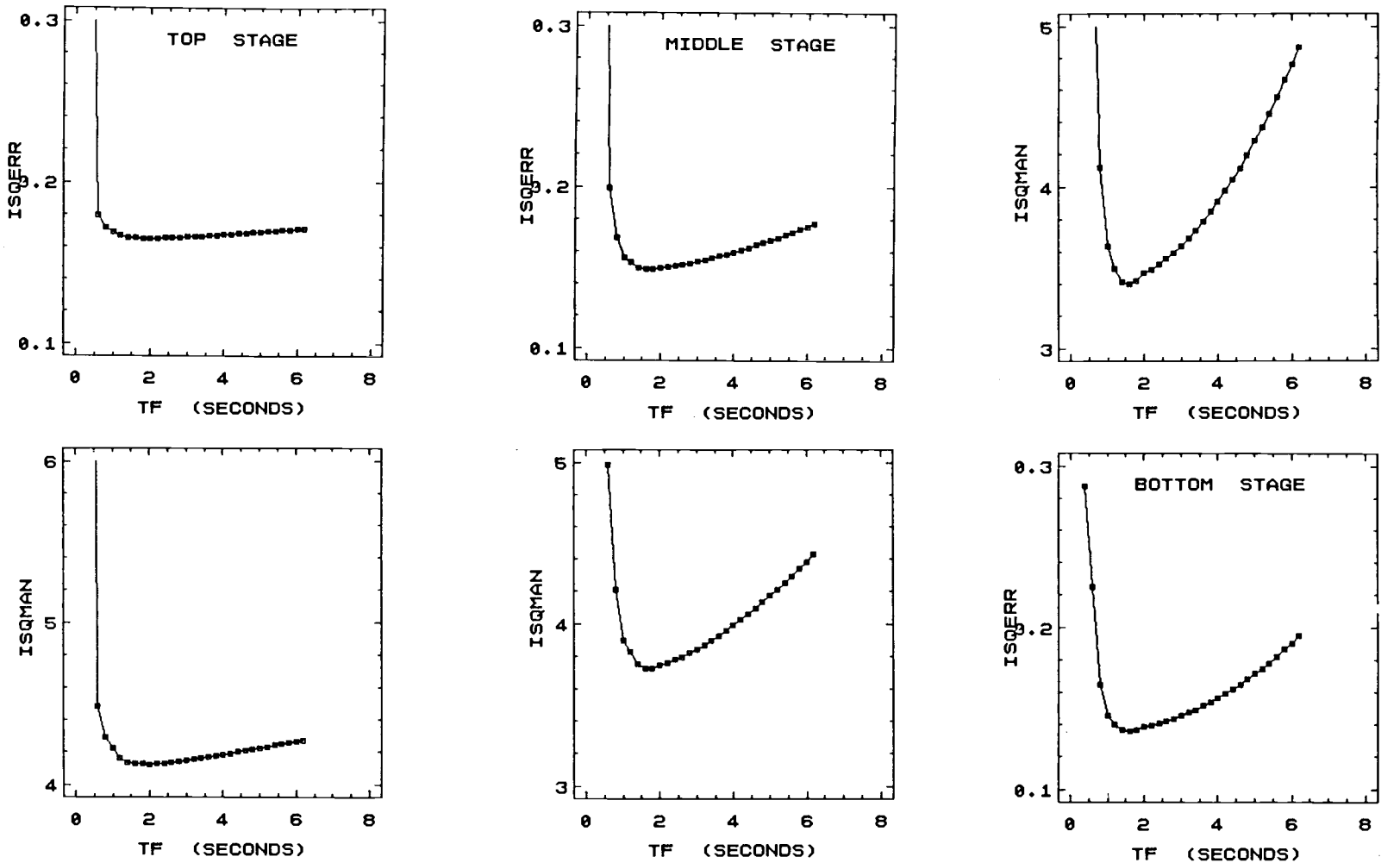

Figure (93) ISQERR and ISQMAN for the Three Stages vs. Filter Time Constant ("Leaking" Valve Operation and 50% Iron).

VII.2.1.3 Input Constraints

As mentioned in section VI.2.3.1.3, the values of the upper and lower constraints on the level of the current are determined experimentally. The upper constraint (I_h) was found to be equal to 100 amps. The value of the lower constraint (I_R) was found to be equal to 56 amps. Figure (94) and (95) show the results of the simulations.They show ISQERR and ISQMAN versus the upper and lower constraints respectively. The figures show that the ISQERR and ISQMAN of each stage are constants when the upper limit values of the current are greater than 86 amps. Figure (95) shows that ISQERR and ISQMAN for the top stage are constants for a lower limit current value less than 60 amps. The plots for the other stages show that ISQERR and ISQMAN are constant for a lower current limit between 60 amps and 20 amps. They increase sharply for a lower limit below 20 amps. The ISQERR and ISQMAN of the top stage for a lower constraint limit greater than 60 amps show a large increase. Therefore, the results of the simulation support the values of the constraints found experimentally.

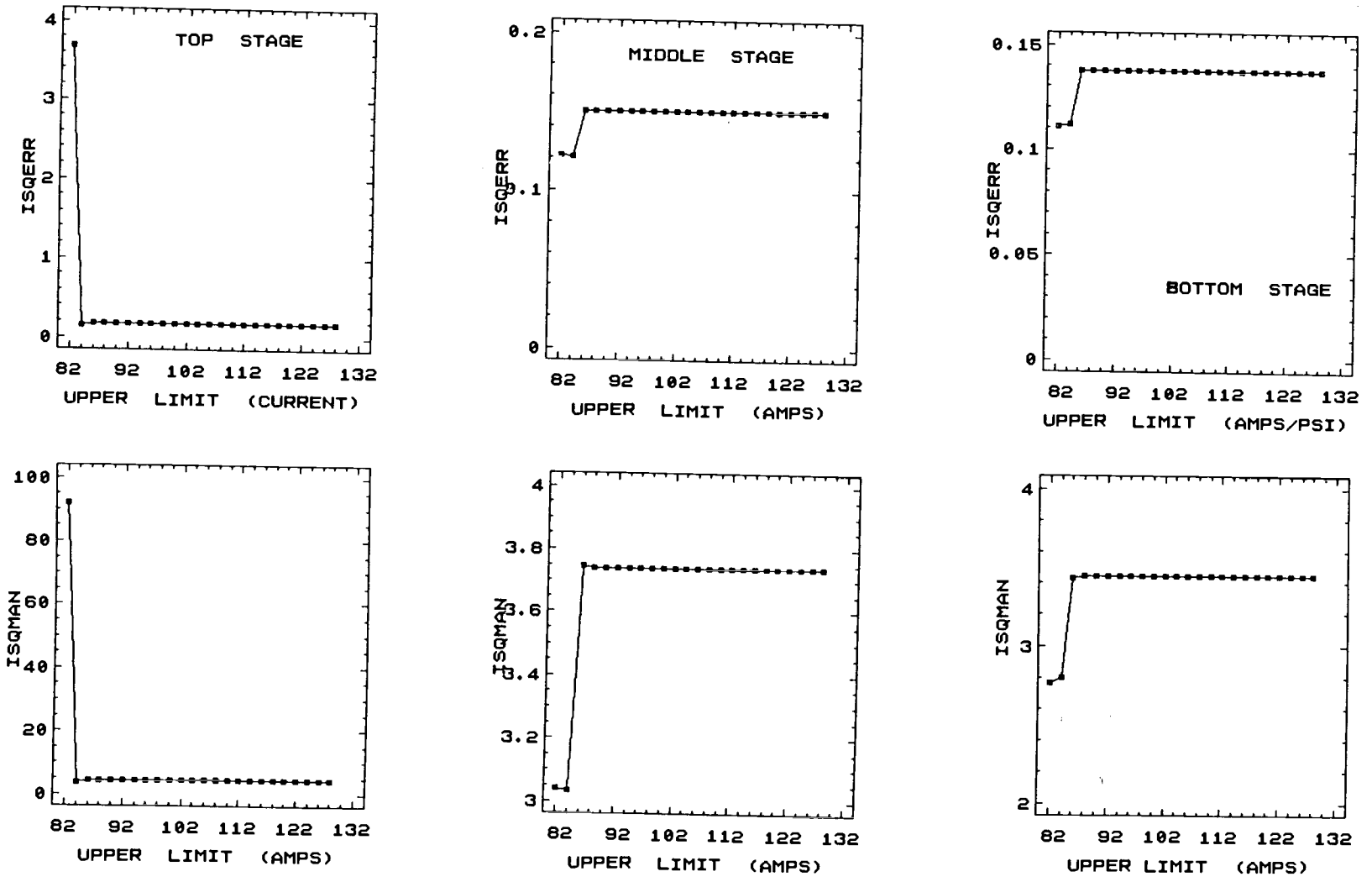

Figure (94) ISQERR and ISQMAN for the Three Stages vs. the Upper Limit on Input Constraint ("Leaking" Valve Operation and 50% Iron).

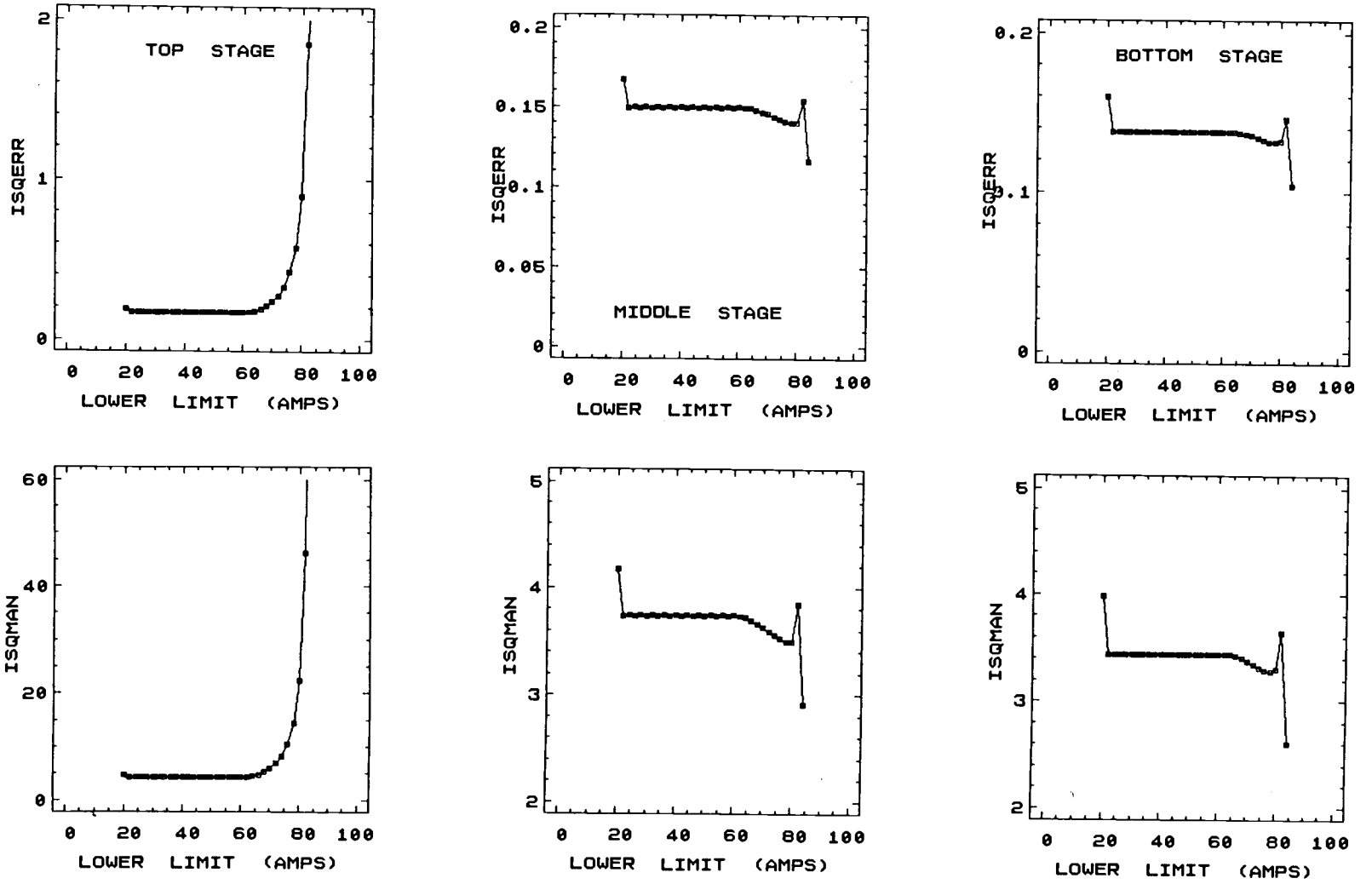

Figure (95) ISQERR and ISQMAN for the Three Stages vs. the Lower Limit on Input Constraint ("Leaking" Valve Operation and 50% Iron).

VII.2.2 Simulated Closed-Loop Performance

VII.2.2.1 Negative Setpoint Change in the Pressure Drop Across a Stage

Figure (96) shows the plots of the pressure drop and the current (controller output) versus time for a -0.2 psi setpoint change in the pressure drop across the top stage. The pressure drop across the top stage undershoots by 0.07 psi below the desired value (0.3 psi) as a result of the setpoint change. The pressure drops across the other stages undershoot by 0.03 psi below the desired value (0.50 psi) at the end of the disturbances. The disturbances in the pressure drop response are slightly attenuated in going from the middle stage ($\Delta P_{max} \approx 0.65$psi) to the bottom stage ($\Delta P_{max} \approx 0.62$psi). The response to the disturbances in the pressure drop is more sluggish in going from the middle to the bottom stages. The response of both the pressure drop and the controller output are oscillatory. The characteristics of the oscillation are similar to those of section VI.2.2.2.1. The controllers output for the top stage hit the lower constraint once. The controller outputs of the other stages have minimum values that lie between the lower constraint (I = 56 amps) and the steady state value (I = 84 amps).

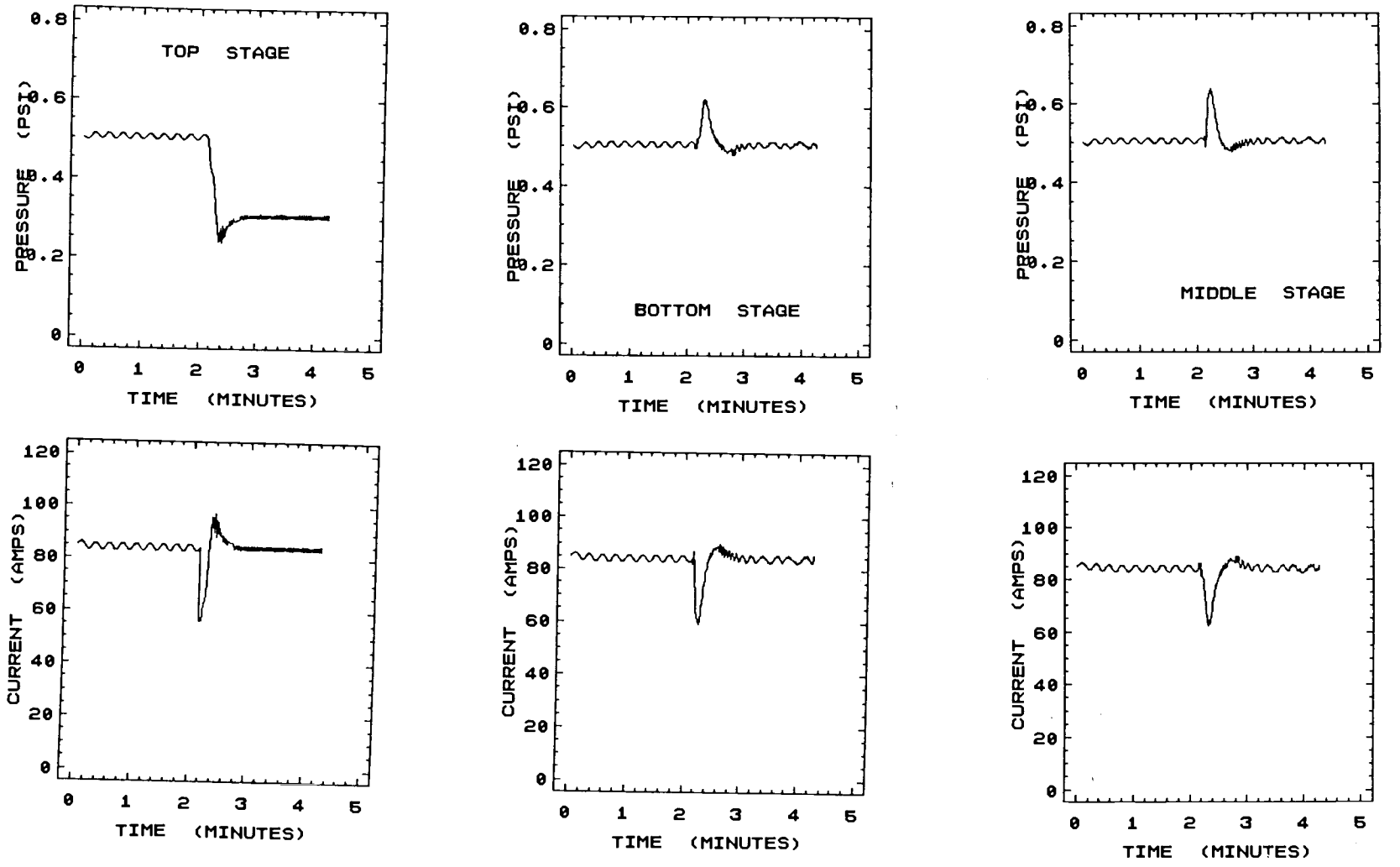

Figure (96) Simulated Closed-loop Performances for a -0.2 psi Setpoint Change in the Top Stage without Decoupling ("Leaking" Valve Operation and 50% Iron).

Figure (97) shows a similar experiment, but with decoupling. The response of the top stage is the same as the last case. However, the disturbances in the pressure drop across the middle and the bottom stages are completely eliminated. The undershoots of the pressure drops across each stage is the same as the last case. All of the controller outputs hit the lower constraint (I = 56 amps) because of the action of decoupling.

Figure (98) shows a similar experiment as the last one with the setpoint change introduced to the middle stage. The undershoots in the pressure drop have a value of 0.03 psi below the desired value of (0.3 psi). Similar reasoning as that used in the similar case in section VI.2.2.2.1 could be used to explain the difference in the behavior between this case and the last one.

VII.2.2.2 Positive Step Change in the Feed Flow Rate of Solids

Figure (99) shows the plots of the pressure drop and current versus time. The pressure drops increase by 0.03 psi when the step is introduced. The pressure response to the step change is sluggish. The disturbances in the pressure drops are delayed in going from the top to the bottom stages. The controller outputs drop to a lower value of the current to increase the flow rate of solids through

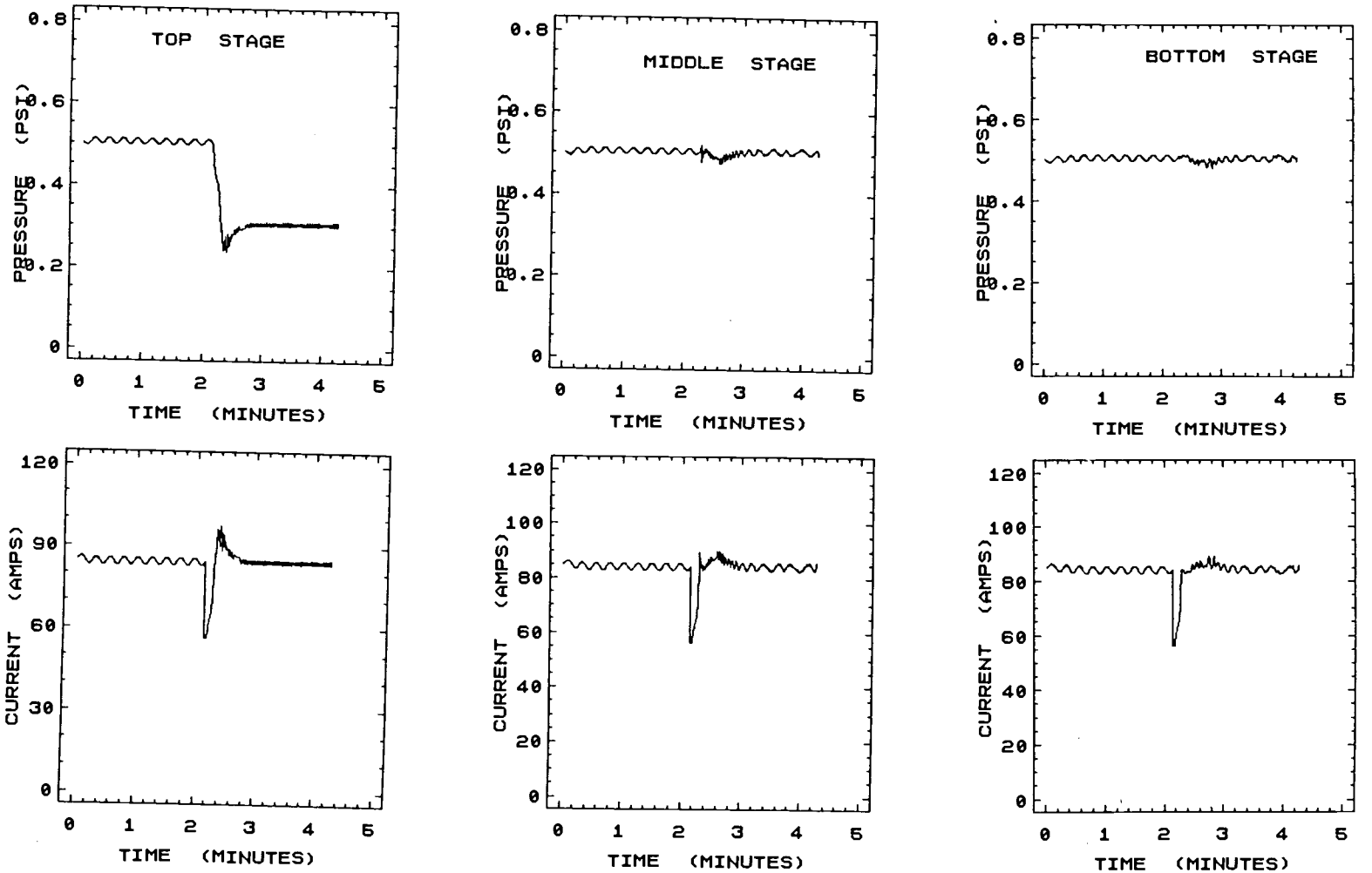

Figure (97) Simulated Closed-loop Performances for a -0.2 psi Setpoint Change in the Top Stage with Decoupling ("Leaking" Valve Operation; 50% Operation).

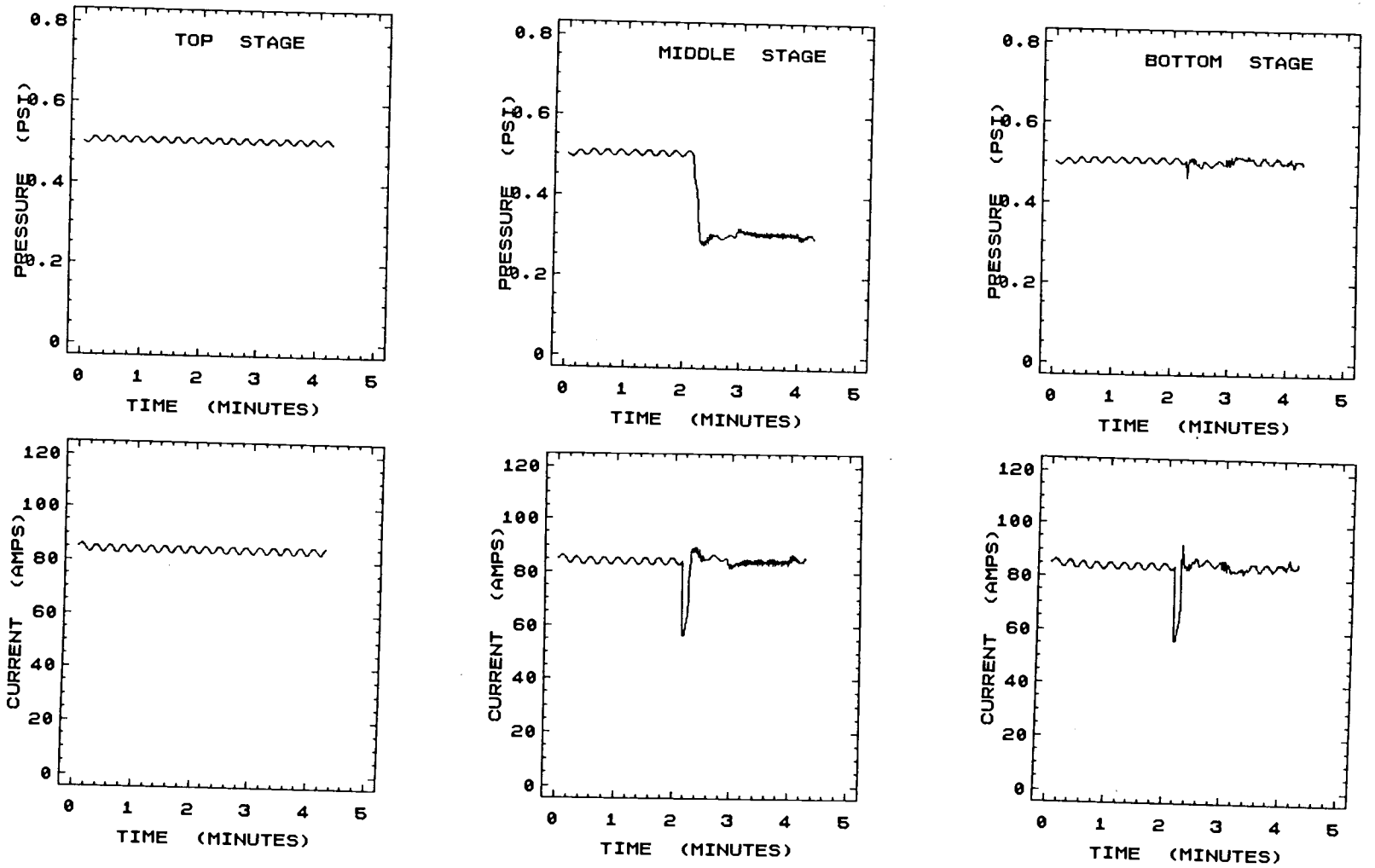

Figure (98) Simulated Closed-loop Performances for a -0.20 psi Setpoint Change in the Middle Stage with Decoupling ("Leaking" Valve Operation; 50% Operation).

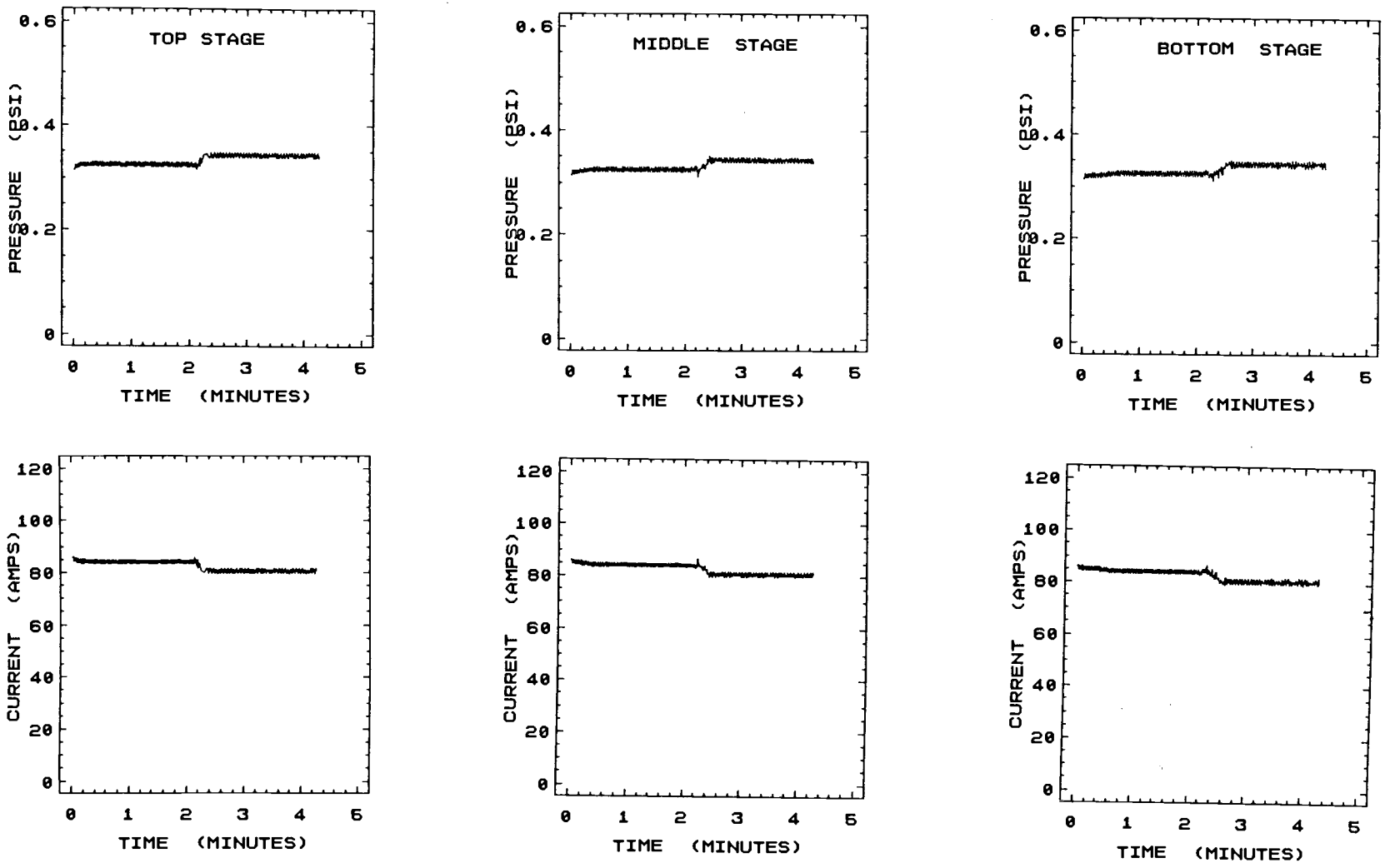

Figure (99) Simulated Closed-loop Performances for a 35 (gm/second) Step Change in the Feed Flow of Solids into the Top Stage.

the valves. However, some offset (-0.03 psi) is observed, as predicted by section VI.1.4. The plots of the pressure drop across each stage show a very slight decrease from the maximum value (.35 psi).

VII.2.3 Closed-Loop Experiment

VII.2.3.1 Negative Setpoint Change in the Pressure Drop Across a Stage

Figure (100) shows the corresponding experimental plots to that of VII.3.2.1. The disturbances in the pressure drop of the middle and the bottom stages are large ($\Delta P_{max} \approx$ 0.7 psi). The pressure drop across the top stage undershoots by a value of 0.07 psi when the step was introduced. The undershoots in the middle and bottom stages at the end of the disturbances are 0.03 psi and .02 psi respectively. The controllers of each stage hit the lower constraint (I = 56 amps) when the setpoint change was introduced. The occurrence of the relatively high peaks in the pressure drop was the result of the fast pressure response of the top stage to the setpoint change and the undershoot of the pressure drop across the top stage below the desired value (0.3 psi). Generally, the performances of both the pressure drop and the controller output are good and their oscillations around the setpoint are small.

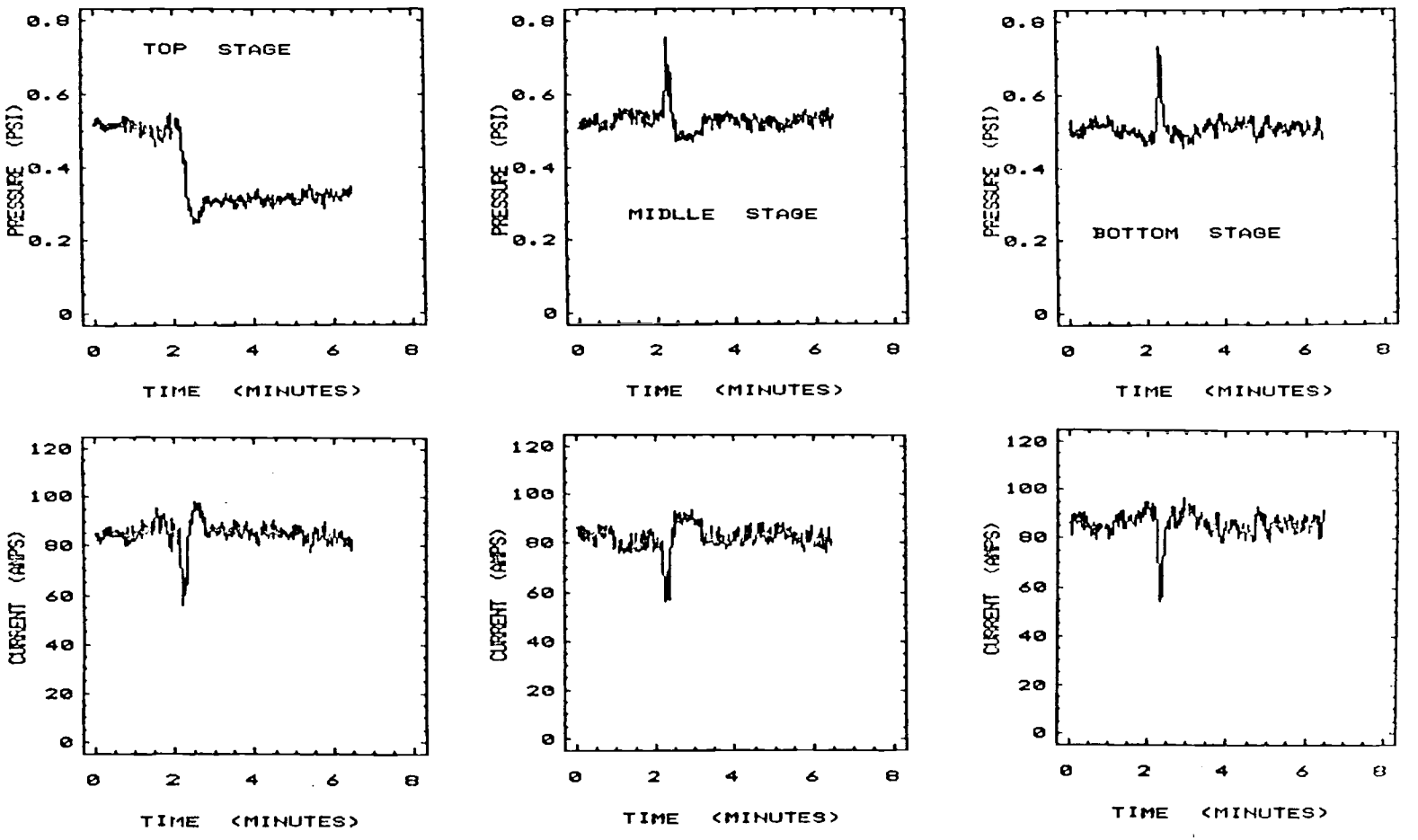

Figure (100) Experimental Closed-loop Performances for a -0.2 psi Setpoint Change in the Top Stage without Decoupling ("Leaking" Valve Operation and 50% Iron).

Figure (101) is a similar experiment with decoupling. The pressure drop response across each stage is very good. The disturbance in the pressure drop of the middle stage is greatly reduced while it is completely eliminated for the bottom stage. The oscillations of the pressure drop across the stages and the current are small. The pressure drops across the top and middle stages undershoot the desired value by 0.05 psi and 0.03 psi respectively. The currents (controller outputs) hit the lower constraint at the same time when the setpoint change is introduced.

Figure (102) shows the same type of experiment when the setpoint change was introduced to the middle stage. Similar behavior is observed as the last case with the exception of the lower undershoot of pressure drop across the middle stage and no undershoot in the pressure drop across the bottom stage.

VII.2.3.2 Positive Step Change in the Feed Flow Rate of Solids

Figure (103) shows the experimental plots of the closed loop performances of the pressure drop across each stage and the current for a step in the feed flow rate of solids (ΔF = 32.3 gm/sec). The pressure drop rose from the desired value (0.35 psi) by approximately .02 psi when the step change is introduced (t=2 minutes). The disturbances in the

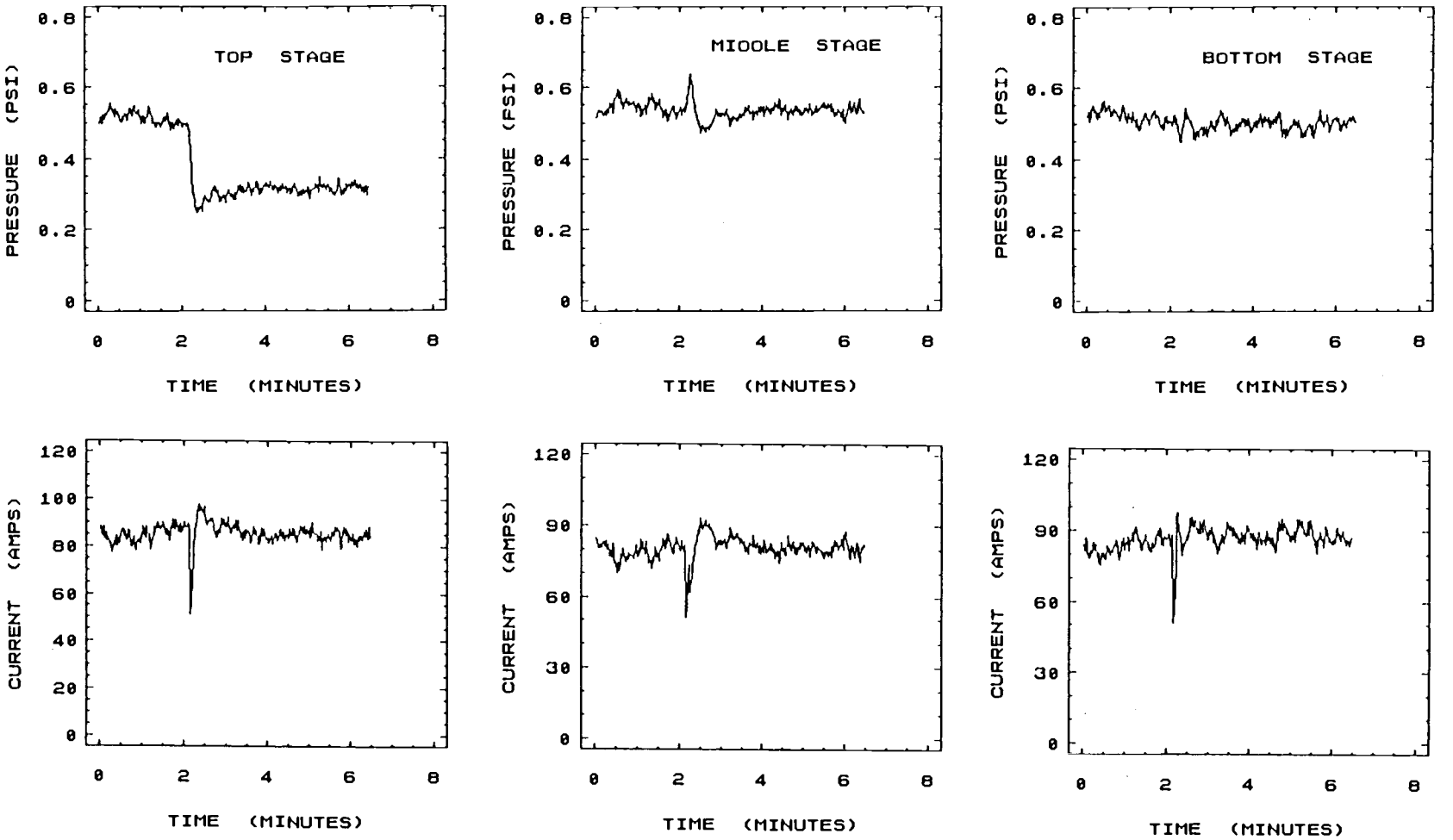

Figure (101) Experimental Closed-loop Performances for a -.20 psi Setpoint Change in the Top Stage with Decoupling ("Leaking" Valve Operation and 50% Iron).

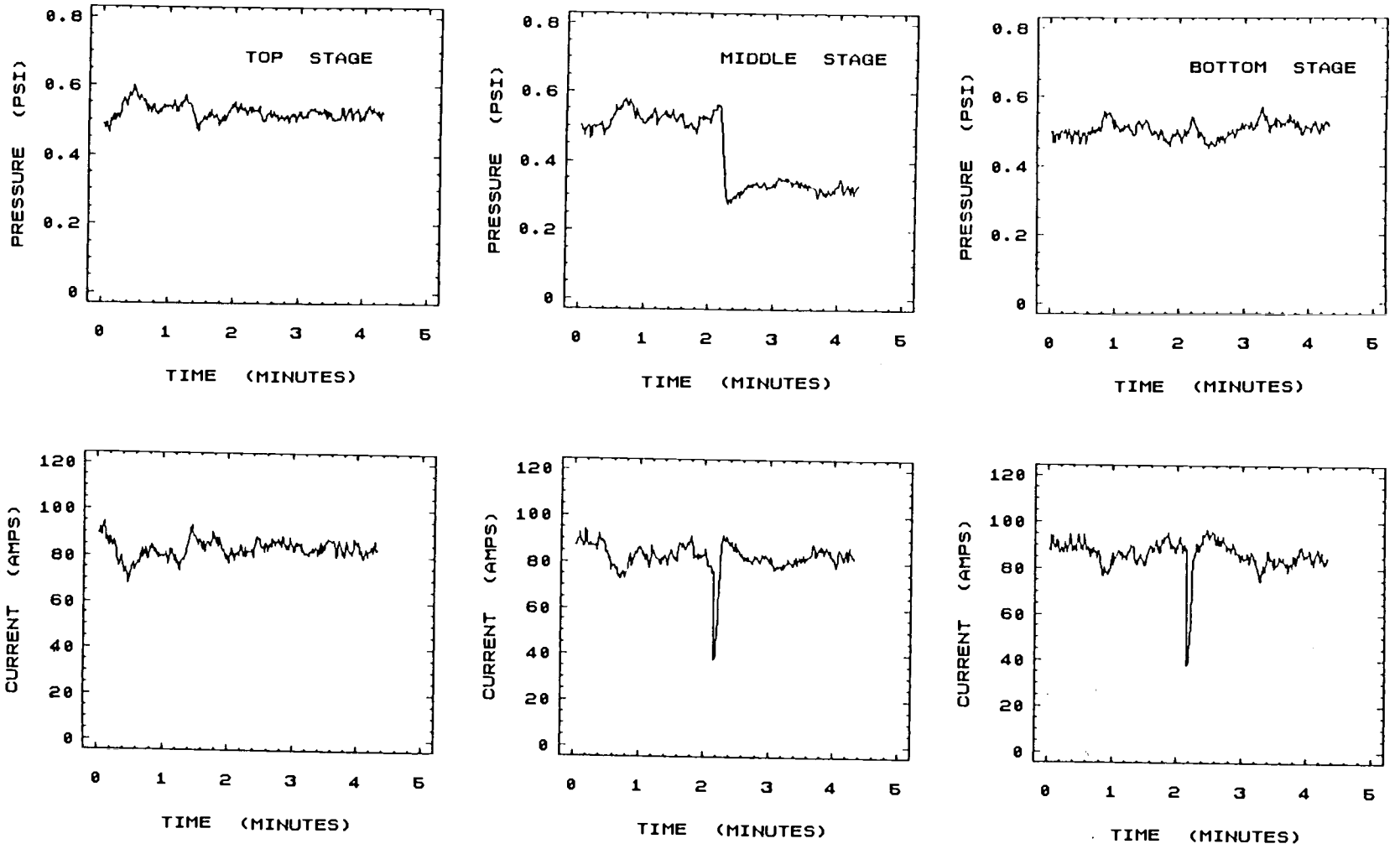

Figure (102) Experimental Closed-loop Performances for a -0.20 psi Setpoint Change in the Middle Stage with Decoupling ("Leaking" Valve Operation and 50% Iron).

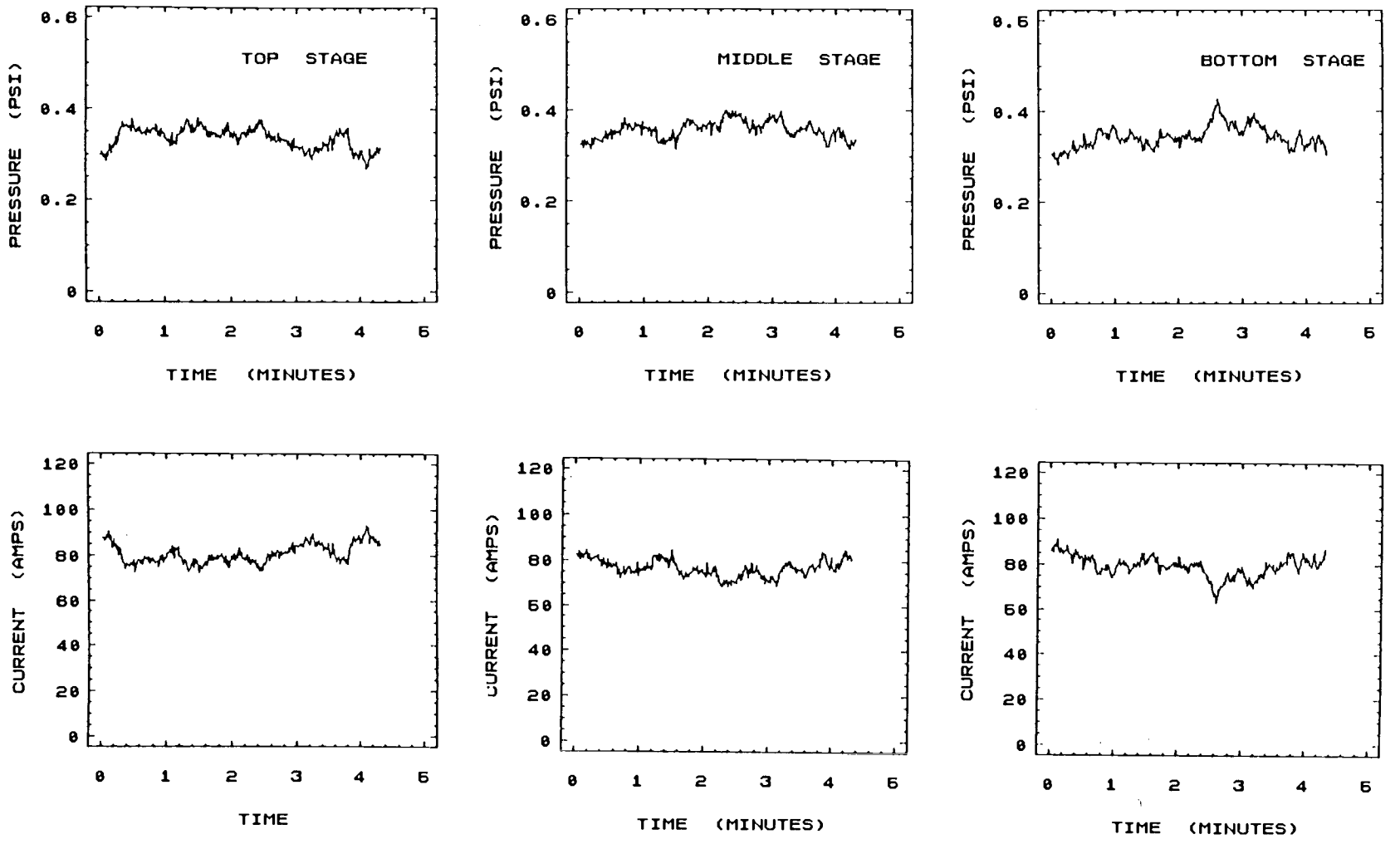

Figure (103) Experimental Closed-loop Performances for a 35 (gm/second) Step Change in the Feed Flow of Solids into the Top Stage ("Leaking" Valve Operation and 50% Iron).

pressure drop are delayed in going from the top to the bottom stages. The pressure responses fluctuate slowly around the setpoint (0.35 psi). The fluctuations have larger amplitude after the step change is introduced. This may be as a result of using solids that are partially magnetic.

VII.2.4 Comparison Between Simulated and Experimental Results

The simulation results agree with the experimental results fairly well. The general behavior of the pressure drop across the stage is accurately predicted by the simulation.

Again, the disturbances in the pressure drop across the middle and bottom stages show higher values than those for the simulation. This case was for the step change in the setpoint of the pressure drop across the top stage without decoupling. The response of the pressure drop predicted by the simulation and observed in the experiment to a step change in setpoint is exactly identical. Similar reasons to those mentioned in chapter VI. may be used to explain the higher heights of the disturbances in the experimental response. The pressure drops and controller outputs performances for the decoupling case looks similar in both the experiment and the simulation with the exception of the occurrence of a small sharp peak disturbance in the middle stage

pressure drop response of the experiment. This could be due to the change in air profile entering the stage which is accompanied with a change in the solids flow rate.

The results of a setpoint change in the pressure drop across the middle stage, when decoupling is implemented, look very similar in both the simulation and experimental performances.

The performances of the pressure drop across the stages to a step in the feed flow rate are different. The experimental pressure drop response to the load change is better and faster than that of the simulation. The simulation shows an offset of -0.03 psi while the experiment shows no offset for time greater than three minutes.

In addition to all of the above, the experimental performances again show slow and irregular fluctuations. The simulation does not show them. The same reasons as those in chapter VI. can be used to explain this.

Generally, the agreement between the simulated and experimental performances are good and better than the on/off operation. The simulation predicted all the behaviors that are shown by experiment.

VII.3 Comparison Between On/Off and "Leaking" Valve Operations

Figure (104) shows the plots of the flow of solids through the valve versus the average current for on/off and "leaking" valve operations. The average current in the on/off operation flow-data is obtained through the conversion of the fraction open-based data to current-based data using equation (25). It is to be noted that the current in this case is an average current which has a large standard deviation while the current in the "leaking" valve operation has a small standard deviation. This large standard deviation is due to the nature of the on/off operation where the current oscillates between high and low values. The figure shows that the "leaking" valve operation is more energy efficient than the on/off operation. It also shows that at low current the curves approach each other as expected. The pressure response to a step change shows the occurrence of an undershoot in the "leaking" valve operation. The corresponding response for the on/off operation does not show any undershoot. When the step was introduced the current goes down to 56 amps in the "leaking" valve operation while the average current goes down to 98 amps in the on/off operation. The lower level of current and the hysteresis behavior (described previously in chapter IV)

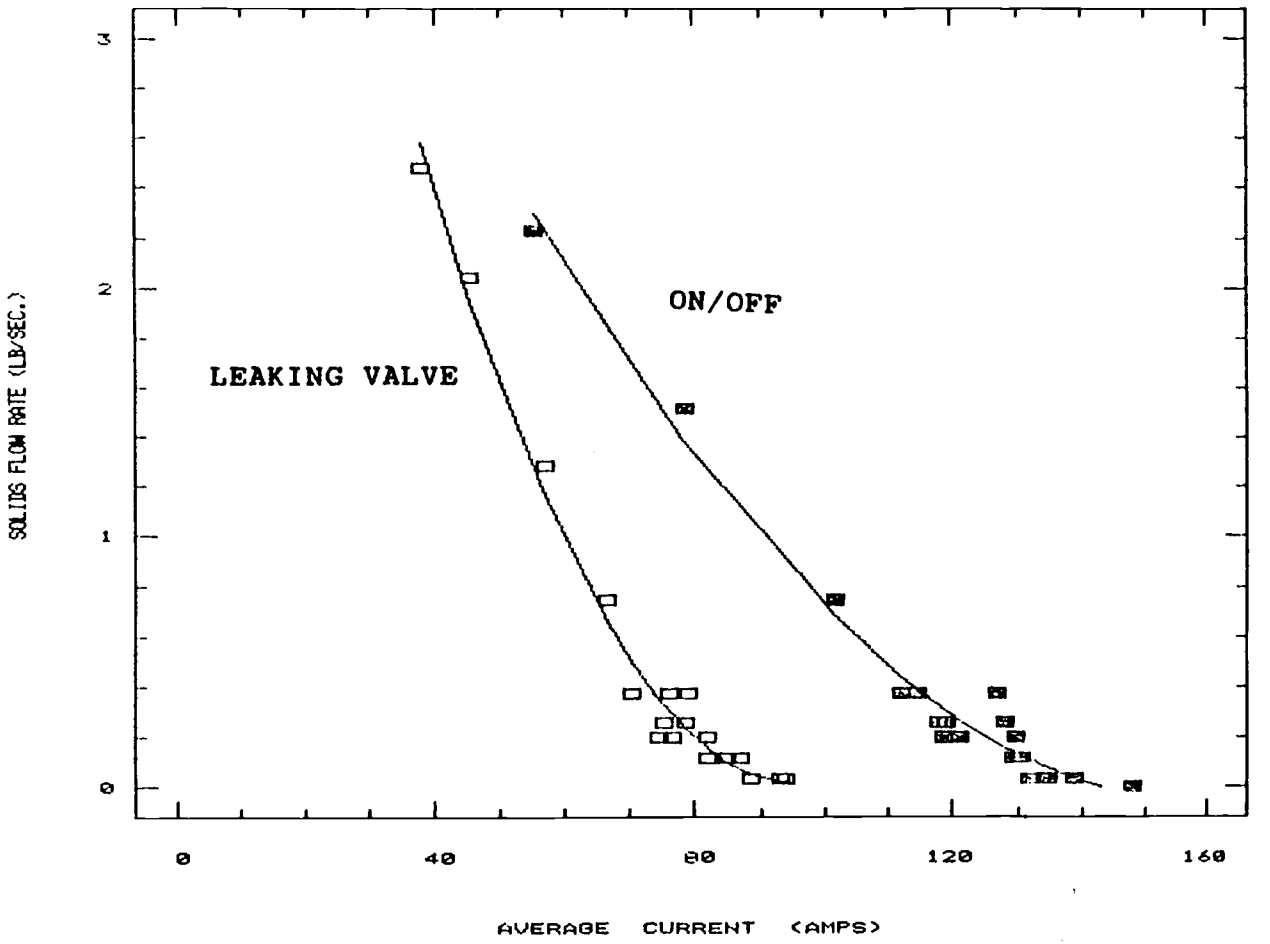

Figure (104) Solids Flow Rate Through the Valve vs. the Average Current for on/off and Leaking Valve Operations.

associated with the "leaking" valve operation explain the occurrence of the undershoot in the "leaking" valve operation. These same reasons can be used to explain the larger disturbance in the pressure response during the "leaking" valve operation.

The response of the pressure drop during the "leaking" valve operation is faster than that of the on/off operation for the same reasons as those mentioned above.

The slow fluctuations of the pressure drop across the stages are similar in both cases.

The "leaking" valve operation is recommended since it is more efficient and has better agreement with the simulation than the on/off operation.

VIII. SEGREGATION AND CLOSED-LOOP STUDIES FOR SOLIDS CONTAINING 25% IRON

The first part of this chapter will cover the segregation of magnetic and non-magnetic particles between the regions close to the grates and the fluidizing region. The mass of solids in the region close to the grates, as well as its height, will be predicted using two different approaches. The rest of the chapter will be organized in a similar way to that of chapter VII.

The segregation studies were undertaken because of the modeling and control difficulties encountered when operating with 25% iron. Also, the separation of the magnetic particles from the mixture is easier and more accurate for this low weight fraction of iron in the solids as will be discussed in chapter VIII.1.1. Some control difficulties and the mechanism of the valve's operation for this low weight fraction will be discussed in the first part of this chapter.

It was noticed also, that the interactions between the stages and the valve hysteresis (especially in the "leaking" valve operation) were the worst when using solids of 0.25 iron weight fraction. This makes the continuous solids throughputs for solids feed with weight fractions of less than 0.25 magnetic extremely difficult and requires higher

currents than those used in this chapter (I_w = 168 amps for on/off operation, I_{av}=105 amps for leaking valve operation).

An additional type of logic control was used in this chapter. The need for this control arose because of the problems mentioned previously (ie. strong hysteresis). This logic is called an override control where the manipulated variable [current or fraction open (t_{op})] is set to be equal to the value of the constraint corresponding to zero flow of solids whenever the average pressure drop across the stage drops below a certain limit. The logic will help minimize the flow rate of solids through the valve. More details will be given in the rest of the chapter.

VIII.1 Iron's Weight Fraction Behavior Inside a Stage with Time

A series of experiments were conducted during which solids samples from each stage were taken at certain time intervals and then analyzed. The experiments were conducted for different flow rates of solids which were either fresh feed of solids or recycled solids.

VIII.1.1 Experimental Procedures

- The power supplies were started and the output current was adjusted to the desired working current.

- The stages were filled with solids from bottom to top by first switching off the current going through the top and middle stages so that the bottom stage was filled with the solids to the desired level. Then the current was allowed to flow through the middle stage which is going to be filled with solids to the desired level. The same was repeated for the top stage.
- The gas flow was started then operated for five minutes. Solids flow rate into the top stage was then started and the process was put under control.
- The samples were drawn from the three stages at certain times. The time interval between drawing the solids samples from two stages was kept as small as possible. The experiment's run time varies between 16 minutes and 100 minutes. Most of the experiments have a run time of 45 minutes. The samples collected during a run were stored then analyzed when the run time was over. The magnetic solids (iron) were separated from the non-magnetic solids (sand) by a permanent magnet and then weighed individually. The procedure was repeated for each sample. The weight fraction was calculated according to the following formula:

$$W_{IM} = \frac{\text{mass of iron}}{\text{mass of iron + mass of sand}} \tag{80}$$

Figure (105) shows the plot of the weight fraction determined by the separation procedure (W_{IM}) versus the actual weight fraction (W_{IA}) obtained by mixing known amounts of iron and sand. The figure shows that the measured value is equal to the actual value for $W_{IA} < 0.3$. The amount of the sample affects the efficiency of separation. As the amount of the sample gets large, the magnetic rod has to be stirred more thoroughly in the sample to achieve good separation. However, the stirring of the sample by the rod was roughly the same when W_{IM} above was determined. The samples drawn from each stage are assumed to represent all of the solids in the stage because of the thorough mixing of the solids in the stage as a result of fluidization.

VIII.1.2 Using Recycled Solids as a Feed to the Top Stage

Figure (106-a, 106-b, 106-c) show the plots of weight fraction of iron in solids versus the time at flow rates 29 (gm/second), 40 (gm/second) and 72 (gm/second) respectively.

Figure (106-a) shows that the weight fraction of iron in each stage drops from the initial value ($W_I = 0.25$) to a lower value then fluctuates around a steady state value. The weight fractions of the middle and bottom stages fluctuate around $W_I = 0.2$ while the weight fraction for the

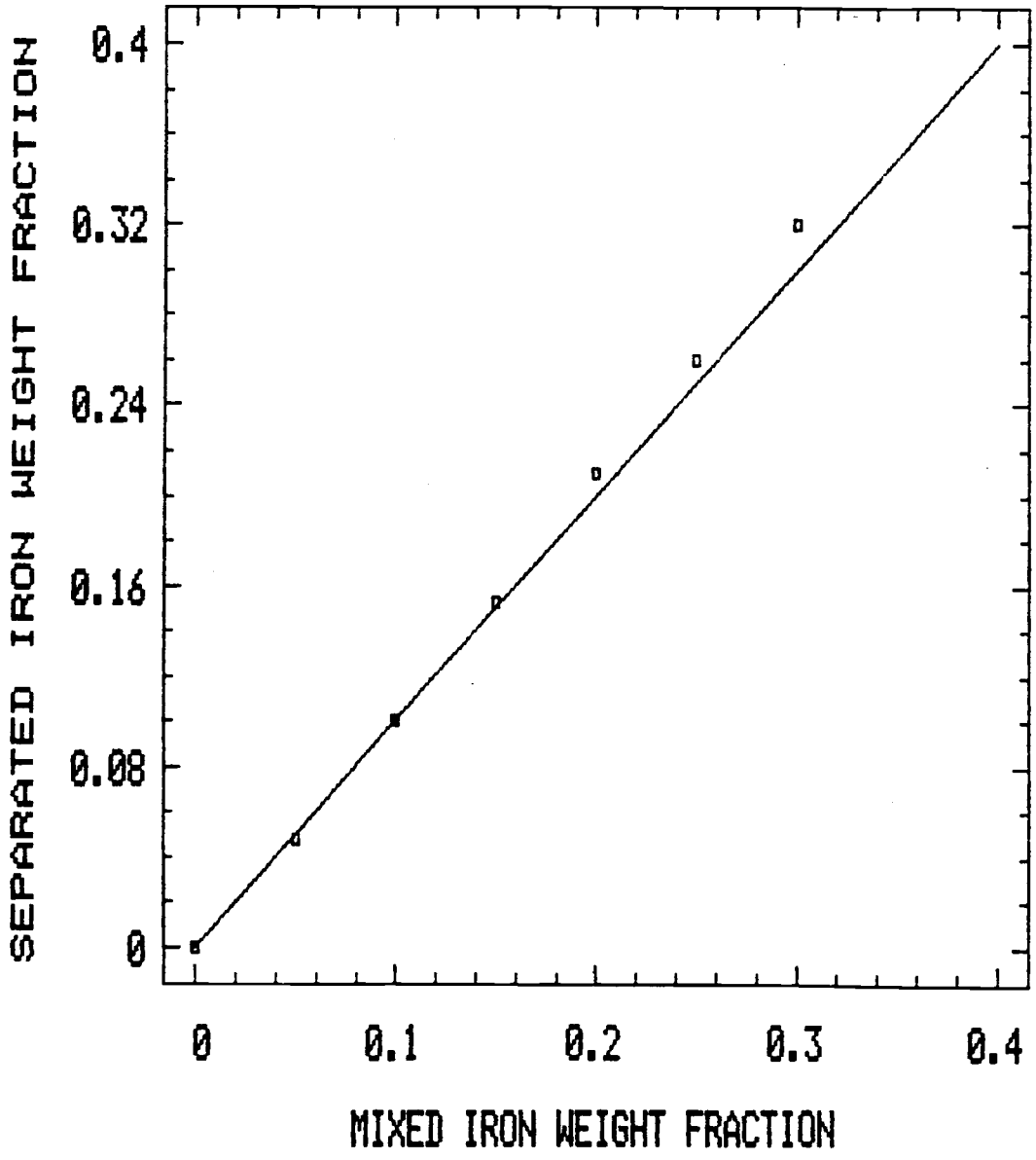

Figure (105) The Plot of the Actual v.s Measured Weight Fractions.

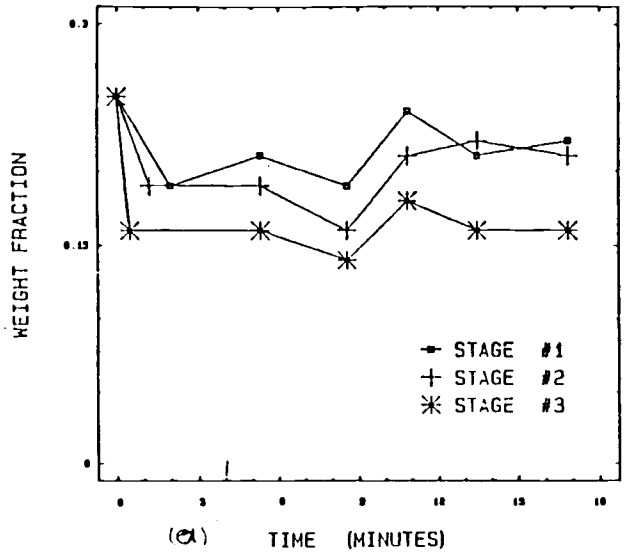

(a)

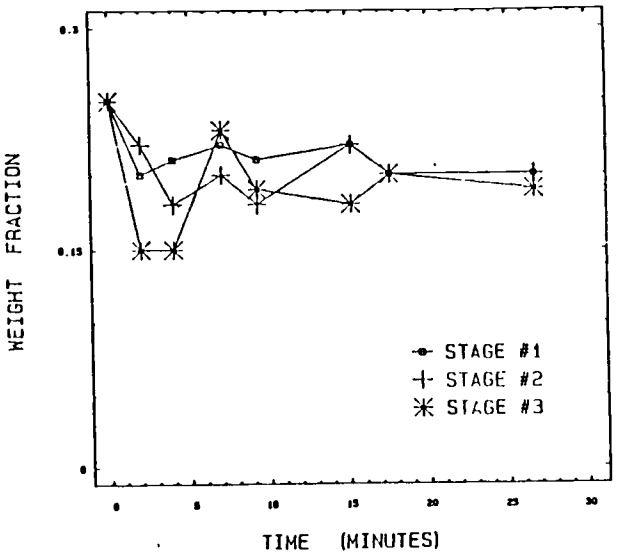

(b)

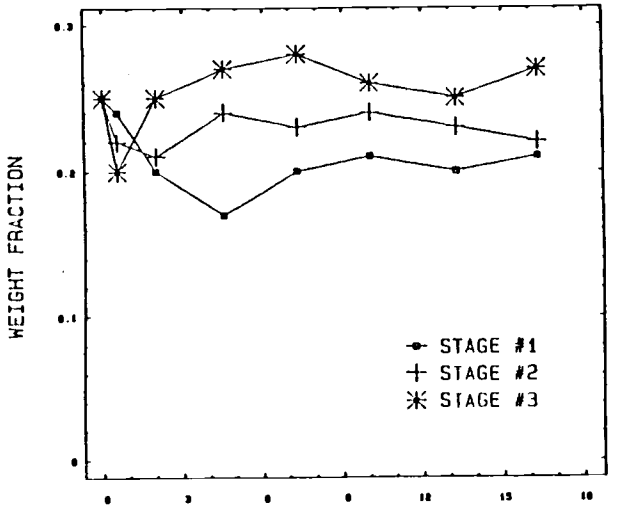

(c)

Figure (106)

Weight Fraction in the Fluidizing Region as a Function of Time for Recycled Solids at a Flow Rate of:
a) 29 gm/second
b) 40 gm/second
c) 50 gm/ second.

top stage has values lower than those for the middle and bottom stages and fluctuates around $W_I = 0.16$.

Figure (106-b) shows similar plots to figure (106-a) when the flow rate of solids is 40 (gm/second). However, the weight fractions of all the stages fluctuate around $W_I = 0.2$.

Figure (106-c) shows the plots of the weight fraction versus time when the feed flow rate is 72 (gm/second). The curves fluctuate around three different values of weight fraction which are $W_I = 0.25$, $W_I = 0.23$, $W_I = 0.2$ for the top, middle and bottom stages respectively.

The above results show that the average weight fraction of iron in the solids in each stage increases with increasing the flow rate of solids into the top stage. The average weight fraction of iron in the top stage fluctuates around a steady-state value that increases from the lowest one among the three stages when the solids flow rate is 29 (gm/second) to the highest one among the three stages when the solids flow rate is 72 (gm/second). The weight fractions of all the stages fluctuate around the same value when the solids flow rate have a value of 40 gm/seconds.

The solids were recycled after they passed through the three stages. A dark layer (W_I is large) followed by a lighter layer (W_I is small) were observed in the plenum (in which solids were stored after they pass through the stages). When the solids were recycled the weight fraction

of the solids entering the top stage fluctuates because of the difference in weight fractions of the different layers. These fluctuations cause the weight fractions inside the stages to fluctuate. However, the fluctuations of the weight fraction are stationary.

The amplitude of weight fraction fluctuation decreases as the feed flow rate of solids increases. It reaches a very small value for high flow rate (72 gm/second). Also, the amplitude of the fluctuations decreases as the time increases until a steady-state value of the weight fraction is reached after which the amplitude of the fluctuations becomes almost constant. The time needed to reach the steady-state operation decreases as the flow rate increases. The time needed for all of the solids to pass through the bed and be recycled (total pass time) is defined as follows:

$$\bar{t}_T = \frac{M_T}{m_i}$$

Where

$\bar{t}$ = total pass time

M_T = total weight of the solids

m_i = flow rate of the solids into the top stage

Recycling the solids causes some mixing between them until the weight fraction reaches almost a steady-state weight fraction. The total pass time (t_T) decreases when m_i increases resulting in a faster occurrence of the steady-state operation.

The average weight fraction of iron in the solids flowing out of the stage is assumed to be equal to that in the feed into the stage.

The fraction open of period, during which the current is zero, is less than 0.15 (20 ms) in all the previous cases discussed. Therefore, the current does not go to zero (based on sections IV.2.2.6 and IV.3.1.5). The fraction open increases from (0.118) for solids flow rate of 29 (gm/second) to 0.15 when the flow rate of solids is 72 (gm/second) which corresponds to an average current of 146 (amps) and 143 (amps) respectively. When the solids have small weight fraction, as is the case in this chapter, the operation is very sensitive to small changes in the fraction open of period during which the current is zero (average current). The amount of magnetic material attracted to the grates increases when the fraction open (t_{op}) decreases which explains the increase in the weight fraction as the flow rate increases.

The residence time is defined by the following equation:

$$\bar{t} = \frac{M_s}{m_i} \tag{81}$$

M_s = solids hold up on the stage

m_i = solids flow rate into the bed

The residence time increases as the flow rate of solids into the stage decreases which results in the attraction of more magnetic materials to the grids as the flow rate decreases.

VIII.1.3 Fresh Feed of Solids

Figures (107-a, 107-b, 107-c) show the behaviors of the iron weight fraction as a function of time when the feed is fresh. Large amounts of solids having an iron weight fraction of 0.25 were prepared. The solids that pass through the stages were thoroughly mixed and their weight fraction is measured and adjusted by adding sand or iron to them.

Figure (107-a) shows similar behavior to that when the feed is recycled. The fluctuations in the weight fraction are much less than that shown in figure (106-a). The weight fraction of the top stage fluctuates around a steady- state

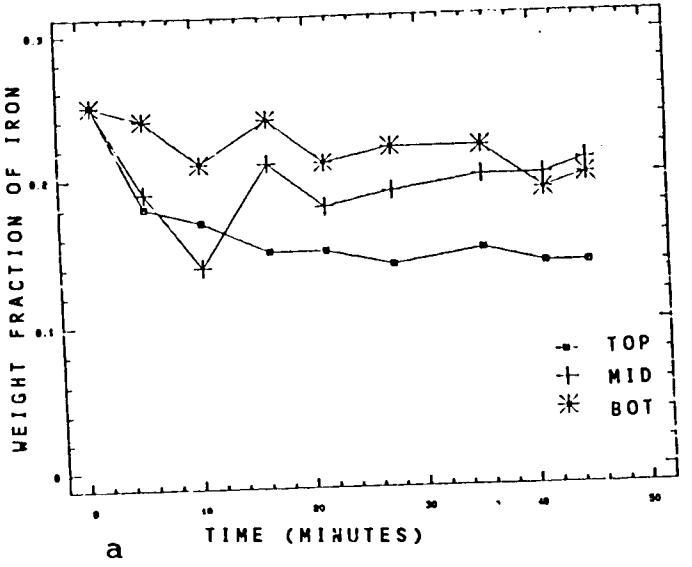

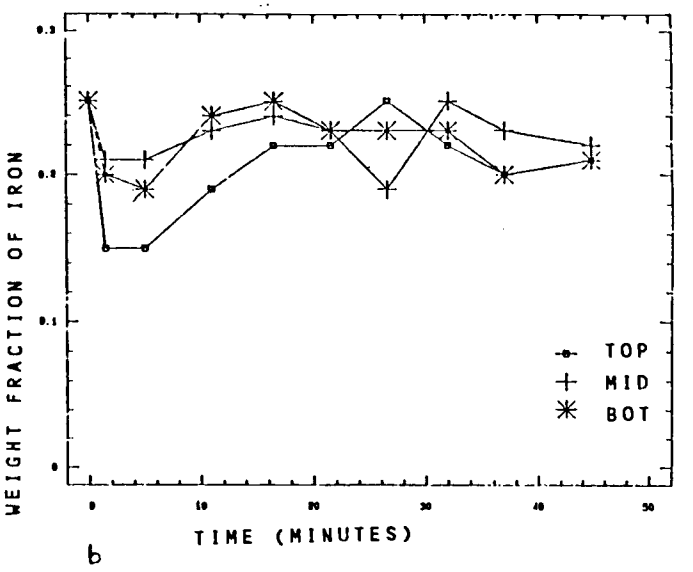

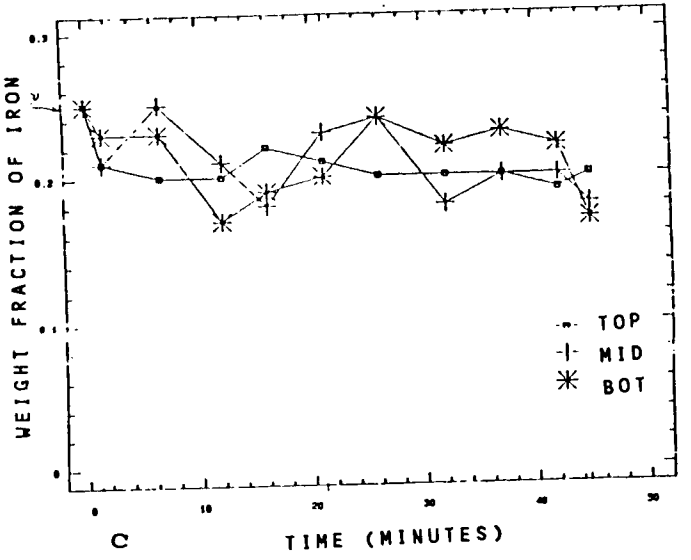

Figure (107)

Weight Fraction in the Fluidizing Region vs. Time for Fresh Solids at a Flow Rate of:
a) 29 gm/second
b) 40 gm/second
c) 50 gm/ second.

value of W_I = 0.15 while that of the middle and bottom stages fluctuate around W_i = 0.20.

Figure (107-b) shows the plots when the flow rate of solids is 40 (gm/second). All of the curves fluctuate approximately around the same weight fraction value (W_i = 0.22).

Figure (107-c) shows the corresponding plots when solids flow rate is equal to 72 (gm/second). The curves representing weight fractions for the three stages fluctuate around W_i =0.23. This case is different from the case where the solids were recycled where the weight fraction curves fluctuate around different weight fractions values.

The weight fraction fluctuations in all the previous cases of fresh feed have smaller amplitudes than those of the recycled solids. The uniformity of the feed composition helps reduce the stage's weight fraction fluctuations. However, some fluctuations still exist even for uniform feed because the magnetic material was observed to flake-off in clumps from the grid which is a feature of the on/off operation. Also, the fluidization of the bed may contribute to the weight fraction fluctuations.

VIII.1.4 Effect of Stage Position on Weight Fraction

Figure (108) shows the results of two separate experiments where the position of the stage with respect to the

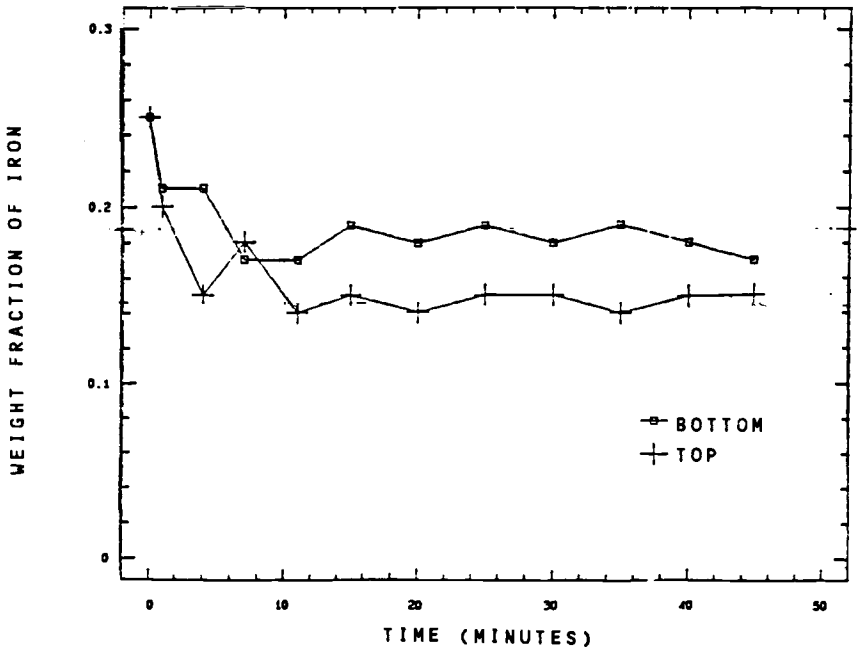

Figure (108) Effect of the Stage Posistion on the Segregation of Solids Between the Two Regions.

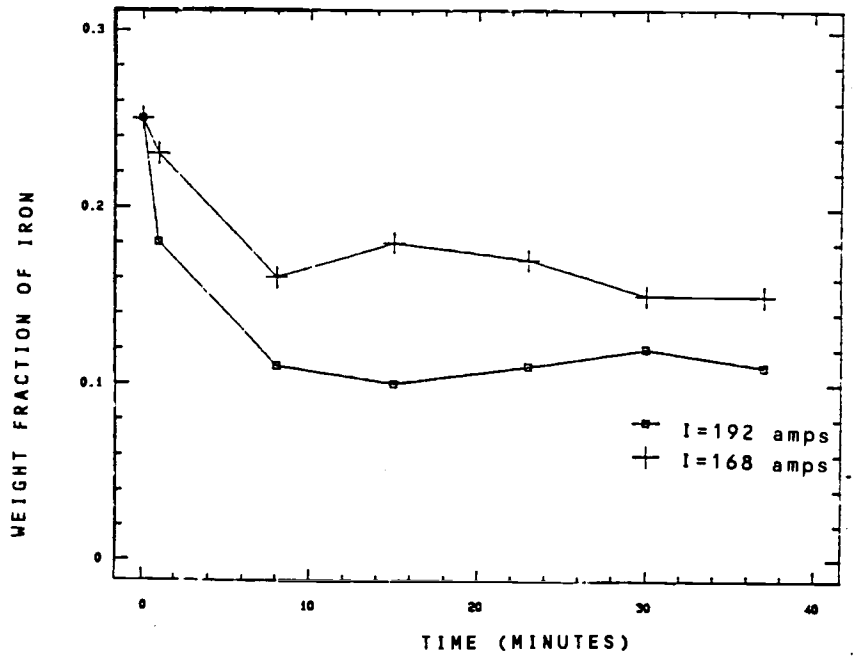

Figure (109) Effect of the Working Current on the Segregation of Solids Between the Two Regions.

air distributor under the bottom stage is changed from one experiment to another. The position is changed by using the top stage in one experiment and the bottom stage in another. The weight fraction for the bottom stage experiment fluctuates around $W_i = 0.19$ while that of the top stage's experiment fluctuates around $W_i = 0.15$. The experiment is done using recycled solids. The fluctuations of the weight fraction are smaller than the cases when three stages were used.

When the top stage is used for the study the distribution of air is better than when the bottom stage is used. In the former case the air passes through the bottom and middle stages which have copper screens and copper tubes (the grates) in addition to those of the top stage. In the latter case, the air passes only through the copper screen and the grates of the bottom stage.

However, the solids distribution is much better when the bottom stage is used. The solids are distributed well by passing through the three screens located below the discharge of the hopper, the copper grids and screens of the top and the middle stages. When the top stage is used, the solids only pass through the three screens located below solids discharge from the hopper.

The effect of stage position on the weight fraction may contribute to the fluctuations of the weight fraction around

different steady states in some of the previous cases discussed.

VIII.1.5 Effect of Current on Weight Fraction

Figure (109) shows the results of two experiments conducted at different working currents using the bottom stage. The weight fractions fluctuate around $W_i = 0.19$ and $W_i = 0.12$ for working currents of 168 (amps) and 192 (amps) respectively. As the working current increases the attraction force between magnetic particles and the grates increases. As a result, the thickness of the layer of magnetic particles close to the grates increases as the current increases. Hence, the average weight fraction of magnetic particles in the fluidized region decreases as the current increases.

VIII.1.6 Determination of the Fixed Layer Thickness and Height

Making a mass balance around the whole stage gives the following equation:

$$W_T M_s = W_1 M_1 + W_2 M_2 \tag{82}$$

W_1 = Average weight fraction of iron in the region close to the grates.

W_2 = Average weight fraction of iron in the fluidized region.

W_T = Average weight fraction of iron in both regions after they are mixed together.

M_1 = The mass of magnetic and non-magnetic particles in the region close to the valve.

M_2 = The mass of magnetic and non-magnetic particles in the fluidized region.

M_s = The total mass of magnetic and non-magnetic particles in the two regions ($=M_1 + M_2$).

The region close to the grate is mainly magnetic material. Also, the weight fraction of the layer attached to the grates is very hard to measure. Therefore, the average weight fraction is assumed to be high and equal to 1.0. This assumption may introduce appreciable error to the results. However, the results represent the minimum conditions ,which are of interest to the operation.

The following equation can be obtained after some algebraic manipulation and after the substitution for W_1.

$$M_1 = \frac{(W_T - W_2)\ M_T}{(1 - W_2)} \tag{83}$$

W_T, W_2, and M_s can be measured experimentally and substituted into equation (83) to obtain a value for M_1. If the average thickness of the region close to the grate is needed, the following equation can be used:

$$M_1 = \rho_s A_1 \delta (1-\epsilon) \tag{84}$$

where ϵ is the voidage of the layer close to the grates

Therefore:

$$\delta = \frac{M_1}{\rho_s A_1 (1 - \epsilon)} \tag{85}$$

where δ = average thickness of the region close to the grates

A_1 can be taken to be approximately equal to the cross-sectional area (see chapter IV.2.2.2).

The existence of the two regions was observed during the experiment. A dark region is observed to exist near the grates while a fluidizing light region was observed to exist a distance away from the grates. The color difference is due to the color of iron (dark) and the color of sand (light). The average height of the region close to the grate (dark region) was measured. The combined weight of the two regions was obtained via a balance. The total solids were then mixed and the weight fraction W_T was de-

termined. The weight of the region close to the grates could be obtained via two ways:

- Using equation (83) and equation (85).
- Using equation (85) along with the measured average height.

The voidage (ϵ) at different weight fractions is discussed in appendix (C). The results shown in tables (8) to (9) represent the end of run conditions for the recycled and fresh feed respectively.

Both of the tables show that the mass of the solids in the region close to the grates (column 5) calculated using equation (83) is very close to that (column 7) calculated using the observed height (H_{obs}) and equation (84). Also, the calculated height (column 8) is very close to the observed height (column 6). This good agreement between the two methods for calculating the mass and height of the layer close to the grates gives some confidence in the theory developed here. Also, this good agreement indicates that the assumption of taking the weight fraction of the magnetic solids near the valve to be one is good.

There is no relation between the flow rate of solids out of the stage or the position of the stage (top, middle or the bottom) and the amount of solids present in the layers close to the grates. This indicates the randomness of the fluctuations of the thickness of the layer.

Table (8) The Weight and Width of the Layer Close to the Grates at Different Flow Rates of Solids. The Recycled Solids are Used for Feed.

m_i (g/S)	Stage Position	M_T (kg)	W_T	W_2	M_1 (kg) Eq(83)	H_{obs} (cm)	M_1 (kg) Eq(84)	H_{cl} (cm) Eq(85)
29	Top	4.25	0.23	0.14	0.44	1.12	0.46	1.10
	Middle	4.89	0.26	0.21	0.31	0.82	0.34	0.80
	Bottom	4.98	0.29	0.22	0.45	1.12	0.46	1.10
29	Top	4.71	0.21	0.14	0.38	0.92	0.38	0.92
	Middle	4.53	0.27	0.16	0.59	1.52	0.62	1.40
	Bottom	4.82	0.31	0.20	0.66	1.82	0.75	1.60
29	Top	5.40	0.24	0.14	0.63	1.82	0.75	1.50
	Middle	5.15	0.25	0.20	0.32	1.02	0.34	0.80
	Bottom	5.42	0.31	0.20	0.74	1.92	0.79	1.80
40	Top	4.68	0.26	0.19	0.41	1.02	0.42	1.00
	Middle	5.30	0.30	0.20	0.69	1.82	0.75	1.70
	Bottom	5.43	0.27	0.20	0.48	1.22	0.50	1.20
72	Top	4.40	0.29	0.23	0.34	0.82	0.34	0.80
	Middle	4.73	0.28	0.21	0.42	1.12	0.46	1.00

Table (9) The Weight and Width of the Layer Close to the Grates at Different Flow Rates of Solids. The Recycled Solids are Used for Feed.

Flow Rate (g/s)	Stage Position	M_T (KG)	W_T	W_2 (KG) Eq(83)	M_1 (CM)	H_{obs} (KG) Eq(84)	M_1 (CM) Eq(85)	H_{cl}
29	Top	5.48	0.23	0.14	0.57	1.42	0.59	1.40
	Middle	5.83	0.28	0.21	0.52	1.32	0.55	1.30
	Bottom	5.46	0.28	0.20	0.55	1.32	0.55	1.30
40	Top	5.79	0.27	0.21	0.44	1.02	0.43	1.10
	Middle	5.35	0.30	0.22	0.55	1.32	0.55	1.30
	Bottom	5.41	0.32	0.21	0.75	1.92	0.80	1.80
72	Top	5.74	0.23	0.16	0.48	1.12	0.47	1.20
	Middle	5.22	0.26	0.18	0.51	1.22	0.40	1.20
	Bottom	5.19	0.31	0.17	0.88	2.32	0.97	2.10
29	Bottom I=168 A	4.92	0.23	0.17	0.46	1.12	0.47	1.10
	Bottom I=192 A	5.42	0.23	0.11	0.73	1.82	0.75	1.80
29	Only TOP	4.98	0.23	0.14	0.52	1.32	0.55	1.30
	Only Bottom	5.33	0.24	0.17	0.45	1.12	0.47	1.10

VIII.2 Control Difficulties

When the weight fraction of magnetic particles in the solids (used for the operation of the staged value) is lower than 0.30, additional problems in controlling the flow of solids through the stage valves arise. The process gain increases rapidly when the weight fraction of magnetic solids decreases. It becomes more sensitive to the changes in the fraction open of period during which the current is zero. As a result, the flow of solids through the valve which corresponds to a certain controller action (t_{op} or current) is very large. There are two kinds of operations that exist when then magnetic staged valve is used.

1) Steady-state operation
2) Operation in which the solids holdups or the flow rate of solids into the top stage are changed.

VIII.2.1 Steady-State Operation

Figures (110) and (111) show the plots of the pressure and the controller outputs versus time for the on/off and "leaking" valve operations respectively.

It was mentioned before that for a small fraction open (FR $\approx$ .12) the average current in an on/off operation is high and the open time (t_{op}) is much smaller than the re-

sponse time for the power supply. Therefore, some solids (mostly magnetic particles) will be always attracted to the copper grates and not released. However, the outside radius of this layer changes depending on whether the current is on or off. Considering two copper grates next to each other, there will be an opening between the two tubes (most likely located in the center between them) the width of which depends on the outside radius of the layers of the solids attracted to the copper grates. The solids flowing through this opening probably have the same average composition as the solids in the stage. However, the average overall composition of the solids coming out of the stage is higher than that flowing through the opening because of the release of some of the highly magnetic solids attracted to the grates when the controller action (t_{op}) is implemented. The above discussion leads us to two possible factors which control the flow of solids through the valve:

A) The width of the opening between two neighboring grates which is a strong function of the magnetic forces (average current).

B) The direct magnetic forces affecting the solids flowing through the opening which have lower magnetic composition than the layer attracted to the individual grates.

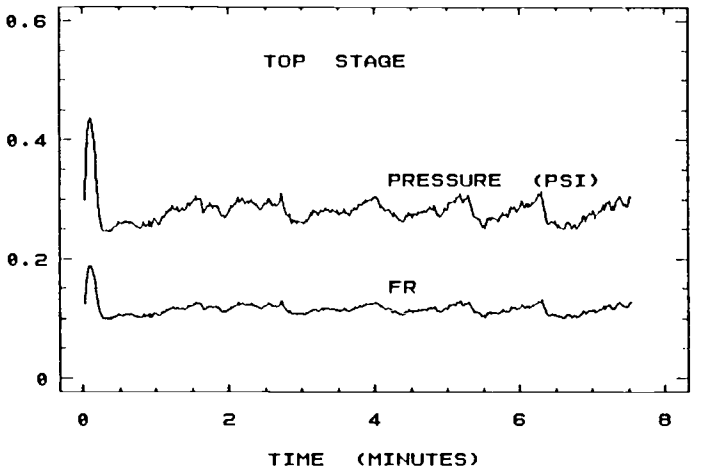

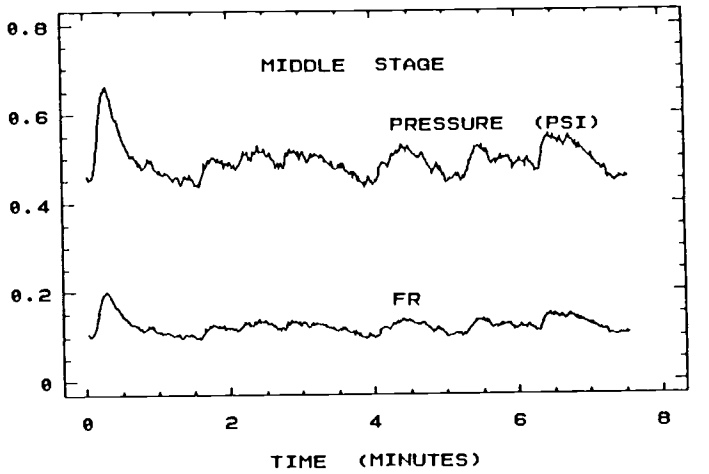

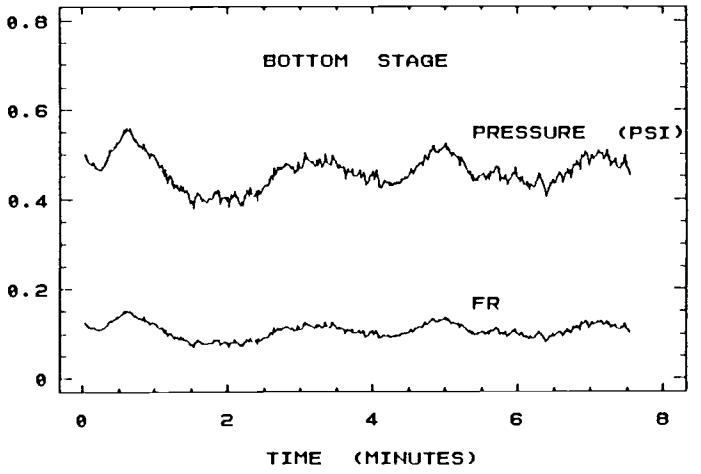

Figure (110)

Pressure Drop Histories Across Each Stage for Steady-State Operation (ON/OFF Operation).

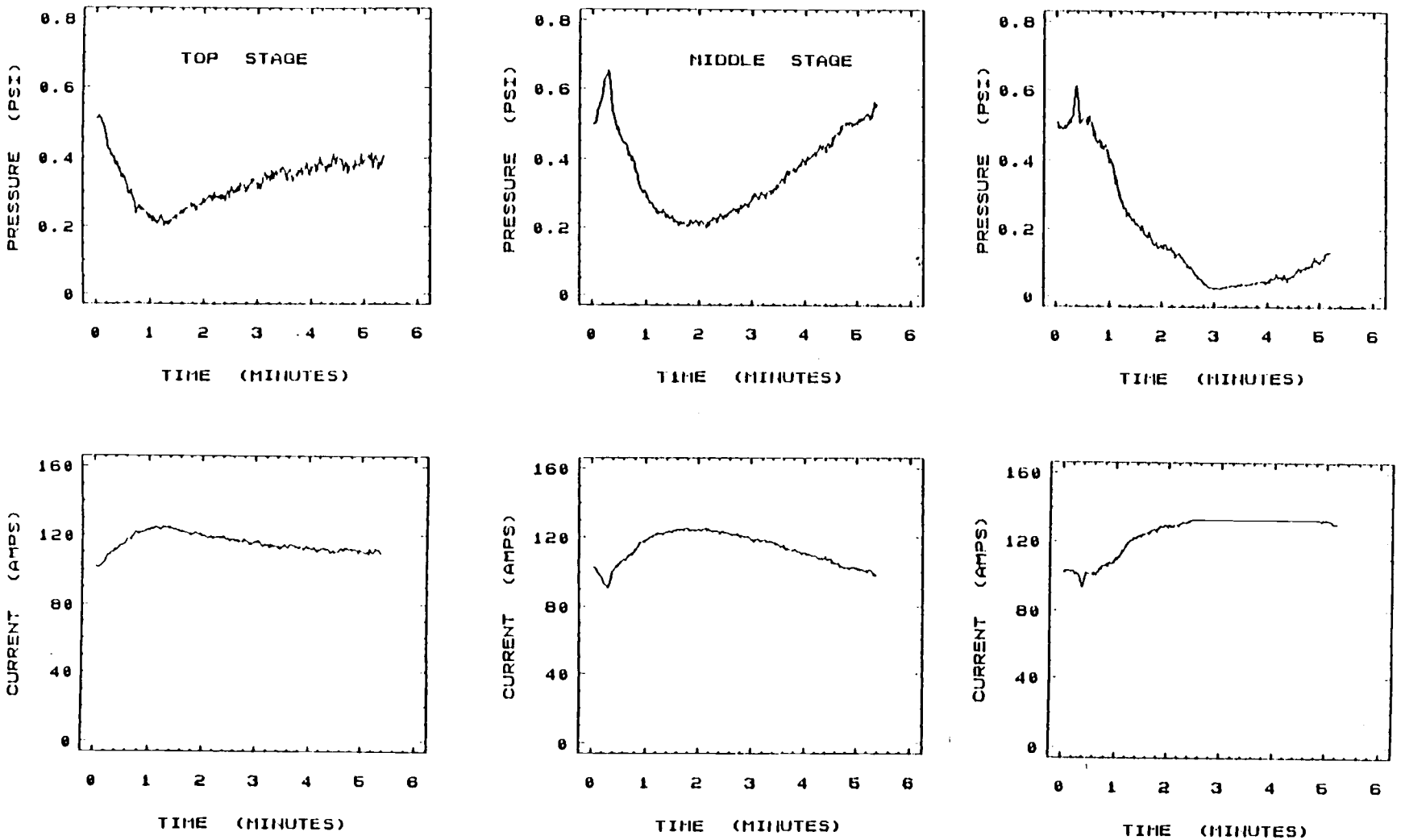

Figure (111) Pressure Drop Histories Across Each Stage for Steady-State Operation (Leaking Valve Operation).

The effect of the factor presented in (a) is probably more pronounced than the one in (b).

A similar discussion as that above can be used to describe the "leaking" valve operation. In fact, the discussion is much more clearer for "leaking" valve operation than on/off operation. The change of the thickness of the layer attracted to the grates is more gradual than the on/off operation where a clump of highly concentrated magnetic particles is released when the current is set to be off which leads to non-uniform thickness of the layer.

In both operations, there is a critical width of the opening corresponding to a certain feed composition and flow rate. If the pressure drop across the stage is more than the setpoint, the average current will be decreased which leads to a wider opening. However, due to the hysteresis nature of the valve, which is more clear for "leaking" valve operation, reducing the width of the opening is not as fast as enlarging it. This will cause the flow of solids to remain large, even after the setpoint requirement is satisfied, which leads to the decrease of the pressure drop to a value below the desired value. As a result, the width of the opening has to be reduced to a value smaller than the critical width for the pressure drop to be the same as the desired value. The cycle is repeated many times during the

operation leading to an oscillatory response of the pressure drop across the stage.

VIII.2.2 Dynamic Operation

When a big disturbance or setpoint change is introduced, the layer attracted to the grate is either reduced below the critical width greatly or completely released depending on the size of the change. Therefore, the problem is much worse than that in the last section and it may lead to a complete depletion of the solids from the stage or to a serious undershoot. Also, the performance will continue to be bad for some time after the change is introduced. The time needed for the opening to reach the critical thickness is longer than the last case and the oscillatory performance is much worse.

The above discussion leads to the necessary use of some kind of control scheme that would make the time needed for reducing the opening width as shorte as possiple. The simplest way is to use an override control where the current is raised to either the higher average current (in the on/ off operation) or to the holding current ("leaking" valve operation) when the solids holdup (pressure drop across each stage) drops below a certain limit. The flow of solids through the valve in both of the cases is then very small (≈ 0).

VIII.3 On/Off Operation

The parameters in the model of flow rate of solids through the valve are determined by fitting the experimental data using linear regression which gives the following equation:

$$M_o = -0.040 - 0.30 * FR + 13.80 * FR^2 \qquad (86)$$

$$R^2 = .982$$

$$0.0658 < FR < 0.31$$

The inequalities correspond to no flow and maximum flow respectively.

Figure (112) shows the plots of both the experimental and theoretical flow rate of solids through the stage valve. The figure shows a good fit of the model to the experimental data. The following equation can be obtained in a similar was as those in chapter VI.

$$\frac{(\bar{V}_p\ K_2)\ (\rho_s\ A_f)}{A_1} = 0.0386 \qquad (87)$$

$$\frac{r\ B}{\mu_0} = 52.89 \qquad (88)$$

$$\frac{(\rho_s\ A_f)}{A_1}\ [\ (A_{cs}\ \delta)\ (1-\epsilon)\ \rho_s - A_1\ u_g = 13.46 \qquad (89)$$

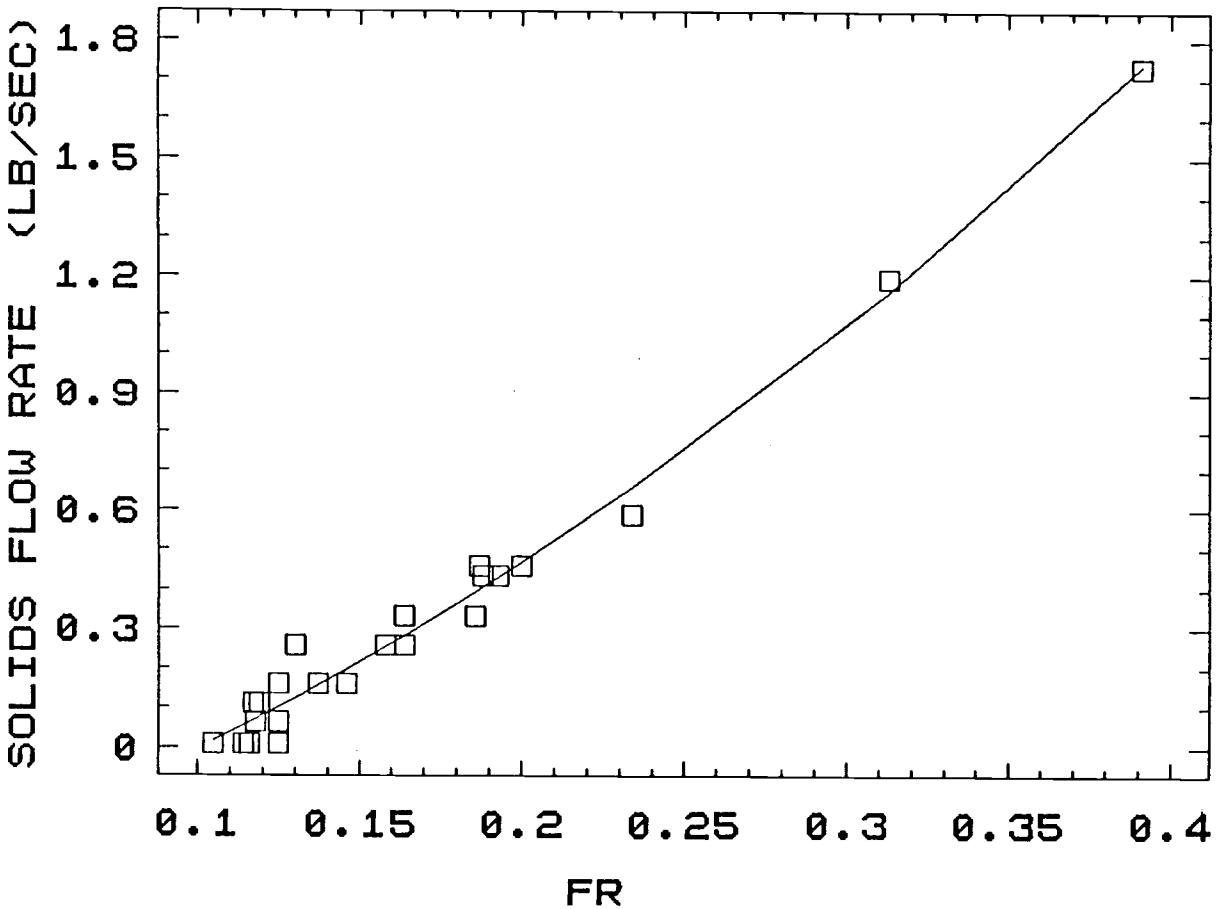

Figure (112) Solids Flow Rate Through the Stage vs. Fraction (ON/OFF Operation and 25% Iron).

VIII.3.1 Design of the Controller Parameters via Simulation

VIII.3.1.1 Controller Gain

Figure (113) shows the plots of ISQERR and ISQMAN versus the controller gain for the three stages. ISQERR and ISQMAN do not change significantly for values of K_C less than 60 ms/psi. ISQERR and ISQMAN for the bottom stage fluctuate for K_C values less than -200 ms/psi which indicates an upper limit of K_C that can be used.

A value of -60 ms/psi is chosen for K_C and is based on the criteria discussed in VI.1.4.

VIII.3.1.2 Filter Time Constant

The plots shown in figure (114) exhibit a minimum at a filter time constant of 1.8 seconds. The minimum is more clearly seen for the plots of the middle and the bottom stages than that for the top stage. The same reasons as those mentioned in section VI.2.1.1.2 can be used to explain the occurrence of the minimums as well as the differences between their shapes in going from the top to the bottom stages.

A filter time constant of 1.8 seconds is chosen to be used in these simulations and experiments.

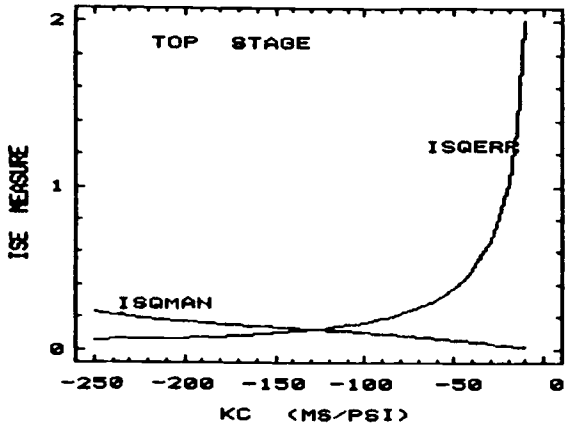

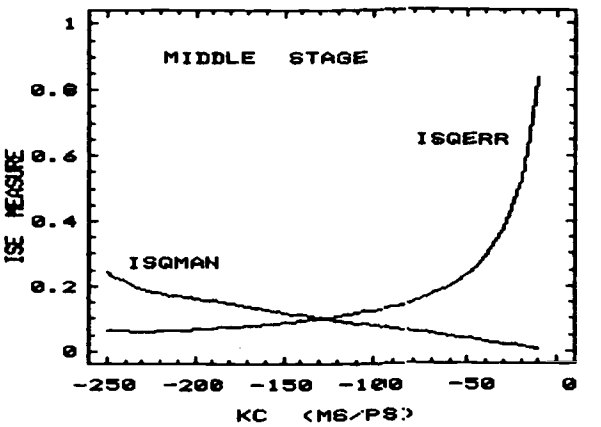

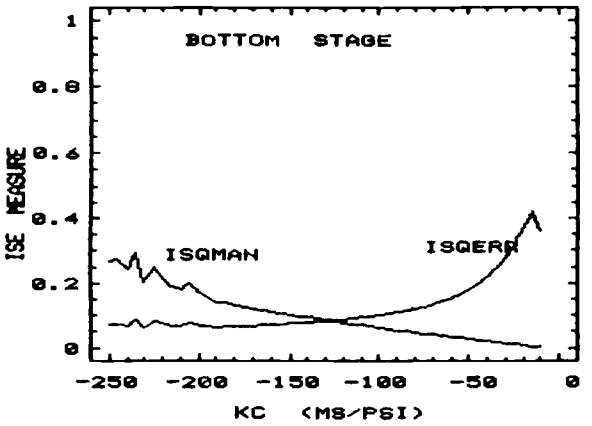

Figure (113)

ISQERR and ISQMAN for the Three Stages vs. the Control Gain (ON/OFF Operation and 25% Iron).

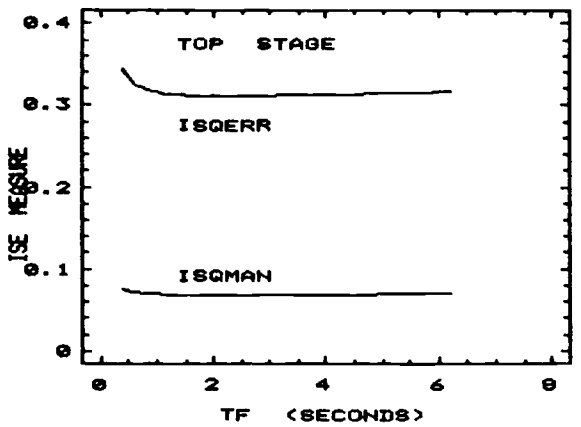

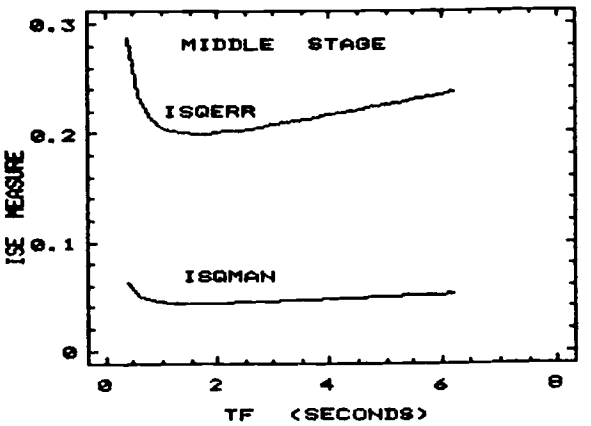

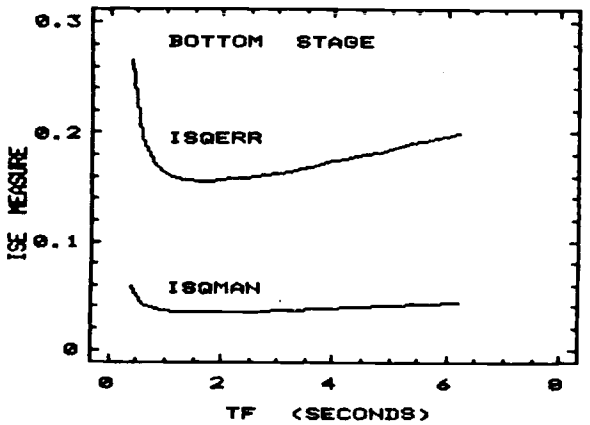

Figure (114)

ISQERR and ISQMAN for the Three Stages vs. Filter Time Constant (ON/OFF Operation and 25% Iron).

VIII.3.1.3 Input Constraints

Figure (115) shows the plots of ISQERR and ISQMAN versus the lower limit of t_{opmax}. ISQERR and ISQMAN are constant for values of t_{op} between 1 ms and 14 ms. The lower limit of t_{op} is chosen so that the solids flow rate out of stage, ISQERR and ISQMAN are as low as possible. A value of 8.4 ms is chosen as the lower limit. The choice is based on the fact that the solids flow rate out of the stage is equal to zero for t_{opmax} equal to 8.4 ms. The choice took into consideration the override control which was used for this kind of process operation with low magnetic solids.

Figure (116) shows the corresponding plots for the upper limit. ISQERR for the top stage decreases as t_{opmax} increases until t_{opmax} is equal to 26 ms, after which ISQERR and ISQMAN reach constant values. ISQERR and ISQMAN for the other two stages increase as t_{opmax} increases until t_{opmax} is equal to 26 ms after which they become constant. However, ISQERR and ISQMAN for the top stage are much larger than the other stages. The choice of the upper limit was based on the performance of the top stage. A value of the upper limit of t_{opmax} of 26 ms was chosen.

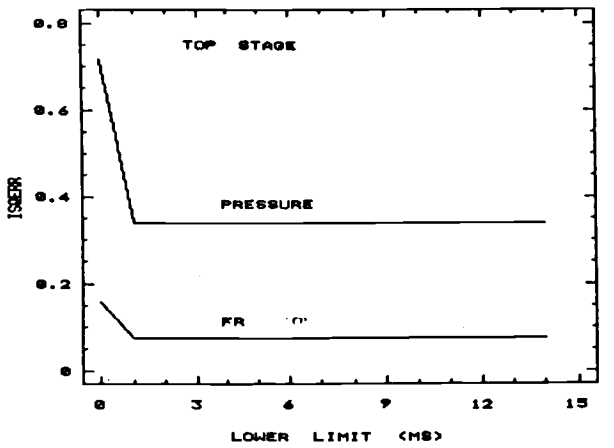

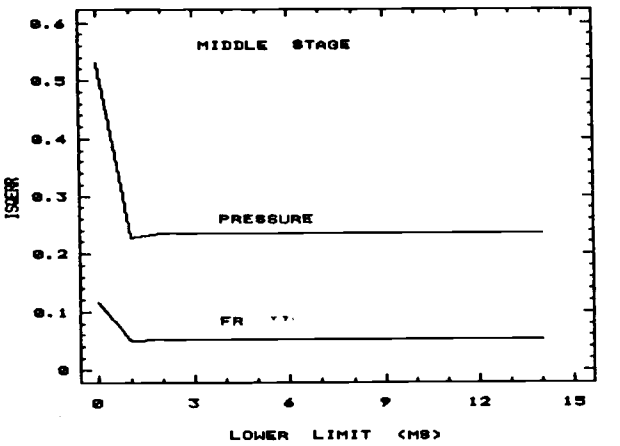

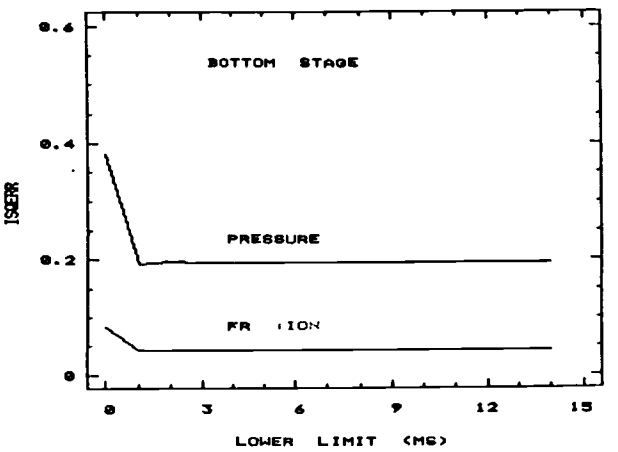

Figure (115)

ISQERR and ISQMAN for the Three Stages vs. the Lower Limit on Input Constraint (ON/OFF Operation and 25% Iron).

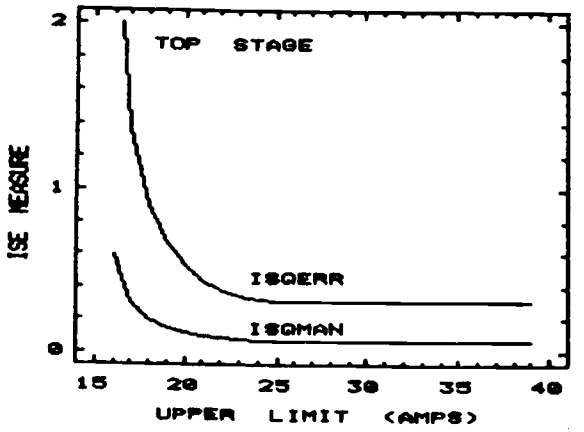

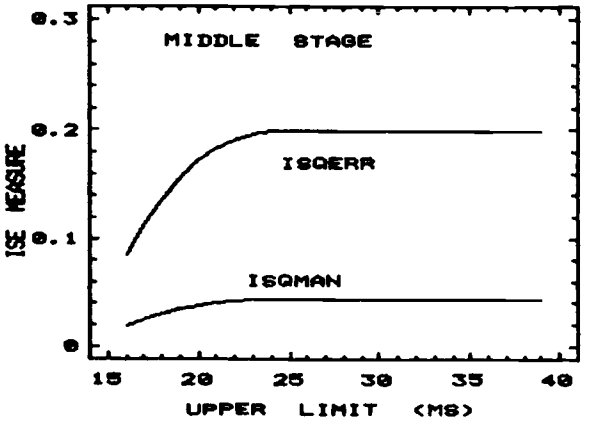

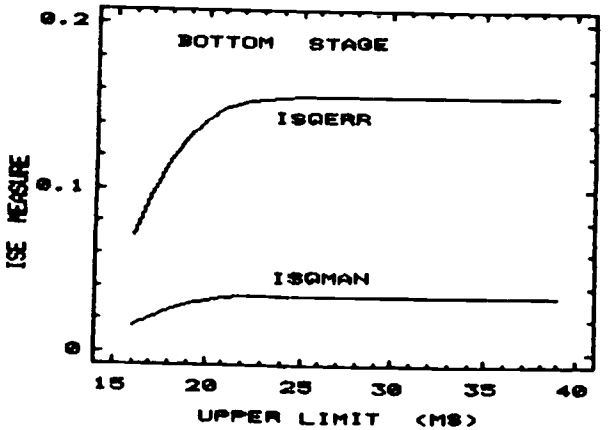

Figure (116)

ISQERR and ISQMAN for the Three Stages vs. the Upper Limit on Input Constraint (ON/OFF Operation and 25% Iron).

VIII.3.2 Simulated Closed-Loop Performance

VIII.3.2.1 Negative Setpoint Change in the Pressure Drop Across a Stage

Figure (117) shows the pressure drop and the controller output's (fraction open) responses for the three stages to a -0.2 psi setpoint change in the pressure drop of the top stage. The response of the pressure drop across the top stage shows an offset which is less than 0.01 psi. The responses of the pressure drops across the middle and bottom stages are more oscillatory than that for the top stage. The disturbances in the pressure drop - caused by the setpoint change of the top stage - across the middle and bottom stages have maximum values of 0.61 psi. The responses to the disturbances are more sluggish for the bottom stage than that for the middle stage. The frequency of hitting the lower constraint of the fraction open (t_{op}) increases in going from the top to the bottom stages. This is because the feed to the top stage is assumed to be constant while those for the middle and bottom stages are fluctuating. Also, the flow through the valve is very sensitive to the fraction open (t_{op}) as discussed previously. Those two reasons may be used to explain the more oscillatory behavior and the larger frequency of hitting the controller in going from the top to the bottom stages.

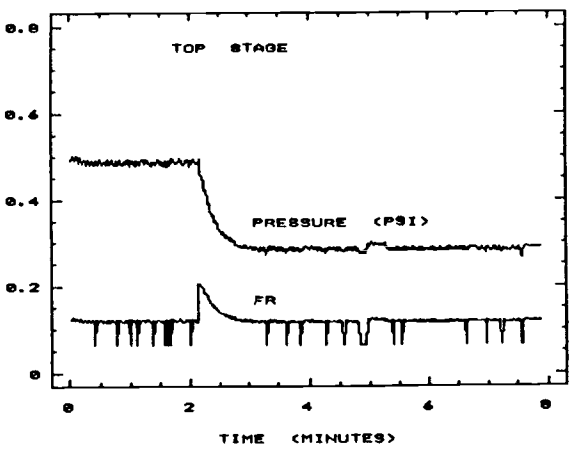

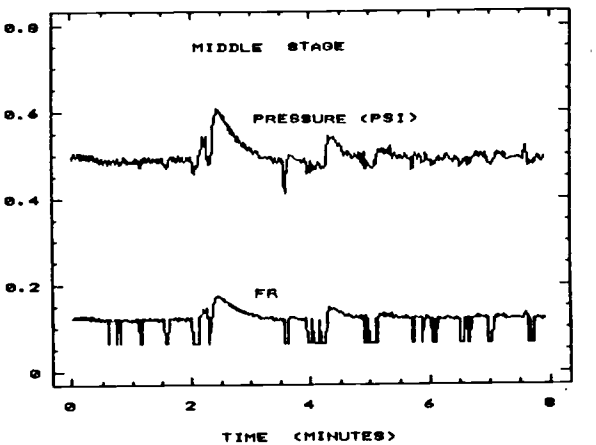

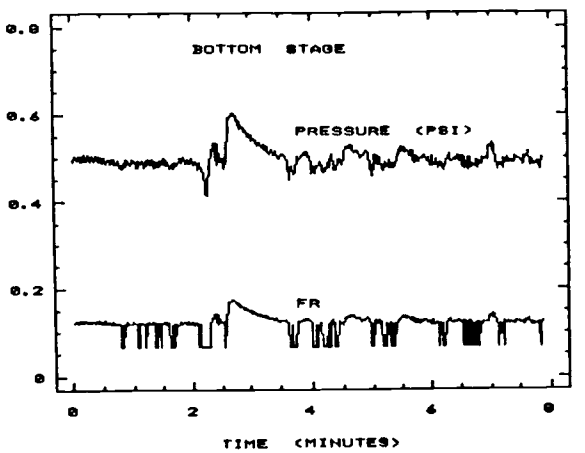

Figure (117)

Simulated Closed-loop Performances for a -0.2 psi Setpoint Change in the Top Stage without Decoupling (ON/OFF Operation and 25% Iron).

Figure (118) shows the responses when decoupling is implemented. The disturbances in the pressure drop responses of the middle and the bottom stages are greatly decreased. The maximum values of the pressure drop across the middle and bottom stages, when the disturbances are introduced, are 0.54 psi and 0.53 psi respectively. The pressure fluctuations are greatly reduced and the performance is generally much better than in the last case.

Figure (49) shows the results when the step change in the setpoint is introduced to the second stage. The pressure drop response across the top stage is not affected by the stages below. The pressure drop responses show some sudden dips which are due to the great sensitivity of the flow rate of solids to the slight increase in the fraction open.

The controller outputs (fraction open) in figures (118) and (119) hit the lower constraint randomly many times. The frequency of hitting the constraint is about equal in all the stages.

VIII.3.2.2 Positive Step Change in the Flow Rate of Solids

Figure (120) shows the response of the pressure drop across each stage to a positive step in the flow rate of solids of 30 gm/second. The pressure across the top stage jumps to a maximum value of 0.34 psi while those for the

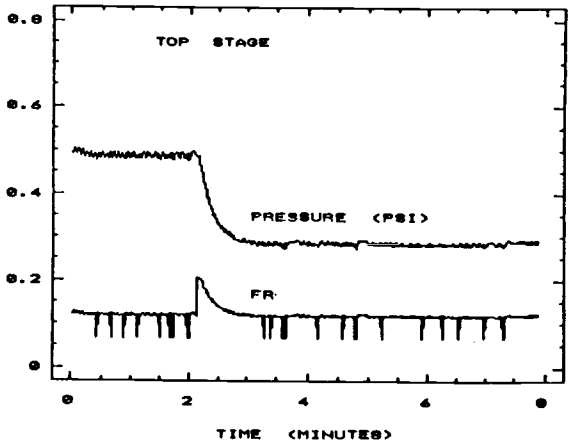

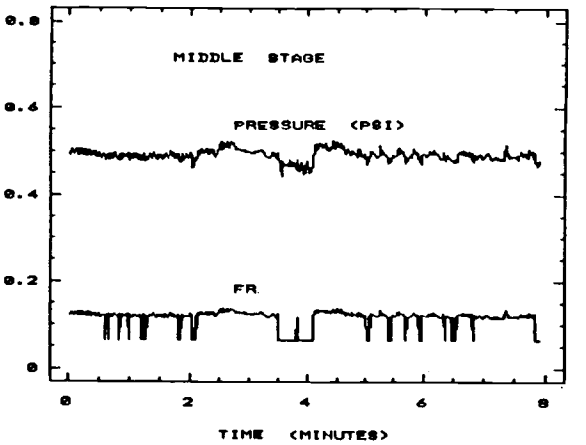

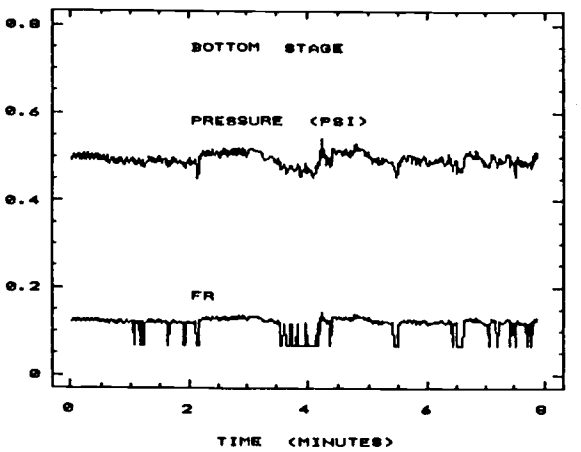

Figure (118)

Simulated Closed-loop Performances for a -0.2 psi Setpoint Change in the Top Stage with Decoupling (ON/OFF Operation and 25% Iron).

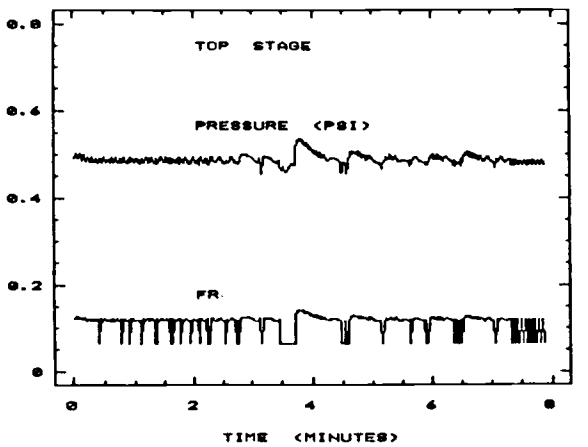

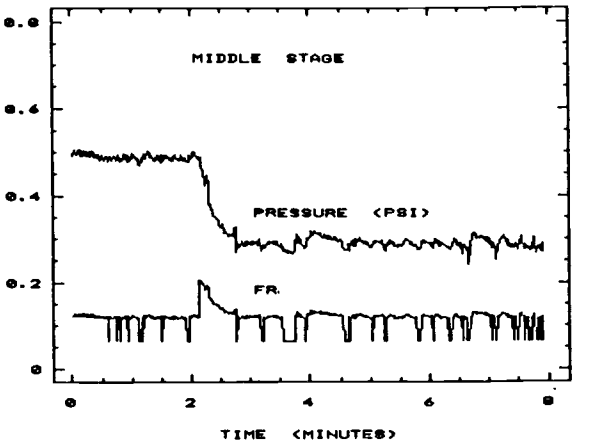

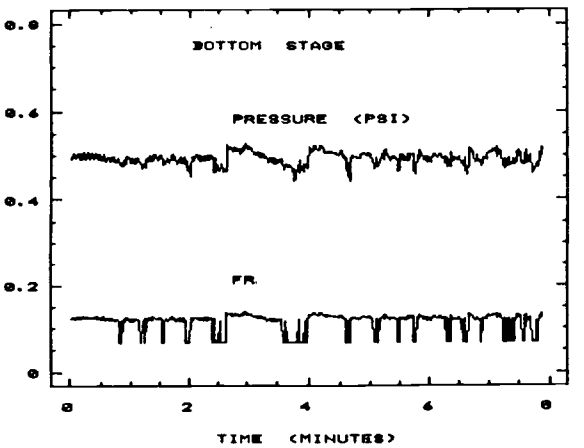

Figure (119)

Simulated Close-loop Performances for a -0.20 psi Setpoint Change in the Middle Stage with Decoupling (ON/OFF Operation and 25% Iron).

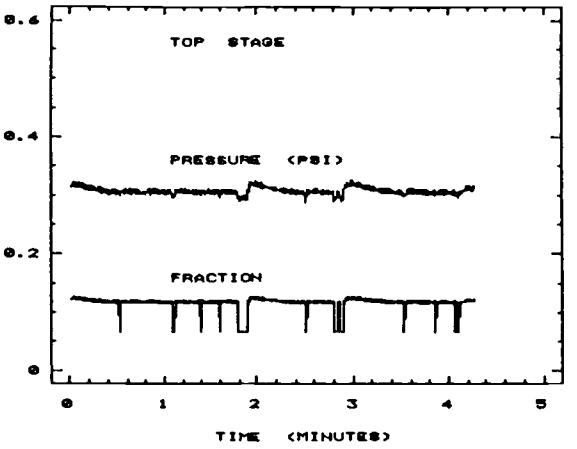

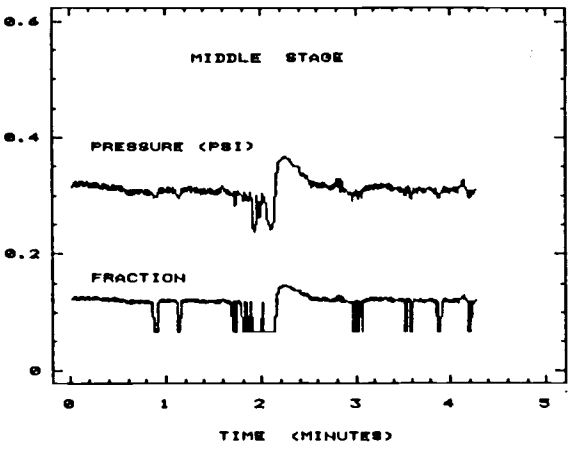

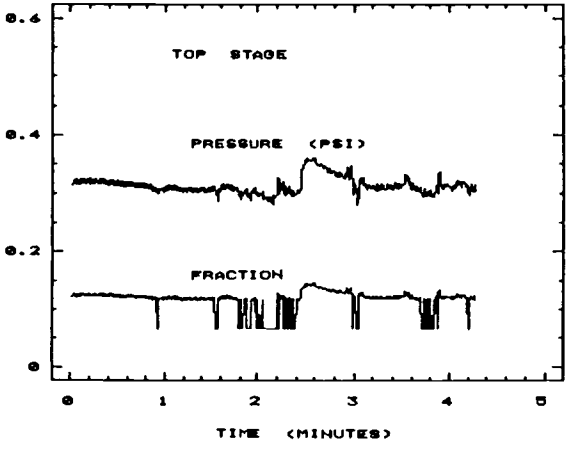

Figure (120)

Simulated Closed-Loop Performances for a 35 gm/second Step Change in the Feed Flow of Solids into the Top Stage (ON/OFF Operation and 50% Iron)

middle and bottom stages jump to values of 0.37 psi and 0.36 psi respectively. The pressure drop across the middle stage is first decreased then increased because of the solids flow rate fluctuations out of the top stage. The amplitude of the slow pressure fluctuations increases in going from the top to the bottom stages which is due to the flow rate fluctuations out of each stage. The pressure drop across each stage returns to the desired value with a response that is more sluggish in going from the top to the bottom stages. Also, the frequency of hitting the lower constraint increases in going from the top to the bottom stages because of the same reasons as those listed above.

VIII.3.3 Closed-Loop Experiments

VIII.3.3.1 Negative Setpoint Change in the Pressure Drop Across a Stage

Figure (121) shows the experimental results of the non-decoupling case. The response of the pressure drop across the top stage is very good. The responses of the middle and bottom stages show very slow oscillation in addition to the disturbances which are due to the setpoint change in the pressure drop. However, the average pressure drop across each stage is equal to the desired value. The disturbances in the pressure drop across the middle and bottoms stage

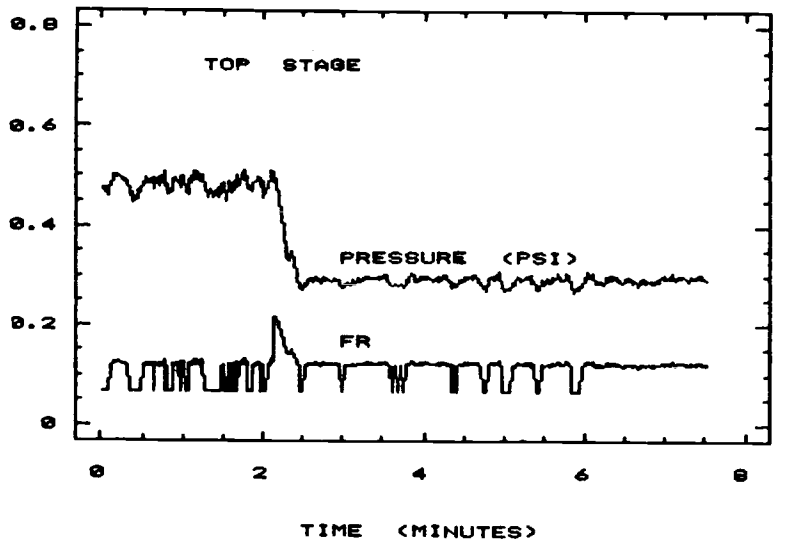

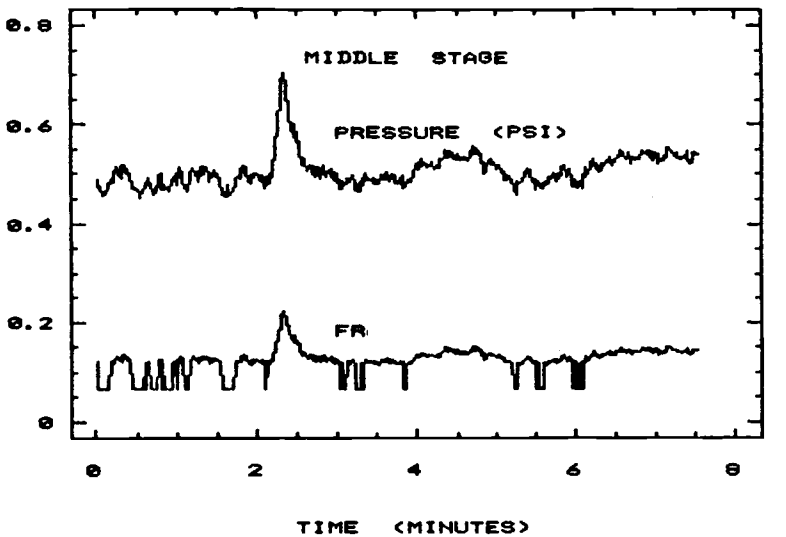

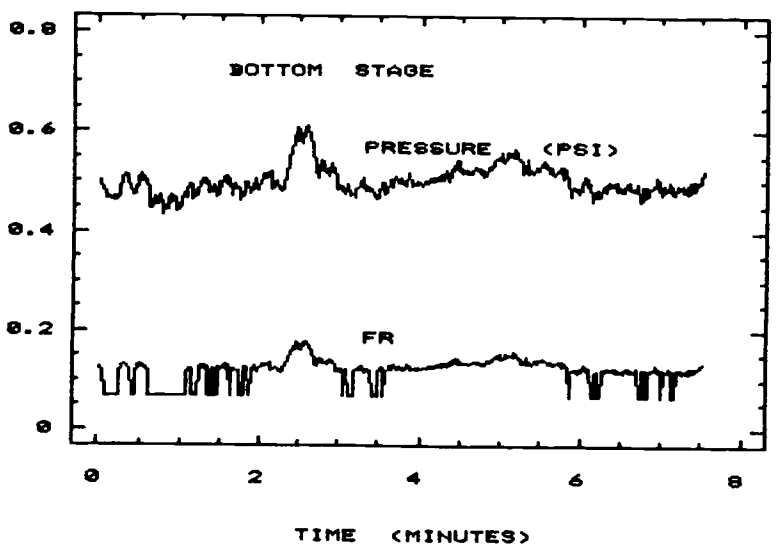

Figure (121)

Experimental Closed-loop Performances for a -0.2 psi Set-point Change in the Top Stage without Decoupling (ON/OFF Operation and 25% Iron).

have maximum values of 0.70 psi and 0.6 psi respectively. The disturbance in the middle stage is more narrow than that for the bottom stage. This could be a result of the fast response of the top stage which means the release of a large amount of solids in a very short time which causes the pressure to jump to a high value (dirac function). The plots show the occurrence of faster oscillations which are random and have very small amplitudes. The controller outputs of all three stages hit the constraint at approximately the same frequency.

Figure (122) shows the results when decoupling is implemented. The disturbances in the middle and bottom stages are reduced to 0.6 psi and 0.57 psi respectively. The pressure drops across the middle and the bottom stages undershot the desired value after the disturbance as a result of the large controller action which is equal to that of the top stage. The large controller action leads to the behavior described previously in sections VIII.2.1 and VIII.2.2. The pressure drops across the top and bottom stages (after and before the disturbances) show an offset which is less than .01 psi. The pressure drop across the middle stage shows slower fluctuations with an average pressure drop close to the desired value. The controller outputs hit the constraint in the top and bottom stages more frequently than the middle stage which may be reason for

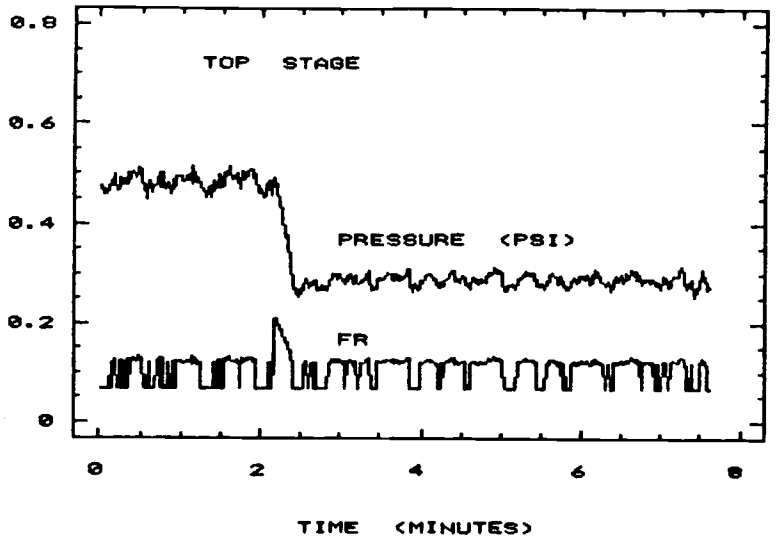

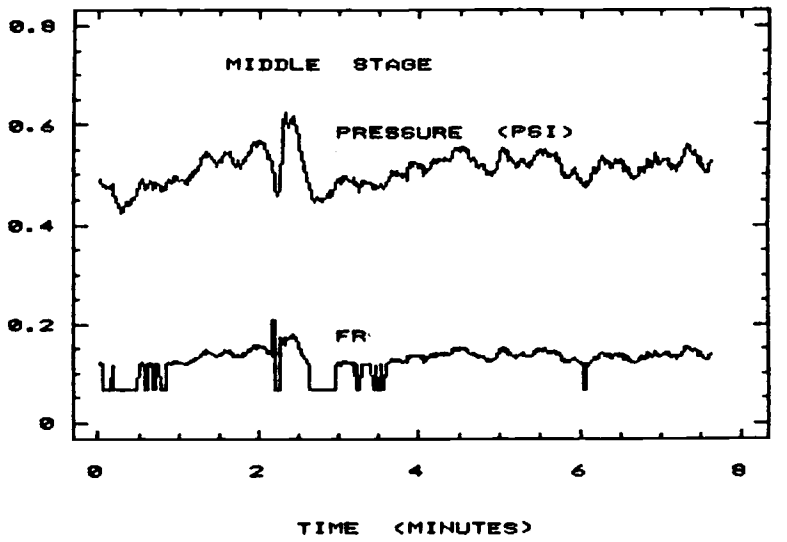

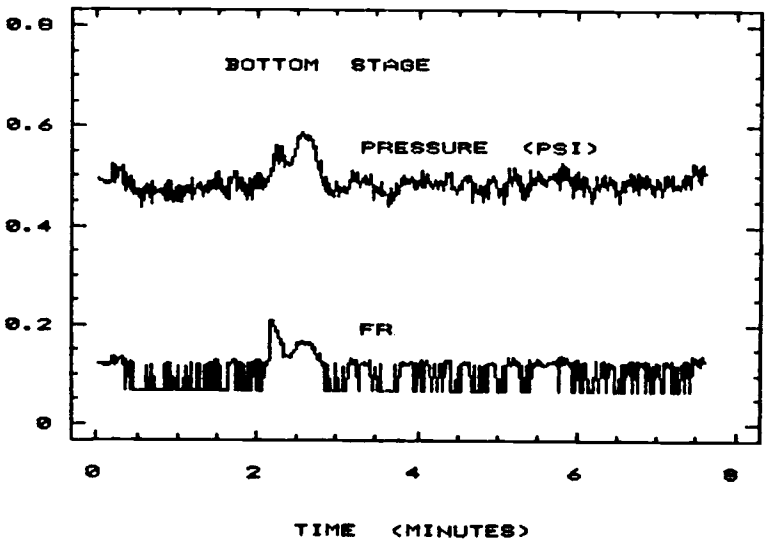

Figure (122)

Experimental Closed-loop Performances for a -.20 psi Setpoint Change in the Top Stage with Decoupling (ON/OFF Operation and 25% Iron).

the offset in the pressure drop as well as the smaller fluctuations associated with the top and bottom stages.

Figure (123) shows the results of a similar type of experiment when the change is introduced to the middle stage. The response of the pressure drop across each stage is very good. The fluctuations are very small and the offset does not exist. The controller outputs show similar behavior as those in the last case.

VIII.3.3.2 Positive Step Change in the Feed Flow Rate of Solids

Figure (124) shows the results when a positive change in the solids flow rate of 30 gm/second is made. The response to the change is good in all three stages. The amplitude and frequency of the fluctuations in the pressure drop across the top stage is greatly reduced when the step is introduced. The pressure response of the middle and bottom stages have similar fluctuations before and after the step is introduced. The fluctuations in the middle stage are slower and have an amplitude which is larger than those for the other stages. The average pressure drop shows a slight increase above the desired value for each stage but then returns to the desired value in a short time. The controller of the top stage hit the constraint much more frequently than the other stages, which might be the reason

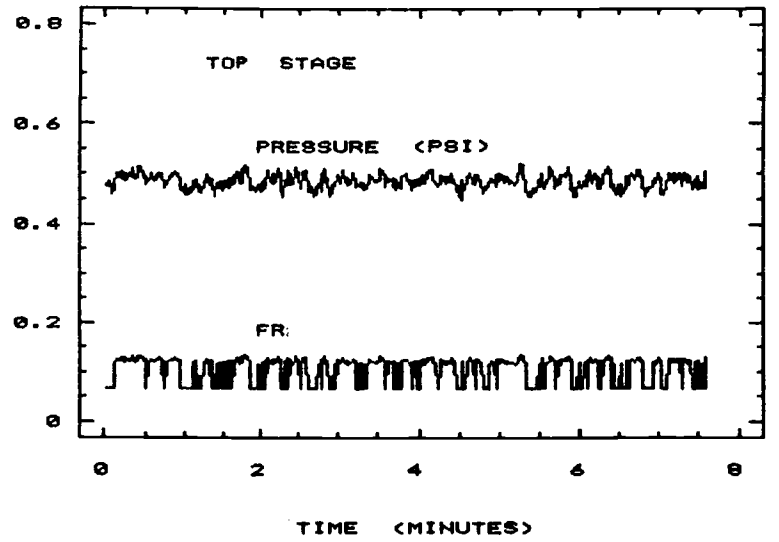

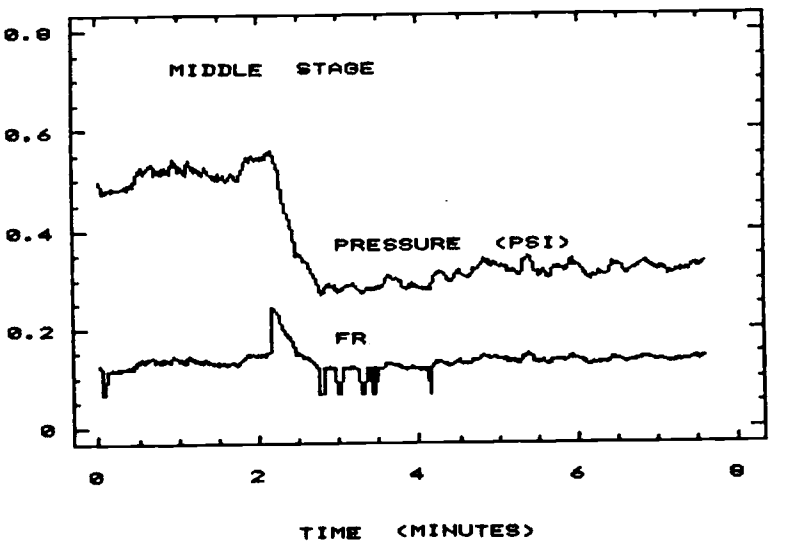

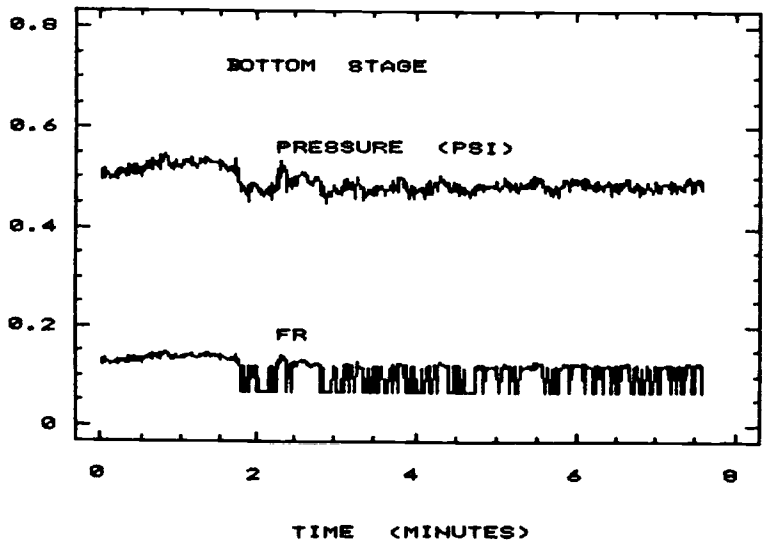

Figure (123)

Experimental Closed-loop Performances for a -0.20 psi Setpoint Change in the Middle Stage with Decoupling (ON/OFF Operation and 25% Iron).

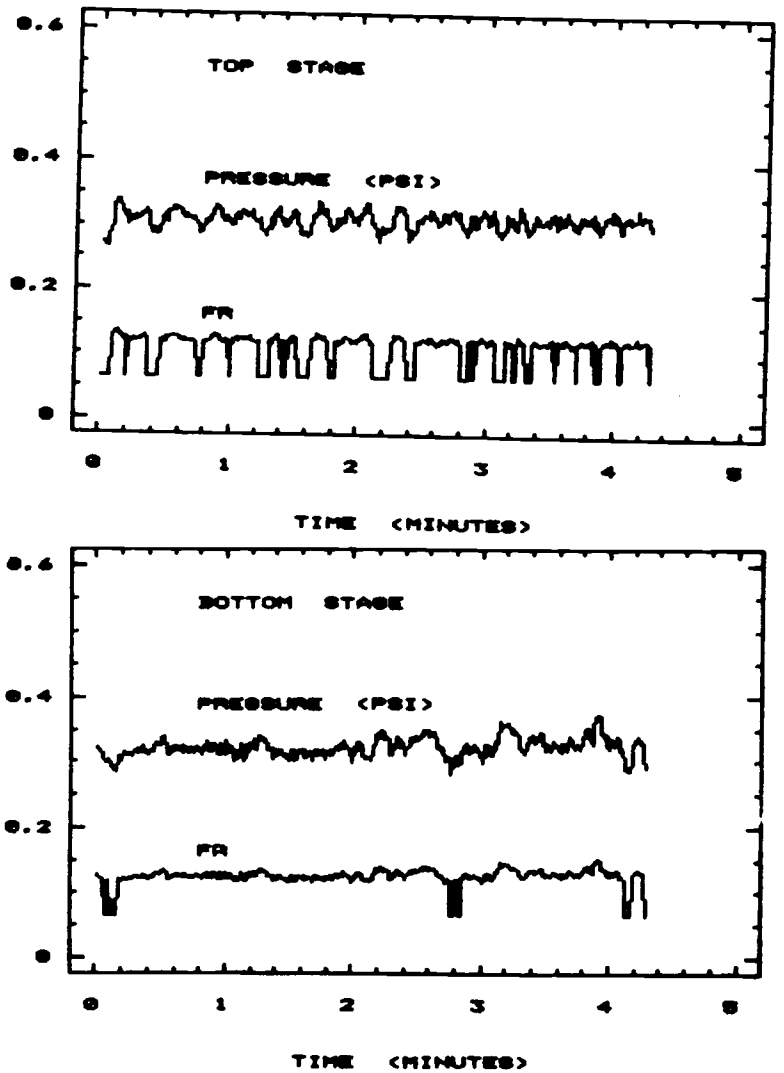

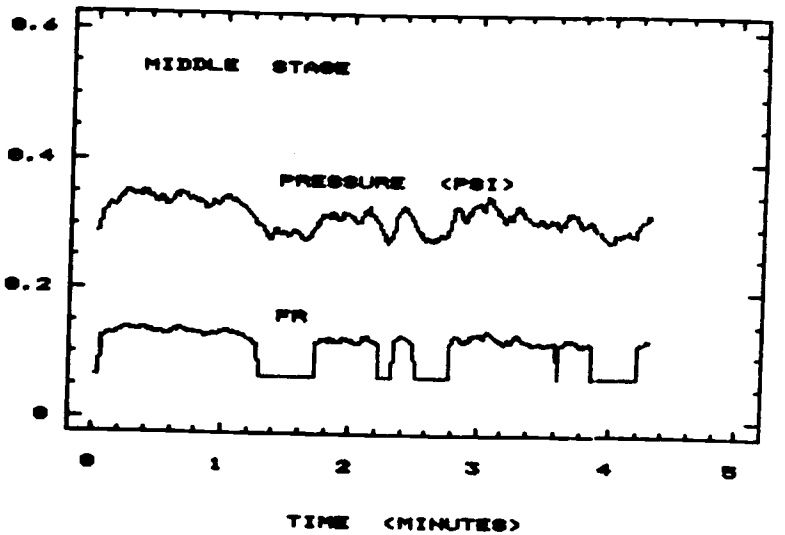

Figure (124)

Experimental Closed-Loop Performances for a 30 gm/second Step Change in the Feed Flow of Solids into the Top Stage (ON/OFF Operation and 50% Iron)

for the small fluctuations as well as the very good response.

VIII.3.4 Comparison Between the Simulated and Experimental Performances

The experimental responses of the pressure drops (20 seconds) across the stage, to which the negative step in the setpoint is introduced, is faster than that for the simulation (23 seconds). This might be the reason for the occurrence of the larger disturbances in the middle and bottom stages that appear in the experimental results. The same reason is responsible for the difference in decoupling efficiency between the experimental and simulated performance. The fluctuations of the pressure drop in the simulation performances are similar to those of the experiments. The disturbances in the pressure drop across each stage, due to a positive change in the feed rate, are larger in the simulation than in the experiment. However, no offset is observed in the simulation or the experimental performances. This is due to the similar reasons discussed previously in sections VIII.2.1 and VIII.2.2.

In general the experimental and simulated responses are in good agreement which indicates that the model is relatively good in describing the process.

VIII.4 "Leaking" Valve Operation

The following equation is the result of linear fitting of the experimental data by the solids flow rate model:

$$m_o = 4.416 - 0.0688 * I + 0.000268 * I^2 \qquad (90)$$

$$R^2 = 0.988$$

Figure (125) shows the plot of the flow rate of the solids out of the stage valve for both the experimental data and the fitted model versus the current. The figure shows a very good agreement between the experimental data and the model predictions.

The following equation, relating the physical properties of solids and geometrical parameters, and the equipment to the model constants, can be obtained by following the same procedures described in section VI.2.1 and VI.2.2.

$$\frac{(\bar{V}_p\ K_2)\ (\rho_s\ A_f)}{A_1} = 0.0212 \qquad (91)$$

$$\frac{r\ B}{\mu_0} = 40.86 \qquad (92)$$

$$\frac{(\rho_s\ A_f)}{A_1}\ [\ (A_{cs}\ \delta)\ (1-\epsilon)\ \rho_s - A_1\ u_g] = 4.416 \qquad (93)$$

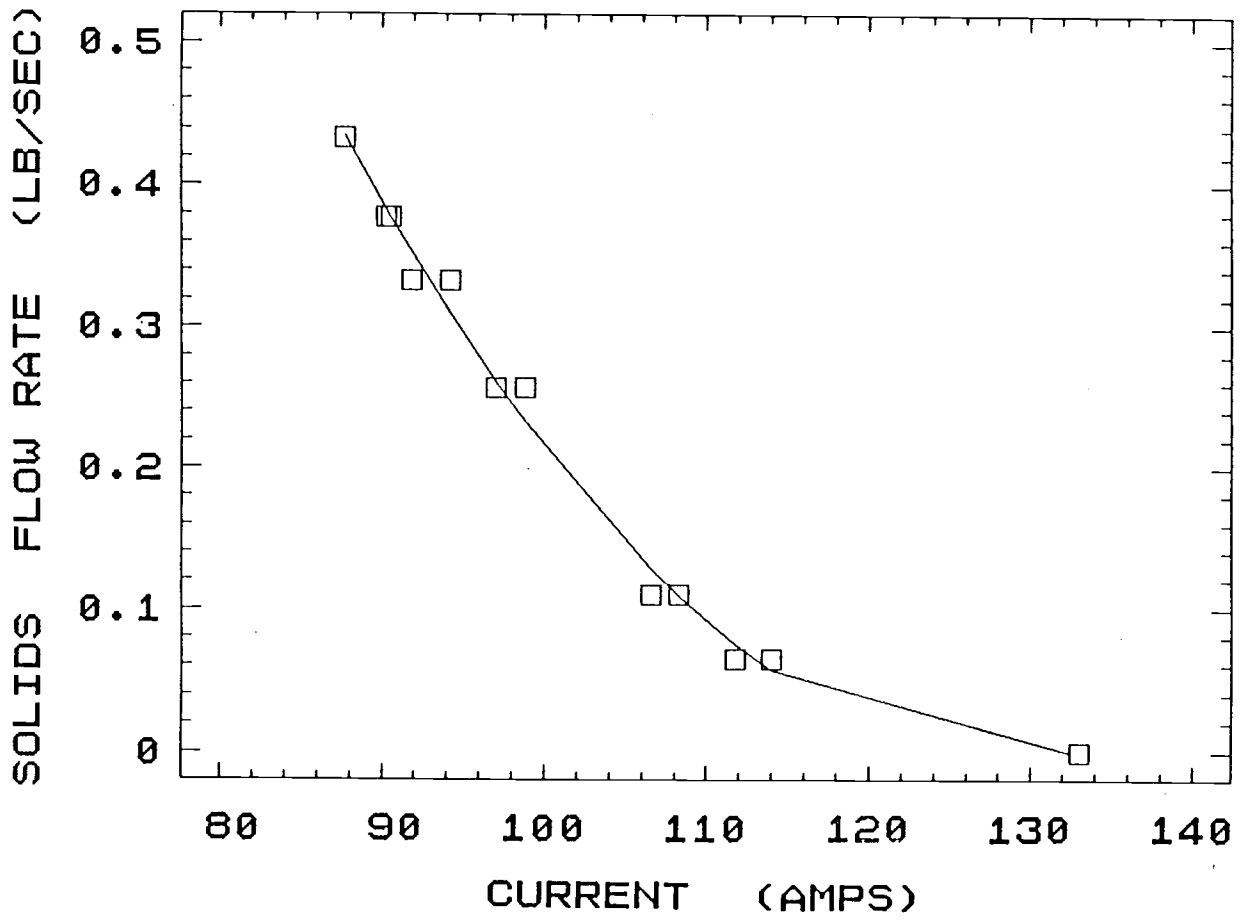

Figure (125) Solids Flow Rate Through the Stage Valve vs. Average Current (Leaking Valve Operation and 25% Iron).

VIII.4.1 Design of Controller Parameters via Simulations

VIII.4.1.1 Controller Gain

Figure (126) shows the results of the simulation. The general curve behavior is similar to those discussed before in section VI.2.2.1.1. However, the curves for the pressure are more sluggish in going from the top to the bottom stages. ISQMANS increase as K_C increases. The curve for the top stage shows an inflection point for K_C = 120 amps/psi. ISQERR in each stage does not show appreciable decrease for K_C grater than 114 amps/psi. Therefore, a value of 114 amps/psi was chosen for K_C based on section VI.1.4. The choice depends mainly on the results of the top stage.

VIII.4.1.2 Filter Time Constant

Figure (127) shows the plots of the simulation results. The curves for the top stage show the occurrence of the minimums at a filter time constant of 2 seconds while those for the middle and bottom stages show minimums at a filter time constant of 1.8 seconds. Therefore, a value of 1.8 seconds was chosen for the filter time constants.

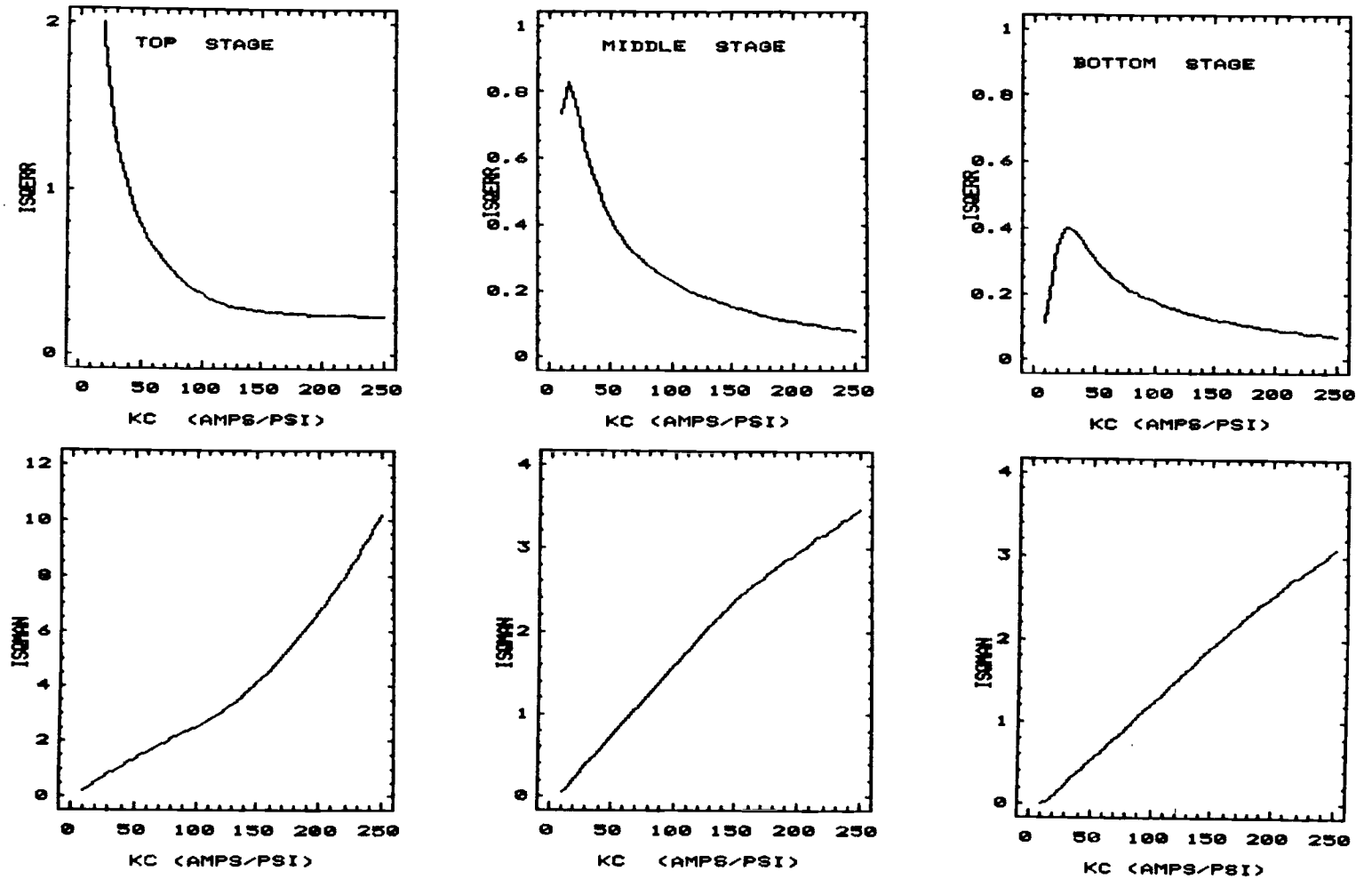

Figure (126) ISQERR an ISQMAN for the Three Stages vs. the Controller Gain.

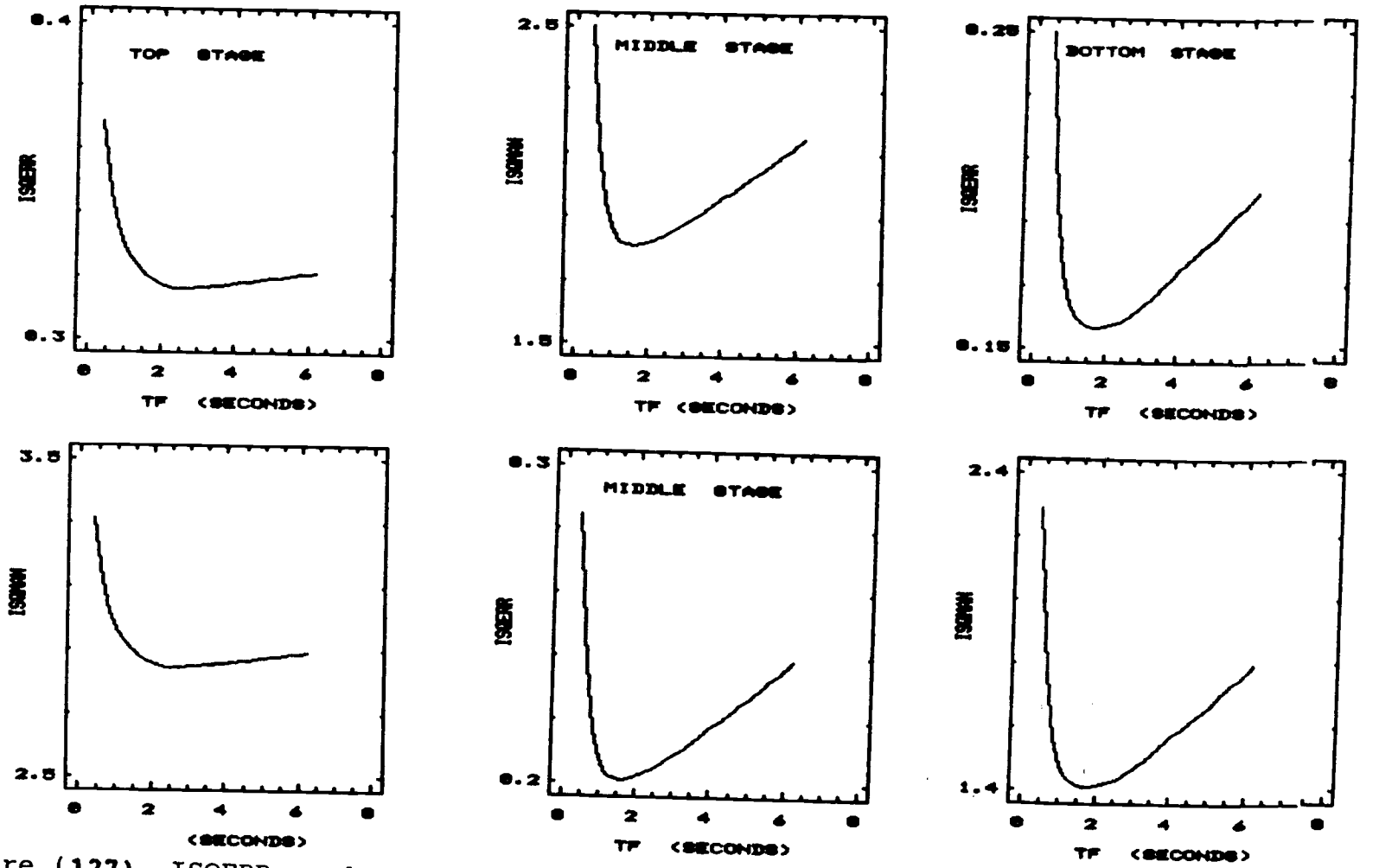

Figure (127) ISQERR and ISQMAN for the Three Stages vs Filter Time Constant ("Leaking" Valve Operation and 25 % Iron).

VIII.4.1.3 Input Constraints

Figure (128) shows the plots for ISQERR and ISQMAN versus the lower limit (constraint) for the three stages. They reach constant values for a lower limit of 88 amps. However, the trends of ISQERR and ISQMAN for the top stage and the middle and the bottom stages are completely different. In the former, the ISQERR and ISQMAN decrease when the lower limit decrease while in the latter, they increase as the lower limit decrease. However, ISQERR and ISQMAN of the top stage are more sensitive to the low limit changes than those for the other stages. Therefore, the lower limit was chosen to be equal to 88 amps. The release current (76 amps) was not chosen as the lower limit because the valve hysteresis behavior for the low weight fraction of the magnetic particles in the solids becomes worse when the lower limit decreases. The performance will deteriorate if the release current is used.

Figure (129) shows the corresponding plots for the upper limit. ISQERR and ISQMAN reach constant values at an upper limit of 110 amps for all the stages. However, due to the strong hysteresis behavior of the valve, a value corresponding to the holding current (132 amps) was chosen as the upper limit. This value corresponds to zero flow of solids through the valve.

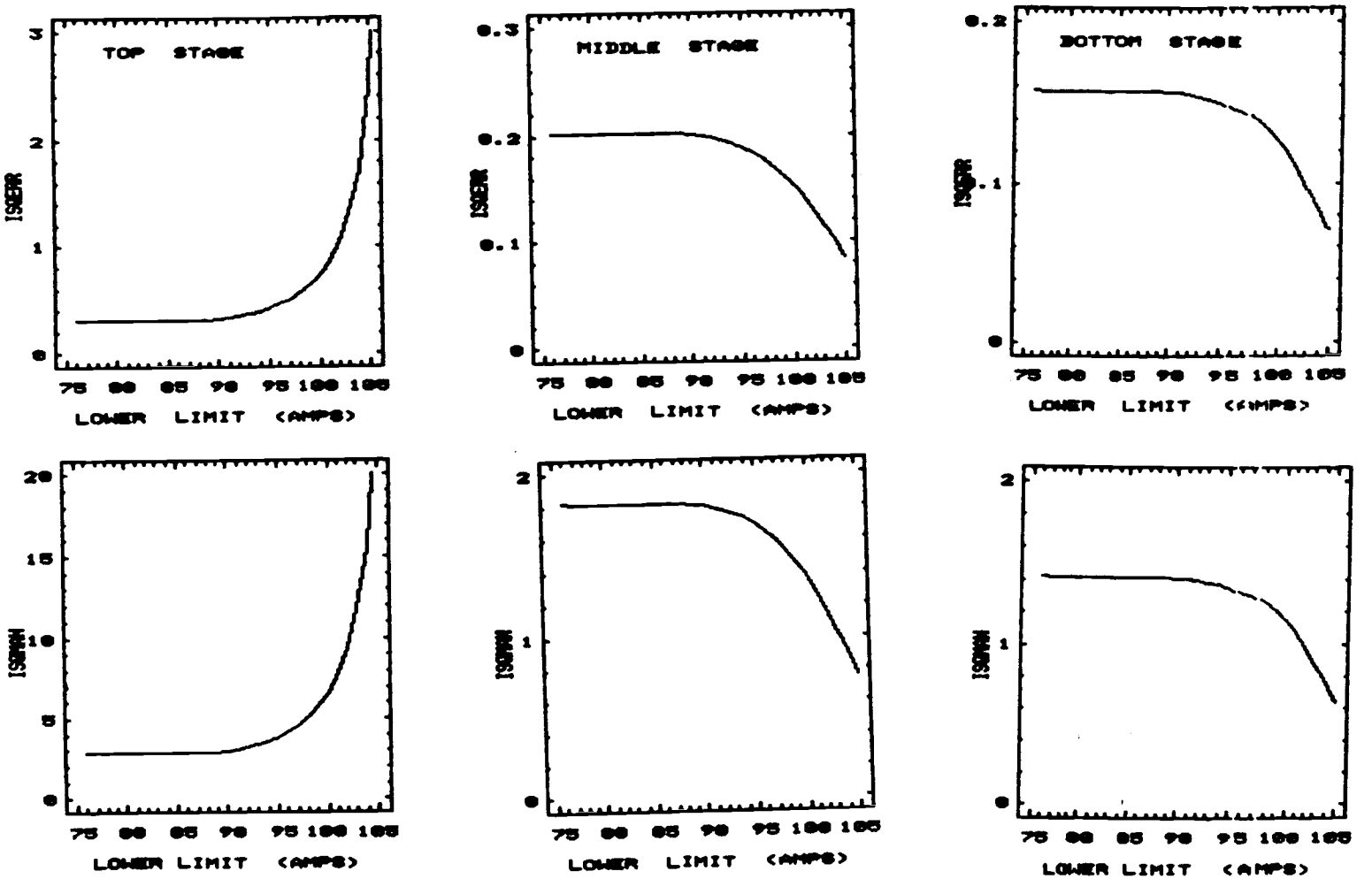

Figure (128) ISQERR and ISQMAN for the Three Stages vs. the Lower Limit on Input Constraint ("Leaking" Valve Operation and 25 % Iron).

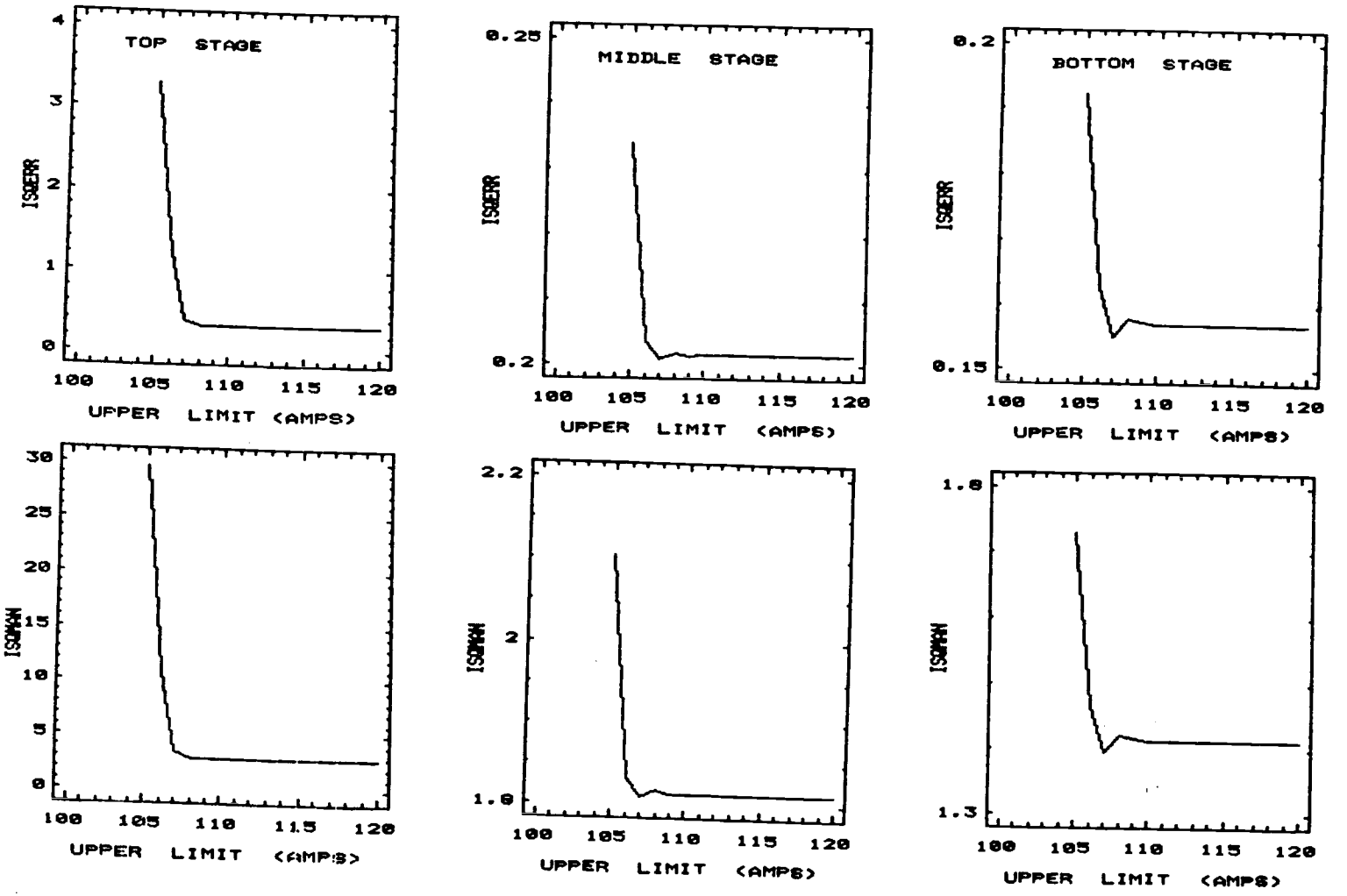

Figure (129) ISQERR and ISQMAN for the Three Stages vs. the Upper Limit on Input Constraint ("Leaking" Valve Operation and 25% Iron).

VIII.4.2 Simulated Closed-loop Performance

VIII.4.2.1 Negative Setpoint Change in the Pressure Drop Across a Stage

Figure (130) shows the simulated performances for the three stages. The top stage response to a negative change in the setpoint is good and relatively fast (≈ 28 seconds). An offset which has a value of less than .01 psi occurs in the pressure response of the top stage. The responses for the middle and bottom stages show the occurrence of the disturbances, resulting from the setpoint change in the top stage, which have values of 0.58 psi and 0.56 psi respectively. As before, the disturbances are delayed from the middle to the bottom stages. The responses of the pressure drops show larger fluctuations after the occurrence of the disturbance. This supports the idea mentioned previously (section VIII.2) which predicts the existence of control difficulties when a disturbance is introduced to any stage. Also, the fluctuations of the flow rate of solids into the middle and bottom stages contribute to the occurrence of the pressure drops' fluctuations. The controller hit the constraints many times which gives an indication of the strong hysteresis behavior of the valve.

Figure (131) shows the results of a similar simulation run when the decoupling is implemented. The perform-

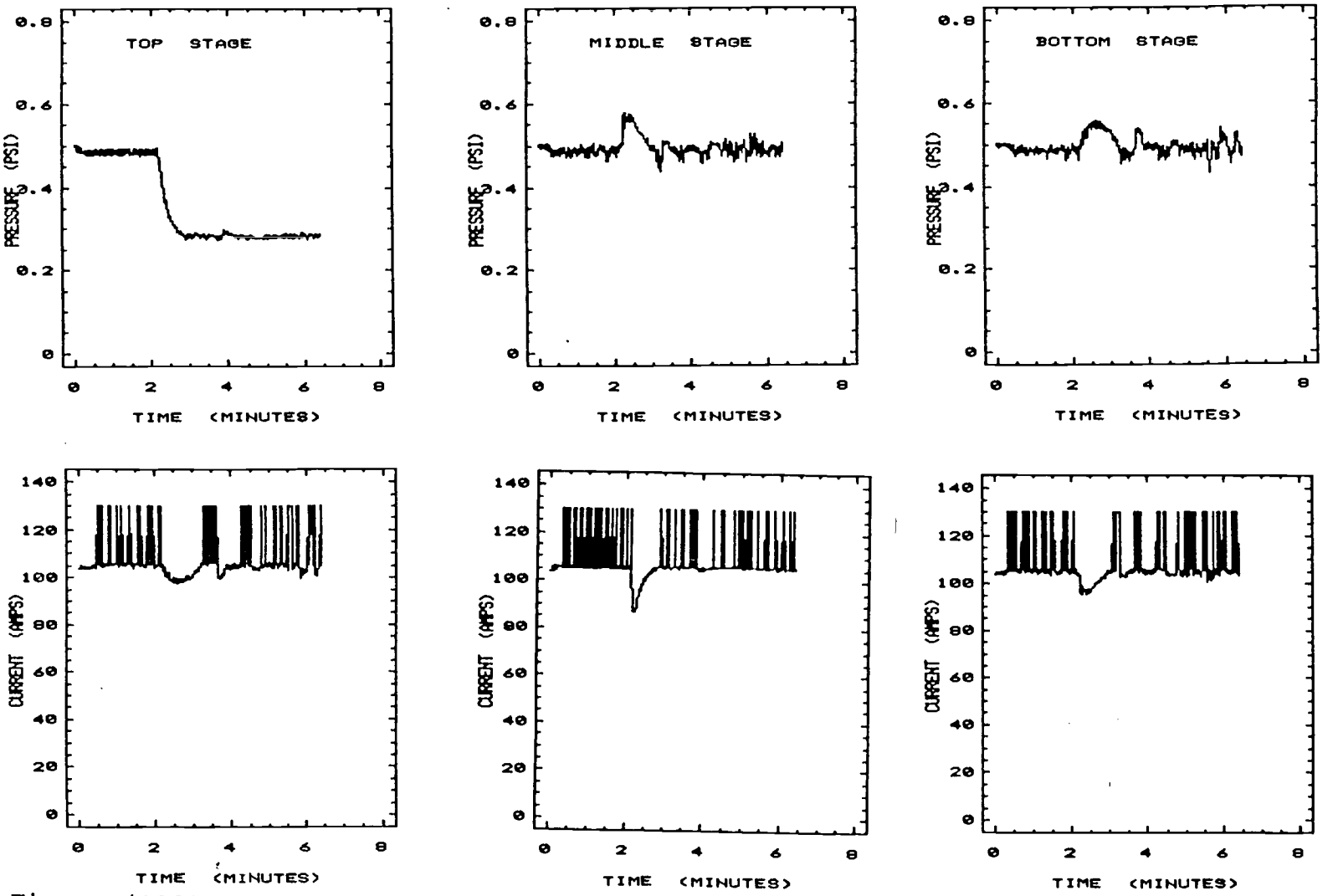

Figure (130) Simulated Closed-loop Performances for a -0.2 psi Setpoint Change in the Top Stage without Decoupling ("Leaking" Valve Operation and 25% Iron).

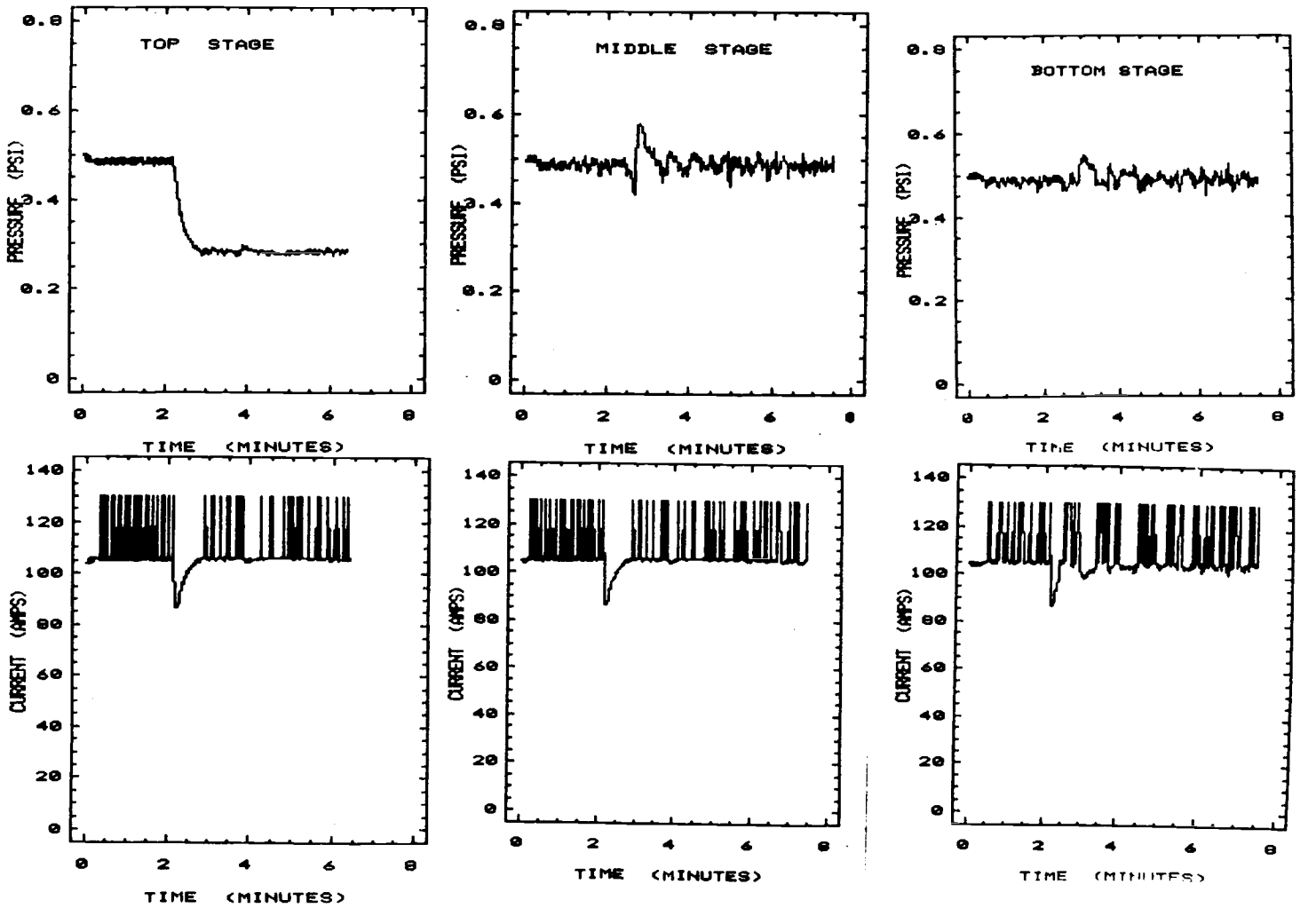

Figure (131) Simulated Closed-loop Performances for a -0.2 psi Setpoint Change in the Top Stage with Decoupling ("Leaking" Valve Operation; 25% Operation).

ances of all stages are improved and the disturbances are reduced in height to 0.57 psi and .55 psi for the middle and bottom stages respectively. The duration of the disturbances is greatly reduced because of the decoupling action. The fluctuations in the middle and bottom stage are random and have small amplitude (≈.01 psi). The average pressure is very close to the desired value (0.5 psi). The response of the top stage is identical to that of the non-decoupling case.

Figure (132) show the results for the case when the step is introduced to the middle stage with decoupling. The top stage performance is good and does not seem to be affected by the changes in pressure across the stages below. The occurrence of the slow fluctuations is due to the hysteresis nature of the valve. The response of the middle stage is similar to that of the last case. However, the pressure fluctuates slowly after the step is introduced, which is due to flow rate fluctuations (section VIII.2.1), to the stage. The disturbance across the bottom stage has a maximum value of .55 psi. Similar to the last cases, the pressure shows larger fluctuations after the disturbances which are due to the same reasons mentioned previously. The output of the controller behaves similarly to those mentioned in the last cases.

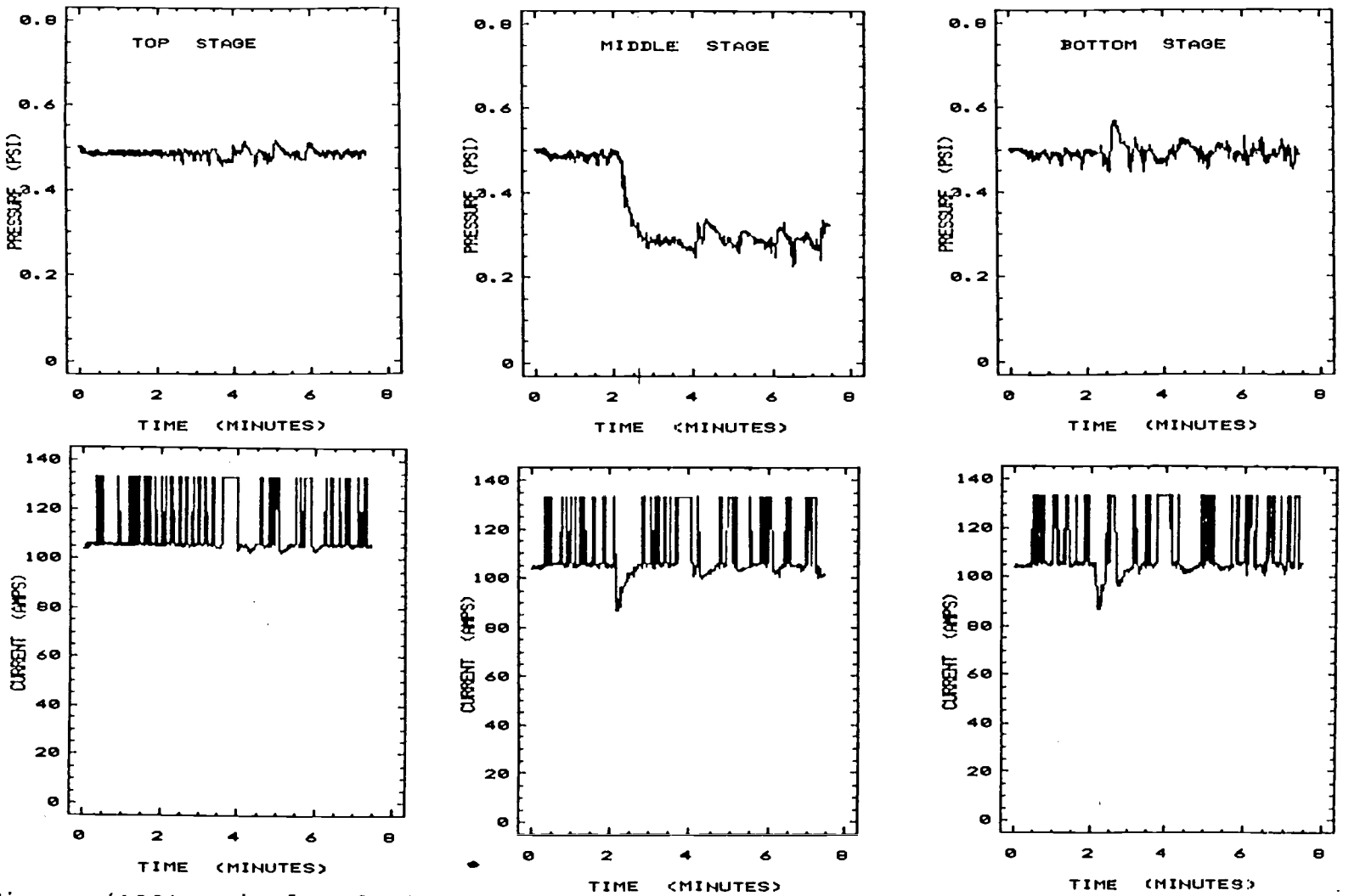

Figure (132) Simulated Closed-loop Performances for a -0.20 psi Setpoint Change in the Middle Stage with Decoupling ("Leaking" Valve Operation; 25% Operation).

VIII.4.2.2 Positive Step Change in the Feed Flow Rate of Solids

Figure (133) shows the pressure response to a positive step in the feed of 30 gm/second. The pressure drop across the each stage increases to a value of 0.34 psi. The responses are delayed and are more sluggish in going from the top to the bottom stages. The offset in the pressure drop across each stage has an average value of -0.02 psi. The controller outputs did not hit the constraint after the step was introduced. This is because the pressure is greater than 0.32 psi during the rest of the simulation.

VIII.4.3 Closed-Loop Experiments

VIII.4.3.1 Negative Setpoint Change in the Pressure Drop Across a Stage

Figure (134) shows the controller output (manipulated variable) and the pressure performances when a setpoint change of -0.2 psi is introduced to the top stage without the implementation of decoupling. The pressure drop response of the top stage is fast (23 seconds). An average offset of 0.01 psi exists in the pressure drop response of the top stage. The fluctuations are small and have

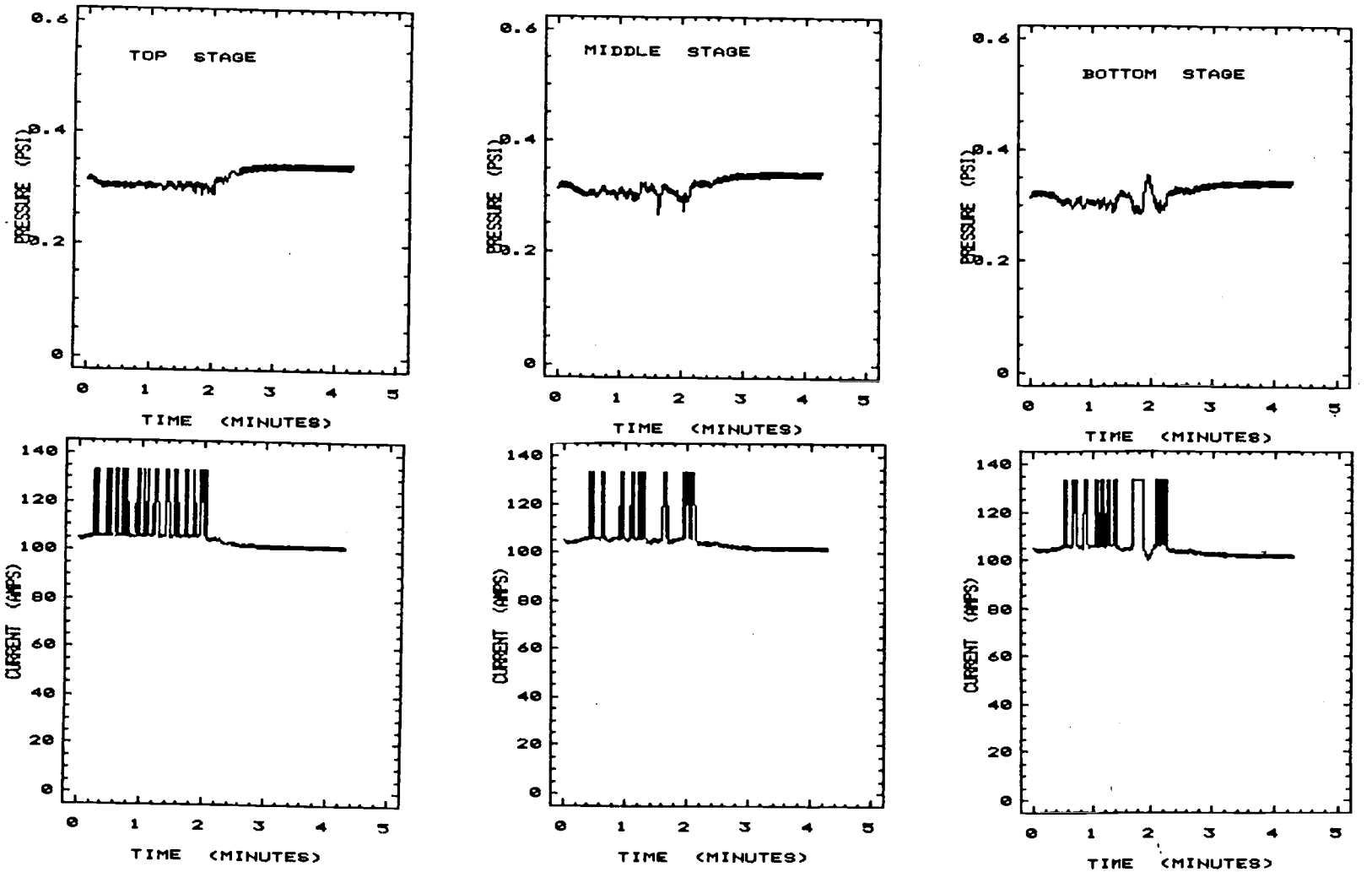

Figure (133) Simulated Closed-loop Performances for a 30 (gm/second) Step Change in the Feed Flow of Solids into the Top Stage (Leaking Valve Operation and 25% Iron).

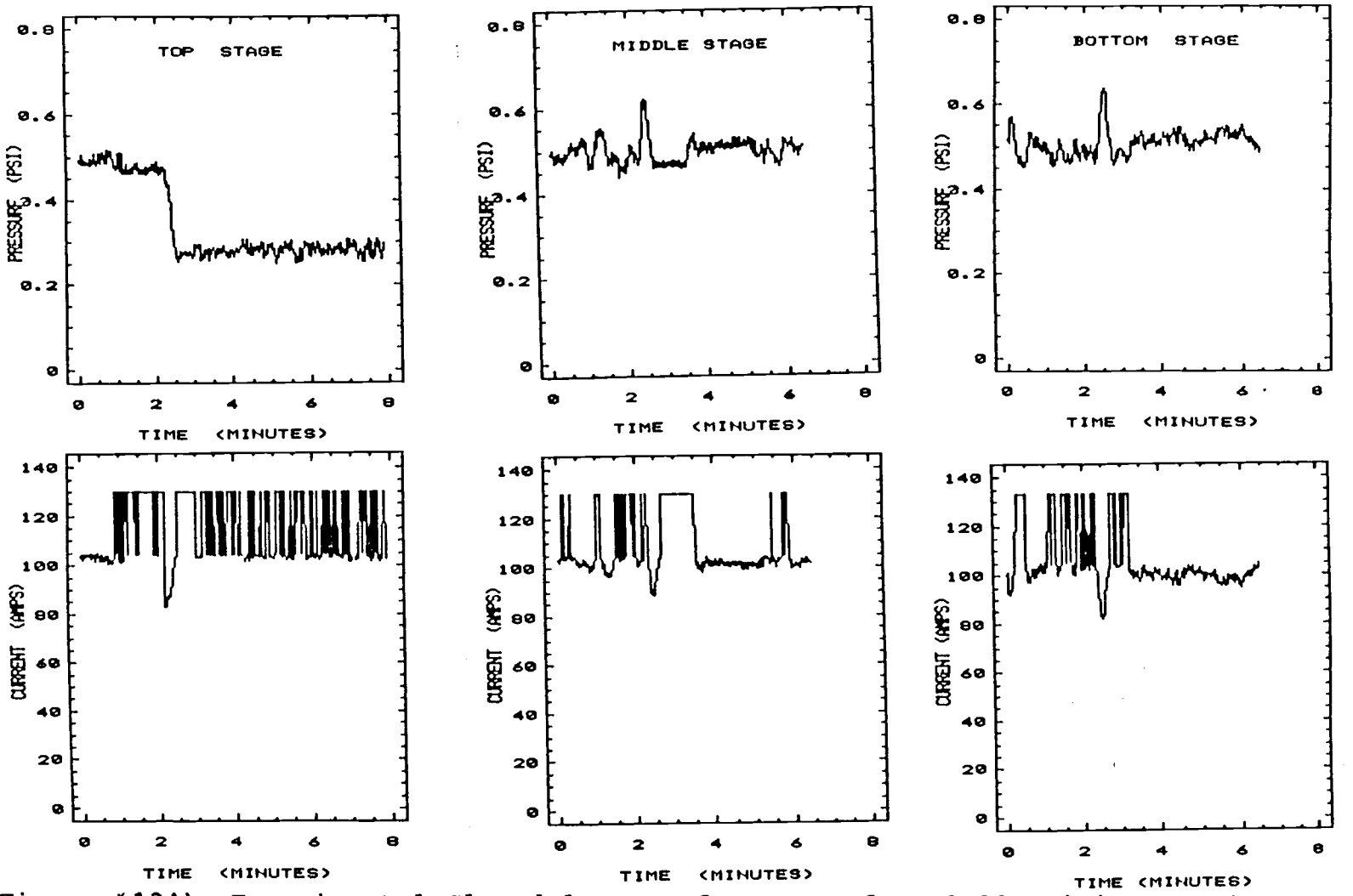

Figure (134) Experimental Closed-loop Performances for -0.20 psi in Setpoint Change in the Top Stage without Decoupling.

average amplitude of 0.01 psi. The pressure drop disturbance in the middle and bottom stages have maximum values of 0.62 psi and 0.63 psi respectively. The durations of the disturbances are small and equal in both stages (≈ 25 seconds). The pressure drop fluctuations are larger and slower than those of the top stage. However, the average pressure drop is equal to the desired value (0.50 psi). The pressure drops across the middle and bottom stages undershoot at the end of the disturbance due to the reasons mentioned in section VIII.2.2.

The frequency of hitting the constraint decreases from the top to the bottom stages. This might explain the difference between the fluctuations in the pressure drop across the different stages.

Figure (135) shows the result of a similar experiment when decoupling is implemented. The pressure drop of the top stage shows slow oscillations with an average pressure drops offset of less than -0.01 psi. The disturbances in the middle and bottom stages are reduced to a value of 0.55 psi. The fluctuations are faster and smaller than that for the top stage and the average pressure is equal to the desired value (0.5 psi).

The controller of the top stage hit the upper constraint limit less frequently than those of the other stages. Again, this may explain the difference in the performances of the different stages.

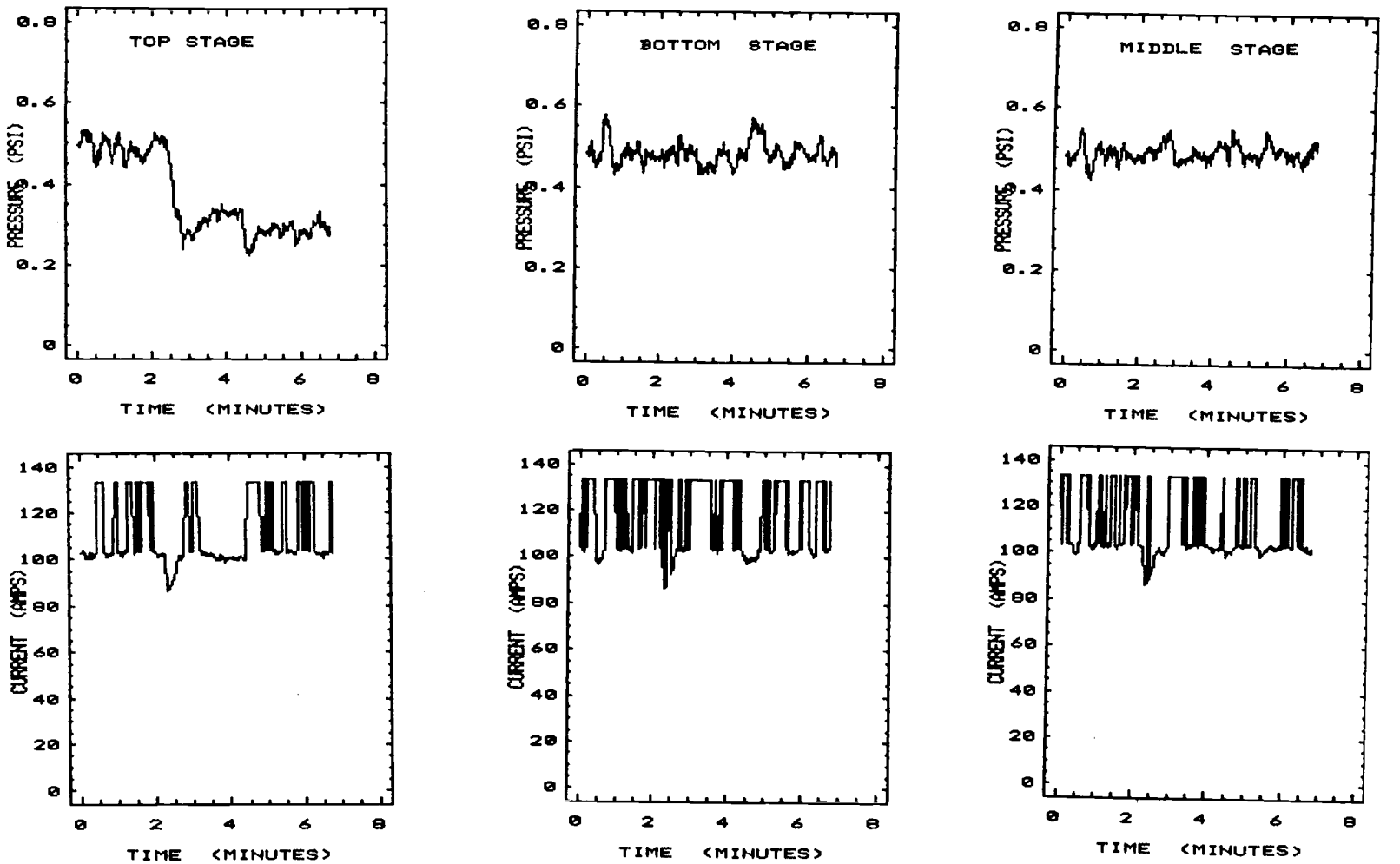

Figure (135) Experimental Closed-loop Performances for a -.20 psi Setpoint Change in the Top Stage with Decoupling ("Leaking" Valve Operation and 50% Iron).

Figure (136) shows the plots of the experimental performance of the pressure when the setpoint change is made in the middle stage with decoupling. The disturbance in the pressure drop is reduced to 0.54 psi due to the decoupling. The pressure drops across the stages show the occurrence of fast fluctuations, which may be due to the very fast fluctuations of the pressure drop discussed in chapter V. and slow fluctuations which are due to the hysteresis nature of the stage valve and the fluctuations of the flow of solids out of each stage. However, the average pressure drop across each stage is equal to the desired pressure (0.5 psi or 0.3 psi). The frequency at which each controller hits the constraint increases in going from the top to the bottom stages for reasons mentioned previously.

VIII.4.3.2 Positive Change in the Feed Flow Rate of Solids

The experimental performances of all three stages are shown in figure (137). The pressure drops across the top and middle stages increase to a value of 0.37 psi while that of the bottom stages increases 0.33 psi respectively. The response of the pressure drop across the top stage is fast and it actually undershoots after the disturbance is introduced because of the reasons mentioned in section VII.2.2

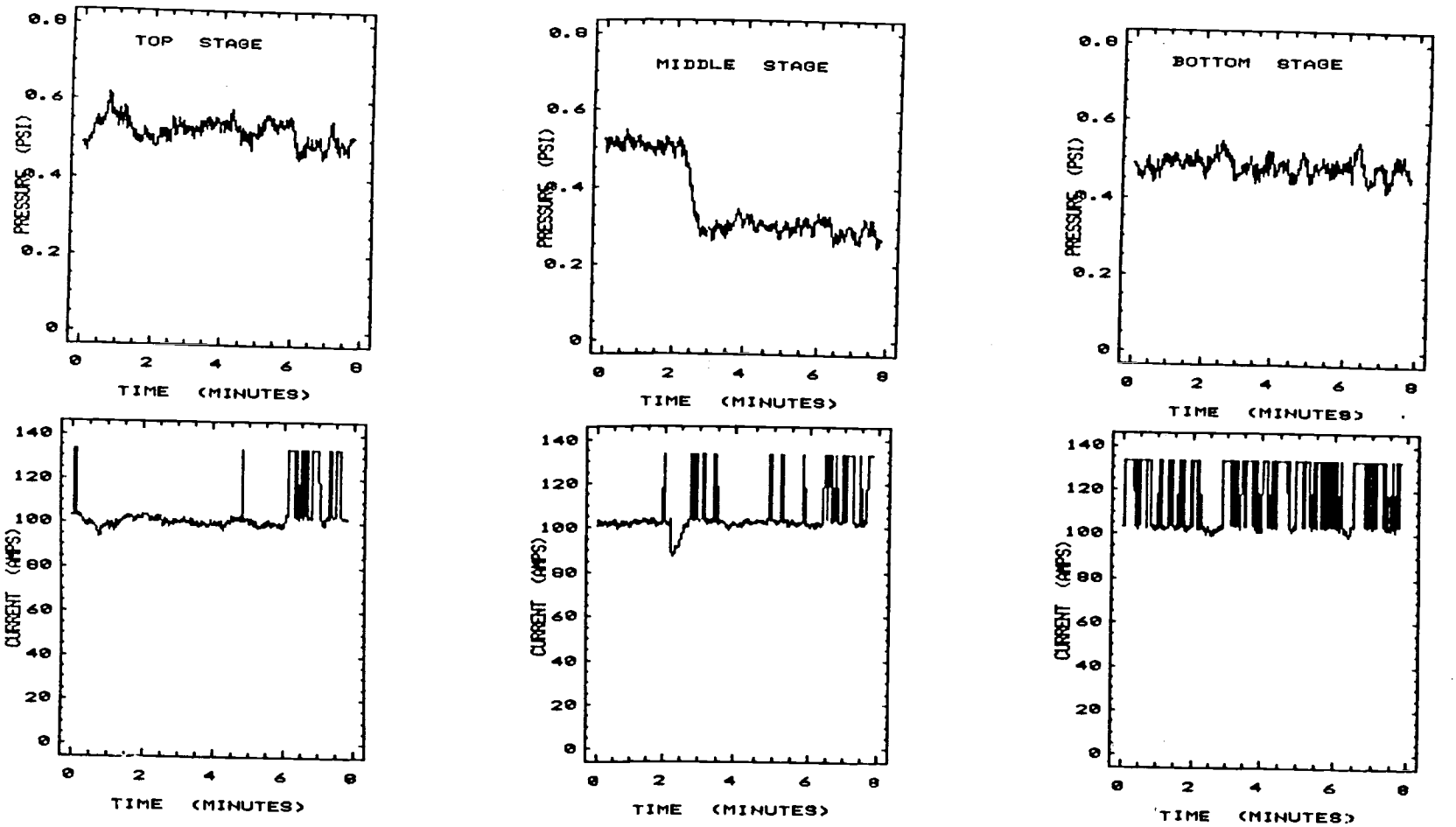

Figure (136) Experimental Closed-loop Performances for a -0.20 psi Setpoint Change in the Middle Stage with Decoupling ("Leaking" Valve Operation and 25% Iron).

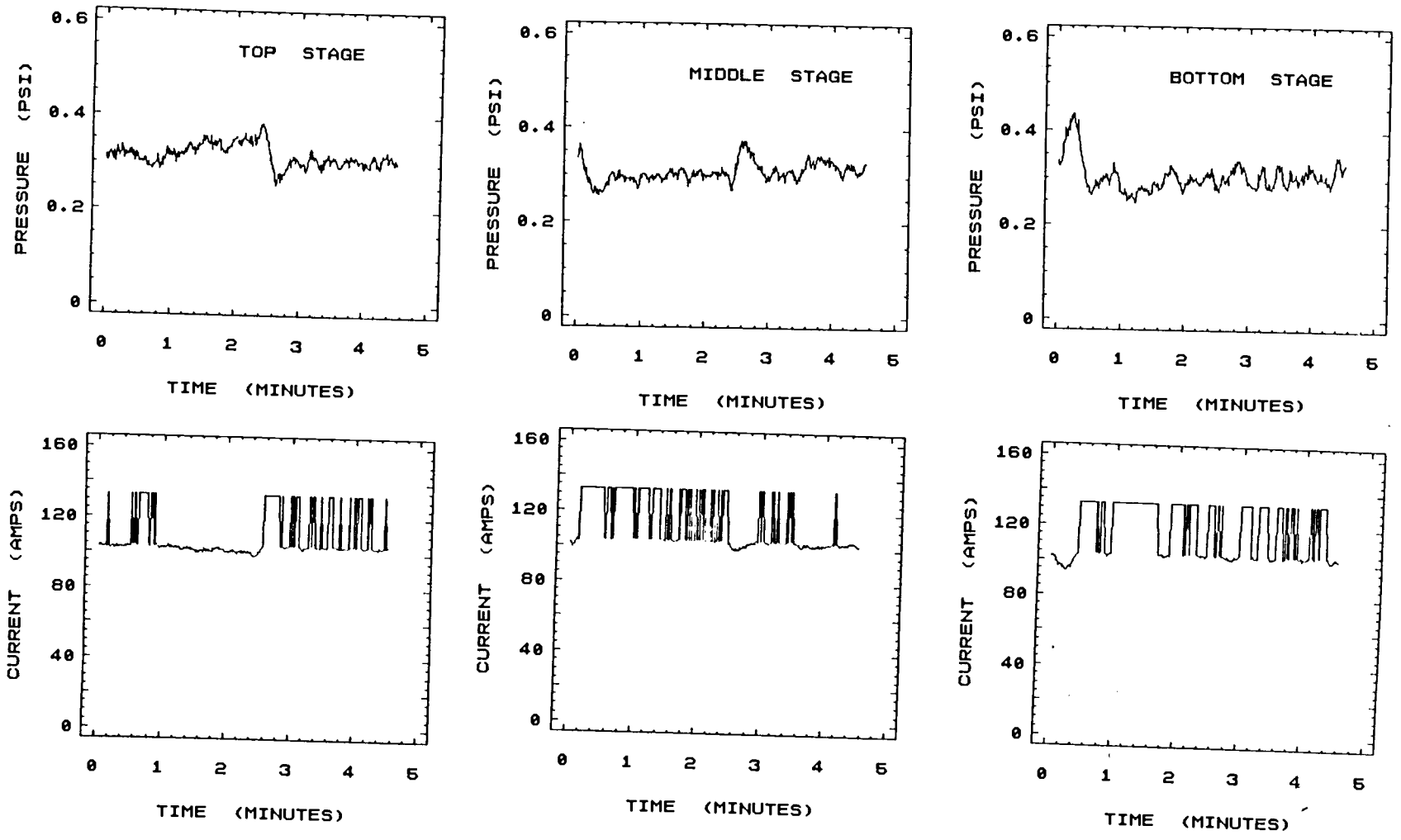

Figure (137) Experimental Closed-loop Performances for a 30 (gm/second) Step Change in the Feed Flow of Solids into the Top Stage (Leaking Valve Operation and 25% Iron).

which happens as a result of the difference between the measured pressure and the setpoint. The effect of the step change in the feed flow rate is delayed from the top to the bottom stages. The response of the pressure drop becomes more sluggish from the top to the bottom stage. However, the average pressure returns to the desired value of .3 psi. Also, the controller outputs hit the constraints more frequently in going from the top to the bottom stages.

VIII.4.4 Comparison Between the Simulated and Experimental Performances

The simulation results show good agreement with the experimental results for the non-decoupled cases. It predicted the occurrence of the disturbances in the pressure drops across the middle and bottom stages. However, the heights of the disturbances are larger in the experimental results while the durations are much smaller than those of the simulation. The simulation predicted fluctuations behavior in the performances of the middle and bottom stages which were also seen in the experiments. The offset in the pressure drop response across the top stage occurred in both the simulation and the experiment. The decoupling cases show very good agreements between the simulation and the experimental results.

The responses to the positive step in the feed show less agreement between the simulation and experimental pressure performances. The responses of the simulations are very sluggish while they are fast in the experiments, especially those of the top and middle stages. The average pressure drops in the simulation results show an offset of -.02 psi, while those in the experiments return to the desired value in relatively short time.

In general, the agreements in all the cases are good and the model can describe the dynamical behavior of the process adequately.

VIII.5 Comparison Between On/Off and "Leaking" Valve Operations

The response of the pressure drop to the load and setpoint changes seem to be better if on/off operation is used. The hysteresis behavior of the valve is more strong when the "leaking" valve operation is used because of the smaller average current used in operation (105 amps) compared to that of the on/off operation (146 amps). The efficiency of decoupling is about the same in both operations. However, the performance of the on/off operation show less slow fluctuation than the "leaking" valve operation which is due to hysteresis nature of the "leaking" valve operation.

The simulation agrees more with the experimental results in the "leaking" valve operation than in the on/off operation except for the case when a step in the feed is made. Figure (138) shows the plots of the flow rate of solids for both the on/off operation (after converting the fraction open data to the current data) and the "leaking" valve operation. The experimental data (points) as well as the fitted models (solid lines) are shown in this figure. The figure shows that, to regulate at a certain flow rate, the "leaking" valve operation is more efficient than the on/off operation. However, the figure shows that the on/off operation can be used to regulate solids flow rate as large 1.89 lbs/second (855 gm/second), while the "leaking" valve operation can only be used to regulate solids flow rate less than 0.5 lbs/seconds (227 gm/second). The operation of the "leaking" valve shows very strong hysteresis for larger flow rates which leads to an unstable operation. The on/off operation uses larger average current than the "leaking" valve operation to regulate the same flow rate of solids through the valve. However, the range of the on/off operation is larger and the regulation of the flow rate of solids is better than the "leaking" valve operation. This is because of the large average current used in the on/off operation which results in a more stable operation.

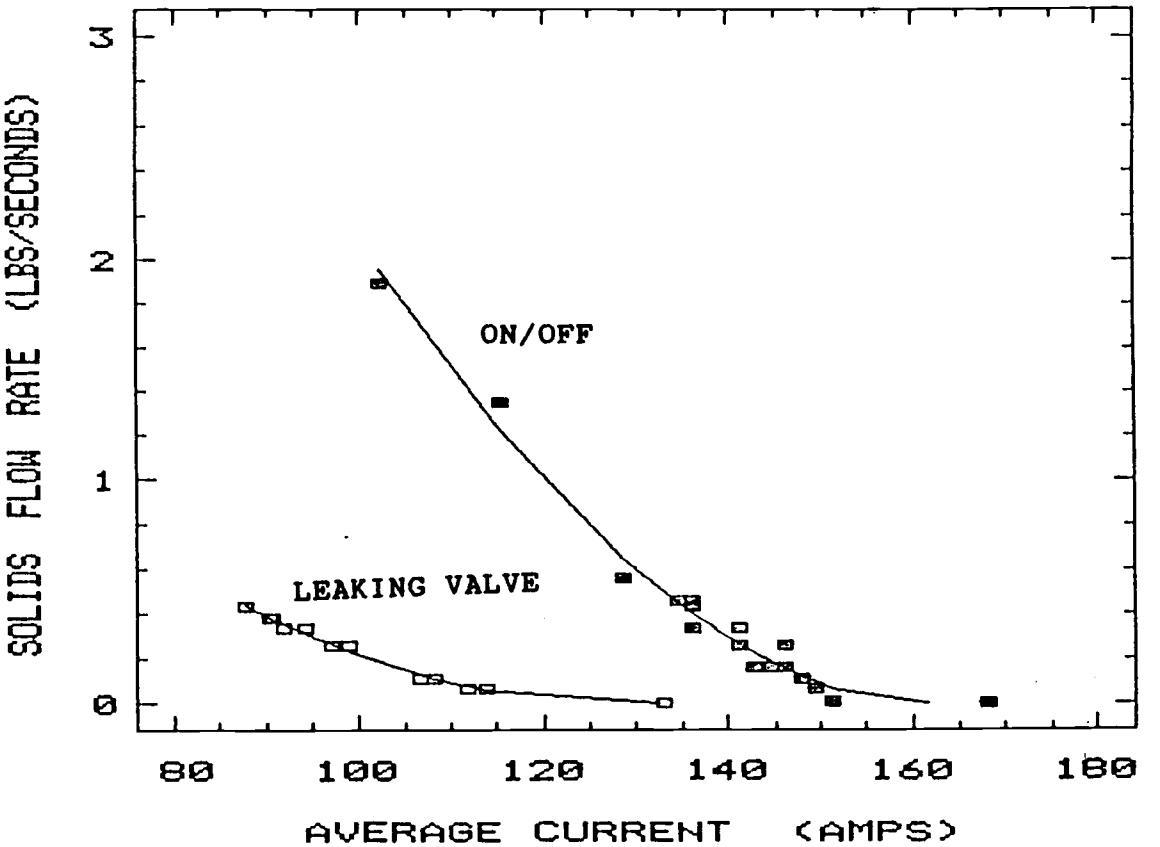

Figure (138) Plots of Solids Flow Rate out of the Stage vs. the Average Current for the ON/OFF and Leaking Valve Operations.

IX. CONCLUSIONS AND RECOMMENDATIONS FOR FUTURE WORK

IX.1 Conclusions

Process Gross Behavior:

- This system behaves as an integrator type process. The fluctuations of the pressure drop across a stage as well as solids flow rates in and out of each stage cause open-loop instability, multiple steady-states and unpredictable behaviors. The use of some kind of controller to stabilize the process is necessary.
- A continuous flow rate of solids through each stage can be achieved with the interface and equipment used in this work.

Pressure Fluctuations:

- The measured pressure fluctuations have fast dynamics and result from the eruption of the bubbles at the surface of the bed. The fluctuations are found to be close to sinusoidal oscillations with the fundamental frequency and the amplitude as the two parameters needed to characterize them. The frequency was found to be a function mainly of the bed height. The other parameters have little effect on the frequency.

The amplitude was also found to depend on bed height. However, other variables which have an effect on the amplitude are gas velocity and particle density.

- A lower limit on the average solids inventory on a stage, which can be inferred from pressure drop measurements, can be determined on the basis of pressure fluctuation studies.

Modeling of the Flow Rate of Solids:

- The effect of the average pressure drop (solids inventory) across the stage on the flow of solids out of the stage was found to be more pronounced for average pressure drops less than 0.2 psi. The average pressure drop across the stage has no effect on the flow out of the stage when the average pressure drop exceeds 0.2 psi.
- A linear relationship between the average pressure drop across the bed and the settled height was found to exist in accordance with the theory presented in the literature.
- During the operation of a stage, the existence of a non-fluidizing region close to the grates and a fluidizing region away from the grates was observed. The existence of the two regions was more clear when using a mixture of 25% iron (dark color) and 75% sand (light color). A model based on the overall mass

balance around the whole stage, the force balance on the region close to the grates and the pressure fluctuations was found to predict the behavior of the process. Time averaged values of variables were used since the instantaneous values cannot be obtained.

Alternative Manipulated Variables:

- The choice of the level of working current in an on/off operation is not critical as long as it is greater than the holding current. The average current needed for a specific operation is the same for all choices of the working current.
- The existence of three regimes for on/off operation (glob, continuous and pulse) of the flow of solids through the stage valve and the collar valve used to control solids flow rate from the hopper was observed. The regimes' boundaries were defined for 100% solids.
- The "leaking" valve operation was found to be more energy efficient and sometimes gives better pressure drop performance than the on/off operation.

Control:

- Proportional control augmented with logic control was found to be sufficient to maintain the desired

pressure levels and to overcome the large positive errors resulting from the setpoint changes.

- The interactions between the stages were found to be one-way interactions from the top to the bottom. Decoupling was found to be efficient in eliminating the interactions between the stages.
- Although the theory and simulation have predicted an offset in the pressure drop across the stage as a result of a step in the load, the experimental results (especially those for "leaking" valve operation) show no offset in the pressure drop. The step in the load results in disturbances in the pressure drop that are attenuated and show sluggish behavior in going from top to bottom stages. In some other cases, such as "leaking" valve operation and on/off operation for 25% iron in the solids, the step in the load shows no effect on the pressure drop.
- The agreement between the simulation and experimental results is generally good. The proposed model is adequate for controller design. The designed controller parameters were found to perform adequately when implemented experimentally. The design of those parameters was based on the trade-off between performance and size of controller actions. Multiple equivalent minimums were found to exist when the optimization was performed and the

choice of the parameters was based on examining the data and the plots of the results.

Effect of the Level of the Working Current:

- The level of working current was found to have some effect on the segregation of solids between the two regions when solids consisting of 25% iron and 75% sand were used in the operation. The thickness of the region close to the grates increases as the current increases. The position of the stage also has some effect on the segregation process. The thickness of the layer close to the grates increases from the top to the bottom stages.
- The minimum fluidization velocity increases as the current increases. Also, the random noise resulted from the fluctuations in the flow rate of the fluidizing gas decreases as the current increases because of the increase in the thickness of the layer close to the grates which serves as a distributor.
- The size distribution of solids reaches a steady state after some operational time when the elutriation and grinding rates of solids become equal. The difference between the initial size distribution and the steady-state size distribution was found to increase as weight fraction of iron in solids increases.

IX.2 Recommendations for Future Work

- Similar studies using composite particles, where the magnetic material is embedded inside non-magnetic materials, especially for low magnetic content, are recommended.
- Similar studies at different operational conditions such as gas velocity, particle density, particle size, valve and bed geometries and different magnetic properties are recommended.
- The speed of the computer was the limiting factor in sampling the pressure drop signal. It is seen that the pressure drop performance improves as the sampling frequency increases. Repeating the previous studies with a faster computer is recommended.
- The pressure fluctuations in this work were modeled as a sinusoidal signal. Actually, the signal is sinusoidal augmented with some noise. Therefore, some improvement in the modeling of the pressure fluctuations is recommended for future work. The improvements may result in a better agreement between the simulation and the experimental results.
- The modeling in this work was based on small particles and on some assumptions which may not hold for other magnetic materials or different geometry. The

improvement of the model to take into account such variables is recommended for future work.

- The interactions between the stages resulting from the small to moderate load changes were not found to be a problem. However, large changes in the load may be a problem. To eliminate the effect of the load changes the model developed in this work can be used to predict the steady-state value of the controller output corresponding to the new flow rate. This feedforward scheme is proposed to take care of the load changes.
- Finally, an applications such as drying, elementary gas-solid reactions or filtering of particulate solids using equipment similar to that developed in this work should be studied to demonstrate the usefulness of staged fluidized beds.

REFERENCES

1. Albert, R. V. and Chi Tien, A.I.CH.E., 31, 1985, 288.

2. Altimer H. K., AICHE Symposium, ser. 79, no. 222, 1983, 55.

3. Arnaldos J., J. Casal, and L. Puigjaner, "Powder Tech nology", 36, 1983, 33.

4. Arnaldos J., J. Casal and L. Puigjaneer, "Powder Tech nology", 44, 1985, 57.

5. Astrom, Karl J., B. Wihenmark, Computer Controlled System, Englewood Cliffs, New Jersey: Prentice Hall, 1984.

6. Avery, D. A. and D. H. Tracy, Symposium on Fluidization, Triportit Chemical Engineering Conference, Monterey, September, 1968.

7. Baird, M. H. I., and A. J. Klein, "Chemical Engineering Science", 28, 1973, 1039.

8. Ballian M. D., and F. E. Block, AICHE Symposium, ser. 66, no. 105, 1970, 229.

9. Baskakov A. P., V. G. Tuponogov, and N. F. Filippovsky, "Powder Technology", 45, 1986, 113.

10. Biscans, B. J. P Ribaer, and J. P. Couderc, "Chemical Engineering Journal", 30, 1985, 81.

11. Bitler, F., Introduction to Ferromagnetism, New York: McGraw-Hill, 1937.

12. Bitter, Francis, Introduction to Ferromagnetism, London: McGraw-Hill Book Company, 1937.

13. Botterill J. S. M., and D. J. Bessant, "Fluidization Technology", 1976, 7.

14. Botterill J. S. M., and M. Van Der Kolk, AICHE Symposium, ser. 67, no. 116, 1971, 70.

15. Botterill, J. S. M., M. Van Der Kolk, D. E., Elliot, and S. MCGuigan,"Powder Technology", 6, 1972, 343.

16. Box, G. E. P., and G. H. Genkins, Time Series Analysis Forecasting and Control, San Francisco: Holden-Day Inc., 1976.

17. Broadhurst T. E., and H. A. Becker, "Fluidization Technology", 1976, 63.

18. Buckley, P. S., "Instrumentation for the Process Industry", p. 80.

19. Burgess K. I., I. I. Inculet, and M. A. Bergougnou, AICHE Symposium, ser. 66, no. 105, 1972, 236.

20. Burk, H. E., Handbook of Magnetic Phenomena, New York: Van Nostrand Reinhold Company, 1986.

21. Burns, M. A., and D. J. Graves, "Biotechnology Progress", 1, 1985, 95.

22. Cheremisinoff, N. P., J. H. Siegell, and C. A. Coulaloglour, "Md. Engineering Chemical Process Design and Development", 24, 1985, 719.

23. Davis, C. E., and N. B. Spedding, "Powder Technology", 53, 1987, 131.

24. Clover, G. M., "Powder Technology", 17, 1977, 9.

25. Cooper, D. J., and D. E. Clough, "AICHE Journal", 32, 1986, 389.

26. Cooper, D. F., and D. E. Clough, "Powder Technology", 44, 1985, 169.

27. Cooper, D. J., and D. E. Clough, "AICHE Journal", 31, 1985, 1202.

28. Coughanour, D. R., and L. B. Koppel, Process Systems Analysis and Control, New York: McGraw-Hill Company, 1965.

29. Dahlin, E. B., "Instruments and Control Systems", 67, 1968, 77.

30. Davidson, J. F., R. D. Lanauze, Fluidization Technology, Hemisphere Publishing Corporation, 1976, 113.

31. Davis, G. F., and O. Levenspiel, "Powder Technology, 44, 1985, 19.

32. Dietz, P. W., and J. R. Melcher, "Industrial Engineering Chemical Fundamentals," 17, 1978, 28.

33. Duffin, W. J., Electricity and Magnetism, Maidenhead, Berkshire, England: McGraw-Hill Book Company, 1980.

34. Eisenstein, Itamar, IEEE "Transactions on Magnetics", Mag. 13, No. 5, 1977, 1646.

35. Eleftheriades and M. R. Judd, "Powder Technology", 21,1978, 217.

36. Encochsen L. D., R. K. Otnes, "Programming and Analysis for Digital Time Series", Shock and Vibration Information Center, Defense Department, 1968.

37. Fertik, H. A., ISA Transactions, 14, 1975, 292.

38. Fink, D. G., and H. W. Beaty, Standard Handbook for Electrical Engineers, 11th ed., New York: McGraw-Hill, 1978, Vol. 2.

39. Gazanchiyanis, M. G., I. G. Martyushin, and A. N. Planovskii, "International Chemical Engineering", 6, 1966, 217.

40. Gilbert N. E., Electricity and Magnetism, New York: MacMillan Company, 1941.

41. Goff, K. W., "ISA Journal", Nov. 1966, 45.

42. Goff, K. W., "ISA Journal", December 1966.

43. Gransden, J. F., J. S. Sheasby, and M. A. Bergougnou, AICHE Symposium, ser. 66, no. 105, 1970, 208.

44. Green, J. R., and D. Margerison, Statistical Treatment of Experimental Data, Amsterdam: Elsevier Scientific Publishing Company, 1979.

45. Grenander, V., and M. R. Blak, Statistical Analysis of Stat Stationary Time Series, New York: John Wiley and Sons, 1957.

46. Gustavsson, I., L. Ljung, and T. Soderstrom, "Automatic", 13, 1977, 59.

47. Harmens, A., "Chemical Engineering Science", 18, 1963,297.

48. Harpavot, G., IEEE "Transactions Magnetics", Mag. 10, 1974, 919.

49. Hatfield, W. B.k, and N. R. Amundson, AICHE Symposium, ser. 67, no. 116, 1971, 54.

50. Hiraoka, S., S. H. Shin, L. T. Fan, and K. C. Kim, "Powder Technology, 38, 1984, 125.

51. Hiraoka, S., S. H. Shin, and L. T. Fan, "Powder Technology", 45, 1986, 245.

52. Hirst, A. W., Electricity and Magnetism, Glasgow: Blackie & Sons Limited, 1963.

53. Hisashi, O. Kono, and J. J. Hwang, AICHE Symposium, ser. 79, no. 222, 1983, 37.

54. Hoselitz, K., Ferromagnetic Properties of Metals and Alloys, Oxford: The Claeendon Press, 1952.

55. Jaraiz, M. E., Y. Wang, Guo Tai Zhang, and O. Levenspiel, "AICHE Journal", 30, 1984, 951.

56. Jaraiz, M. E., Octave Levenspiel, and T. J. Fitzgerald, "Powder Technology", 38, 1982, 107.

57. Jaraiz, M. E., Guo Tai Zhang, Yang Wang, and O. Levenspiel, "Powder Technology", 38, 1984, 53.

58. Jenkins, G. M., and D. G. Watts, Spectral Analysis and its Applications, San Francisco: Holden-Day Inc., 1968.

59. Jobes, C. W., "Chemical Engineering", 61, 1954, 166.

60. Johnson, T. W., and J. P. Melcher, "Md. Engineering Chemical Fundamentals", 14, 1975, 146.

61. Jones, A. L., and T. D. Wheelock, AICHE Symposium, ser. 66, 1970, 157.

62. Jones, T. B., G. L. Whittaker, and T. J. Sulenski, "Powder Technology", 49, 1987, 149.

63. Jones, B. R. E., and D. L. Pyle, AICHE Symposium, ser. 67, no.116, 1971, 1.

64. Katz, H., and J. R. Sears," Con. J. of Chemical Engineering", 47, 1969, 50.

65. Kirko, I. M., and M. V. Filippov, "Jhurad Rekhnicheskoi Figiki", 30, 1960, 1081.

66. Koppel, L. B., "I & EC Fundamentals", 5, 1966, 397.

67. Kunii, D., and O. Levenspiel, Fluidization Engineering, New York: Wiley, 1969.

68. Labine, R. A., "Chemical Engineering", 96, February, 1960.

69. Lanauze and J. F. Davidson, "Fluidization Technology", 1976, 113.

70. Lee, E. B., and D. A. Spyner, IEEE "Transactions on Automatic Control", Feb. 1973, 39.

71. Lirag, R. C., Jr., and H. Lihman, AICHE Symposium, ser. 67. no. 116, 1971, 11

72. Lucchesi, P. J., W. H. Hatch, G. X. Mayo, R. E. Rosensweig, Proc. 19th World Pet. Cong., Bucharest, 1979, 4, Sp 4, Heyden, Philadelphia.

73. Maitre, J. F. IE, J. G. Paquer, and J. C. Gille, "Automatica", 6, 1970, 609.

74. Mark A. B., and D. J. Graves, "Biotechnology Progress", 1, 1985, 95.

75. Martin T. L., Basic Physics for Electrical Engineering, Englewood Cliffs, N.J., Prenice-Hall, 1956.

76. McFarlane, R. C., T. W. Hoffman, P. A. Taylor, and MacGregor, "Industrial Engineering Chemical Process Design and Development", 22, 1983, 22.

77. McFarlane, R. C., T. W. Hoftman, P. A. Taylor, and J. F. MacGregor, "Md. Engineering Chemical Process Design and Development", 22, 1983, 22.

78. Morina, I. M., R. K. Chernysheva, M. G. Gazanchiyanis, and I. G. Martyushin, "International Chemical Engineering", 10, 1970, 27.

79. Mulay, L. N., Magnetics Susceptibility, New York: John Wiley and Sons, Inc., 1963.

80. Nander, V. G., M. R. Blak, Statistical Treatment of Experimental Data, New York: John Wilery and Sons, 1957.

81. Nguyen, V. T., M. A. Bergougnou, and C. G. J. Baker, "Canadian Journal of Chemical Engineering", 51, 1973, 573.

82. Oberteuffer, J. A., IEEE "Transactions on Magnetics", Mag. 10, 1974, 223.

83. Onyshko, S. and C. Woo, "International Journal Control", 36, 1982, 775.

84. Ototake, N. and Fan T., "Powder Technology", 48, 1986, 31.

85. Overcashier, R. H., D. B. Todd, and R. B. Olney, "AICHE Journal", 1954, 54.

86. Panofsky, W. K. H., and M. Phillips, Classical Electricity and Magnetism, Reading, Massachusetts: Addison-Wesley Publishing, 1962.

87. Papadatos, K. , W. Y. Svrcek, and M. A. Bergougnou, "Canadian Journal of Chemical Engineering", 55, 1976, 686.

88. Patrose, B., H. S. Caram, AICHE Symposium, ser. 80, no. 241, 1984, 48.

89. Patterson, R. G., and M. L. Jackson, AICHE Symposium, ser. 73, no. 161, 1977, 64.

90. Pillay, P. S., and B. G. Varma, "Powder Technology, 35, 1983, 223.

91. Press, W. H., B. P. Flennery, S. A. Teukolsky and W. T. Vetterling, "Numerical Recipes", Cambridge University Press, 1986.

92. Priel, Z., "Journal Phys. E. Sci. Instrum.", 11, 1973, 27.

93. Raghhuraman J., and Y. B. G. Varma, "Chemical Engineering Science", 28, 1973, 305.

94. Raghumaman J., and Y. B. G. Varma, "Chemical Engineering Science", 28, 1973, 585.

95. Raghuraman J. and Y. B. G. Varma, "Chemical Engineering Science", 29, 1974, 697.

96. Ray, W. H., Advanced Process Control, New York: McGraw Hill Book Company, 1979.

97. Rosensweig, R. E., "Industrial Engineering Chemical Fundamentals", 18, 1977, 260.

98. Rosensweig, R. E., "Science", 204, 1979, 57.

99. Rosensweig, R. E., U. S. Patent 4, 115, 927, September, 1978.

100. Rosesweig, R. E., J. H. Siegell, W. K. Lee, and T. Mikus, AICHE, 77, 1981, 8.

101. Rosensweig, R. E., "Industrial Engineering Chemical Fundamentals", 18, 1979.

102. Rowson, H. M., "Brit. Chemical Engineering", 8, 3, 180, 1963.

103. Segall, N. L., and P. A. Taylor, "Industrial Engineering Chemical Process Design and Development", 25, 1986, 495.

104. Serviant, G. A., M. A. Bergougnou, C. G. J. Baker, and W. Bulani, "Canadian Journal of Chemical Engineering", 48, 1970, 496.

105. Serviant, G. A., M. A. Bergougnou, and C. G. J. Baker, "Canadian Journal of Chemical Engineering", 50, 1972, 690.

106. Shinskey, G., "Instruments and Control Systems", November, 1974, p. 69.

107. Siegell, J. H., and J. C. Pirkle Jr., "Separation Science and Technology", 19, 1984 - 1985, 977.

108. Siegell, J. H., and C. A. Coulaloglov, "Powder Technology", 39, 1984, 215.

109. Si-elling, PJ. O., Jernkontores Ann., 141, 237, 1957.

110. Slater, M. J., "British Chemical Engineering", 14, 1969, 41.

111. Sonoliker, R. L., S. G. Ingle, J. R. Giradkar, and P. S. "Mengindia Journal of Technology", 10, 1972, 373.

112. Spooner, Thomas, Properties and Testing of Magnetic Materials, New York: McGraw-Hill Book Company, Inc., 1927.

113. Stephanoupoulos, G., Chemical Process Control, Englewood Cliffs, New Jersey: Prentice Hall 1984.

114. Stokes, and E. B. Nauman, "Canadian Journal of Chemical Engineering", 48, 1970, 723.

115. Stratton, J. A., Electromagnetic Theory, New York: McGraw-Hill, Inc., 1941

116. Tardos, G. I., D. Mazzone, and R. Pfeffer, "Powder Technology", 41, 1985, 135.

117. Toei, R., "Chemical Engineering Jap.", 20, 1956, 551, 695.

118. Tsu, J. C., and A. V. Meyers, Modern Control Principles and Application, New York: McGraw-Hill, 1968.

119. Turton, R., and N. N. Clark, "Powder Technology", 53, 1987, 127.

120. Valdez, E. G., H. Dolezal, and K. R. Dean, AICHE Symposium, ser. 66, no. 105. 1970, 22.

121. Vaneck V., M. Markvart, R. Orbohlav, and R. L. Hummel, AICHE Symposium, ser. 66, no. 105, 1970, 243.

122. Varma, Y. B. G., "Powder Technology", 12, 1975, 167.

123. Verloop J., and P. M. Heertjes, "Chemical Engineering Science", 29, 1974, 1035.

124. Wei-kuo Lee, AICHE Symposium, ser. 79. no. 22, 1983, 87.

125. Weil, N. A., and F. A. Zenz, "AICHE Journal", 4, 1958, 472.

126. Wellstead, P. E., and J. M. Edmunds, "J. Control", 21, 1975, 689.

127. Winch, R. P., Electricity and Magnetism, Sec. Edition, Englewood Cliffs, New Jersey: Prentice-Hall, 1963.

128. Wong, Pui Man, P. A. Taylor, and J. D. Wright, "Md. Engineering Chemical Res.", 26, 1987, 1117.

129. Wong, H. W., and M. H. I., Baird, "Chemical Engineering Journal", 2, 1971, 104.

130. Yang, W.E., Jaraiz, M., Octave Levenspiel and T. J. Fitzgerald, "Industrial Engineering Chemical Process Design and Development", no. 4, 21, 1982, 717.

131. Yang, J. S., Y. A. Liu, and A. M. Squires, "Powder Technology", 49, 1987, 177.

132. Yarmchulk, E. J., and J. F. Janak, IEE "Transactions Magnetics", Mag. 18, 1982, 1268.

133. Zabrodsky, S. S., Hydrodynamics and Heat Transfer in Fluidized Bed, Cambridge, Massachusetts, M. I. T. Press, 1966.

134. Zhang, Guo-tai, M. Jaraiz, Y. Wang, and O. Levenspiel, "AICHE Journal", 30, 1984, 959.

APPENDICES

APPENDIX A: DETAILS ABOUT THE INTERFACE

A-1 The Three Channel 8-bit Programmable Timer

A-1.1 Introduction

The three channel timer was built by R. T. Chan of Virginia Polytechnic Institute, Blacksburg, Virginia.

The block and timing diagrams of the three channels programable timer are shown in figures A-1 and A-2. The numbers shown in the small boxes in figures A-1 are the integrated circuits manufacturing numbers used for labeling. The standard electronics manuals have more information about them.

This timer was used in this work as an interface between the computer and the circuit card which controls the output of the power supply. More information about the timer and its operation can be found in section II.2.1.

A-1.2 Description of the Three Channel Programmable Timer

On the front of the THREE CHANNEL 8-bit PROGRAMMABLE TIMER are located a thumb operated push button switch, three manual mode select switches, and three status LED indicators. To use the TIMER, a suitable time base is selected by adjusting the push button switch to give the proper time

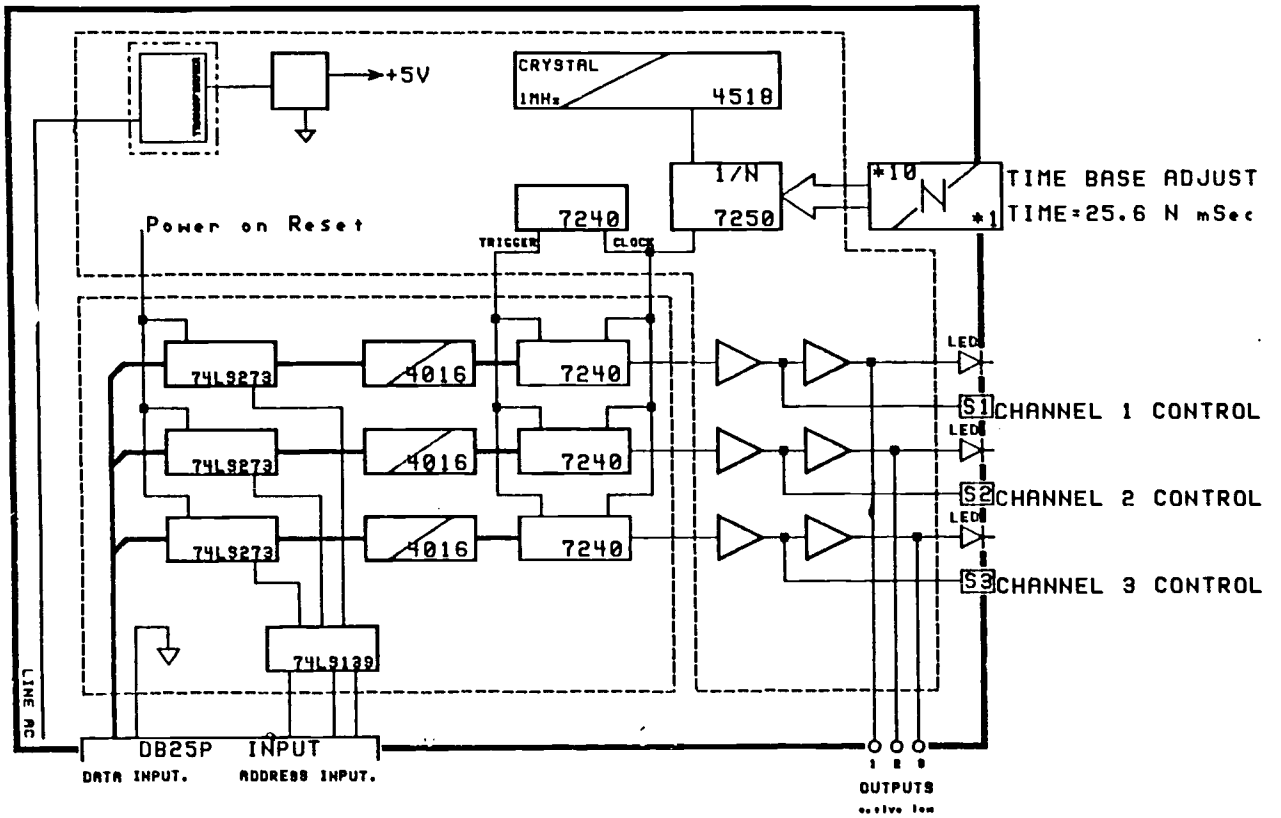

Figure (A-1) Three Channel 8-bit Computer Interfaced Programmable Timer Block Diagram.

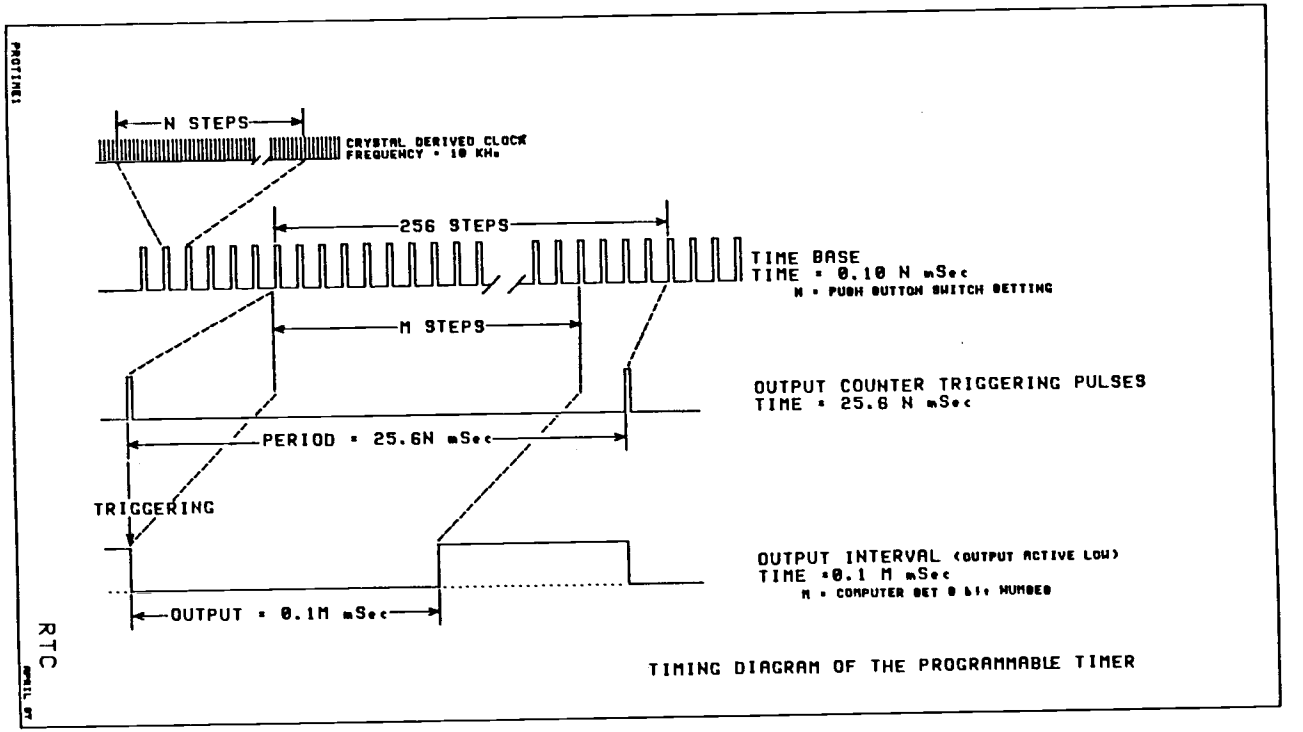

Figure (A-2) Timing Diagram of the Programmable Timer.

interval. For example, to obtain a pulse period of about one second, actually, .998 second, the push button switch is set to 39, (i.e. N = 39), and the time of 0.998 second is obtained from 25.6xN mSecond. This gives an interval of one second between pulses which are used to trigger the computer controlled 8-bit counters. These counters count to the 8-bit numbers set by the computer after they are triggered by the time base interval counter and reset. The outputs, active low state, are then functions of the binary values of the 8-bit computer input to the counters and is given by TIME OUTPUT = 0.1 M mSecond, where M is the 8-bit binary number for the counter channel.

The three mode select switches allow the outputs to be controlled manually to either an ON, OFF, or AUTOMATIC (internal timer) state, which are indicated by the LED status monitors.

On the rear panel are located the DB25P input connector, the three BNC output connectors, and the power AC cord. The input DB25P connector is configured with an 8-bit parallel data input lines, two channel select lines, and a data latch configuration as shown in table A-1.

Table A-1 Connections to the Inputs of the Timer

1	data bit 0
2	data bit 1
3	data bit 2
4	data bit 3
5	data bit 4
6	data bit 5
7	data bit 6
8	data bit 7
9	ground
10	ground
15	channel select B
16	channel select A
17	data latch enable

A-1.3 The Timer Operation

The timing output of the counters is a function of the 8-bit computer word latched into the appropriate channel. For example, if the 8-bit word latched into channel 1 is logic 00000000, the output is disabled, giving a continuous logic 1 for the channel, and if it is subsequently changed to 00000001, the output will be of a length of [(1 * 25.6)/(256)] * N mSecond. If then the input word of channel 2 is

10000000, the output will be [(128 * 25.6)/(256)] * N mSeconds, or 12.8 N mSeconds. The inputs are all tied to logic 1 through a 1.0 kohm (Logic 0) at power on so that the outputs are all at logic high initially.

The channel select lines are configured as below:

CHANNEL	CHANNEL SELECT A	CHANNEL SELECT B
0, not used	0	0
1	1	0
2	0	1
3	1	1

To access one of the three channels to adjust the output timing of the channel, the appropriate channel select address lines, A and B, must be brought to the correct logic level. The data latch enable must be brought from a logic low to a logic high only after the data lines and channel select lines are set up and for a period of not shorter than one microsecond, otherwise the data entered into the counters may not be valid.

The outputs TTL logic level, active low for the duration of t_{op} can drive a standard TTL load.

A-2 The One Channel Programmable 8-bit Programmable Timer

The electronics of this timer are similar to that described in the last section. The diagrams and descrip-

tions in the last section can be used here. However, this timer has a built-in power supply that has a maximum output of 11.8 volts and 1.6 amps. The timer is used to control the time (off-time) during which the output current of the power supply should be zero. The input to the timer is similar to that described in the last section and to that in chapter II.2.1..

This timer is used for regulating the feed flow rate of solids from the hopper by controlling the current off-time which flows through the copper coil surrounding the outlet tube connected to the hopper.

The various pin connections to the input of the timer are similar to those in table A-1 with data latch enable as pin 10 and pin 15 through 17 are eliminated.

A-2.1 The Current Controlling Circuit Card

The description of the card operation in connection with the timer and the power supply was presented in section I.2.2. The main purpose of the card is to produce a perfect square wave which cannot be produced by the timer. The schematic and the block diagrams of the current controller circuit are shown in Figures A-2.1 and A-2.2.

The front and back panels layouts of the current controller cards are shown in figure A-2.3. Also, this circuit card was made by R. T. Chan.

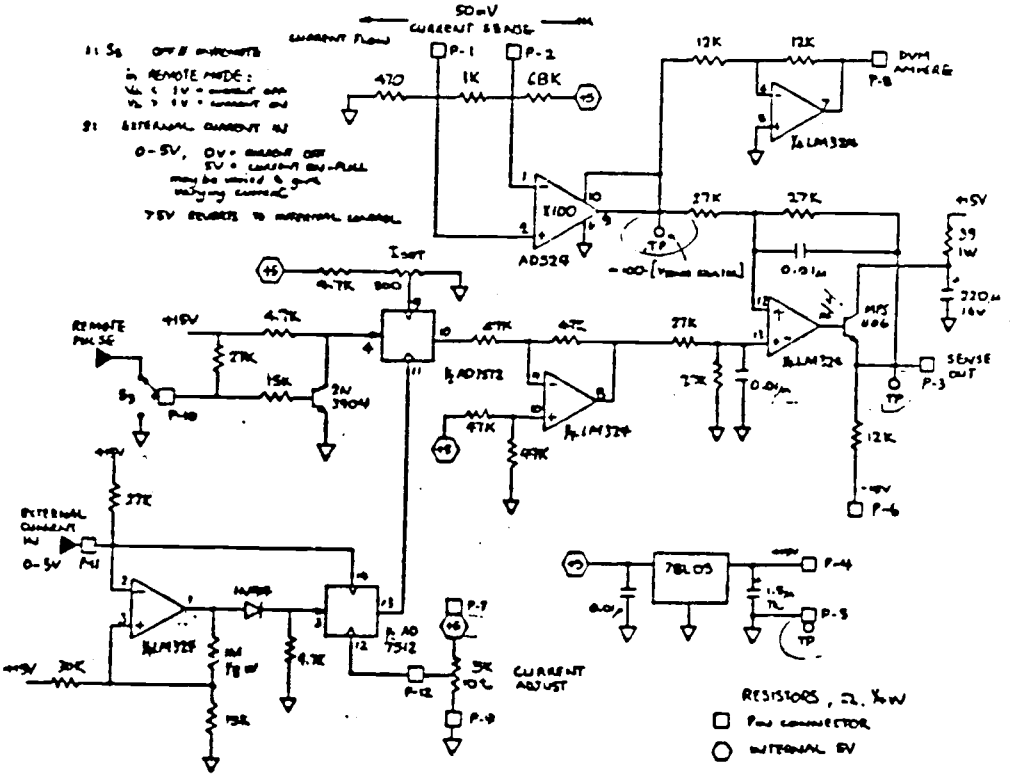

Figure (A-2.1) Schematic Diagram of Current Controller Circuit Card.

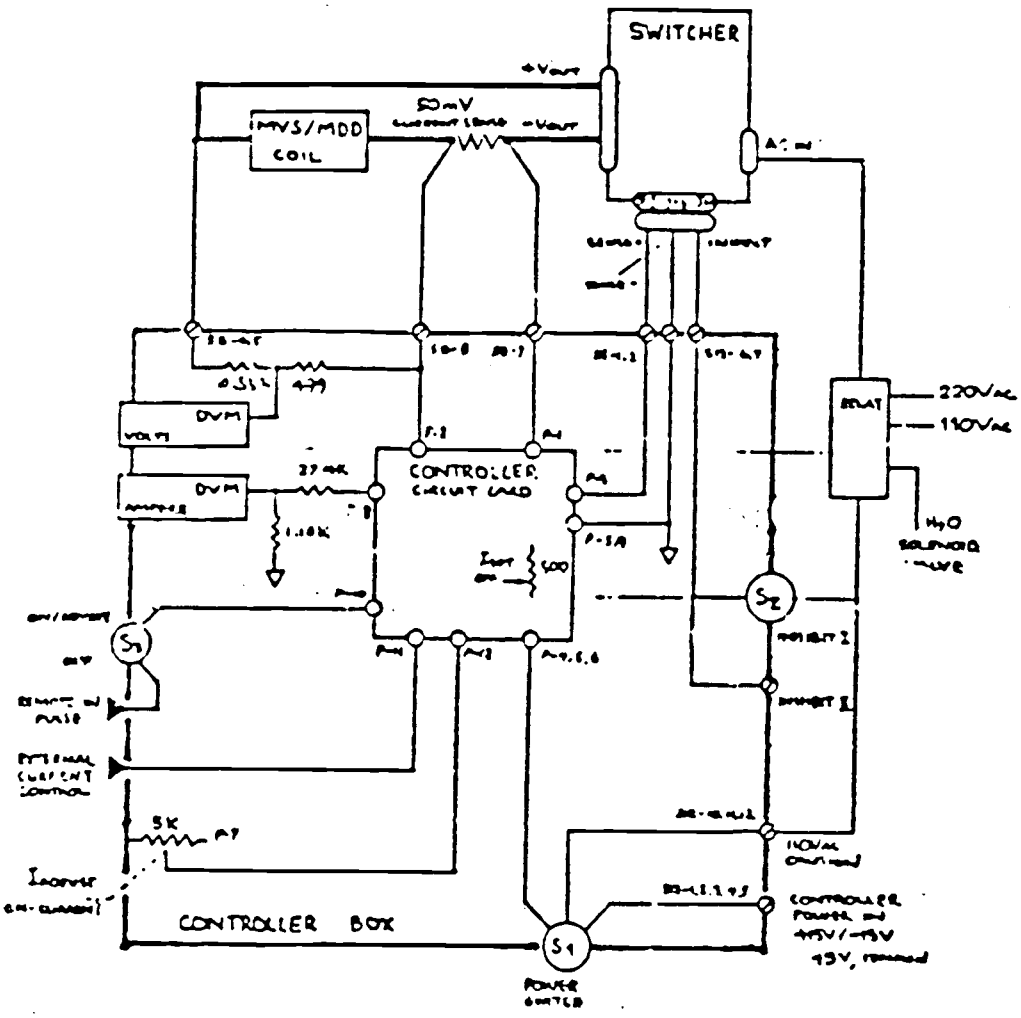

Figure (A-2.2) Block Diagram of the Current Controller Circuit Card.

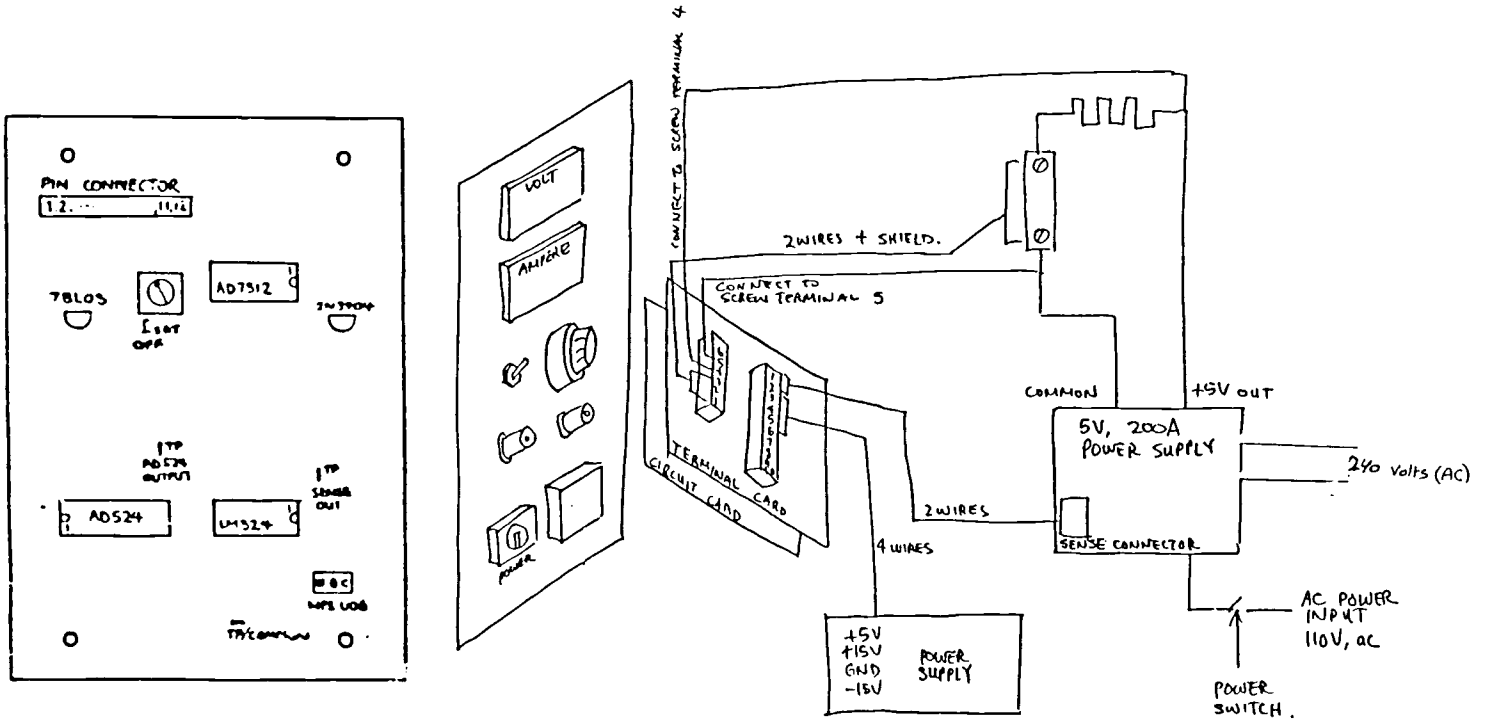

Figure (A-2.3) The Front and Back Panels Layouts of the Current Controller Circuit Card.

A-3 The Pressure Transducer

The pressure transducer used in this research is made by Validyne Engineering Corporation, Northridge, California.

A-3.1 Specifications:

Name	P305D
Range	= 0.08 to 2 psi full scale
Accuracy	= 0.01 psi
Over Pressure	4 psi
Operating temperature	-65 to 250° F
Output noise	≤ 5 mv rms
Power input	10.8 to 32 VDC
Output range	0 to 5 VDC

The power input to the differential pressure cell used in this work was 15 VDC.

Connector Wiring:

A	(+) excitation (10 - 32 VDC)
B	signal output
C	signal return
D	excitation return
E	no connections
F	no connections

A-3.2 Calibration of the Differential Pressure Cell

- The front cover of the cell is first removed. The cell should be placed during the calibration in the same position as that during the operation.
- The positive end of the cell is connected to a constant pressure source via a "T" valve. The other end of the "T" valve is connected to a manometer. The negative end of the cell is left open to the atmosphere.
- The 15 volts power supply for the cell is started. The voltage output of the differential pressure cell is connected to an accurate voltmeter. The reading on the voltmeter should be zero since the valve leading to the pressure source is closed. If the reading is not zero, the pin on the front panel of the differential pressure cell with a mark "Z" is then adjusted until the reading is zero.
- The T-valve connected to the pressure source is then opened slowly and carefully until the reading of the manometer is 2 psi. The pin marked as "o" is then adjusted until the reading of the voltmeter is exactly 5 volts. The positive end of the cell is then disconnected from the pressure source and the reading of the voltmeter is checked and adjusted if it is not zero. The pin located in the

middle between "z" and "o" pins should not be touched.

- The front cover of the cell is returned to its place and the pressure signal to be measured is connected to the positive end of the cell.

APPENDIX B: CALIBRATION OF THE FEED FLOW RATE FROM THE HOPPER

B-1. Calibration of Solids Flow Rate into the Bed

B-1.1 Calibration for Solids Containing 100% Iron

A valve for controlling the solids flow rate was described by Levenspiel et. al. (31, 55, 56) and others (3, 4). This valve consist of a copper coil which slides around the tube through which the solids flow. A copper screen must be placed directly below the coil for a reliable operation. The same principles as those for the grate design are used to regulate the flow of solids through the tube. In this thesis, a completed study is done for defining all the flow rate regions of solids through the coil valve. The boundaries of the regions of solids flow are defined for 100% iron. Three regions were found to exist. They are:

1) Glob Region
2) Continuous Region
3) Pulsed Flow Region

The boundaries are drawn on the basis of visual

inspection. They are much clearer and easier to distinguish from each other than those of the grate design.

Procedures:

- A binary number representing the fraction of period the current flowing through the coil should be zero is sent to a timer connected to the coil. Upon receiving the binary number, the timer will send a square signal to the coil with an amplitude of 1.6 or zero amps.
- The timer continues sending the signal and the solids flowing through the valve is collected for a certain time. The solids are weighed and the procedure is repeated for different fractions open and different periods. The periods are varied from 25.6 to 1230 milliseconds while the fraction open is varied from 0 to 1. By varying the fraction open at constant period, the flow pattern through the valve is watched and the fraction open corresponding to the boundaries for each region is registered. The response of the timer is very fast, so the analysis done before for the stage valve does not apply here. This is due to the low current needed for the operation of the valve. Therefore, the time needed to bring the current down to zero and again to 1.6

amps is so small that it can be considered neglible.

Figure (B-1.1.1) shows the boundaries for the three regions, where, the flow rate is a function of the fraction open at different periods. It shows the different regions that exist in the operation of this kind of valve. The solids flow rates used in the operation of the three-staged fluidized bed lie in the continuous flow region. Because the flow pattern of solids through the valve is somewhat different from the grate design, a brief explanation about the different flow regions is given:

1) <u>Glob Flow Region:</u>

Solids flow through the valve is very slow, and continuous. The solids which is aligned along the magnetic flux line below the coil, detached from the solids, closer to the valve, in forms of clumps. At the detachment point the gravity force is greater than the magnetic and friction forces. The distance at which this occurs is not constant. A value of 3.8 cm may be taken as an average value of this distance. The flow of solids in this region may be divided into two types:

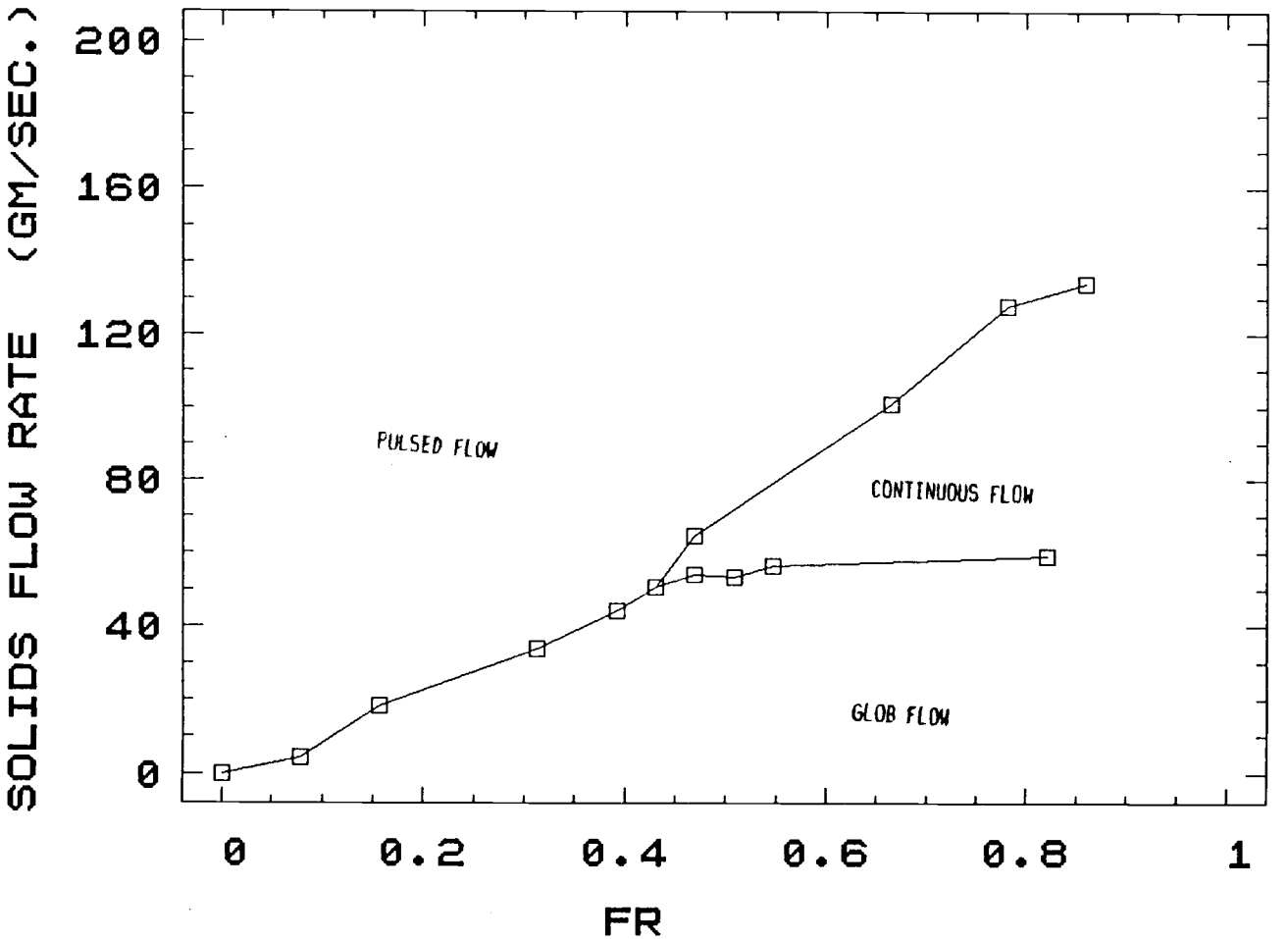

Figure (B-1.1.1) The Three Flow Regimes of Solids Flow Through the Collar Valve of the Hopper.

- Continuous through the valve (very slow)
- Discontinuous at 3.8 cm away from the valve. The discontinuation is represented by the irregular detachment of the solids in the form of clumps.

The flow in this region (Figure B-1.1.1) is a characteristic of small periods T < 51.6 milliseconds and for small fraction open (Fr < .2) for larger periods. Figure (B-1.1.2) shows that the calibration curve is different for each period.

2) <u>Continuous Flow Region:</u>

In this region the flow of solids through the valve is fast and continuous. The detachment of clumps is so frequent that the flow out of the tube is continuous. Therefore, the continuous region is a glob region with flow through the valve and dettachment of clumps at the end of the tube happening at much faster rate. The flow in this region is a characteristic of periods between 51.6 and 384.0 milliseconds and fractions open greater than 0.4. Also, it is a characteristic of fractions open greater than 0.8 for all periods. The flow in the case of larger fraction open is more constant because there is no formation of

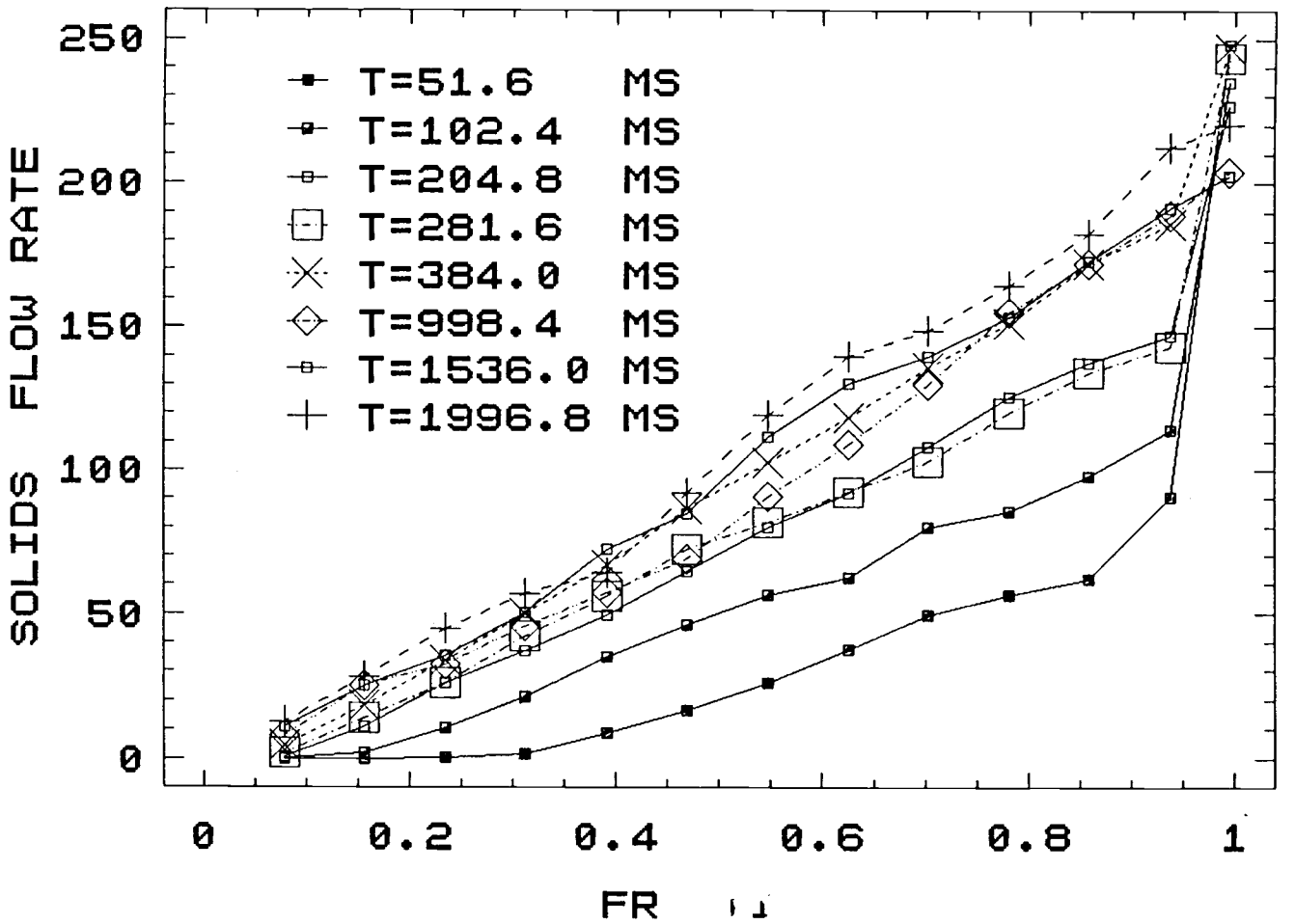

Figure (B-1.1.2) The Calibration of Solids Flow Rate Through the Stage at Different Periods for Solids Consisting of 100% Iron.

clumps. The solids flow pattern in the valve is similar to that at the end of the tube. Figure (B-1.1.2) shows that the calibration at each period is represented by a different line than the other periods.

3) <u>Pulse Flow:</u>

The flow in this region can be represented by the following equation:

$$F \begin{array}{lll} = F_{max} & I = 0 & \text{for } t = t_{op} \\ = 0 & I = 1.6 \text{ amps} & \text{for } t = t_{cl} \end{array}$$

Because of the large open time, hence, the high flow rate, there are no clumps formed. The flow rate of solids is oscillatory. This causes large disturbances to the fluidized bed. In the case of mixtures, the operation in this region is unreliable. This operation is characteristic of periods larger than 281.6 milliseconds. Figure (B-1.1.2) shows that the data representing solids flow rate versus fractions open scatter around one straight line which has the following form:

$$F = S * FR$$

Where S is the slope of the line.

B-1.2 Calibration for Solids Containing 50% by Weight Iron

The calibration (Figure B-1.2) is done only at one period (T = 102.4 milliseconds). The operation is continuous for a fraction open greater than 0.2. For a fraction open of less than 0.2, the flow is similar to a glob flow. However, the flow of solids exhibit occasionally a periodic nature which is due to the uncontrolled flow of non-magnetic material. The formation of clumps is not as clear as that of 100% iron. Only small clumps (some times no clumps) are formed at the end of tube. In this case, the magnetic flux lines are not as strong (due to the presence of non-magnetic particles) as that of 100% iron.

The pulsed operation is not reliable and the flow rate is not reproducible. A high current is needed for more reliable operation.

B-1.3 Calibration of Solids Containing 25% by Weight Magnetic

Figure (B-1.2) shows the calibration of solids flow rate through the valve which is done at a period of 102.4 milliseconds. The operation is continuous when a fraction

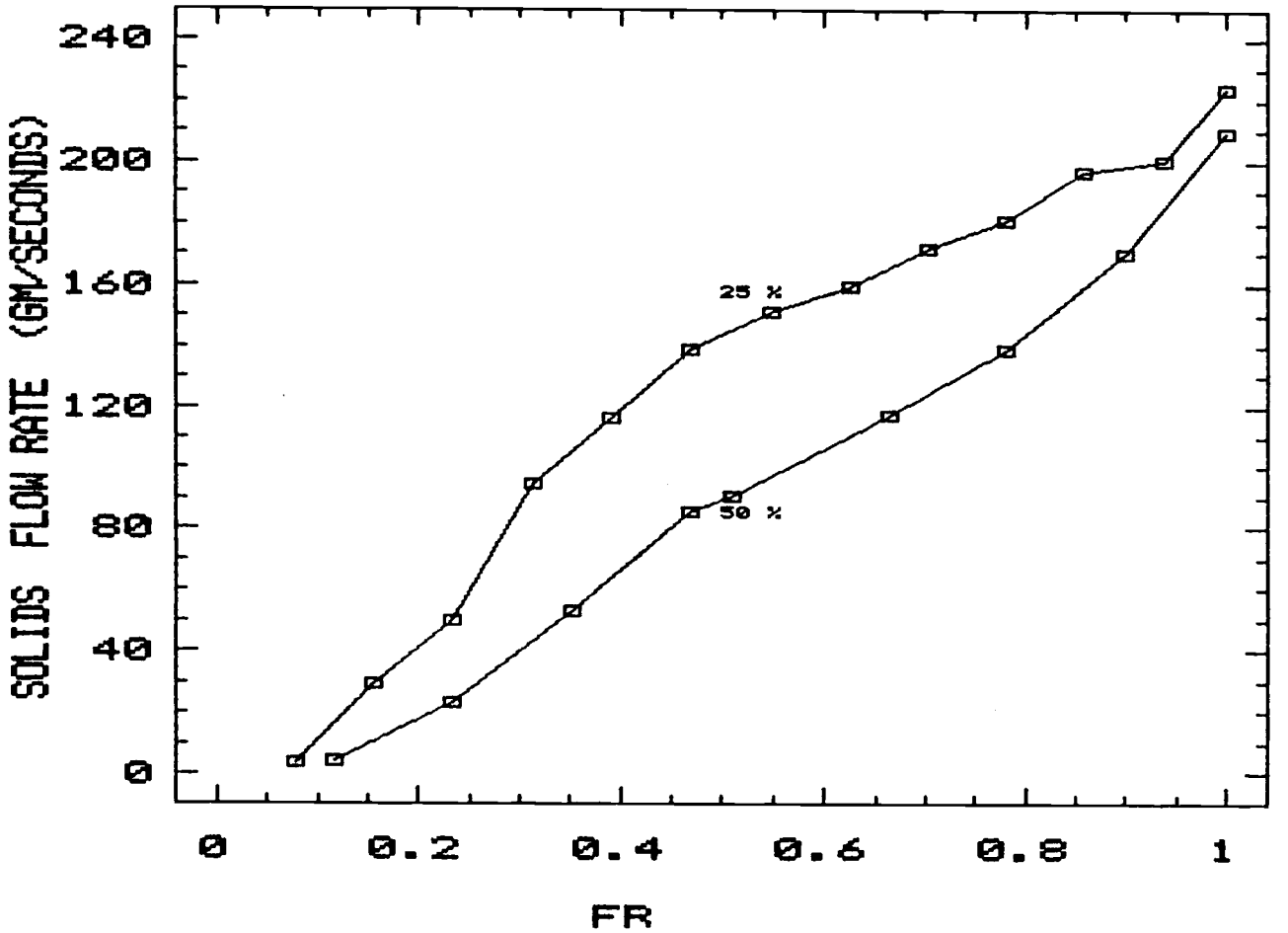

Figure (B-1.2) Calibration of the Flow Rate of Solids Through the Stage Valve

open is greater than 0.1.

The glob region is different from those at 100% and 50% iron. No clumps are seen to be formed and the flow rate is periodic because the flow of non-magnetic solids is also periodic and depends on how much magnetic particles exist in the value which oscillates according to the current being on or off. No pulsed operation is observed in this case and that is due to the high weight fraction of non-magnetic in solids.

B-2 Effect of Screen Location On the Flow Rate of Solids Out of the Hopper

It is mentioned in chapter IV that placing a copper screen some place inside the tube and close to the lower end of the coil makes the operation of the coil valve more reliable. So, the question to be asked is: "What is the distance at which the screen should be placed?". To answer this question, a series of experiments are conducted during which the vertical distance from the coil is varied.

Figures (B-2.1) and (B-2.2) show the plot of solids flow rate through the valve as a function of the vertical distance from the bottom of the coil which is considered to be the origin. The data are obtained for a timer period of .996 second. It can be concluded, from the figure, that the flow rate is a weak function of the vertical distance. The same type of experiments are conducted when a second screen is placed at the very end of the tube below the coil to help, as we thought, distributing the solids into the bed. This screen is fixed in place. It is found that its existence does not help to achieve that and the same pattern of solids flow persist whether one or two screens are used. However,in that case the solids flow rate through the valve seemed to be more affected when the position of the first screen is changed. It is believed that the presence of the second screen affects the flux lines.

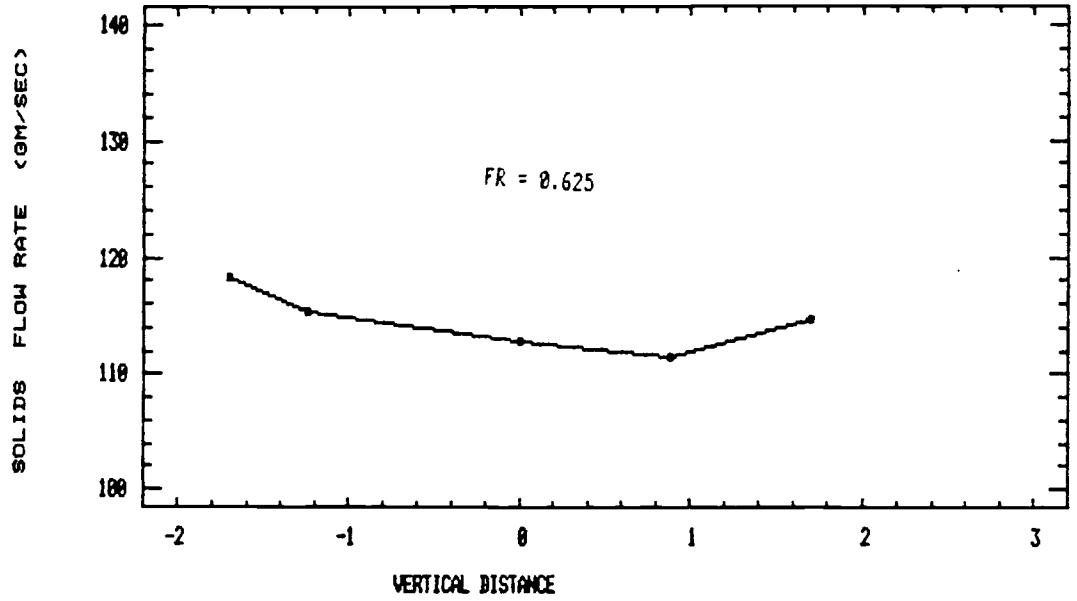

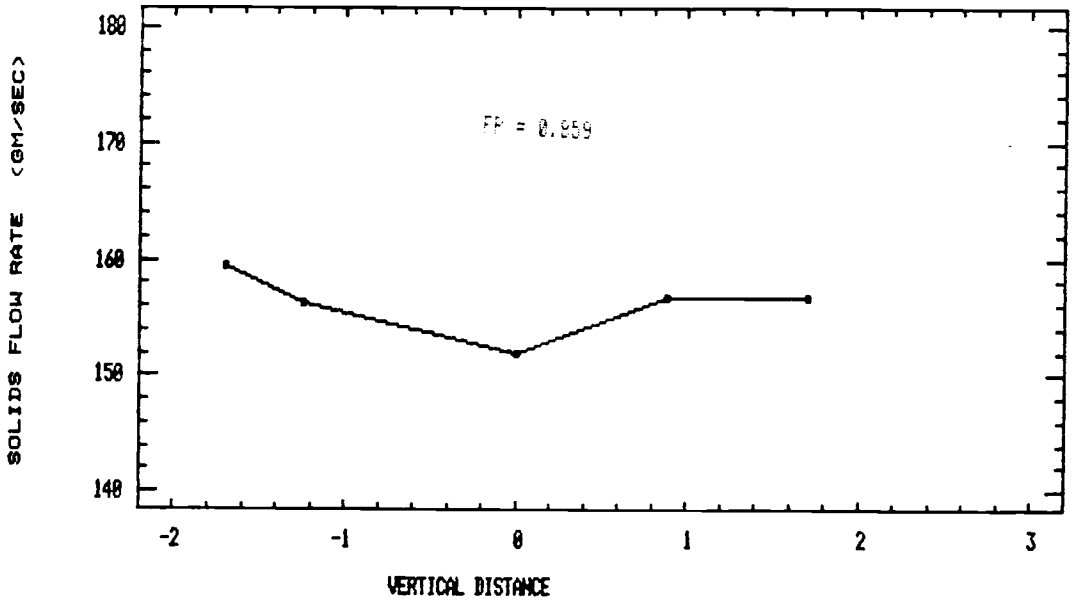

Figure (B-2.1) Effect of Screen's Position on the Flow Rate of Solids Through the Collar Valve Without Another Screen at the End of the Tube.

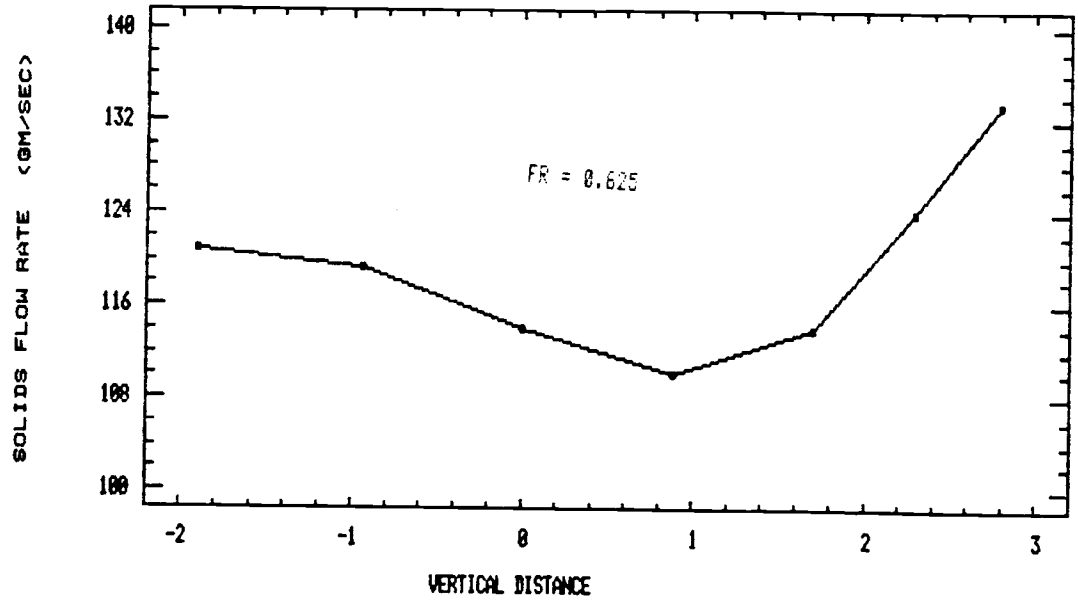

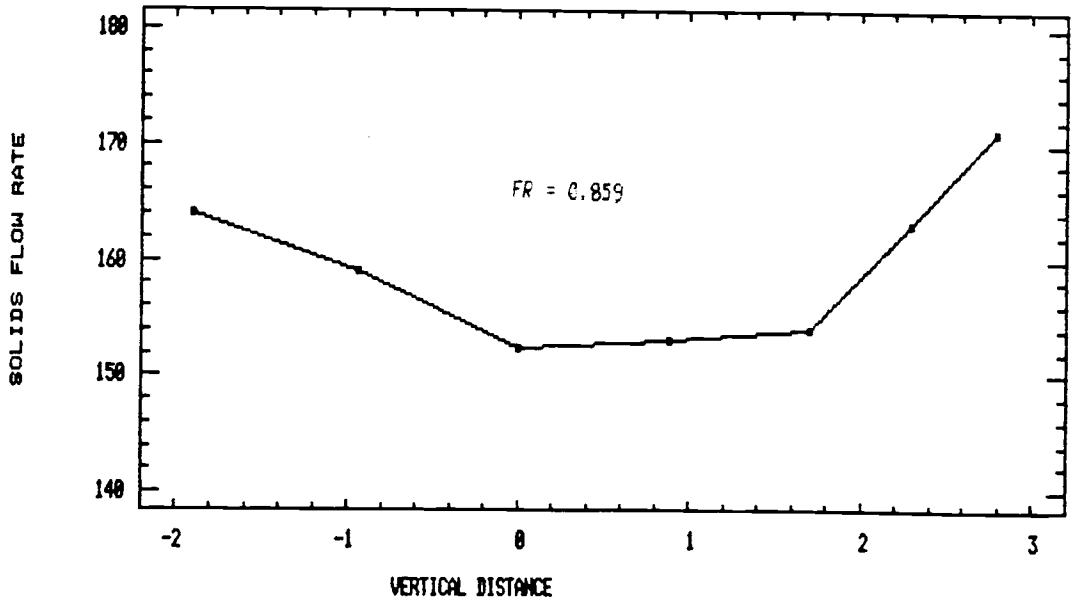

Figure (B-2.2) Effect of the Screen's Position on the Flow Rate of Solids Through the Collar Valve With Another Screen at the End of the Tube.

Figure (B-2.1) shows that a minimum flow rate is reached when the distance is 1 cm while figure (B-2.2) shows that the minimum is reached at a distance of 0 cm.

The top plots which are shown in figures (B-2.1) and (B-2.2) are obtained for a fraction open of 0.625, while the bottom plots are done for a fraction open of 0.894.

B-3 Effect of Solids Inventory in the Hopper On the Flow Rate of Solids

Figure (B-3) shows the plot of the solids flow rate out of the hopper as a function of the solids inventory in the hopper. The total inventory of the solids is first weighed and then transported to the hopper. Then the current through the coil is allowed to oscillate between 1.6 and 0 amps according to the fraction open of period the current should be on which is sent by the computer to the timer. The solids are collected and weighed. The arithmetic average of solids present in the hopper before the flow started and after it stopped is taken to represent the average solids inventory. The procedure is repeated until the hopper is empty.

$$Mavg = \frac{M_i + M_{i+1}}{2}$$

From Figure (B-3), it can be seen that the flow rate of solids out of the hopper is essentially constant for $M_{avg} \geq 4$ kg. So, the solids inventory is kept always above this limit.

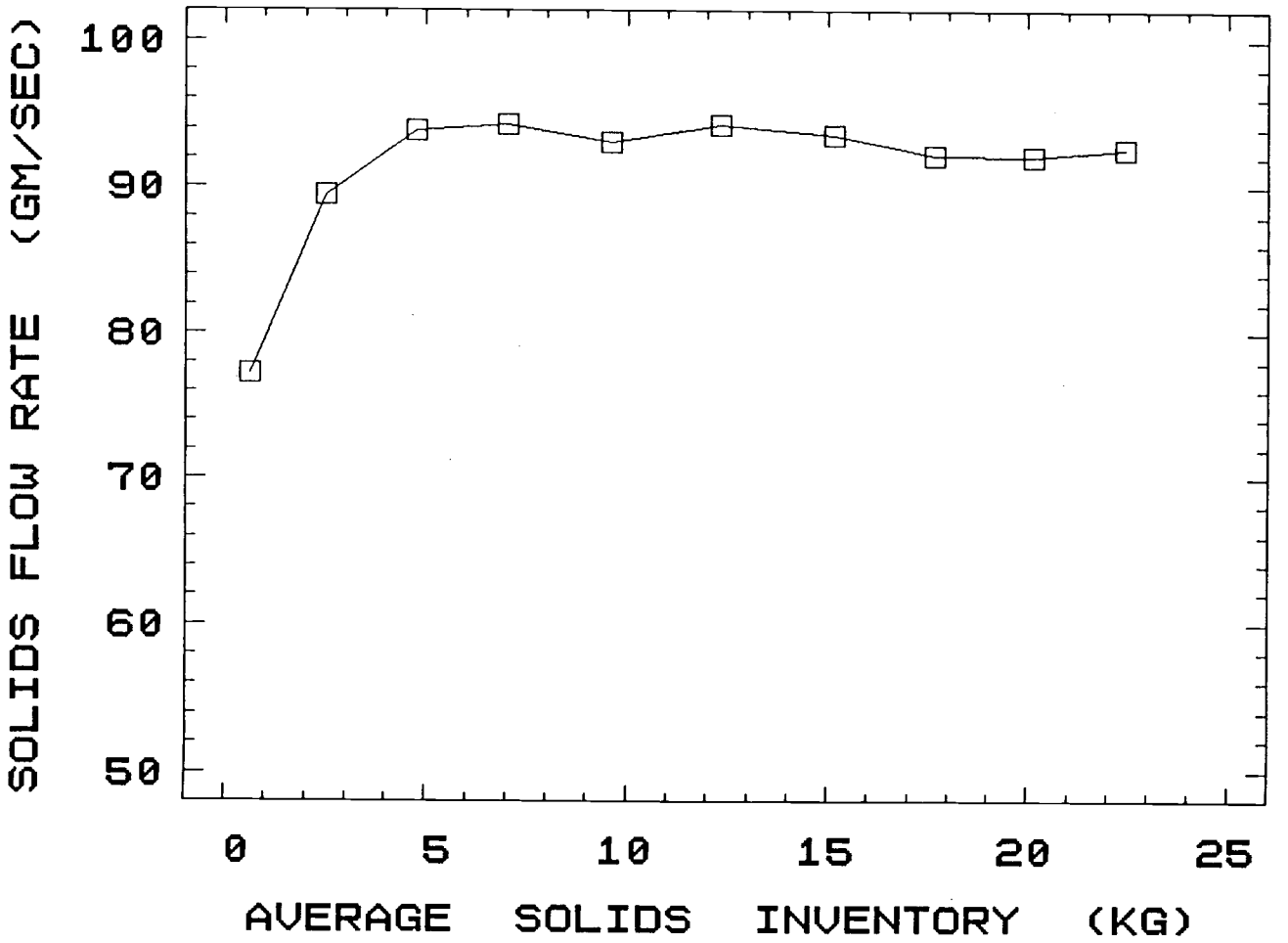

Figure (B-3) Effect of Solids Inventory in the Hopper on the Flow Rate of Solids Through the Collar Valve.

APPENDIX C: CHARACTERIZATION OF SOLIDS

C-1 Size Distribution of Solids

Figure (C-1) shows the particles size distribution of the solids used in the operation of the stage valve. The solids are 100% iron. Different size distributions of the solids are shown in the figure. The samples are taken at different times to see how the size distribution of the particles change with time. The sample is obtained by collecting the whole solids in the equipment in a large container and mixing them thoroughly. Then, a large sample of solids is drawn to determine the size distribution by sieving them. The figure shows that the particles size distribution reaches steady state as the operational time increases. As the time increases, the fresh solids particles, which have larger amounts of big particles, experience grinding and sheer stresses as a result of the friction between them and the walls of the bed, copper grates, screens, and the recycle tube. This results in more fine particles. However, the fluidizing air will cause some solids elutriation of those fine particles. Those two opposing factors cancel each other after some time leading to a steady-state size distribution, as shown by Figure (C-1). Similar results are shown by Figure (C-2) which is the plots of the size distribution of the particles that consist

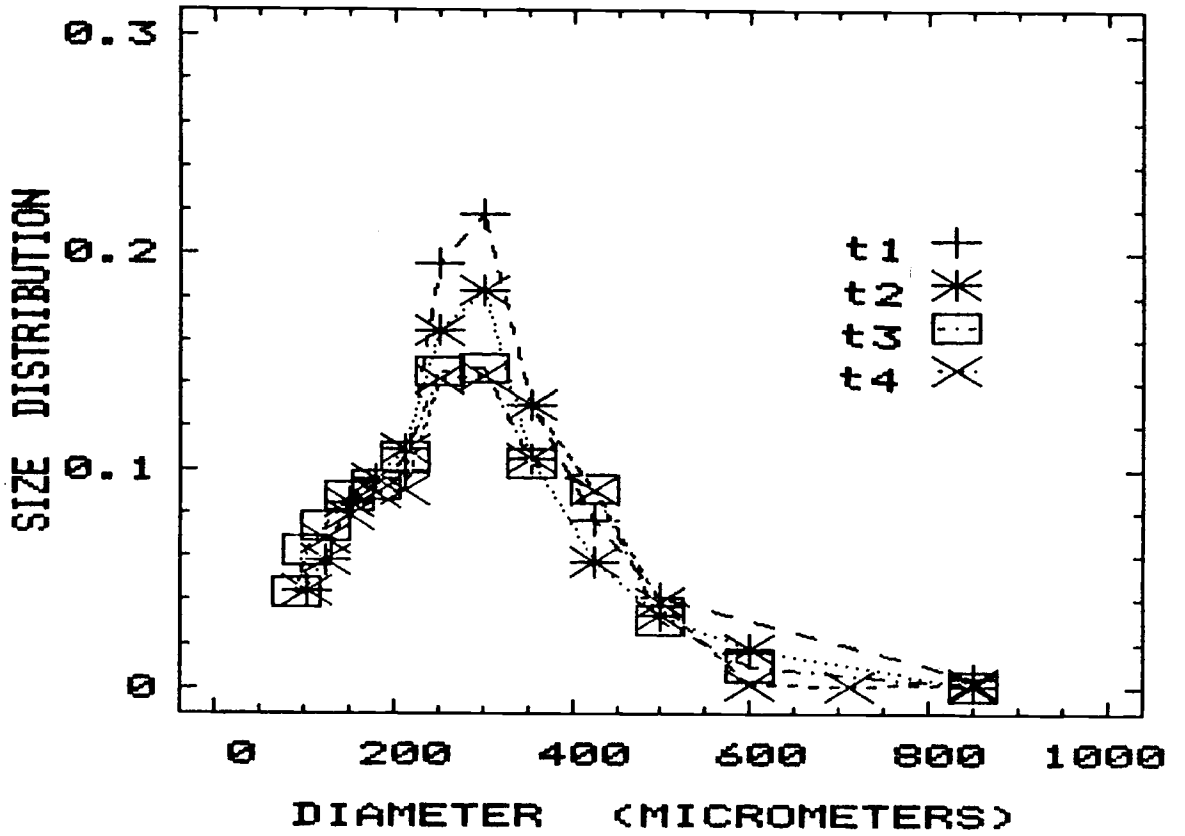

Figure (C-1) Size Distributions of the Solids Consisting of 100% by Weight Iron at Various Times.

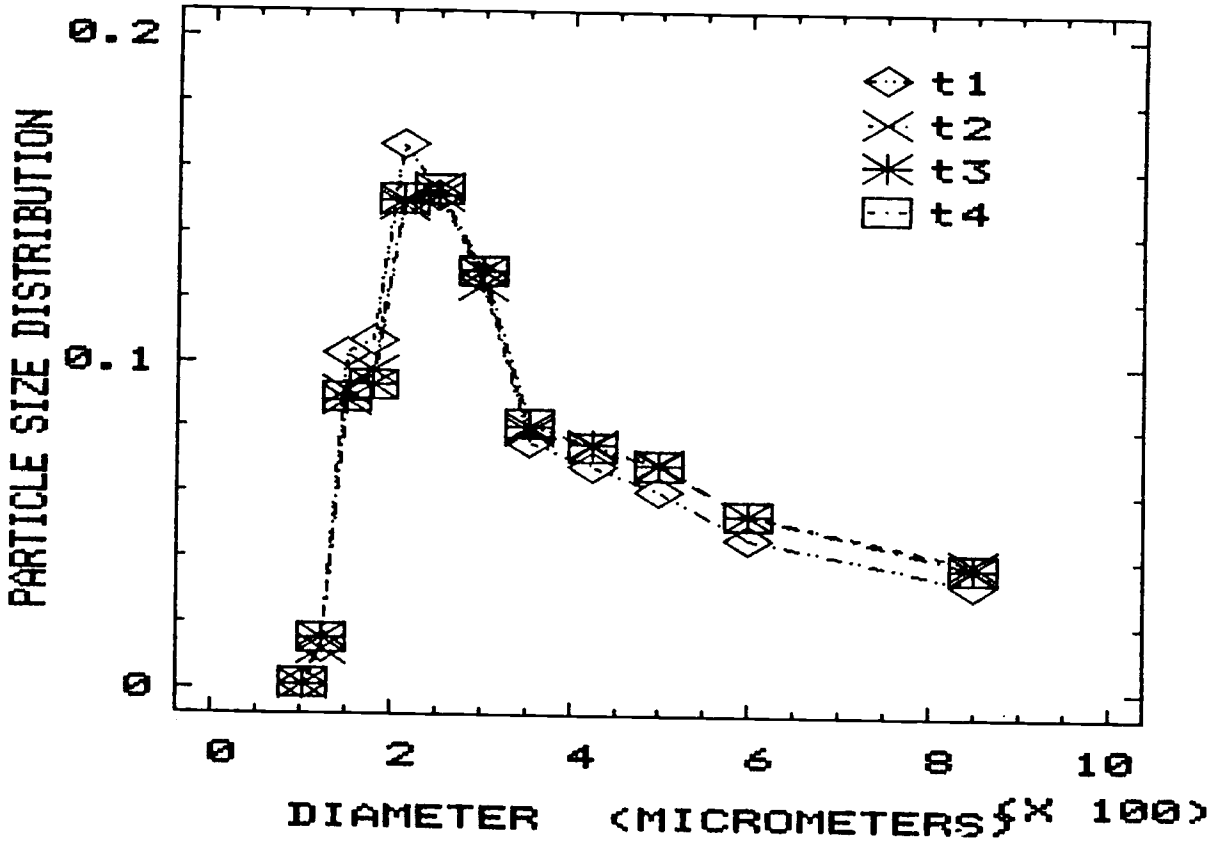

Figure (C-2) Size Distributions of the Solids Consisting of 50% by Weight Iron at Various Times.

of 50% by weight magnetic particles. The curves are very close to each other with little change between the size distribution of the fresh solids and that of the steady state.

The plots of the size distribution of solid that contain 25% by weight iron are shown in figure (C-3). The figure shows similar behavior to that of the 100% magnetic particles.

The figures show that the average particles diameter decreases in going from 100% by weight iron to 25% weight iron. The figures show that the difference between the particle size distribution of the fresh solids and the steady state particle distribution increases as the weight fraction increases. This is because the iron particles are more porous than the sand, which results in more grinding of the particles with large iron's weight fraction.

Tables (C-1), (C-2), and (C-3) show the size distributions data for 100%, 50% and 25% respectively. Some of the data of those tables are used in plotting Figures (C-1) to (C-3).

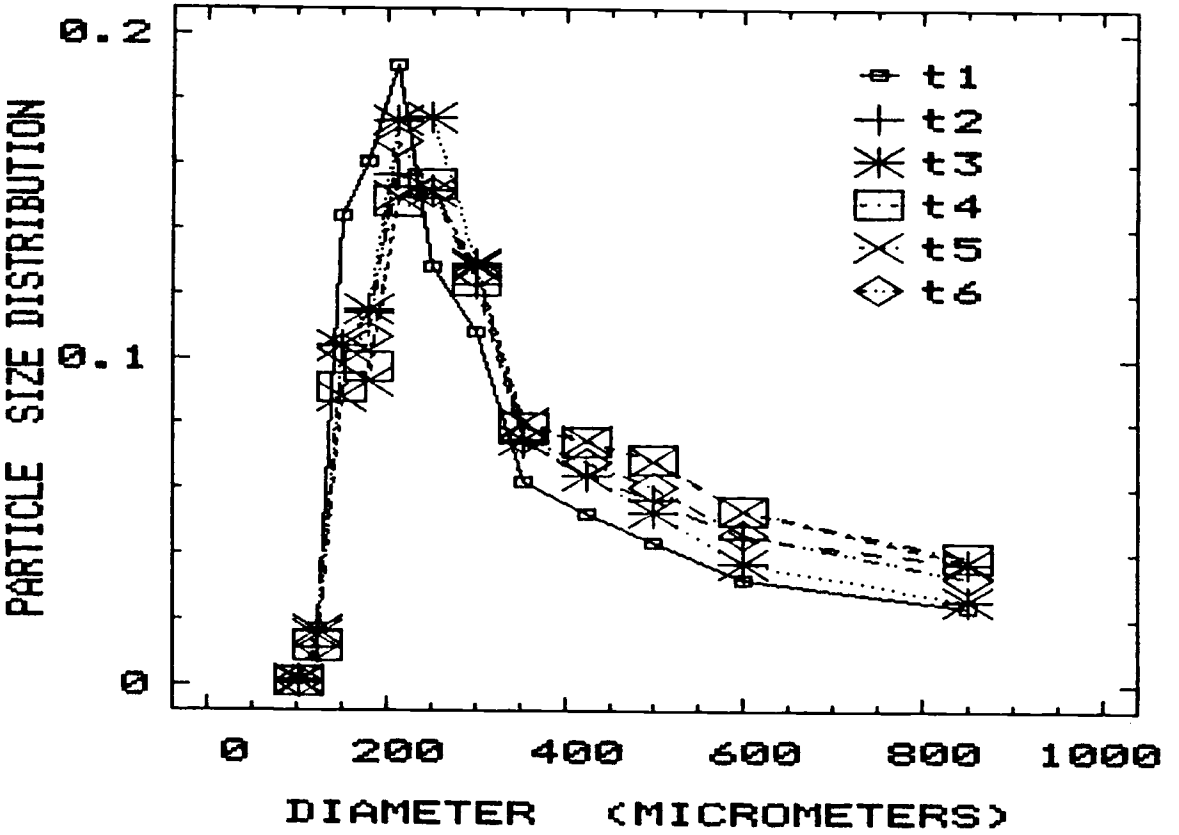

Figure (C-3) Size Distribution of the Solids Consisting of 25% Iron at Various Times.

Table (C-1) Size Distribution of Solids Containing 100% Iron at Various Operational Time.

Dia. (μm)	10 HR	0 HR	Dia. (μm)	40 HR	Dia. (μm)	30 HR	Dia. (μm)	20 HR
212	0.102	0.098	125	0.068	90	0.044	104	0.044
250	0.216	0.195	150	0.078	104	0.062	125	0.058
300	0.209	0.218	180	0.089	125	0.073	150	0.084
355	0.110	0.130	212	0.090	150	0.087	180	0.095
425	0.055	0.076	250	0.142	180	0.093	212	0.110
500	0.021	0.041	300	0.143	212	0.105	250	0.164
850	0.004		355	0.130	250	0.145	300	0.182
			425	0.090	300	0.146	355	0.105
			500	0.038	355	0.103	425	0.057
			600	0.002	425	0.091	500	0.033
			710	0.001	500	0.031	600	0.018
			850	0.002	600	0.009	850	0.001

Table (C-2) Size Distribution of Solids, Containing 50% by W Iron and 50% by Weight Sand, at Various operat Times.

Dia. (μm)	10 HR	30 HR	0 HR	20 HR
104	0.001	0.001	0.001	0.001
125	0.012	0.015	0.012	0.015
150	0.091	0.088	0.103	0.089
180	0.097	0.093	0.107	0.093
212	0.148	0.150	0.167	0.150
250	0.154	0.151	0.151	0.153
300	0.124	0.128	0.126	0.128
425	0.074	0.075	0.068	0.074
500	0.069	0.068	0.061	0.069
600	0.053	0.053	0.046	0.054
850	0.039	0.038	0.033	0.038

Table (C-3) Size Distribution of the Solids Containing 25% by Iron and 75% by weight sand, at Different Times.

DIAMETER				SIZE DISTRIBUTION		
(μm)	T=0.0	35 HRS	25 HRS	30 HRS	20 HRS	5 HRS
104	0.0030	0.009	0.0010	0.0011	0.001	0.0012
125	0.0174	0.0281	0.0115	0.0150	0.012	0.0173
150	0.2014	0.0510	0.0911	0.0880	0.103	0.1440
180	0.1416	0.0644	0.0973	0.0928	0.107	0.1606
212	0.1247	0.1016	0.1480	0.1499	0.167	0.1905
250	0.1362	0.1474	0.1537	0.1510	0.151	0.1282
300	0.0872	0.1286	0.1236	0.1283	0.126	0.1081
355	0.0813	0.0959	0.0787	0.0800	0.076	0.0622
425	0.0609	0.0908	0.0744	0.0746	0.068	0.0522
500	0.0487	0.0880	0.0688	0.0683	0.061	0.0436
600	0.0345	0.0481	0.0532	0.0532	0.046	0.0321
850	0.0262	0.0766	0.0393	0.0378	0.033	0.0240

C-2 Typical Properties of the Solids Used in the Operation

C-2.1 The Magnetic Material

NAME: Pyron R-12 Iron Powder

Chemical Analysis, %

Total Iron	> 97
Carbon	0.01
Sulfur	0.002
Phosphorus	0.002
Manganese	< 0.6
Hydrogen Loss	1.75

Apparent Density = 1.3 gm/cm3

True Density = 7.85 gm/cm3

Curie Point = 770 ^{o}C (after this point the iron turns to paramagnetic material)

Sand:

Apparent Density = 1.1 gm/cm3

True Density = 2.55 gm/cm3

C-2.2 Bulk and Void Fraction

The void fractions for a bed of particles at minimum fluidization conditions and for the closely packed bed are determined as follows:

- A small test bed 5 cm ID plexiglass tubing was filled with known mass of the particles. Then the

bed is tapped and shaken until the height of the bed would not decrease. Then the height of the bed is recorded. The process is repeated four times for each kind of particles and the arithmetic average of the packed bed height is determined.

The gas flow through the bed is started until the minimum fluidization conditions is achieved and the corresponding height of the bed is recorded. Again, the experiment is repeated four times for each particle size and the arithmetic average height at minimum fluidization conditions is determined.

The void fractions are determined using the following equations:

For packed be : $\rho_b = (1 - \epsilon_b) \rho_s$ (C-1)

$$\rho_b = \frac{M_{pb}}{h_{pb} A_{cs}} \quad (C-2)$$

where ρ_b, ϵ_{pb} = Bulk density and height of the packed bed of solids.

At minimum fluidization conditions, the following equation applies:

$$h_{mf} (1-\epsilon_{mf}) = h_{pb} (1-\epsilon_{pb}) \quad (C-3)$$

h_{mf}, ϵ_{mf} = Height and voidage of the bed at minimum fluidization conditions.

$$\epsilon_{mf} = \frac{(1 - h_{pb})}{h_{mf}} (1- \epsilon_{pb}) \quad (C-4)$$

The various values for the different variables are listed below in table (C-4).

Table C-4 Physical and Geometric Properties of Solids at Different Composition.

% wt. Sand	% wt. Iron	d_p M	ρ_b (gm/cm^3)	ρ_s (gm/cm^3)	ρ_{p_b}	ρ_{m_f}	U_{mf} (cm/s)	Current (Amps)
100	0	224	1.53	2.55	.4	.45	7.20	0
75	25	240	1.65	3.88	.57	.61	7.72	168
50	50	264	1.90	5.20	.63	.67	8.80	148
0	100	308	2.39	7.85	.70	.75	11.20	148

APPENDIX D: PRESSURE FLUCTUATIONS STUDIES

D-1 Some Information About Sampling

In addition to the information chapter V, the following sampling experiments were conducted in the early stages of this research.

D-1.1 Very Fast Sampling Frequency

Five experiments were conducted at sampling frequencies of 20,000, 10,000, 5,000, 3,000, 1,000, and 100 samples/ second. Figure (D-1.1) shows the experimental results for the last three frequencies. The purpose of the fast frequencies (20,000, 10,000, and 5,0000 sample/second) is to be sure that no abnormal behavior in the pressure drop signal are taking place. The other experiments done at the last three frequencies show that the shape of the pressure drop signal shape across each stage is the same for all the three frequencies. Therefore, a sampling frequency of 100 samples/second is adequate for capturing the pressure drop signal used for the different studies (i.e. autocorrelation, power spectrum, etc.).

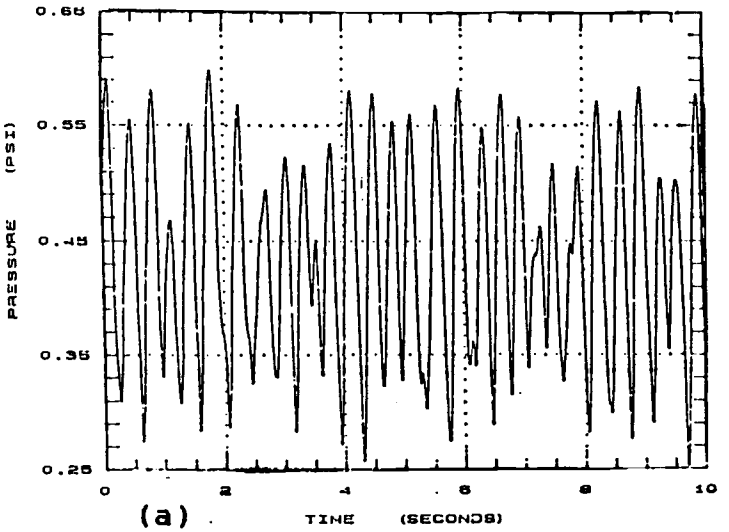

(a)

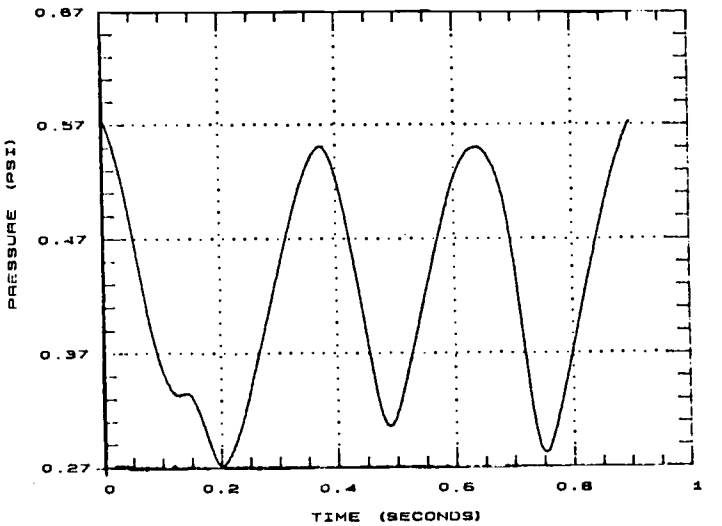

(b)

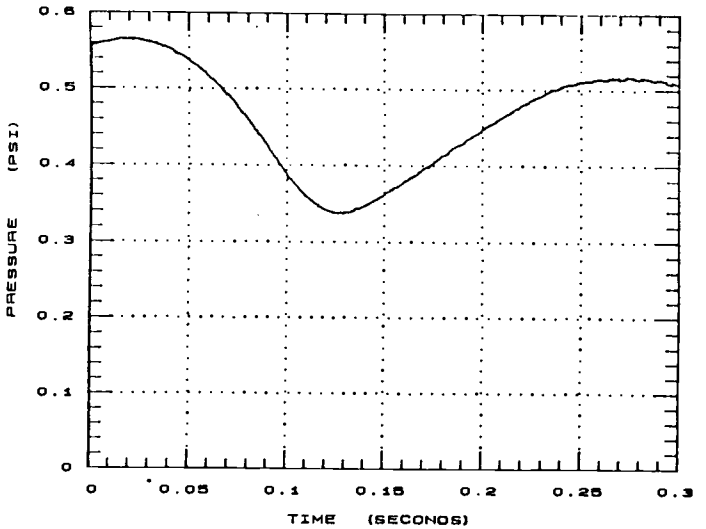

(c)

Figure (D-1.1)
Fast Sampling Of Pressure Drop Across the Stage
a)100 Samples/Second b)1000 Samples/Second
c)3000 Samples/Second

D-1.2 Controller Sampling Rate

Some limitations are imposed by the computer speed and the timer setting on the sampling frequency. More details can be found in sections V.2.1.2 and V.2.3. Some experiments are conducted to see the behavior of the pressure drop signal which the controller sees during the solids flow at a sampling rate of 7.8 samples/second. The signal is also sampled at higher frequency (100 samples/second), to compare it with the last signal, using a second computer. The results are shown in Figure (D-1.2). The figure shows that the controller sampling frequency of 7.8 samples/second is adequate to capture the process behavior.

Figure (D-1.3) shows the pressure drop across (after filtering) the stage for continuous operation at different sampling rate. The pressure drop performance deteriorates as the sampling time increases from 0.128 seconds to .512 seconds.

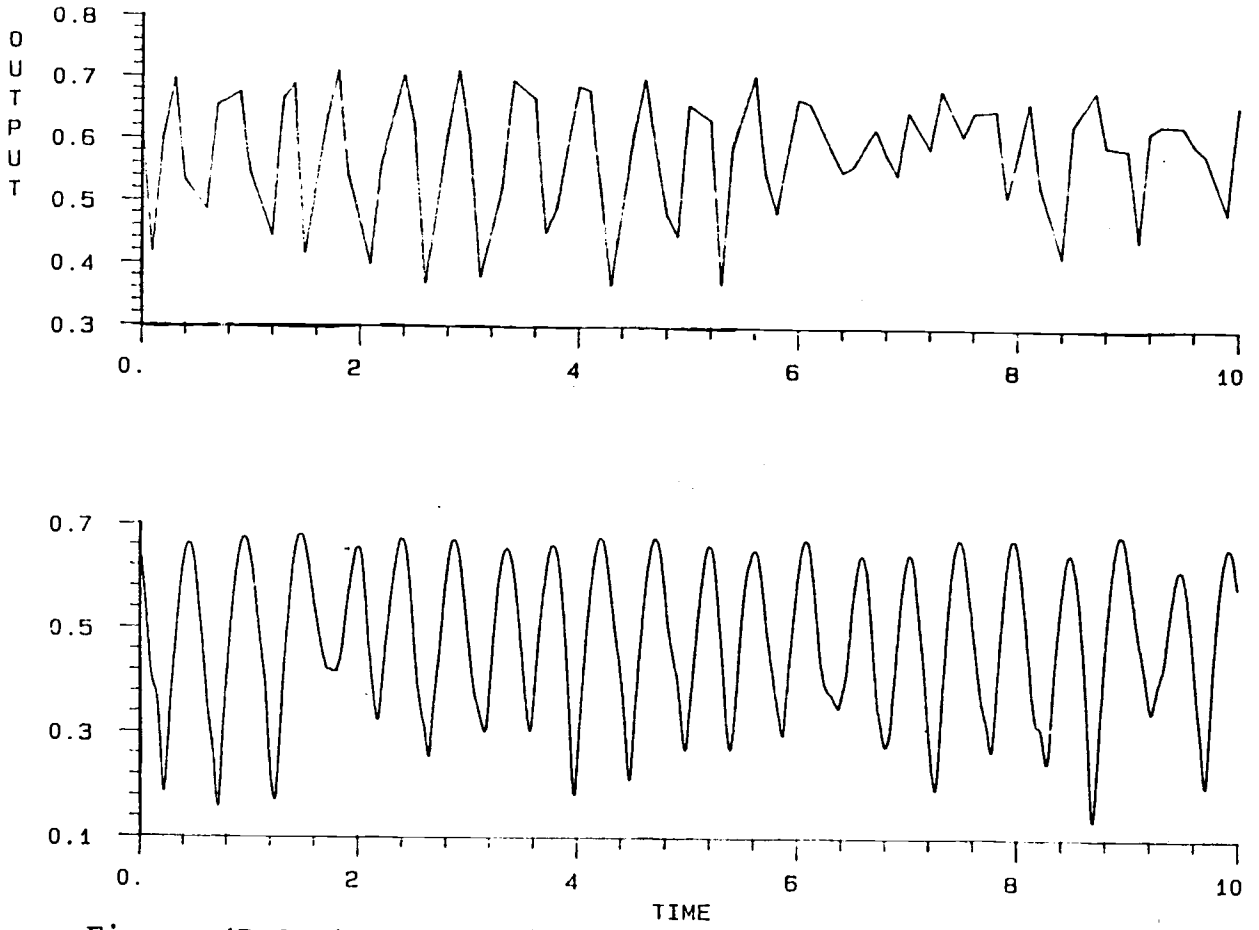

Figure (D-1.2) Comparison Between the Controller Signal and the Actual Signal.
a) 7.8 Samples/second (Controller's Sampling Frequency)
b) 100 samples/second (Actual Signal)

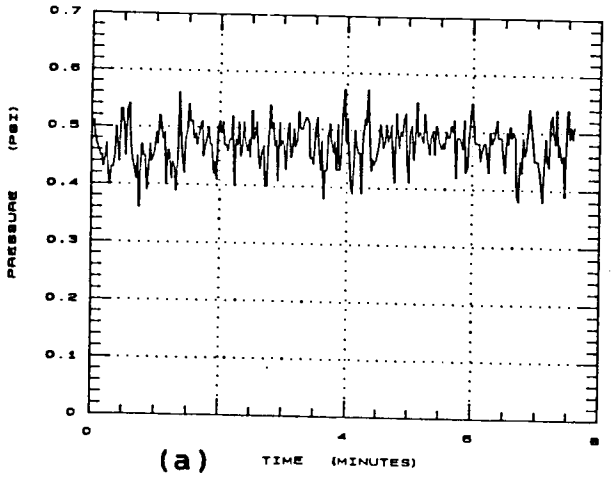

(a)

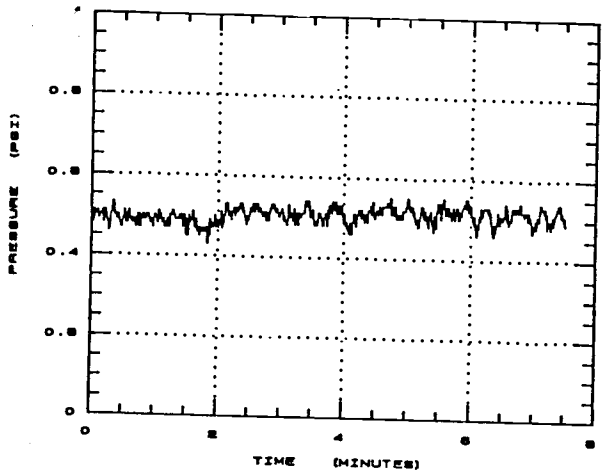

(b)

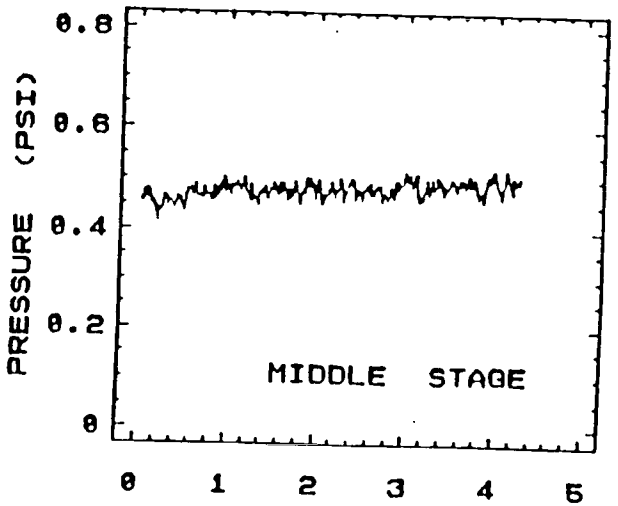

(c) TIME (MINUTES)

Figure (D-1.3)
Pressure Drop Across The Stage at Different Slow Sampling Frequencies
a)2 Samples/Second b)3.9 Samples/Second c)7.8 Samples/Scond

D-2 Approximate Model for Pressure Fluctuations

The existence of the harmonic oscillations in the pressure fluctuations can be deduced from the oscillatory behavior of the autocorrelation as will as the appearance of the large peak at a certain frequency in the spectral plot.

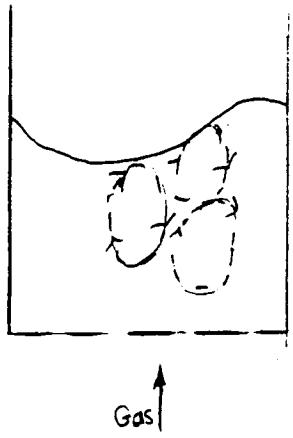

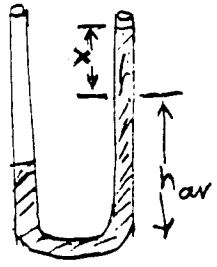

The major effect on the pressure fluctuations is exerted by the bubbles that rise from the bed which cause the bed surface to rise at the spots of their emergence. The height adjacent to the spot varies. Figure (D-2.1.1) shows the circulations of the material inside the bed and the most probable sites for emergence in the bed. The fluctuations in the bed are determined by the vertical displacement of the materials in the bed. This picture is adopted from Baskakov et al (9). The natural frequency of the fluctuations can be obtained by assuming that it can be represented by a U-shaped manometer filled with an ideal liquid.

Making a force balance around the manometer gives:

$$F = m\ a$$

$$m = 2\ h_{av}\ A\ \rho_f$$

h_{av} = average height at fluidization. ρ_f = density at fluidization .

$$a = \frac{d^2\ X}{d\ t^2}$$

Assuming that the major force is that caused by hydrostatic pressure in the tubes gives:

$$F = 2\ \rho_f\ g\ X\ \ A$$

Then:

$$2\ \rho_f\ g\ X\ A + 2\ h_{av}\ A\ \rho_f\ \frac{d^2\ X}{d\ t^2} = 0$$

Which gives

$$\frac{d^2\ X}{d\ t^2} + \frac{g\ \ x}{h_{av}} = 0$$

This equation has a solution of the form:

$$X = A * COS\ \left(\sqrt{\frac{g}{h_{av}}}\right)\ t$$

Making a force balance around the manometer shown in Figure (D-2.1.2) gives an expression for the pressure at the bottom:

$$\Sigma\ F = A_{cs}\ P - (\ h_{av} + X\ )\ A_{cs}\ \rho_f\ g$$

$$m\ a = A_{cs}\ (\ h_{av} + X\ )\ \rho_f \frac{d^2\ X}{d\ t^2}$$

which can be simplified to :

$$P = h_{av}\ \rho_f\ g + \rho_f\ X \frac{d^2\ X}{d\ t^2}$$

$$P = h_{av}\ \rho_f\ g - \frac{A^2\ g}{h_{av}} \quad \cos^2 \left[\ 2\ \left(\sqrt{\frac{g}{h_{av}}}\ \right)\ t\ \right]$$

Therefore :

$$\omega = 2\ \pi\ f = 2\ \sqrt{\frac{g}{h_{av}}}$$

D-2.1 <u>Frequency</u>

From the last equation:

$$f = \frac{1}{\pi}\ \sqrt{\frac{g}{h_{av}}}$$

assume that $h_{av} = h_{mf}$

also $h_{mf} = h_{pb} \dfrac{(\ 1 - \epsilon_{pb}\ )}{(\ 1 - \epsilon_{mf}\ )}$

therefore:

$$f = \frac{1}{\pi}\ \sqrt{\frac{g\ (\ 1 - \epsilon_{mf})}{(\ 1 - \epsilon_{pb}\ )\ h_{pb}}} \qquad \text{(D-2.1)}$$

The above equation shows that the dominant frequency of the pressure fluctuations is a function of the average packed bed height (settled height) across the bed to a power of (-0.5). Figure (D-2.2) shows the theoretical line along with the experimental data.

D-2.2 Amplitude

It has been reported (9,17,123,129) that the amplitude of pressure fluctuations above the distributor (A_{fl}) is a function of the following variables:

1) The excess fluidization velocity ($U - U_{mf}$)
2) g (gravitational acceleration)
3) ρ bed density
4) h bed height

The experiments done in this research on the above variables influence on A_{fl} agreed with the literature. Doing dimensional analysis on the five dominant quantities (A_{fl}, $U - U_{mf}$, g, ρ, h), the following two dimensionless groups result:

$$\frac{A_{fl}}{g\ h_{av}} = f\left[\frac{(U - U_{mf})^2}{g\ h_{av}}\right.$$

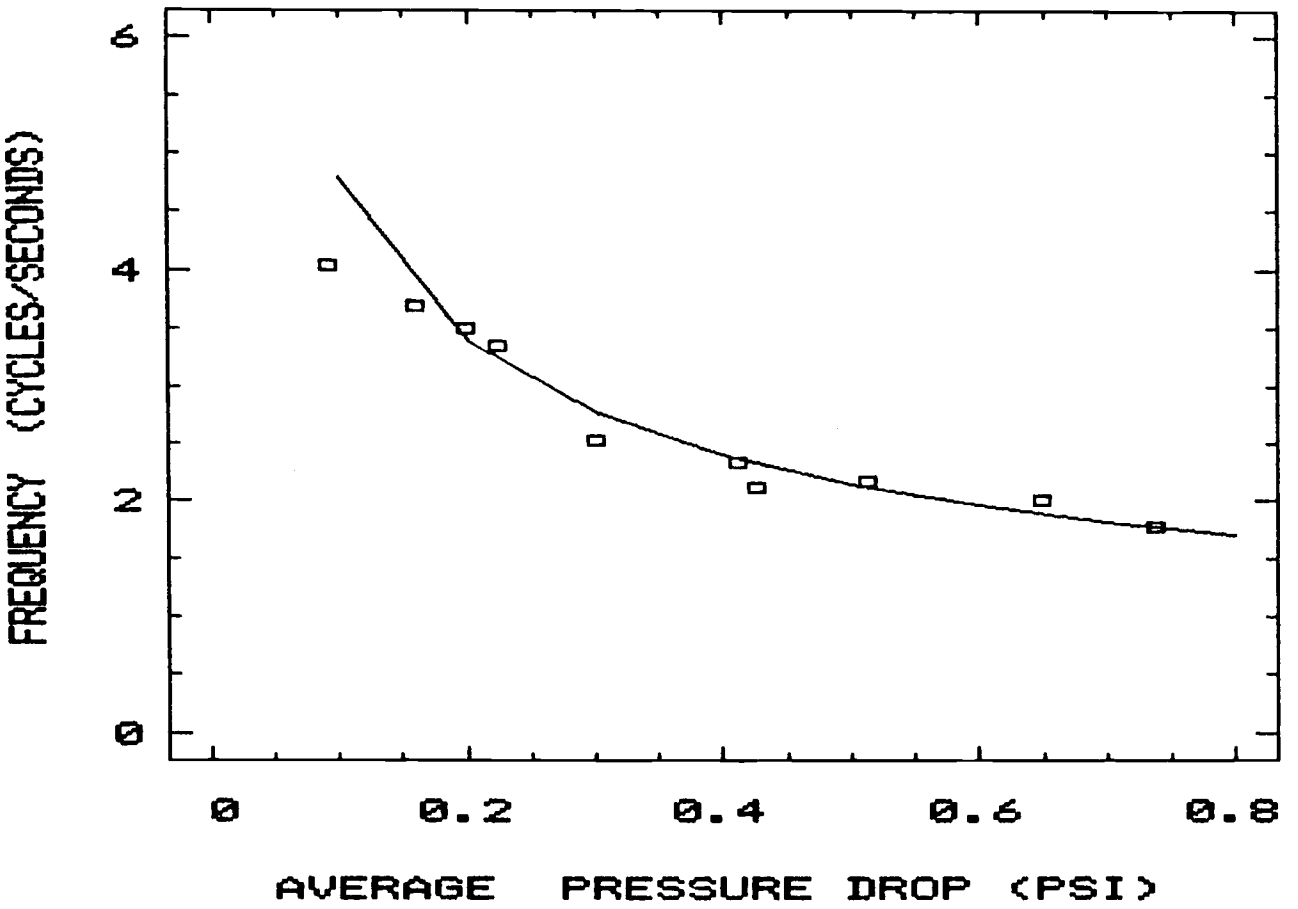

Figure (D-2.2) Experimental Data and the Theoretical Model (Line) for the Frequency of the Pressure Drop Fluctuations.

which can be rewritten in the following form:

$$\frac{A_{fl}}{P_{av}} = f\left[\frac{\rho_{mf}\,(U - U_{mf})^2}{P_{av}}\right]$$

where

$$P_{av} = \rho_{mf}\, g\, h_{av}$$

It is assumed that $\rho = \rho_{mf}$ (density of the bed at minimum fluidization)

The following dimensionless relation can be written based on the last equation.

$$\frac{A_{fl}}{P_{av}} = \text{Constant} * \frac{[\,\rho_{mf}\,(U - U_{mf})^2\,]^n}{P_{av}}$$

The values of the constant and the power (n) is obtained from experimental data. A value of the constant of 0.061 and a value for the power of 0.5 are found by non-linear regression of experimental data. The final equation can be written in the following form:

$$A_{fl} = 0.061 \sqrt{\rho_{mf}\,(U - U_{mf})^2\, P_{av}} \qquad \text{(D-2.2)}$$

Figure (D-2.3) shows the theoretical line representing equation (D-2.2) along with the experimental data.

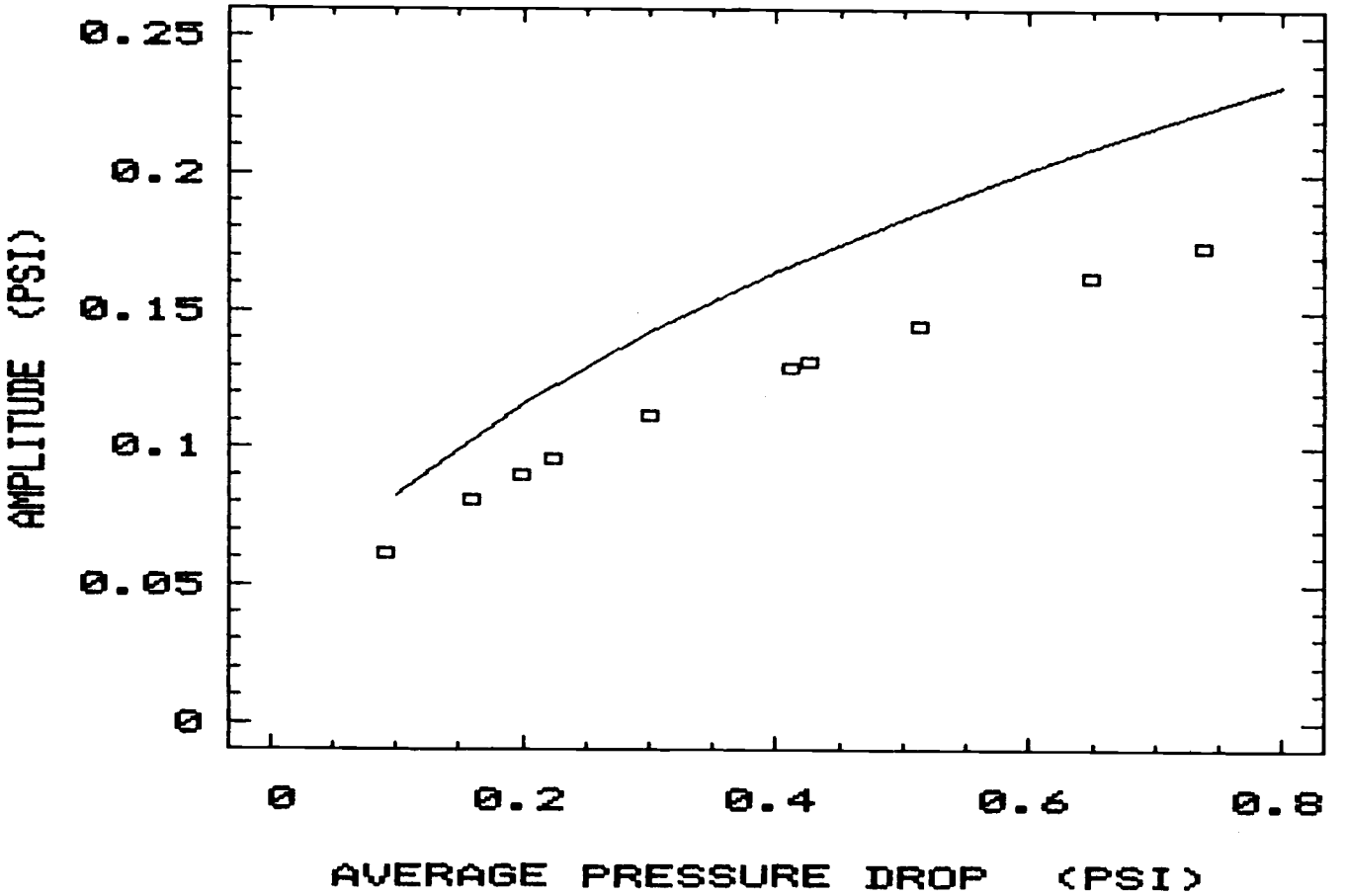

Figure (D-2.3) Experimental Data and Theoretical Model (Line) for the Amplitude of the Pressure Drop Fluctuations.

D-3 Pressure Fluctuations Without Solids Flow Through the Stage (Batch Fluidizaion)

Some experiments are conducted to study the effect of P_{av} (settled height) on the pressure fluctuations' frequency and amplitude without solids flow from or into the stage. The typical signal plot is shown in chapter V.2.4. The signal shows an oscillation which is closer to harmonic oscillation than the case of continuous solids flow through the stage. The experimental procedure is similar to that of section V.2.4. The first experiment begins with a small amount of solids (i. e. average pressure). The amount of solids then can be increased to other desired levels by adding solids from the hopper. These experiments are done for solids that are 100% magnetic. Again, the sampling time is equal to 100 samples/ second. The following equations are the result of curve fitting using non-linear regression routines:

$$f = 1.583 * P_{av}^{-0.57} \qquad R^2 = 0.98$$

$$A_{fl} = 0.195 * P_{av}^{0.498} \qquad R^2 = 0.99$$

The experimental data is shown in Table (D-3). The plots of the experimental data as well as the fitted curve for the frequency and amplitude are shown in figure (D-3).

Table (D-3) Amplitude and Frequency Data Obtained from Spectral Analysis for Batch Fluidization.

Average Pressure Drop (PSI)	Amplitude (PSI)	Frequency (Cycles/sec.)
0.097	0.061	6.05
0.172	0.089	4.41
0.194	0.086	3.81
0.213	0.090	3.58
0.290	0.105	3.53
0.366	0.118	2.54
0.427	0.127	2.86
0.431	0.128	2.62
0.505	0.144	2.27
0.530	0.142	2.38
0.575	0.147	2.14
0.596	0.150	2.14
0.596	0.150	2.14
0.713	0.164	1.90
0.778	0.171	1.90

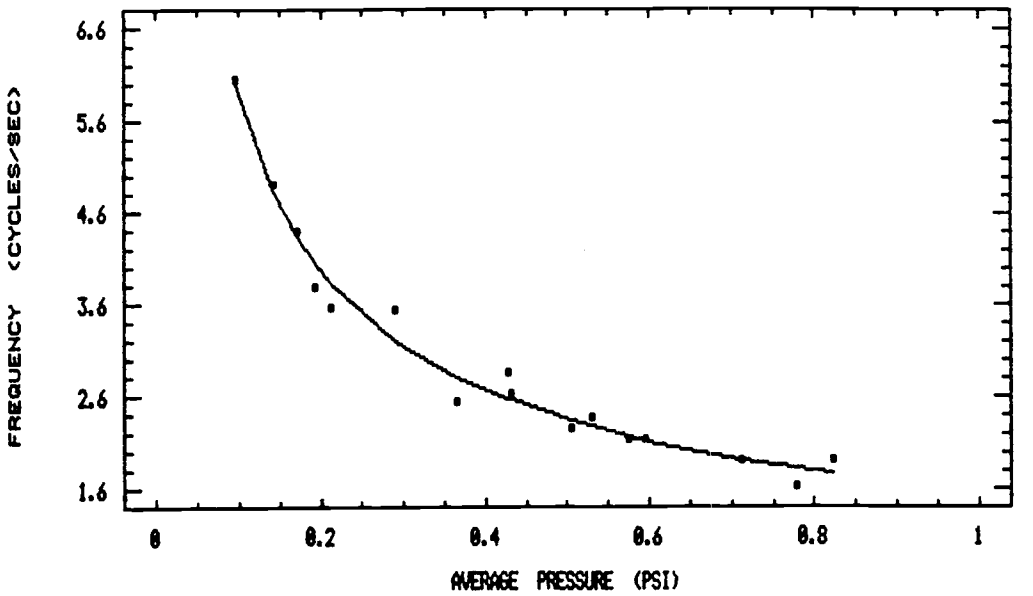

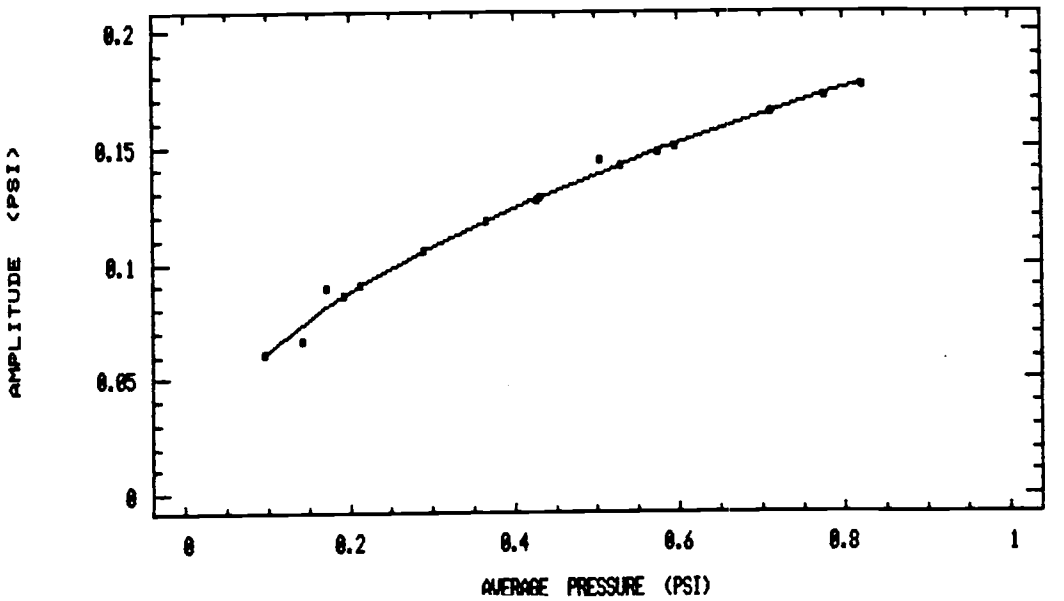

Figure (D-3) Frequency and Amplitude of the Fluctuations vs. Average Pressure for 100% by Weight Iron and Batch Fluidization.

D-4 Pressure Fluctuations with Solids Flow and 0.256 Second as a Controller in Sampling Time

The experimental procedures are exactly similar to that of section V.2.4. Also, two computers were used where one of them was used for fast sampling (100 samples/second) and the other was used for the slow sampling for the controller (T_c = 0.256 second). The study was done to see the effect of the controller sampling rate on the pressure fluctuations. The following correlations are obtained by non-linear curve fitting:

$$f = 1.67 * P_{av}^{-0.4} \qquad R^2 = 0.95$$

$$A_{fl} = 0.202 * P_{av}^{0.499} \qquad R^2 = 1.0$$

The experimental data, as well as the fitted curves for the frequency and amplitude, are shown in Figure (D-4). The experimental data are shown in Table D-4. The above results show that the frequency of the pressure fluctuations at a controller sampling time of 0.256 seconds is larger than when the controller sampling time is equal to 0.128 second. The amplitude at T_c = 0.256 second is slightly larger than that at T_c = 0.128 second. This is partially due to the larger change in the orientation of the solids layer attached to the grates which serves as a distributor. The air flow is influenced by the distributor orientation

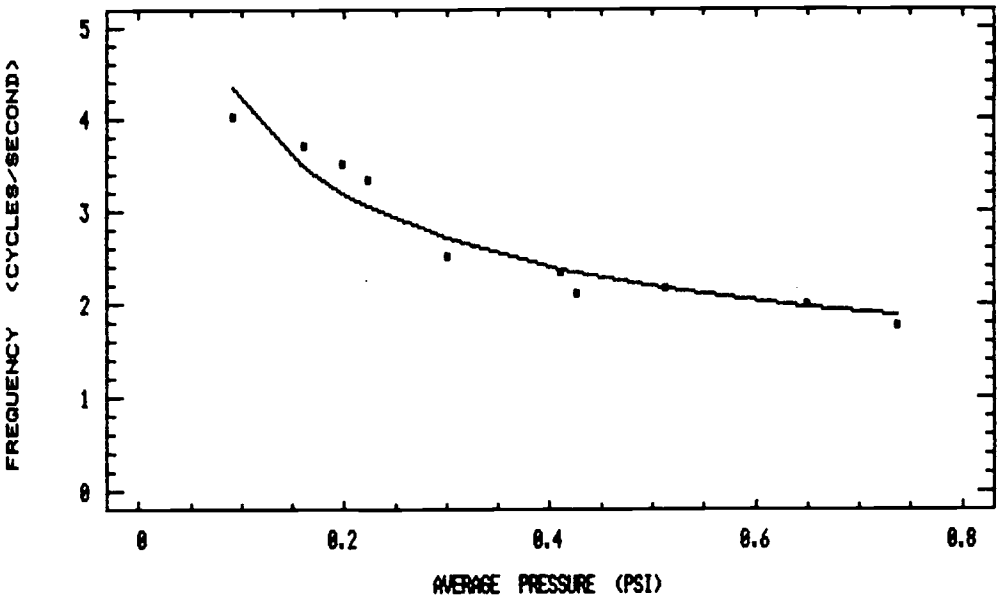

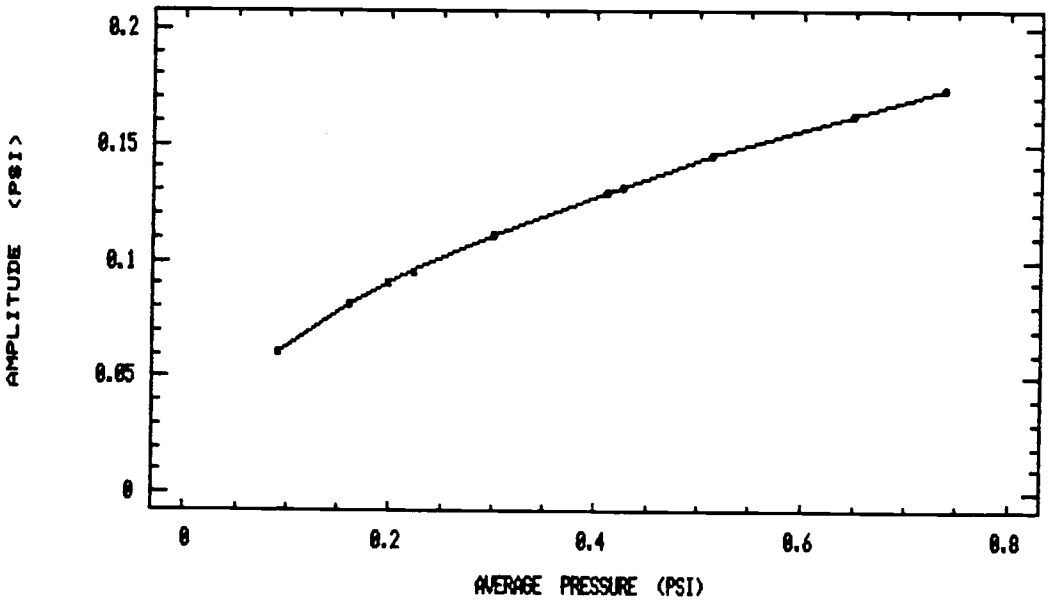

Figure (D-4) Frequency and Amplitude the Fluctuations vs.Average Pressure for 100% by Weight Iron in Solids and Continuous Solids Throughputs. T_C= 0.256 Second.

and larger bubbles start to evolve more frequently. The study was done on solids that are 100% iron.

Table (D-4) Amplitude and Frequency Data Obtained from Spectral Analysis for Continuous Solids Throughputs and for T_C = 0.250 Second.

Average Pressure Drop (PSI)	Amplitude (PSI)	Frequency (Cycles/sec.)
0.091	0.061	4.04
0.160	0.081	3.70
0.199	0.090	3.50
0.223	0.095	3.35
0.301	0.114	2.52
0.411	0.130	2.33
0.425	0.132	2.12
0.512	0.145	2.17
0.650	0.163	2.00
0.737	0.173	1.77

D-5 Effect of Level of Current on the Minimum Fluidization Velocity

Some experiments were conducted to study the effect of working current on the fluidization velocity.

The current flowing through the grates is adjusted via the current controller circuit card to the desired level. Then, the stage is filled with solids, which are 100% iron, to the desired level. The superficial gas velocity is increased from zero to a value higher than the value used in the normal operation (20 cm/sec). The increase in the velocity was done at uniform increments with a time interval which was always greater than 15 minutes between the consecutive increments. The pressure drop across the stage was recorded during the 15 minutes time interval. The superficial gas velocities and the corresponding pressure drops at different working currents are shown in Table D-5. The same data are plotted in Figures D-5.a to D-5.c.

The figures, tables and other data support the following conclusions:

1) The minimum fluidization gas velocity increases as the working current increases.
2) The pressure fluctuations decrease as the working current increases.

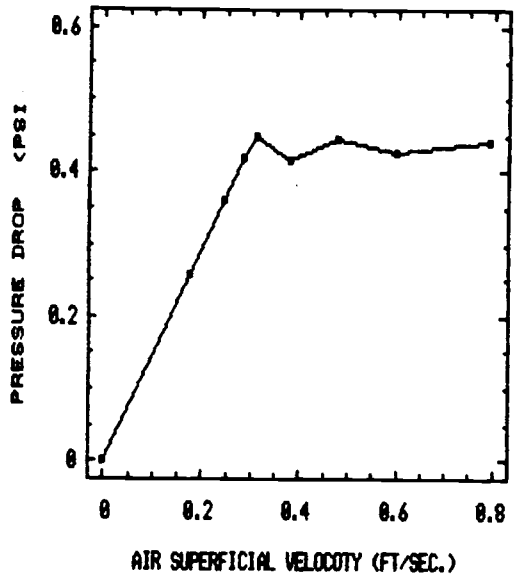

(a)

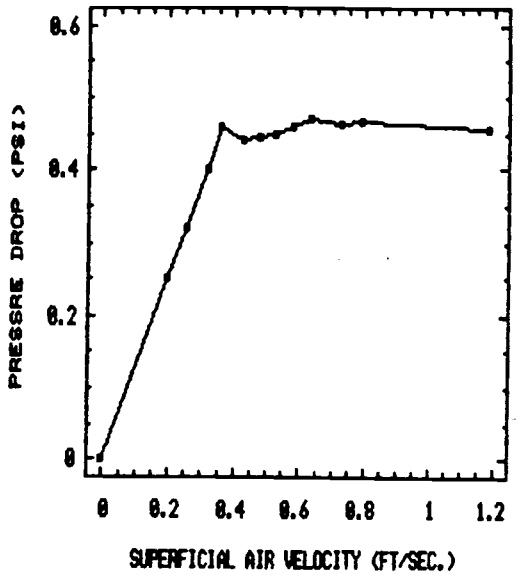

(b)

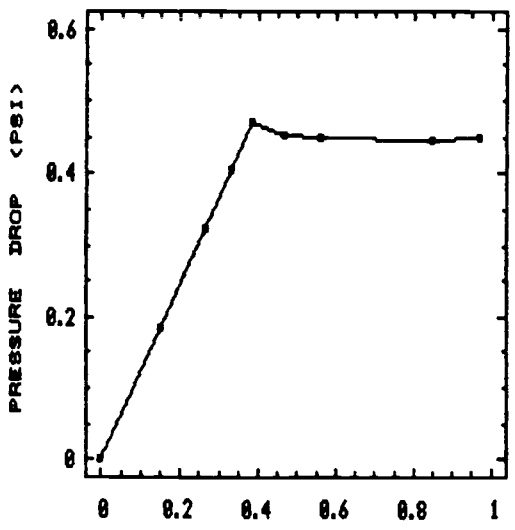

(c)

Figure (D-5) The Effect of the Level of Current on Minimum Fluidization Velocities.
a) No Current; b) I = 148 amps;
C) I = 192 amps

Table (D-5) Superficial Gas Velocities and the Corresponding Pressure Drops at Different Working Currents.

CURRENT = 148 AMPS		CURRENT = 192 AMPS		NO CURRENT	
VELOCITY (FT/SEC.)	PRESSURE (PSI)	VELOCITY (FT/SEC.)	PRESSURE (PSI)	VELOCITY (FT/SEC.)	PRES (PSI)
0.000	0.00	0.000	0.00	0.00	0.00
0.193	0.25	0.152	0.19	0.18	0.26
0.254	0.32	0.264	0.32	0.25	0.36
0.316	0.40	0.330	0.40	0.29	0.42
0.357	0.46	0.383	0.47	0.31	0.45
0.424	0.44	0.464	0.45	0.38	0.42
0.476	0.45	0.560	0.45	0.48	0.45
0.523	0.45	0.847	0.45	0.60	0.43
0.579	0.46	0.967	0.45	0.79	0.44
0.631	0.47				
0.725	0.46				
0.791	0.47				
1.183	0.45				

The above conclusions support the previous postulationse:

1) There are two regions in the stage which are the fluidized region and the region close to the grates.

2) The region close to the grates serves as a distributor for the fluidizing gas. Therefore, as the thickness of the layer increases (the current increases) the pressure drop increases and the distribution of the gas is improved.